MONOCYTE RESPONSE TO EXTRACELLULAR MATRIX DERIVED SEMI-INTERPENETRATING NETWORK SCAFFOLD

by

Amy S. Chung

A dissertation submitted in partial fulfillment of

the requirements for the degree of

Doctor of Philosophy

(Pharmaceutical Sciences)

at the

UNIVERSITY OF WISCONSIN-MADISON

2009

A dissertation entitled

MONOCYTE RESPONSE TO EXTRACELLULAR MATRIX DERIVED

SEMI-INTERPENETRATING NETWORK SCAFFOLD

submitted to the Graduate School of the
University of Wisconsin-Madison
in partial fulfillment of the requirements for the
degree of Doctor of Philosophy

by

AMY S. CHUNG

Date of Final Oral Examination: MAY 12, 2009

Month & Year Degree to be awarded: **December** **May** 2009 **August**

****

Approval Signatures of Dissertation Committee

Signature, Dean of Graduate School

Committee's Page. This page is not to be hand-written except for the signatures

To my Family who eternally stand by me:

My Dad, my hero

My Mom, who sacrificed anything and everything for our education

My Sister, my best friend, my soul, and my spirit

And…

To my advisor Dr. Weiyuan John Kao.

It has been the greatest honor to grow as a scientist under his guidance all these years.

Acknowledgements

I would first like to thank my family for their eternal support and unconditional love. It has only been through their selfless sacrifices and their loving encouragement that I was able to make it this far.

The words thank you cannot express how much gratitude I feel toward everyone around me during my graduate career. Without everyone's inspiration, support and friendship, this enlightening journey would have been impossible. I thank my committee members, Dr. Ronald Burnette, Dr. Melgardt deVilliers, Dr. Darin Furgeson, Dr. Glen Kwon, and Dr. Kristyn Masters for their ingenious ideas, their enthusiastic guidance and encouragement. I would also like to express my gratitude toward the National Science Foundation for the predoctoral fellowship that funded my graduate career for three years. I am very grateful for my friends in Rennebohm, the "Pharmers," for their camaraderie and their support: Kwadwo Owusu-Ofori, Sheng "Penny" Tu, Dr. Joe Su, Heather Waldeck, Dr. Hak Auth, Dr. Adam Alani, Howard Chen, Dr. Oana Martin, Dr. James Dowell, and Ho Chul Shin. I thank Dr. Hu Yang for guiding me during his postdoctoral training in the Kao lab and jumpstarting my growth as a scientist. Special thanks to Heather Waldeck for all her insightful scientific discussions, moral support and her friendship. I thank my KASA dance team, Heeyoon Kim, Yoonsun Park, Jenny Ko, and Jane Lee. Without all our fun teamwork, laughs and love I could not have completed this journey. And I especially thank the inspirational women by my side: to my rock stars, Grace Lee and Narae Lee and my rock, Dr. Susan Lee, for her solid support, trust, and friendship. I am deeply grateful for her tremendous help, and wish to express my sincere respect for her as a scientist, a friend, and a woman.

And lastly, but mostly, I express my deepest gratitude and respect toward my advisor, Dr. Weiyuan John Kao. It has been truly an honor for me to have been a part of his group and to have experienced graduate school under his advisement. He has been most inspirational and only through his patience and his warm guidance am I here today. He always knew best, even if it involved watching me sometimes learn things the hard way, and rooted for my every achievement, no matter how trivial. People say that graduate school is part skill and part luck. I feel all my luck was in meeting the perfect advisor. I know no one will live up to my boss, but as they say it is better to have had the perfect boss than to never have had one. I am forever grateful for the opportunity to have grown as a scientist under his extraordinary scientific knowledge and wisdom and to have thrived under his wholehearted encouragement all these years.

Monocyte response to extracellular matrix derived semi-interpenetrating network scaffold

Amy S. Chung

Under the guidance of Professor Weiyuan John Kao

at the University of Wisconsin-Madison

Understanding the complex intermolecular interactions between the host and the bioengineered substrate is critical to the field of bioengineering and drug delivery. Monocytes/macrophages are commonly observed at the biomaterial-tissue interface and their adhesion onto a biomaterial and the subsequent protein release represents a critical component of biocompatibility. Cell adhesion onto peptide sequences in the extracellular matrix (ECM) proteins such as arginine-glycine-aspartic acid (RGD) through integrin receptors and the subsequent protein release also play a significant role in wound healing.

By conjugating RGD onto a polyethylene glycol (PEG) tether and grafting the RGD-PEG onto a gelatin and PEG based semi-interpenetrating network (sIPN), monocyte adhesion was enhanced. In addition, we observed that β1 and β3 containing integrin receptors were critical in mediating monocyte adhesion and the subsequent matrixin and inflammatory protein expression in the presence of RGD grafted ECM-derived scaffolds. The density of the RGD presented on the sIPN surface was also observed to modulate monocyte adhesion and the expression of matrixin and inflammatory protein expression over time.

We further probed monocyte response to the sIPN in a more physiologically relevant environment by creating a monocyte-fibroblast co-culture system to study the direct influence of fibroblasts on monocyte interaction with the ECM-based substrata. Molecular mechanisms behind monocyte adhesion onto the ECM scaffold and expression of key wound healing factors

in inflammation, matrix remodeling and regeneration were analyzed. We observed that fibroblasts decreased monocyte adhesion onto RGD-PEG grafted sIPN. However, fibroblasts did not decrease monocyte adhesion by decreasing monocyte viability on RGD-PEG grafted sIPN. Fibroblasts increased monocyte GM-CSF drastically except on RGD and PHSRN grafted sIPNs at later stages. Monocytes decreased initial fibroblast IL-1α and TGF-α, but drastically increased fibroblast MMP-2 and GM-CSF at selective time points on all surfaces, including ligand-PEG grafted sIPNs. When the ligand immobilized was RGD, monocyte TGF-α, MIP-1β and VEGF expression was increased while monocyte GM-CSF was decreased at selected time points. These results showed a dynamic monocyte response to selected ECM components in the presence of fibroblasts and the interrelated role of regulation in modulating monocyte-fibroblast interaction in the presence of the ECM-derived matrix.

Approved 

Professor Weiyuan John Kao

Date 6/8/2009

Table of Contents

Chapter 2: Integrin dependent monocyte interaction with ECM-derived peptide functionalized sIPN: adhesion and subsequent IL-1beta, MMP-2 and MMP-9 protein and mRNA regulation

Chapter 3: Monocyte interaction with varying ECM-derived ligand concentration on the sIPN substrate: inflammatory and matrix remodeling protein and mRNA regulation

Chapter 4: Monocyte interactions with ECM-mimic sIPN as modulated by fibroblasts: the effects on monocyte adhesion and the production of inflammatory, matrix remodeling and growth factor proteins

Figures/Tables

Chapter 1.

Chapter 2.

Chapter 3.

Chapter 4.

Chapter 5.

Appendix

List of Abbreviations

Bis-COOH-PEG	bis-carboxylate-PEG
Bis-NSu-PEG	bis-*N*-succinimidyl-acetate-PEG
BCA	bicinchoninic acid
BSA	bovine serum albumin
DIPEA	*N, N*-diisopropyl ethylamine
ECM	extracellular matrix
ELISA	enzyme linked immunosorbent assay
ELS	evaporative light scattering
FN	fibronectin
GAPDH	glyceraldehydes-3-phosphate-dehydrogenase
GGG	glycine-glycine-glycine
GM-CSF	granulocyte-macrophage colony-stimulating factor
GPC	gel permeation chromatography
HPLC	high performance liquid chromatography
HRP	horse radish peroxidase
IL-1α	interleukin-1alpha
IL-1β	interleukin-1beta
IL-6	interleukin-6
LDV	leucine-aspartate-valine
M-MLV	moloney murine leukemia virus
M-PER	mammalian protein extraction reagent
MCP-1	monocyte chemoattractant protein-1
MIP-1α	monocyte inflammatory protein-1alpha
MIP-1β	monocyte inflammatory protein-1beta
MMP-2	matrix metalloprotease-2
MMP-9	matrix metalloprotease-9
MPEG	polyethylene glycol monomethyl ether
RT-PCR	reverse transcription polymerase chain reaction
PBS	phosphate buffer saline
PEG	polyethylene glycol (diol) 2kDa
PEGdA	polyethylene glycol diacrylate
PHSRN	proline-histidine-serine-arginine-asparagine
RGD	arginine-glycine-aspartic acid
RI	refractive index
RPMI	Roswell Park Memorial Institute
sIPN	semi-interpenetrating network
TCPS	tissue culture polystyrene
TGF-α	transforming growth factor-alpha
TNF-α	tumor necrosis factor-alpha
VEGF	vascular endothelial growth factor

Chapter 1. Introduction

1.1 Wound Healing

Wound healing is a dynamic process involving many cell types such as macrophages and fibroblasts and depends on the communication of cells in the wound bed for a healthy progression of healing. In general, the wound healing process involves three phases: inflammation, proliferation, and matrix formation and remodeling and Figure 1-1 and 1-2 display these events at the site of injury [1-6]. During wound repair a large number of monocytes are quickly recruited into the site of injury or site of implant and monocytes differentiate into macrophages in the injured tissue. The number of macrophages increases to five times in the wound compared to the number of resident macrophages in the normal skin [7,8]. Fibroblasts follow the monocyte migration into the injury site and fibroblasts and collagen are often found in close contact with inflammatory cells such as monocytes. Thus, the examination of monocyte and fibroblast behavior in the presence of the extracellular matrix (ECM) is crucial in understanding the host response.

When the human body cannot resolve the injury by itself due to the size and nature of the trauma, infection, pressure on the wound or other factors, the wound becomes chronic. Chronic wounds are characterized by the body's response detained at one or more of the major phases of wound healing described above, often the inflammatory stage [9-11]. An artificial ECM scaffold for chronic, unresolvable wounds on which cells can infiltrate and proliferate, is central in facilitating the wound healing process.

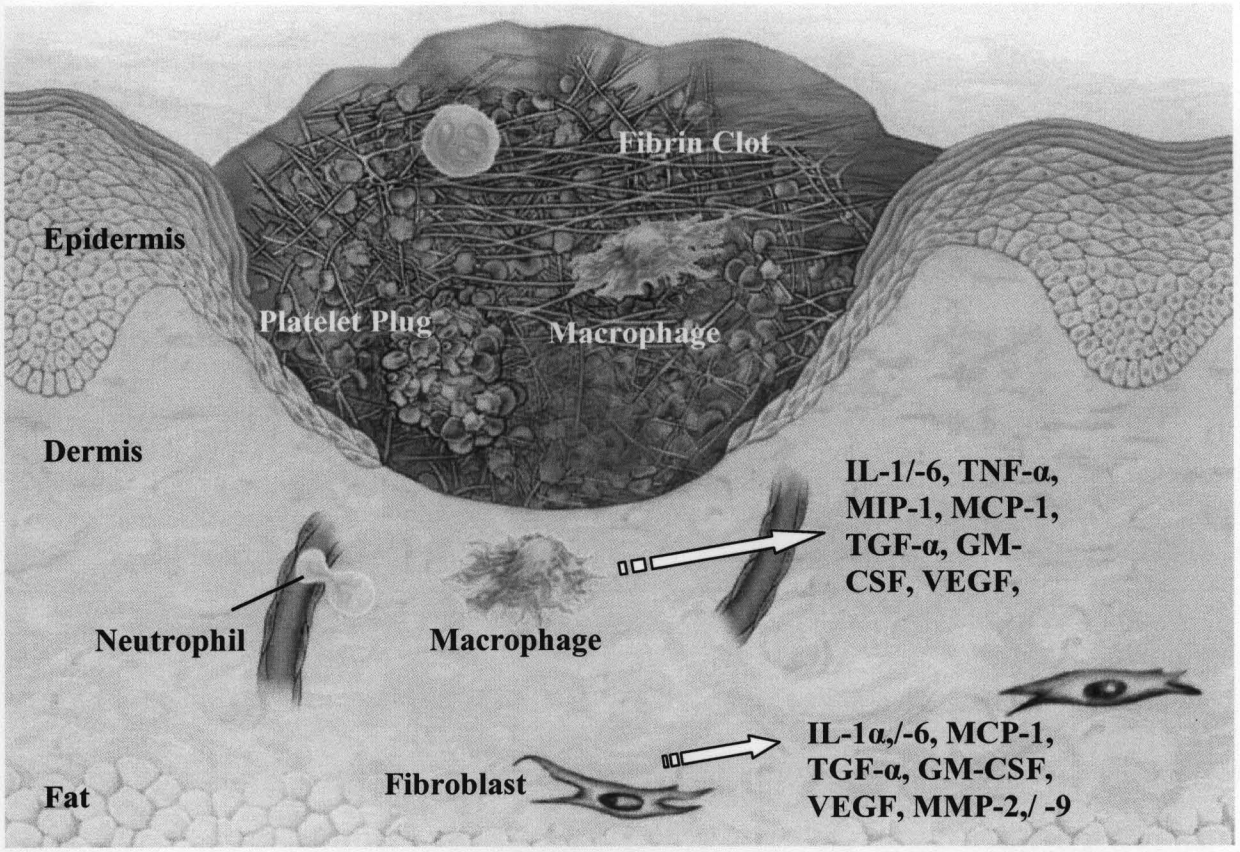

Figure 1-1. Initial injury and inflammatory phase and key wound healing inflammatory proteins and growth factors expressed by macrophages and fibroblasts (adapted from [2]).

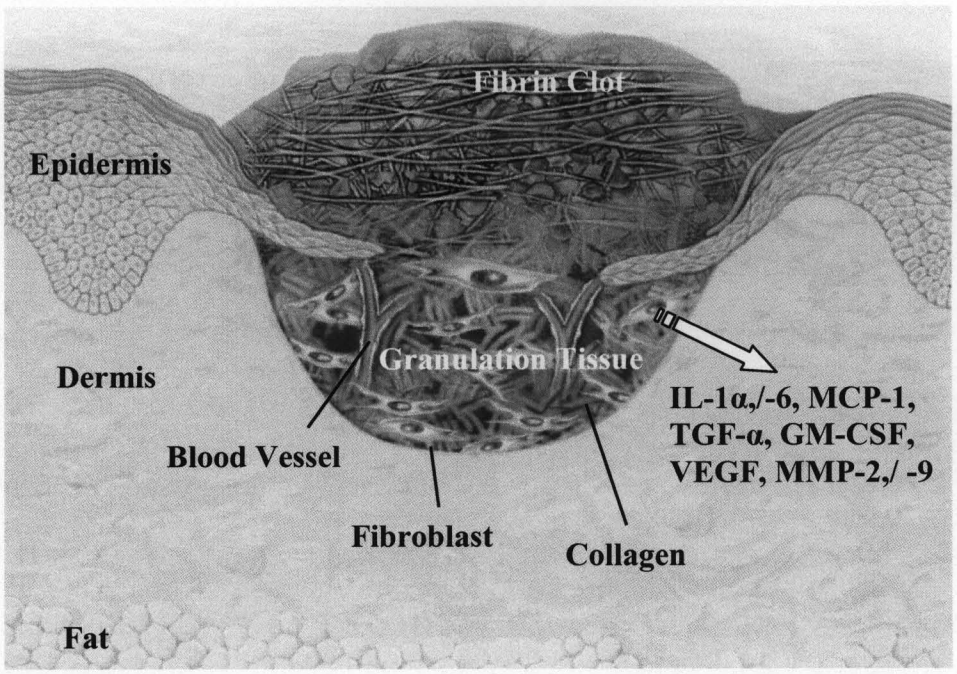

Figure 1-2. Proliferative and matrix remodeling phase and key wound healing proteins and matrix remodeling and growth factors expressed by fibroblasts (adapted from [2]).

1.2 Biomaterials for Wound Healing Therapy

As new biomaterials and the reformulation of existing materials continue to advance, evaluation and intervention of the host response to these materials through extensive material and biological characterization remains imperative. Host response to materials can range from acute inflammation that eventually becomes resolved as the material integrates into the body, to fibrosis and fibrous capsule development to rejection of the material. The shift from passively observing material interaction with the host to actively tailoring and guiding the host response at the implant-tissue interface has been steady, but with our currently limited mechanistic understanding of the host-material interaction, actively guiding the material's biocompatibility remains a critical challenge. Thus, a more thorough understanding of both the host response and the physicochemical properties of biomaterials will ultimately lead to controlled biocompatibility with desired wound healing therapies.

1.2.1 Host Response to Biomaterials: Process and Progression

Host response to materials remains a developing area of study and is a highly complex process comprised of finely orchestrated cascade of overlapping and interrelated events. Upon injury, including the introduction of a biomaterial to the host, the body begins a wound healing response to the foreign entity [12]. Wound healing is divided into three major phases: inflammation, tissue formation, and remodeling. When there are biomaterials involved, the progression of wound healing is modified to compensate for the persistent presence of the material in the host [13]. Thus, the progression of wound healing response in the presence of a biomaterial can be divided into the following phases: injury, blood-material interactions,

provisional matrix formation, acute inflammation, chronic inflammation, granulation tissue, foreign-body reaction, and fibrous encapsulment.

Figure 1-3 highlights the cascade of host response events depending on the presence of the implant. The phases during wound healing without implant versus with implant materials do not completely differ and often overlap. For example, granulation tissue is not a response unique to wounds with implants and can occur during normal tissue healing without implant.

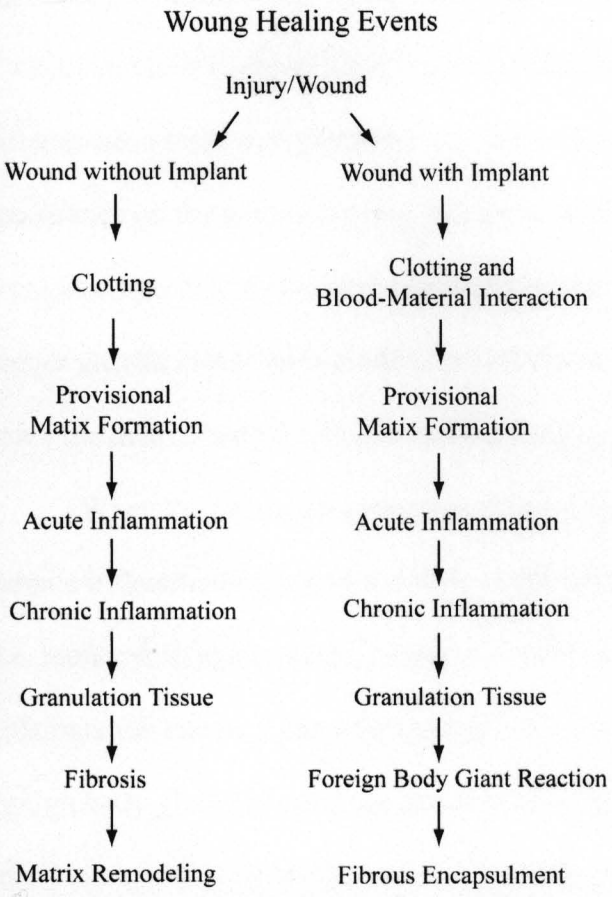

Figure 1-3. Wound healing process with and without implant in the host. In the presence of an implant, the cascade of events that occur include the foreign body giant reaction in the host's attempt to wall off the foreign material.

Host interaction with biomaterials begins with the Vroman effect, where blood protein adsorption on the biomaterial surface starts the development of the provisional matrix [14-16]. With the highly dynamic protein adsorption on the material surface begins the host's coagulation and inflammation events. Clotting and blood-material interaction involve the formation of bulk fibrin around the injured site and the implant while inflammation brings the recruitment of cells including platelets, leukocytes such as neutrophils and other white blood cells [17].

Inflammatory response to material serves as a normal event to wall off and locally contain the material at the injury site. In acute inflammation, neutrophils and monocytes that enter the wound site as a part of exudation and begin to degrade the material and release a myriad of proteases, cytokines and oxygen-derived free radicals. However, depending on the physical and chemical properties of the material, the acute inflammatory phase may be prolonged (i.e. beyond 1 week) and lead to chronic inflammation [18]. If wound healing proceeds normally, acute inflammation leads into granulation tissue, a phase that is marked by a soft, pink, granular appearance on the wound healing surface as well as signs of neovascularization [12]. The lysosomal agents and chemical mediators produced during acute inflammation activate and trigger growth factor upregulation by endothelial cells and fibroblasts, and these cells also lay down the matrix bed of collagen and proteoglycans to resolve the tissue repair process [2].

When the persistent presence of the biomaterial in the host and the incompatibility lead to chronic inflammation however, much of the cells recruited during the acute inflammatory phase (i.e. monocytes, macrophage, lymphocytes) remain and a foreign body reaction ensues. Chronic inflammation can be a part of a foreign body reaction, which is characterized by the presence of foreign body giant cells and the encapsulation of the foreign object at the local implant site in the host's attempt to wall off the material [12]. Macrophages attempt to phagocytose the material and the material is too large to be phagocytosed, they undergo "frustrated phagocytosis" and macrophages fuse to form foreign body giant cells, an indicator of a foreign body reaction. When foreign body reaction leads to fibrous encapsulation, densely packed avascular collagen around the material forms to locally contain the foreign body from the rest of the host. Host tolerance of the material will result in matrix remodeling progresses as fibroblasts and endothelial cells that infiltrate the site produce extracellular matrix (ECM) components such as collagen, fibronectin

and hyaluronic acid and form the new ECM, scar tissue. While the matrix bed is laid down, matrix degrading agents such as matrix metalloproteases and collagenases help rearrange and organize a structured ECM.

The host response is a delicately orchestrated complex process that is often determined by the chemistry of the material's surface. Controlling each host response event and achieving complete restoration of normal tissue structure and function is a difficult task given our currently limited mechanistic understanding of host response. However, rather than a relatively passive approach of implanting a material and observing the host response, an active approach of tailoring host response through the presentation of biofunctional peptides may prove to be one significant stride toward avoiding host rejection of the material.

1.2.2 *In vitro* response to biomaterials

In vitro assays allow the assessment of material cytotoxicity on cells and are invaluable in screening biomaterials to gain insight into material degradation, mechanical strength over time and whether the materials leech toxic substances that affect the viability of cells. Three major assays for testing material biocompatibility and toxicity *in vitro* include agar diffusion, extraction, and direct cell-biomaterial contact method. Material toxicity can be investigated through the agar diffusion method by covering a confluent layer of cells with agar containing a viability stain, then placing the biomaterial on the agar surface and examining the extent of the viable cells under and around the material after an incubation period. Thus agar diffusion assays are useful in evaluating material toxicity, and the method is often applied to highly dense materials [19,20]. Extraction studies (i.e., elution, extract dilution) are also employed to observe any linear relationship between cell cytotoxicity and the concentration of extracted biomaterial.

The threshold concentration of material extract on minimal and maximal cytotoxicity can be investigated with a confluent layer of cells being exposed to serially diluted material extract and assessing cell viability after the incubation period. Usually, the cells in the targeted implant area are candidates for the extract dilution test and how much of the material extract is absorbed by these cells can also be determined [21].

Direct contact is the most widely applied test in cell-material *in vitro* analysis, and it involves placing the material directly on top of a confluent layer of cells or directly placing cells on top of the material. After incubation, cells are microscopically evaluated for toxicity (through viability staining), adherent density and morphology. Direct cell-material contact studies are the most prevalent in testing material biocompatibility and can reveal the intermediate zone of damaged cells. Especially when testing for cell response to peptide conjugated materials, the assessment of the cells direct interaction with the peptide presented on the material surface is imperative. Cell adhesion and spreading as modulated by various peptides are central to the study of biologically responsive peptide conjugated materials. Since its discovery by Pierschbacher and Ruoslahti in 1984, the arginine-glycine-aspartic acid (RGD) sequence has been the most effective peptide sequence for enhanced integrin-mediated cell adhesion and has been applied to a myriad of materials and assessed for enhanced cell adhesion and wound repair [22]. The tripeptide sequence has been shown to enhance osteoblast adhesion *in vivo* and a myriad of cells *in vitro*, including osteoblasts, chondrocytes, human umbilical vein endothelial cells, fibroblasts and monocytes [23-31]. Table 1 shows increased monocyte adherent cell density on RGD-PEG grafted on a semi-interpenetrating network (sIPN) of gelatin and PEGdiacrylate (PEGdA) compared to that on sIPNs grafted with control ligands triglycine (GGG) or a methoxy group [31].

Table 1-1. Adherent monocyte density on RGD-PEG grafted sIPN and control ligand-PEG grafted sIPN (adapted from [31]).

	Adherent Monocyte Density (cells/mm^2)			
Ligand-PEG grafted onto gelatin of sIPN	**Culture Time: 2 h**	**24 h**	**96 h**	**168 h**
GGG	328 ± 69	444 ± 16	207 ± 52	74 ± 40
Methoxy	145 ± 18	233 ± 14	106 ± 2	95 ± 12
RGD	1321 ± 74*	1071 ± 190	350 ± 42*	157 ± 8

* Significantly higher than all other ligand-PEG grafted sIPN ($p<0.001$)

Direct cell-biomaterial *in vitro* testing and high throughput assays have been coupled in current studies to screen biomaterials more rapidly while testing for cell adhesion and material influence on cell morphology and proliferation. Figure 1-4 below outlines a study by Mochizuki and others where twelve biologically active peptides derived from ECM components were conjugated to chitosan membranes and microscopically observed using a 96 well plate as a high throughput system [32]. Table 1-2 describes two of the peptides used and Figure 1-4 shows cell response to the peptide-grafted chitosan membranes.

Table 1-2. Synthetic peptides derived from ECM components and biological activities of peptide-chitosan membranes (adapted from [32]).

Peptide	**Sequence**	**Protein Source (Residues)**	**Fibroblast Attachment**	**Neurite Outgrowth**
531	GEFYFDLRLKGDKY	Human collagen alpha1, type IV	++	-
AG73	RKRLQVQLSIRT	Murine laminin alpha1 chain	++	+

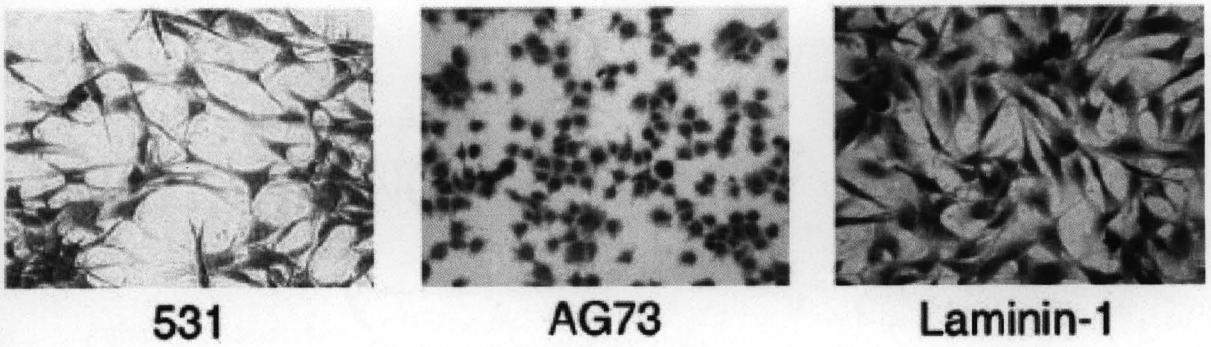

Figure 1-4. Human foreskin fibroblasts adhered to chitosan membranes conjugated with different bioadhesive peptide sequences. 531 conjugated chitosan membranes and laminin support cell adhesion and spreading while AG73 supports cell adhesion but not spreading. Cells are stained with crystal violet [32].

Though *in vitro* studies offer the advantage of providing information on a specific cell type response to the biomaterial, *in vitro* work has the limitation of being too simple of a system compared to the highly complex and dynamic *in vivo* system with all the physiologically relevant players present interacting with the material of interest. Recent direct cell-biomaterial contact studies have been developed to accommodate higher complexity and closer physiological relevance, such as the addition of a cell type to create a co-culture environment. In a work by Chung and Kao, monocyte interaction with an RGD-PEG conjugated hydrogel was examined in the presence of a confluent layer of fibroblasts [33]. Figure 1-5 below shows the co-culture schematic where monocyte response to the RGD presenting sIPN as perturbed by fibroblasts could be evaluated and key wound healing proteins could be profiled over time.

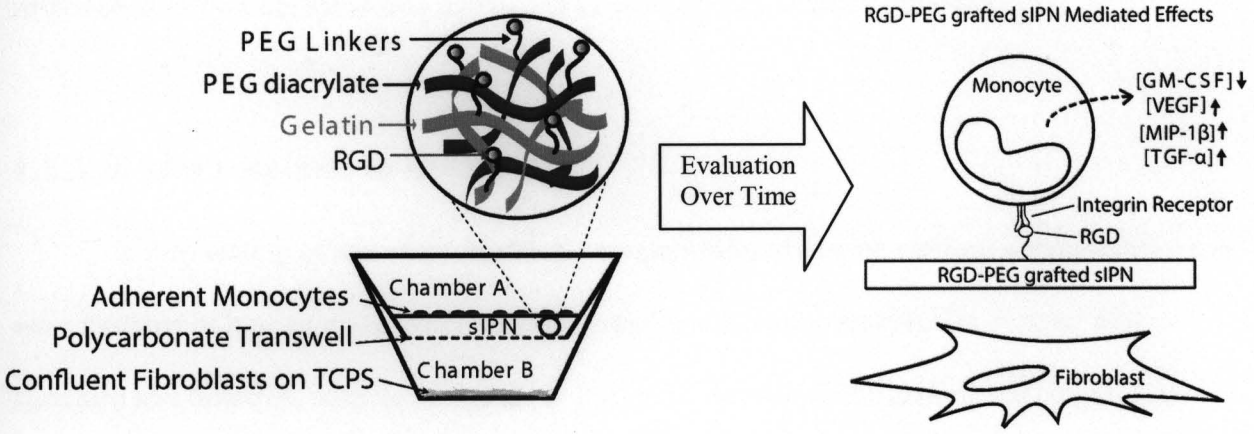

Figure 1-5. A schematic of a co-culture of monocytes and fibroblasts with RGD-PEG grafted sIPN wound healing scaffold. Monocyte response to the RGD presenting sIPN and the communication between monocytes and fibroblasts in the presence of the RGD presenting sIPN scaffold were evaluated. Key wound healing factor expression in response to RGD-PEG grafted sIPN over time in the presence of fibroblasts could be evaluated [33].

The co-culture setting allowed the evaluation of cell-material interaction in an environment closer to physiological conditions as well as the assessment of the biomaterial as a communicative barrier between two key wound healing cell types. Key wound healing factors including vascular endothelial growth factor (VEGF), monocyte inflammatory protein-1beta (MIP-1β), and tumor growth factor-alpha (TGF-α) were upregulated in a ligand specific response to RGD-PEG grafted sIPN in the presence of fibroblasts while granulocyte-macrophage colony-stimulating factor (GM-CSF) was downregulated. Other approaches to making the *in vitro* system more advanced have included the addition of dynamic components such as flow of media and nutrients on the system and making the cell culture 3D [34]. Although this type of work adds

to the already challenging task of parsing out specific causal effects and the source of each response, it allows the system to more closely mimicking the tissue environment.

1.2.3 *In vivo* response to biomaterials

In vivo testing of materials for tissue compatibility offers the obvious advantage over *in vitro* systems of having all the appropriate physiological components (cells, matrix, tissue structure and function, soluble proteins, etc.) present. *In vivo* investigations are intended to simulate end-use applications and thus the direct application of the biomaterial is used to assess biocompatibility in the clinical use setting. Where the assessment can vary is the duration, frequency, and the location of exposure, as well as the physicochemical stability and compatibility of the biomaterial itself. *In vivo* tests can reveal critical information on the biomaterial's compatibility at the tissue site, as well as on the function and the stability of the material in the host. *In vivo* analyses can reveal much information on host response including blood material interactions, matrix formation, inflammation, fibrous encapsulment and the other events as outlined in Figure 1-3. In addition, *in vivo* assays can also yield information on local and system toxicity, genotoxicity and local and systemic immune response.

In the case of biomaterial implantation, histological examination of the implant site after a given duration has remained a widely applied evaluation of host tissue response. The presence and the abundance of certain cell types at the tissue-implant interface are examined for tissue compatibility by immunohistochemical staining or immunofluorescent labeling the histological sections. For example, polymorphonuclear leukocytes at the implant site indicate acute inflammation, the presence of mononuclear cells such as plasma cells and lymphocytes indicates chronic inflammation, lymphocytes and monocytes in high numbers suggesting possible

infection. Other indications of pathology include the examination of granulation tissue with key markers such as infiltrating fibroblasts, soft granular appearance of the healing site as well as collagen deposition and small capillary development. Foreign body giant cells and fibrous capsule of densely packed collagen indicate foreign body reaction and fibrous encapsulment, respectively. Figure 1-6 highlights key wound healing events in a dermal wound repair of a full thickness wound treated with a collagen implant in a mouse model [35]. Reepithelization and the newly formed epidermis along with granular tissue that mark the late stages of wound repair are shown along with the resorbed collagen implant. Thus, the biocompatibility of the material at the tissue level and the incorporation of the implant material and the host tolerance of the material can be gauged by histology.

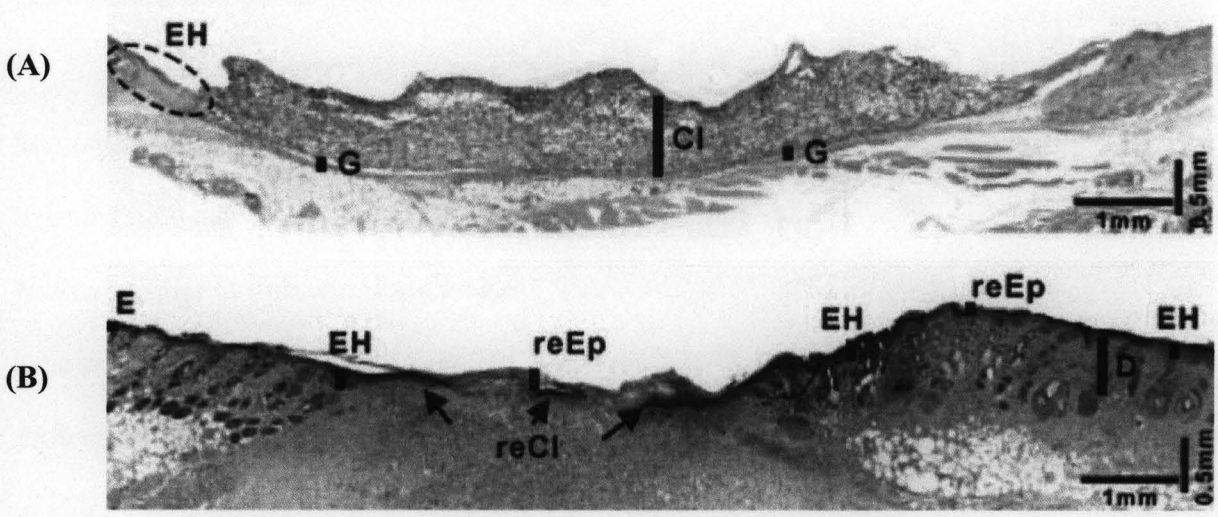

Figure 1-6. Wound healing assessments at day 3 (A) and at day 14 (B) post collagen implantation. reEp: early re-Reepithelization; E: epidermis; D: dermis; EH; epidermal hyperplasia (new grown epidermis); reCI: resorption of collagen implant; G: granular tissue [35].

In addition to histological evaluations, host response is also analyzed by the use of various biomarkers. Tissue homogenate and exudates are often collected and analyzed for biomarkers including inflammatory biomarker proteins such as interleukins and tumor necrosis factors and matrix remodeling matrix metalloproteases often screened at the implant site [36]. Biomarkers can be identified in many ways, western blotting, enzyme linked immunosorbant assay (ELISA) can identify markers at the protein level and currently applications of mass spectroscopy to profile the tissue and analyze host response to biomaterials is rapidly developing [37]. Consistent with trends in *in vitro* analyses, high throughput approaches are becoming rapidly incorporated into *in vivo* analyses. Thus, protein microarray chips and multiplexed cytokine assays can be employed to analyze tissue homogenate or wound exudates to provide reproducible and global protein analysis rapidly.

Genetic analysis of the tissue site can be carried out by northern blot analysis of the tissue homogenate or wound exudates, similar to western blot analysis for proteins. In situ hybridization can be applied to the tissue section to localize DNA or RNA of interest with probes, similar to immunohistochemistry that localizes proteins. Reverse transcriptase or real time polymerase chain reaction (RT-PCR and qRT-PCR, respectively) and ribonuclease protection assays can analyze mRNA at the tissue site. However, both northern blot analysis and in situ hybridization require a larger amount of sample and polymerase chain reactions are time consuming and cannot target many genes per assay. Analysis of tissue lysate or exudates employing cDNA microarrays can also provide a global gene expression at the wound site and can uncover cell signaling and transcription genes critical to wound healing that were not targeted with the other assays [38].

The protein and genetic analysis of tissue homogenates or exudates described above can be coupled within *in vivo* analyses, as well as with *in vitro* analyses. For example, analysis of inflammatory interleukins can be analyzed *in vitro* by investigating the protein levels through ELISA or western blot and the genetic interleukin expression by PCR. *In vivo*, ELISA or western blot can also be applied to analyze the tissue homogenate or exudates to observe interleukin protein levels, and PCR or ribonuclease protection assay can reveal genetic interleukin regulation *in vivo*. Microarrays can also be useful in coupling *in vitro* and *in vivo* host response analyses.

1.2.4 Enhancing biological response: host interaction with peptide-polymer conjugates

Peptide sequences can enhance adhesion and elicit specific intracellular signaling events upon peptide-cell interaction [39,40]. Due to their relatively robust stability compared to the whole protein and their ability to direct specific downstream effects upon interaction with the cell, peptide conjugated materials are emerging as a new class of materials that combine unique advantages from both the natural and synthetic world to yield a material with unique biological properties compared to conventional therapies.

Peptides have been conjugated to natural and synthetic polymers for tissue repair applications [39, 41]. Directing the host response by presenting biofunctional peptides on the material surface is one approach to improving host biocompatibility while simultaneously taking advantage of the mechanical and structural properties of the natural or synthetic polymer scaffold. Natural polymers possess highly ordered and complex quaternary structures that have excellent aqueous solubility, *in vivo* compatibility and controlled degradation, and break down into natural amino acids that can be metabolized in the host with minimal immune response and

cytotoxicity [42,43] Thus, peptide conjugated natural polymers can offer a complex yet highly biocompatible platform that also has biofunctional sequences to direct cell response and tissue function. Peptides can also be grafted onto synthetic polymers and though they cannot provide the level of complexity that natural polymers can, synthetic polymers offer better availability, stability, chemical control and innertness in the host. Synthetic polymers are readily available at often lower cost than natural polymers and offer practicality as well as control over the physicochemical properties including chain length, functional groups, degree of crosslinking, chain architecture, and subsequently the elasticity, tensile strength and rheological properties and others. In addition, polymers such as polyethylene glycol have been established as a nonfouling polymer that resists nonspecific protein adsorption, and polymers such as polydimethoxysilane do not support bacterial growth [44]. Depending on the targeted tissue, the polymer can be tailored to provide the structural template close to the tissue site, and by conjugating critically active portions of the naturally derived material to synthetic polymers, specific signaling from the natural material and the inertness of the synthetic material can be combined to yield a controlled biomaterial with predictable and desired host response.

1.3 Peptide-Polymer Conjugate Systems: Synthesis and Interaction with the Host

1.3.1 Overview: Conjugation Chemistry

The most common method used to conjugate bioactive peptides to polymers is with thiol or succinimide ester groups to create a covalent amide bond. This linkage is created by the activation of a carboxylic group on the material to react with the peptide's amine-terminus. Carboxylic acids can be activated by carbodiimide peptide coupling reagents, most commonly

dicyclohexylcarbodiimide (DCC) or diisopropylcarbodiimide (DIC), and sometimes ethyl-(N', N'-dimethylamino)propylcarbodiimide hydrochloride (EDC). Outlined in Figure 1-7 is a reaction scheme demonstrating the conjugation of peptides onto polyethylene glycol by activating the carboxy groups with DCC, then conjugating N-hydroxysuccinimide (NH-Su) to ultimately serve as a leaving group for peptide conjugation [45]. More examples of these chemistries will be highlighted in the case studies to follow.

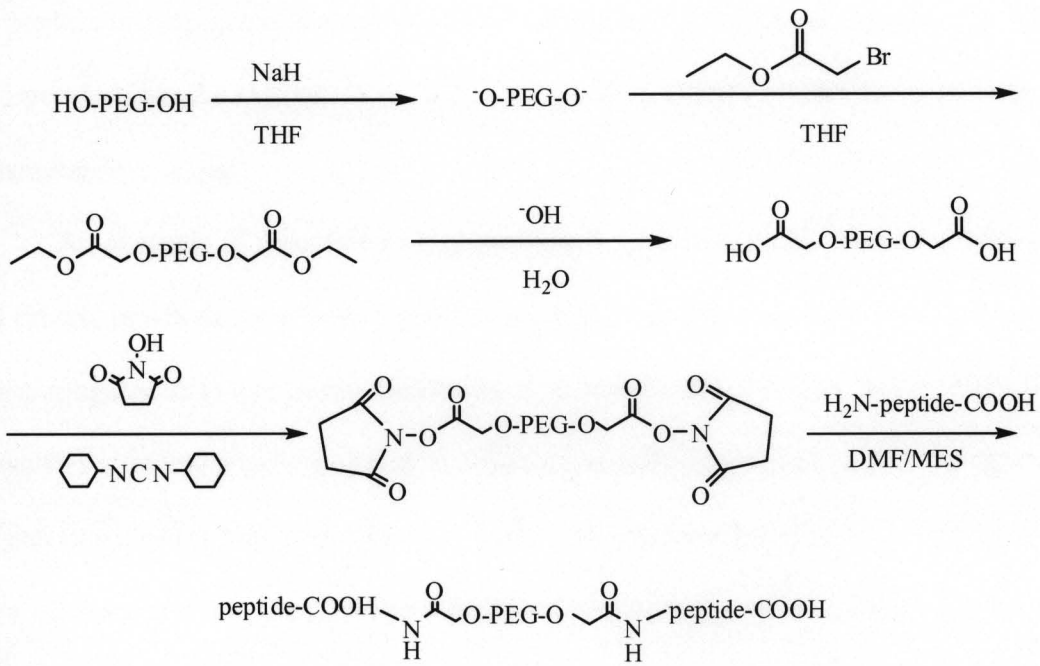

Figure 1-7. Schematic of peptide conjugation onto polyethylene glycol by first activating the carboxy group with DCC and using N-hydroxysuccinimide as a leaving group adapted from [45].

1.3.2 Peptide Conjugated Natural Polymers

The ideal treatment for wounds is the application of natural tissue. However, as tissue sources are limited, components of the natural tissue can be used to substitute as a tissue repair scaffold to achieve maximal biocompatibility. Natural polymers include many of the ECM

proteins such as collagen, fibronectin, laminin, chitosan, hyaluronic acid, and others. These polymers can provide multiple functions, for example, collagen provides structural function, but also contains biofunctional peptide sequences that have been demonstrated to enhance the stability and differentiation of encapsulated cells [46-48]. By conjugating bioactive peptide sequences onto these ECM-derived scaffolds, ligand-specific activity and signaling can be achieved to enhance cell attachment and support cell proliferation. As the scaffold onto which the peptide is conjugated is a naturally derived material, the biomaterial platform will be better incorporated into the injured tissue and subsequently cleared from the body in a non-inflammatory manner.

An example of a peptide conjugated natural polymer is exhibited in a work by Masuko and others, in which the adhesive peptide sequence Arg-Gly-Asp-Ser-Gly-Gly-Cys (RGDSGGC) was conjugated onto a chitosan membrane with reactive thiol groups incorporated [49]. RGD, an adhesive sequence, was conjugated to chitosan, as chitosan has shown to be promising polysaccharides for biocompatible and wound healing materials [50-53]. Reactive thiol groups were incorporated into the chitosan membrane by reacting it with 2-iminothiolane, as it has been demonstrated that the 2-iminothiolane undergoes a ring opening reaction with primary amines, including N-terminal α-and ε-amino groups of peptides or proteins (Figure 1-8) [54].

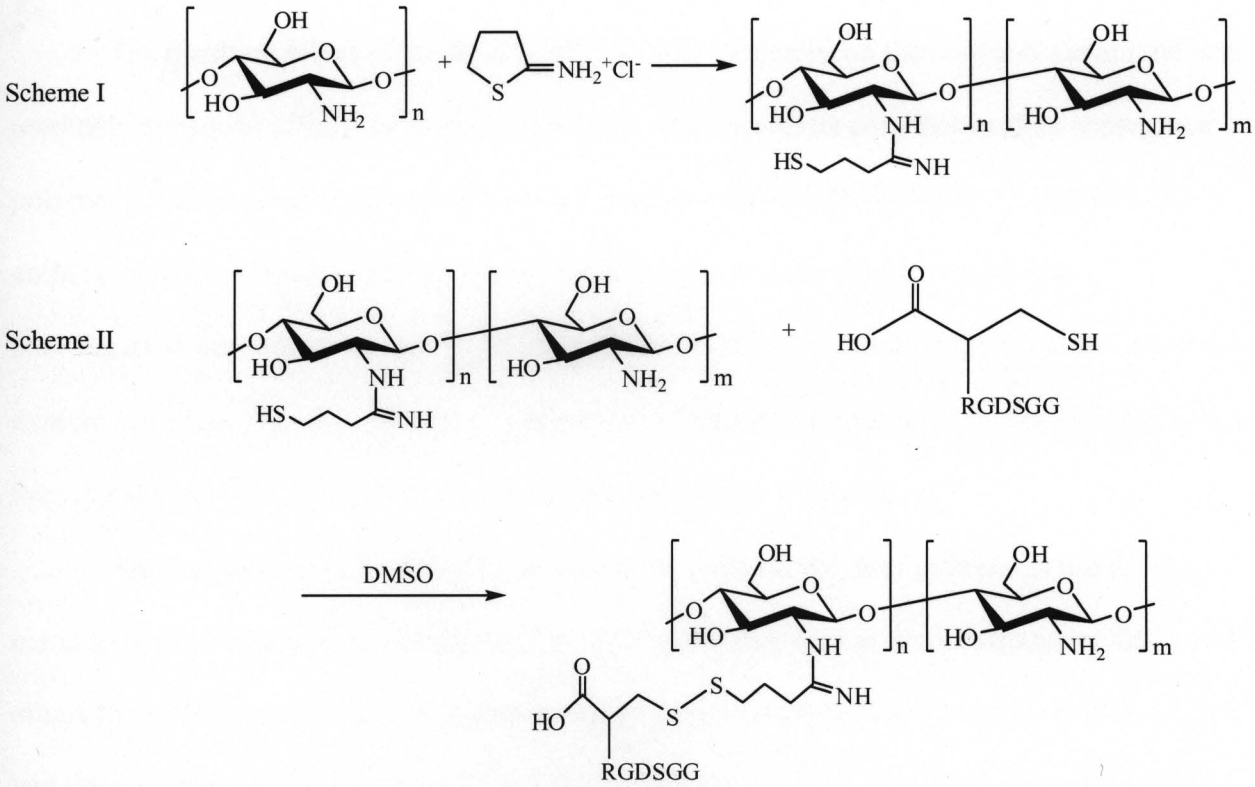

Figure 1-8. Scheme I outlines incorporation of a thiol group through a ring opening reaction of 2-iminothiolane with chitosan and scheme II shows the coupling reaction of SH-chitosan with RGDSGGC (adapted from [49]).

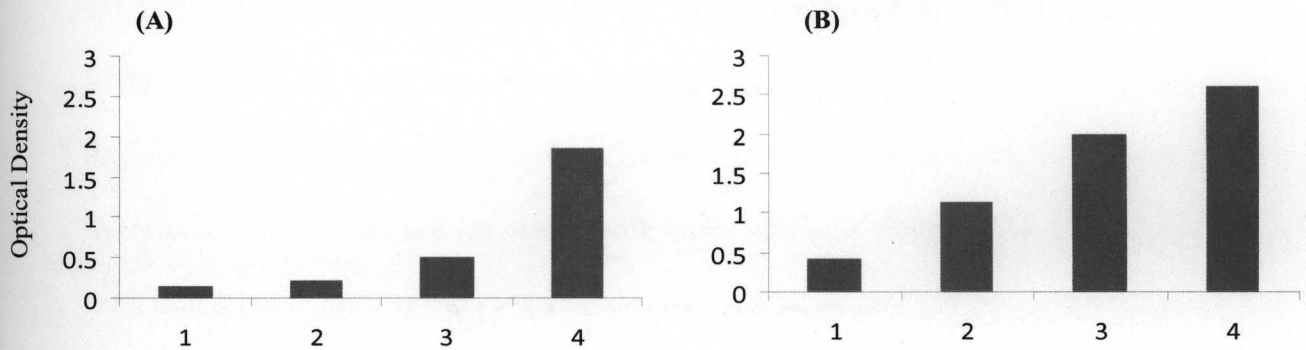

Figure 1-9. Adhesivity of (A) chondrocytes and (B) fibroblasts: (1) Control (2) 0.0012% RGDSGGC-chitosan (3) 0.012% RGDSGGC-chitosan (4) 0.12% RGDSGGC-chitosan (adapted from [49]).

The resulting effect of the RGDSGGC peptide presented on the chitosan membrane was markedly enhanced affinity of both chondrocytes and fibroblasts onto this peptide conjugated polymer scaffold when compared to that on a plate coated with RGDSGGC. In addition, the authors showed enhanced affinity of both chondrocytes and fibroblasts in a peptide-concentration dependent manner. With increased RGDSGGC-chitosan concentration coated onto a microtiter plate, chondrocyte and fibroblast cell adhesivity, as measured by optical density of the crystal violet dye, was proportionally increased (Figure 1-9A,B).

Another example of a peptide conjugated to a natural polymer material is the RGD containing peptide sequence covalently linked to hyaluronic acid as demonstrated by Glass and others [55]. Hyaluronic acid, a non-immunogenic polysaccharide found in many human tissues and upregulated during wound repair and naturally cleared by the host, has been extensively studied and applied. Though hyaluronic acid modifications with synthetic polymers have been commonly reported, studies on peptide conjugation on the polysaccharide are to date elusive. Hyaluronic acid crosslinked with a diepoxide is reacted with periodate to create reactive aldehydes by peroxidate oxidation of the polyhydroxyls of glucuronic acid (Figure 1-10A). A RGD containing 18 amino acid peptide sequence, Gly-Arg-Arg-Arg-Arg-Arg-Gly-Gly-Gly-Arg-Gly-Asp-Ser-Pro-Ala-Ser-Ser-Lys (GR_5G_3RGDSPASSK, or WH18), was then conjugated to hyaluronic acid through sodium cyanoborohydride reduction. Primary amines of the peptide sequence serve as nucleophiles to form secondary amine bonds, which are reduced by sodium cyanoborohyride, creating a more stable primary amine, and covalently linking the peptide to the carbonyl chains on hyaluronic acid (Figure 1-10B). The WH18 peptide sequence, while designed to present the RGD sequence recognized by the integrin receptors, was also designed with the D-

isomer or arginine to protect it against a number of serine proteases known to be present in wounds.

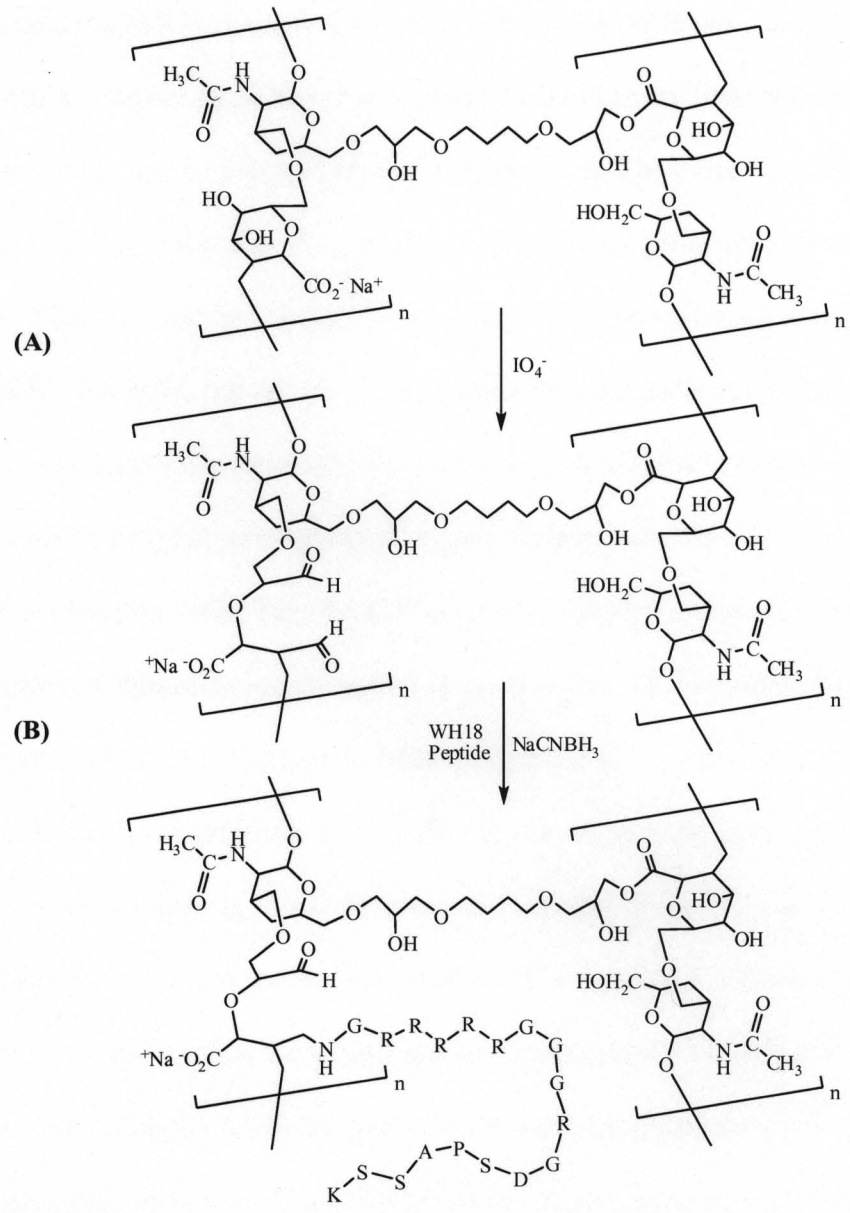

Figure 1-10. Reaction of (A) diepoxide crosslinked hyaluronic acid with periodate to oxidize the polyhydroxyls of the glucuronic acid to create reactive aldehydes and of (B) activated aldehydes of the hyaluronic acid with the peptide sequence, followed by a reduction with sodium cyanoborohydride to form a stable amine on the conjugation site [55].

The conjugation of the RGD containing WH18 peptide sequence onto hyaluronic acid resulted in a 90% or greater attachment and subsequently supported spreading of human osteosarcoma cells (MG63). On surfaces that were treated with periodate in the absence of peptide, or that were not treated with periodate resulted in very little attachment of the osteosarcoma cells and no cell spreading on the material. They also described enhanced attachment of human colon fibroblasts, primary bovine epithelial cells and human gingival fibroblasts. Thus, by conjugating an adhesive peptide sequence onto a naturally occurring polysaccharide material, cell adhesion and proliferation could be supported.

In a simultaneously reported study, the $GR_5G_3RGDSPASSK$ conjugated hyaluronic acid matrix was tested for healing response of second-degree burn wounds in pigs. The RGD-hyaluronic acid matrix (with Tegaderm™ as outer secondary dressing) showed significantly increased rates of epithelization compared to air exposed control and the hyaluronic acid vehicle alone after one week [56]. Along with enhanced epithelization, the RGD-hyaluronic acid matrix showed marked cellular infiltrate compared to the air exposed control and the hyaluronic acid without peptide conjugation. In addition, increased granulation tissue was also observed with RGD-hyaluronic acid treated burns compared to the air exposed control. Hyaluronic acid has been tested in several models for wound healing applications, but with varying results. With the RGD-hyaluronic acid matrix, Glass and others demonstrated enhanced osteosarcoma cell adhesion and proliferation *in vitro* while Mertz and others showed significantly improved epithelization rate, cellular infiltration and granulation of tissue, complex processes that lead to the total repair of second degree burns *in vivo*.

1.3.3 Peptide Conjugated Synthetic Polymers

Synthetic polymers can also offer biochemical inertness in the body, and offer other advantages over natural polymers, including precise control over the physicochemical properties of readily available materials. Polymers can also better withstand processing events such as autoclaving, dry heating, gamma-radiation, alcohol washes, and electron beam treatments compared to the natural polymer, which can denature more readily with its protein based structure. Thus, synthetic polymers offer a practical alternative to naturally derived polymers and are widely applied in biomedical devices and implants. However, though they offer advantages in terms of mechanical plasticity and lower cost, they are not engineered for specificity and biorecognition. Thus, peptide conjugated polymers steadily increased in development to provide a well controlled and practical tissue repair platform with chemical innertness as well as peptide signals to direct cell events and promote wound repair.

Polymers can offer a practical and chemically and mechanically controllable option for biomedical applications, and polymers such as poly(dimethylsiloxane) (PDMS) have been widely used in the clinical setting, including surgical implants and catheters [57,58]. PDMS elastomers, with good compatibility with the human tissue and biological innertness, and excellent elasticity and transparency, are widely applied as surgical implants and catheters. However, though they are biocompatible and resist bacterial growth, these silicone elastomers do not support cell adhesion, a critical process in wound healing. Thus, Li and others attempted to merge the excellent elasticity of the material with cell adhesion promoting properties by conjugating the bioadhesive peptide sequence RGD peptide onto the PDMS [59]. The conjugation of RGD onto PDMS was carried out through a succinimide based chemistry, using sulfosuccinimidyl 6-(4'-azido-2'-nitro-phenylamino) hexanoate (sulfo-SANPAH) (Figure 1-11).

Unique to this photochemical, succinimide based conjugation of peptides onto a polymer surface is that it is similarly convenient to peptide coating or adsorption approaches, but distinct in that the ultimate peptide conjugation is achieved through a covalent amide bond. Figure 1-11 outlines the two step photochemical based conjugation of the RGD peptide onto the PDMS surface.

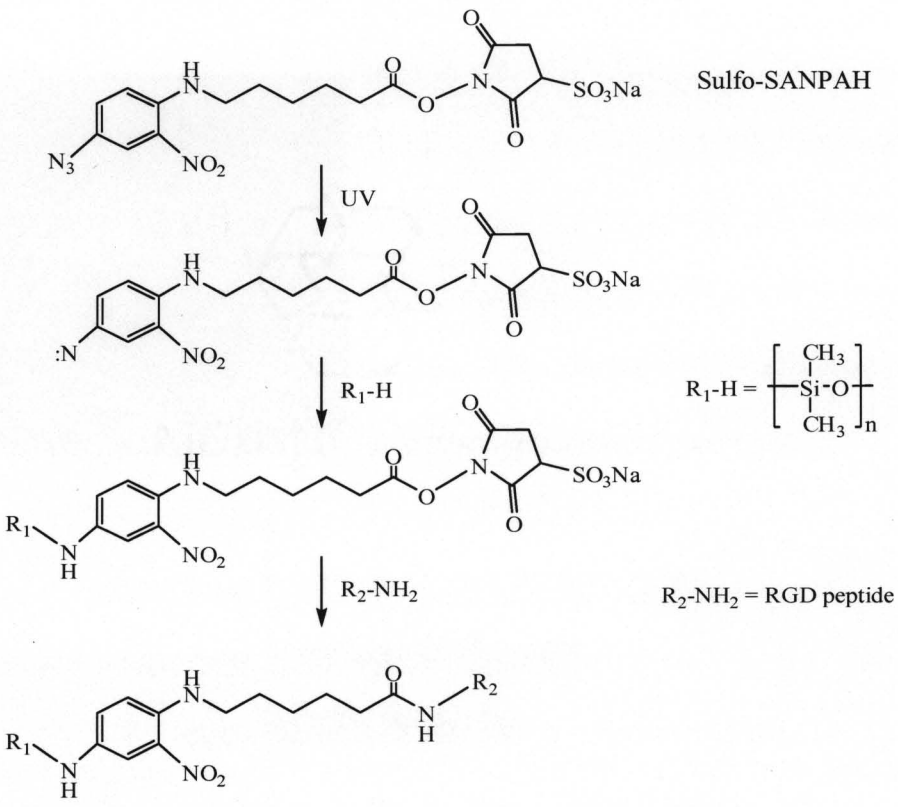

Figure 1-11. A two step succinimide based process for conjugating RGD peptide onto PDMS surfaces [59].

The RGD conjugated PDMS surfaces promoted adhesion, proliferation, and collagen secretion of human skin fibroblasts (HSFs). While few cells attached onto the PDMS surface, RGD-peptide conjugation on to the PDMS surface resulted in an enhanced adhesion and rapid proliferation of HSFs. RGD conjugated surfaces yielded a well spread and elongated fibroblasts

that showed increased formation of actin microfilament bundles and focal adhesions, indicating strong cell-substrate interaction (Figure 1-12). Furthermore, the RGD conjugated PDMS surface promoted fibroblast collagen production when compared with that produced on sulfo-SANPAH activated PDMS surfaces and TCPS (Figure 1-13).

Figure 1-12. Fluorescence microscopy images of HSFs cultured on a RGD-conjugated PDMS substrate. The cells contain bundles of stress fibers (solid arrows), and their focal adhesions are also clearly seen (blank arrows). The cells were fixed and stained after 2 days in culture; Scale bar, 20 μm [59].

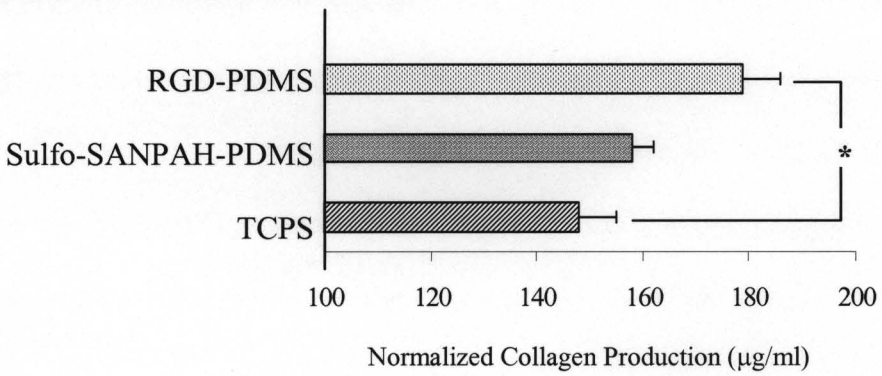

Figure 1-13. Total soluble collagen production by human skin fibroblasts cultured on RGD-conjugated PDMS, sulfo-SANPAH activated PDMS surface (without RGD conjugation) and TCPS. Collagen concentrations are normalized to cell number *p<0.01 (adapted from [59]).

Literature on the *in vivo* biocompatibility and immune response to peptide conjugated synthetic polymer substrates is curiously elusive. However, an example of an *in vivo* response to a ligand conjugated to polyethylene glycol (PEG) tethered onto a gelatin and polyethylene glycol diacrylate (PEGdA) hybrid material demonstrates host response. PEG, which is a widely applied polymer that has been established in biocompatibility, is not only commonly found in biomedical devices and materials, but is also found in food, cosmetics and drugs [60]. In a work by Waldeck and others, a wound healing scaffold composed of polyethylene glycol diacrylate (PEGdA) and gelatin semi-interpenetrating network (sIPN) was constructed to present the RGD peptide on a PEG linker [61]. Gelatin, a denatured form of collagen, has been widely accepted as biocompatible and often found in food products and applied in bridging nerves and nerve tissue engineering [62,63]. The chemistry was carried out similar to the succinimide based chemistry shown in Figure 1-7, except with one functional group of the polyethylene glycol used for the RGD peptide conjugation and the remaining functional group used to covalently link the RGD-PEG onto the lysyl group of the gelatin backbone to yield RGD-PEG grafted gelatin (Figure 1-14). When the RGD-PEG grafted gelatin was polymerized with PEGdA, the resulting hybrid sIPN presented the RGD peptide on the matrix surface on a PEG tether.

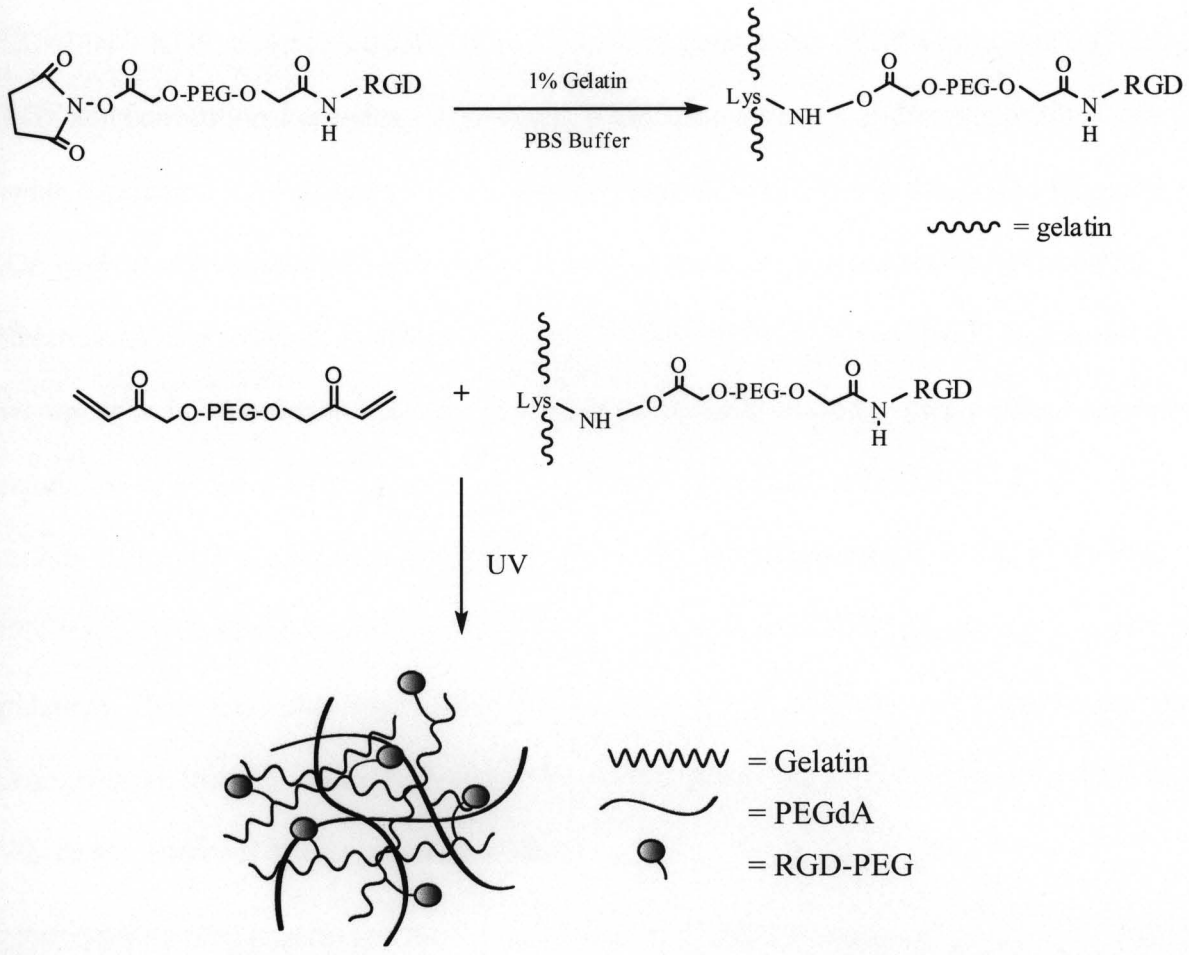

Figure 1-14. Chemical schematic of the RGD-PEG grafted gelatin and PEGdA interpenetrating network scaffold. The RGD peptide is grafted onto a PEG linker via a succinimide based conjugation and the RGD-PEG grafted gelatin is polymerized with PEGdA to create a natural and synthetic polymer hybrid scaffold that presents a biofunctional peptide (adapted from [45]).

The RGD-PEG grafted sIPN with keratinocyte growth factor (KGF) incorporated into the matrix was applied onto a full-thickness wound on a rat model to investigate wound healing response *in vivo* [61]. The resulting *in vivo* analysis revealed enhanced cell recruitment and granulation of tissue along with higher extracellular matrix organization, neovascularization and

rate of contraction was observed (Figure 1-15). Shown in Figure 1-15 are the effects of RGD-PEG sIPN + KGF, unmodified sIPN (i.e., unmodified gelatin and PEGdA only, and no RGD-PEG), and conventional dressing, Silverlon®. While the conventional dressing resulted in a visible depression in the healing wound, both the unmodified sIPN and the RGD-PEG sIPN + KGF supported formation of tissue with no visible depression, demonstrating its structural effectiveness as a scaffold. In addition, the RGD-PEG sIPN + KGF resulted in high levels of macrophages and fibroblasts that were similar to undamaged tissue by three weeks, suggesting granulation of tissue at the later stages of wound healing for RGD-PEG sIPN + KGF treated wounds. The epidermis was restored to a thicker degree with more ridges for the RGD-PEG sIPN + KGF treated wounds as well as a basket-weave patterned ECM developing toward the epidermis. There were also larger occurrences of neovascularization as well as thicker and more dense collagen bundles in the RGD-PEG + KGF treated wounds when compared to unmodified sIPN or conventional dressing treated wounds.

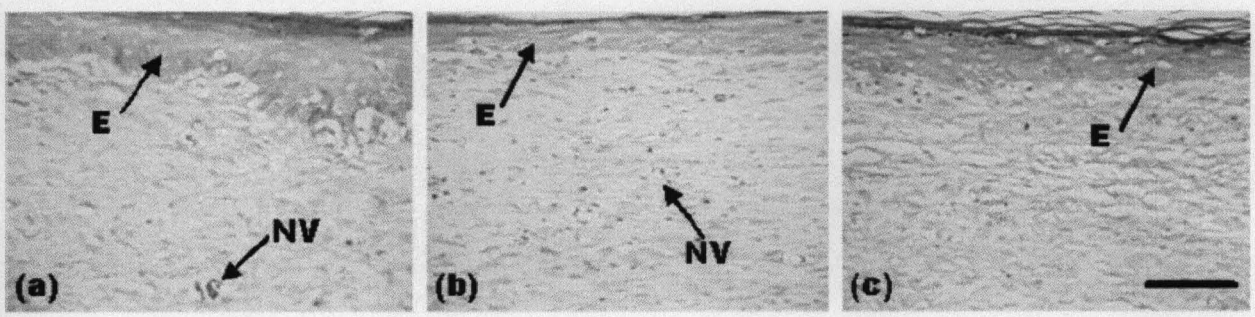

Figure 1-15. Photomicrographs (x20) of (a) RGD modified sIPN + Keratinocyte growth factor interface at 3 weeks. (b) unmodified gelatin sIPN interface area at 3 weeks. (c) conventional dressing interface area at 3 weeks. Areas identified include neovascularization (NV) and epidermis (E) [61].

1.4 Extracellular matrix-derived semi-Interpenetrating Network as Wound Healing Scaffold

We designed a semi-interpenetrating network of bio and synthetic polymers as an ECM building block for tissue repair. The ECM-mimic composed of porcine gelatin, which has been widely accepted as biocompatible and often found in food products, and polyethylene glycol, which is also a known biocompatible product found in food, cosmetics and drugs [62,63]. By tethering the biofunctional peptide RGD, an adhesive peptide sequence through which cells interact and communicate with the ECM, we aimed to attracted monocytes to the wound site. Others have grafted biofunctional peptides to enhance cellular attachment [64,65]. With the sIPN, we aimed to attract monocyte adhesion and interaction with the scaffold and analyze monocytes interaction with and response to the ECM-mimic to ultimately yield directed cytokine and growth factor release after complexation onto the RGD-PEG grafted sIPN.

Thus, the ECM-analog composed of ligand-PEG grafted gelatin and polyethylene glycol diacrylate (PEGdA) was designed as shown in Figure 1-16. Once the lysyl groups of the gelatin strands were grafted with ligand-PEG, the modified gelatin was combined with PEGdA and polymerized with photoinitiator to create a semi-interpenetrating network.

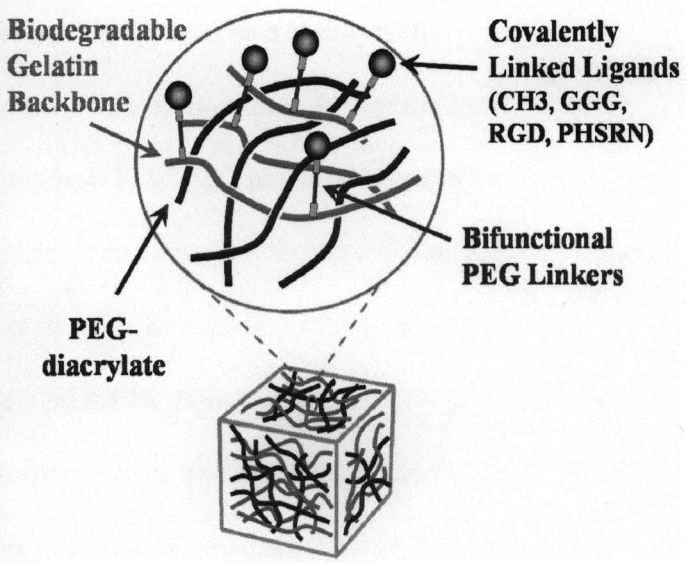

Figure 1-16. Semi-interpenetrating network of ligand-PEG grafted gelatin and PEGdA schematic.

Thus, the tethered RGD (or other ligand group) could be presented on the sIPN surface. Others have grafted the bioadhesive peptide RGD onto a substrate to attracted additional macrophages to the site of implant [66-68]. Our approach has been to present the RGD peptide on a flexible PEG linker of a gelatin (i.e. denatured form of collagen) and PEGdA based ECM-like network to enhance monocyte adhesion and modulate subsequent protein expression over time.

1.5 Monocyte interaction with biomaterials: molecular mechanisms and insight into cell-material interaction and biocompatibility

The presence of monocytes and macrophages at the site of injury plays a crucial role in orchestrating wound repair [7, 69-71]. One of the therapeutic approaches to facilitate wound healing has been to inject additional macrophages to the wound bed to increase repair rate [72]. As key players in wound healing, monocyte/macrophage interaction with biomaterials is also crucial as they often determine the fate of the biomaterial as a result of the impact that monocytes have on the host response [73-76]. Thus it is essential to characterize the monocyte response and behavior in the context of the ECM-analog sIPN, as severe inflammatory response from monocytes can lead to the recruitment of other immune cells and ultimately lead to the destruction of the

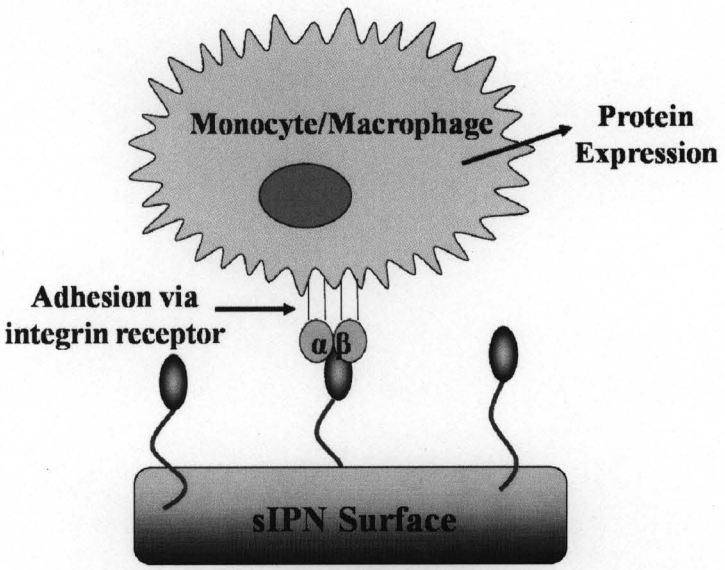

Figure 1-17. Molecular depiction of monocyte interaction with ligand-PEG grafted sIPN.

biomaterial or rejection of the material from the host system. It is also essential to evaluate monocyte response to and interaction with biomaterials in the presence of other wound healing cells as the injury repair process is a highly complex and delicately orchestrated progression of events. The presence of fibroblasts and how they influence monocyte response to the ECM-derived sIPN is crucial as fibroblast regulate the proliferation, regeneration and remodeling phase of wound healing and are found in the same wound environment as monocytes, communicating through proteins [2, 77-79]. Thus, monocyte and fibroblast response to an implanted material as well as the cells' interaction with each other in the context of materials is crucial in understanding a central component of host response and biocompatibility. In order to maximize the understanding of host response to materials, studies that take the *in vitro* system closest to physiological settings will need to be designed.

1.6 References

1. Anderson JM. Biological response to materials. Annu Rev Mater Res 2001;31:81-110.
2. Singer AJ, Clark RA. Cutaneous wound healing. N Engl J Med. 1999;341(10):738-46.
3. Clark, RA. Cutaneous tissue repair: basic biologic considerations. J Am Acad Dermatol 1985;13:701–725.
4. Schaffer CJ, Nanney LB. Cell biology of wound healing. Int Rev Cytol 1996;169:151-181.
5. Gottrup F, Lorentzen H, Jørgensen LN. Human models. In: Mani R, Falanga V, Shearman CP, Sandeman D, eds. Chronic Wound Healing: Clinical Measurements and Basic Science. London, England: Saunders 1999:156–169.
6. Iba Y, Shibata A, Kato M, and Masukawa T. Possible involvement of mast cells in collagen remodeling in the late phase of cutaneous wound healing in mice. Int J Immunopharm 2004;4(14): 1873-1880.
7. Fukasawa M, Campeau JD, Yanagihara DL, Rodgers KE, diZerega GS. Regulation of proliferation of peritoneal tissue repair cells by peritoneal macrophages. J Surg Res 1990;49(1), 81-7.
8. DiPietro LA. Wound healing: the role of the macrophage and other immune cells. Shock 1995; 4(4), 233-40. Boughton II G, Janis JE, Attinger CE. The basic science of wound healing. Plast Reconst Surg 2006; 117: 7S, 12-34S.
9. Snyder RJ. Treatment of nonhealing ulcers with allografts. Clin Derm, 2005; 23(4):388-395.
10. Taylor JE, Laity PR, Hicks J, Wong SS, Norris K, Khunkamchoo P, Johnson AF, and Cameron RE. Extent of iron pick-up in deforoxamine-coupled polyurethane materials for therapy of chronic wounds. Biomaterials 2005;26(30): 6024-6033.
11. Woolverton CJ, Fulton JA, Lopina ST and Landis WJ. Tissue Engineering and Biodegradable Equivalents. 2002:43-75. (Eds. Lewandrowski KU, Wise DL, Trantolo DJ, Gresser JD, Yaszemski MJ, Altobelli DE,) Marcel Dekker, Inc. New York, NY.
12. Ratner BD, Hoffman AS, Schoen FJ, Lemons JE, eds. An introduction to materials in medicine: Host reactions to biomaterials and their evaluation. San Diego, CA: 2004:293-354.

13. Ratner BD, Hoffman AS, Schoen FJ, Lemons JE, eds. An introduction to materials in medicine: Biological Testing of Biomaterials. San Diego, CA: 2004: 355-409.

14. Vroman, L. Effect of adsorbed proteins on the wettability of hydrophilic and hydrophobic solids. Nature 1962;196:476-477.

15. Jung SY, Lim SM, Albertorio F, Kim G, Gurau MC, Yang RD, Holden MA, Cremer PS. The Vroman Effect : A Molecular Level Description of Fibrinogen Displacement. J Am Chem Soc 2003;125: 12782-12786.

16. Turbill P, Beugeling T, Poot AA. Proteins involved in the Vroman effect during exposure of human blood plasma to glass and polyethylene. Biomaterials 1996;17:1279-1287.

17. Chang DT, Jones JA, Meyerson H, Colton E, Kwon IK, Matsuda T, Anderson JM Lymphocyte/macrophage interactions: Biomaterial surface-dependent cytokine, chemokine, and matrix protein production. J Biomed Mater Res 2008;87A:676-687.

18. Luttikhuizen DT, van Amerongen MJ, de Feijter PC, Petersen Arjen H; Harmsen MC, van Luyn MJA. The correlation between difference in foreign body reaction between implant locations and cytokine and MMP expression. Biomaterials 2006;27:5763-5770.

19. C. Hendrich, M. Geyer D. Sheddin, N. Schutze, J. Eulert, R. Thull, A new osteoblast culture system for standardized testing of biomaterials. Biomed Tech (Berl) 1996;41:278-2836.

20. Tsuchiya T. Studies on the standardization of cytotoxity tests and new standard reference materials useful for evaluating the safety of biomaterials. J Biomat App, 1994;138-157.

21. Huhtala A, Pohjonen TL, Salminen A, Salminen K, Kaarniranta H, Uusitalo. *In vitro* biocompatibility of degradable biopolymers in cell cultures from various ocular tissues: extraction studies. J Mater Sci Med 2008;19:645-649.

22. Pierschbacher MD, and Ruoslahti E, Cell attachment activity of fibronectin can be duplicated by small synthetic fragments of the molecule. Nature 1984;309:30-33.

23. Shin HS, Jo SB, Mikos AG. Modulation of marrow stromal osteoblast adhesion on biomimetic oligo[poly(ethylene glycol) fumarate] hydrogels modified with Arg-Gly-Asp peptides and a poly(ethylene glycol) spacer. J Biomed Mater Res 2002;61:169-179.

24. Kantlehner M, Schaffner P, Finsinger D, Meyer J, Jonczyk A, Diefenbach B, Nies B, Holzemann G, Goodman SL, Kessler H. Surface coating with cyclic RGD peptides

stimulates osteoblast adhesion and proliferation as well as bone formation. Chembiochem 2000;1:107-114.

25. Rezania A and Healy KE. Integrin subunits responsible for adhesion of human osteoblast-like cells to biomimetic peptide surfaces. J Orthop Res 1999;17:615-623.

26. Massia SP and Stark J. Immobilized RGD peptides on surface-grafted dextran promote biospecific cell attachment. J Biomed Mater Res 2001;56:390-399.

27. Verrier S, Pallu S, Bareille R, Jonczyk A, Meyer J, Dard M, Amedee J. Function of linear and cyclic RGD-containing peptides in osteoprogenitor cells adhesion process. Biomaterials 2002;23:585-596.

28. Yu J, Gu Y, Du KT, Mihardja S, Sievers RE, Lee RJ. The effect of injected RGD modified alginate on angiogenesis and left ventricular function in a chronic rat infarct model. Biomaterials 2009;30:754-756.

29. Zhao B, Yi Z, Tian W, Cui F, Feng H, Hu H, Kawakami T, Tagaki T, Nagai N. Improvement of adhesion and spreading of human gingival fibroblasts to RGD-grafted titanium surface. J Hard Tissue Biol 2006;15:65-68.

30. Karakecili AG, Dermirtas TT, Satriano C, Gumusderelioglu M, Marletta G. Evaluation of L292 fibroblast attachment and proliferation on Arg-Gly-Asp-Ser (RGDS)-immobilized chitosan in serum-containing /serum-free cultures. J Biosci and Bioeng 2007;104:69-77.

31. Chung AS, Waldeck HM, Schmidt DR, Kao WJ. Monocyte inflammatory and matrix remodeling response modulated by grafted ECM-derived ligand identity and concentration." J Biomed Mater Res published online Dec 2, 2008.

32. Mochizuki M, Yamagata N, Philp D, Hozymi K, Watanabe T, Kikkawa Y, Kadoya Y, Kleinman HK, Nomizu M. Integrin-dependent cell behavior on ECM peptide conjugated chitosan membranes. Pept Sci 2007;88:122-130.

33. Chung AS and Kao WJ. Fibroblasts regulate monocyte response to ECM-derived matrix: The effects on monocyte adhesion and the production of inflammatory, matrix remodeling and growth factor proteins. J Biomed Mater Res, published online Apr 2, 2009.

34. Stephens JS, Cooper JA, Phelan FR, Jr., Dunkers JP. Perfusion flow bioreactor for 3D in situ imaging: investigating cell/biomaterials interactions. Biotechnol Bioeng 2006;97:952-961.

35. Wang X, Yu X, Yan Y, Zhang R. Liver tissue responses to gelatin and gelatin/chitosan gels. J Biomed Mater Res 2008;87:62-68.

36. Kalltorp M, Oblogina S, Jacobsson S, Karlsson A, Tengvall P, Thomsen P. In vivo recruitment, cytokine release and chemiluminescence response at gold, and thiol functionalized surfaces. Biomaterials 1999;20:736-742.

37. Caldwell RK, Opalenik SR, Davidson JM, Caprioli RM, Nanney LB. Tissue profiling MALDI mass spectrometry reveals prominent calcium binding proteins in the proteome of regenerative MRL mouse wounds. Wound Repair Regen 2008;16:442-449.

38. Gibran NS and Isik FF. Use of high-throughput microarray membranes for cDNA analysis of cutaneous wound repair. Methods in Molecular Medicine: Wound Healing Methods and Protocols, 2008;78:425-432 (Ed. Luisa A DiPietro and Aime L. Burns) Humana Press Inc., Totowa, NJ.

39. Neff JA, Tresco PA, Caldwell KD. Surface modification for controlled studies of cell-ligand interactions. Biomaterials 1999;20:2377-2393.

40. Chaikof EL. Biomaterials that imitate cell microenvironments. Chemtech 1996;26:17-22.

41. VandeVondele S, Voros J, Hubbell JA. RGD-grafted poly -L-lysine-graft-(polyethylene glycol) copolymers block non-specific protein adsorption while promoting cell adhesion. Biotechnol Bioeng 2003;82:784-790.

42. Mishra S, Bajpai R, Katare R, Bajpai AK. Preparation and characterization of polyvinyl alcohol based biomaterials: water sorption and in vitro blood compatibility study. J App Polym Sci 2006;100:2402-2408.

43. Sethuraman S, Nair LS, El-Amin S, Farrar R, Nguyen MTN, Singh A, Allcock HR, Greish YE, Brown PW, Laurencin CT. In vivo biodegradability and biocompatibility evaluation of novel alanine ester based polyphosphazenes in a rat model. J Biomed Mater Res 2006;77A:679-687.

44. Harris JM. Poly(ethylene glycol) chemistry and biotechnical and biomedical applications. App Biochem Biotechnol 1992;41.

45. Chung AS, Gao Q, Kao WJ. Either integrin subunit β1 or β3 is involved in mediating monocyte adhesion, IL-1β protein and mRNA expression in response to surfaces functionalized with fibronectin-derived peptides. J Biomater Sci Polym Ed 2007;18:713-729.

46. Aigner T and Stove J. Collagens—major component of the physiological cartilage matrix, major target of cartilage degeneration, major tool in cartilage repair. Adv Drug Deliv Rev 2003;55:1569-1593.

47. Wallace DG and Rosenblatt J. Collagen gel systems for sustained delivery and tissue engineering. Adv Drug Deliv Rev 2003;55:1631-1639.

48. Lee CR, Grodzinsky AJ, Spector M. Biosynthetic response of passaged chondrocytein a type II collagen scaffold to a mechanical compression. J Biomed Mater Res A 2003;64:560-569.

49. Masuko T, Iwasaki N, Yamane S, Funakoshi T, Majima T, Minami A, Ohsuga N, Ohta T, Nishimura SI. Chitosan-RGDSGGC conjugate as a scaffold material for musculoskeletal tissue engineering. Biomaterials 2005;26:5339-5347.

50. Madihally SV and Matthew HWT. Porous chitosan scaffold for tissue engineering. Biomaterials 1999;20:1133-1142.

51. Suh JKF and Matthew HWT. Application of chitosan based polysaccharide biomaterials in cartilage tissue engineering: a review. Biomateirals 2000;21:2589-2598.

52. Degim Z, Celebi N, Sayan H, Babul A, Erdogan D, Take G. An investigation on skin wound healing in mice with a taurine-chitosan gel formation. Amino Acids 2002;22:187-198.

53. Peh K, Kahn T, Ching H. Mechanical, bioadhesive strength and biological evaluations of chitosan films for wound dressing. J Pharm Sci 2000;3:303-311.

54. Fu Q and Gowda DC. Carbohydrate-directed conjugation of cobra venom factor to antibody by selective derivatization of the terminal galactose residues. Bioconjugate Chem 2001;12:271-279.

55. Glass JR, Dickerson KT, Stecker K, Polarek JW. Characterization of a hyaluronic acid-Arg-Gly-Asp peptide cell attachment matrix" Biomaterials 1996;17:1101-1108.

56. Mertz PM, Davis SC, Franzen L, Uchima FD, Pickett MP, Pierschbacher MD, Polarek JW. Effects of an arginine-glycine-aspartic acid peptide-containing artificial matrix on epithelial migration in vitro and experimental second-degree burn wound healing in vivo. J Burn Care Rehabil 1996;17:199-206.

57. Gorman SP and Woolfson AD. Novel biomimetic and bioactive silicones. Med Device Technol 2002;13:14-15.

58. Gumargalieva KZ, Zaikov GE, Mioseev YV. Quantitative foundations of polymer biocompatibility and biodestructibility. Int J Polym Mater 1996;31:183-214.

59. Li B, Chen J, Wang JHC. RGD peptide conjugated poly(dimethylsiloxane) promotes adhesion, proliferation, and collagen secretion of human fibroblasts." J Biomed Mater Res 2006;79:989-998.

60. Hooftman G, Herman E, Schacht. Review: poly(ethylene glycol)s with reactive endgroups. II. Practical consideration for the preparation of protein-PEG conjugates. J Bioact Compat Polymers 1996;11:135-159.

61. Waldeck HM, Chung AS, Kao WJ. Interpenetrating polymer networks containing gelatin modified with PEGylated RGD and soluble KGF: Synthesis, characterization, and application in in vivo critical dermal wound. J Biomed Mater Res 2007;82:861-871.

62. Li J, Wang F, Zhou L, Cui J. Application of gelatin tube in bridge repair of sciatic nerve defect. Zhongguo Linchuang Kangfu 2005;9:158-159.

63. Wu B, Luo Z, Meng H, Hu H, Zhang Y, Li M. Preparation of crosslinked collagen-gelatin biomaterial and experiment of its cytotoxicity. Shengwu Yixue Gongcheng Yu Linchuang 2007;11:420-425.

64. Massia SP and Hubbell JA. An RGD spacing of 440 nm is sufficient for integrin alphaVbeta3 mediated fibroblast spreading and 140 nm for focal contact and stress fiber formation. J Cell Biol 1991;14:1089-1100.

65. Yahalom D, Wittelsberger A, Mierke DF, Rosenblatt M, Alexander JM, Chorey M. Identification of the principal binding site for RGD-containing ligand in the alphaVbeta3 integrin: a photoaffinity cross-linking study. Biochem 2002;41:8321-8331.

66. McNally AK and Anderson JM. Beta1 and beta2 integrins mediate adhesion during macrophage fusion and multinucleated foreign body giant cell formation. Am J Path 2002;160:621-630.

67. Rowley JA and Mooney DJ. Alginate type and RGD density control myoblast phenotype. J Biomed Mater Res 2001;60:217-223.

68. Sawyer AA, Hennessy KM, and Bellis SL. The effect of adsorbed serum proteins, RGD and proteoglycan-binding peptides on the adhesion of mesenchymal stem cells to hydroxyapatite. Biomaterials 2007;28:383-392.

69. DiPietro LA, Polverini PG, Rahbe SM, Kovacs EJ. Modulation of JE/MCP-1 expression in dermal wound repair. Am J Pathol 1995;146:868-875.

70. Brown LF, Daniel D, Lavigne L, Logan B, Dvorak HF, Livingston VDW. Macrophages and fibroblasts express embryonic fibronectins during cutaneous wound healing. Am J of Path 1993;142(3):793-801.

71. Hunt TK, Knighton DR, Thakral KK, Goodson, William H., III; Andrews, Walter S. Studies on inflammation and wound healing: angiogenesis and collagen synthesis stimulated in vivo by resident and activated wound macrophages. Surgery 1984;96(1): 48-54.

72. Danon D, Kowatch MA, Roth GS: Promotion of wound repair in old mice by local injection of macrophages. Proc Natl Acad Sci USA 1989;86:2018-2020.

73. Brodbeck WG, Nakayama Y, Matsuda T, Colton E, Ziats NP, Anderson JM. Biomaterial surface chemistry dictates adherent monocyte /macrophage cytokine expression in vitro. Cytokine+ 2002;18(6):311-319.

74. Schachtrupp A, Klinge U, Bhardwaj R, Rosch R, Schumpelick V. Individual response of human blood monocytes on mesh materials in the cell culture. Chirurgisches Forum fuer Experimentelle und Klinische Forschung 2002;69-172.

75. Cardona MA, Simmons RL, Kaplan SS. TNF and IL-1 generation by human monocytes in response to biomaterials. J of Biomed Mater Res 1992;26(7):851-9.

76. Shanbhag AS, Jacobs JJ, Black J, Galante JO, Glant TT. Human monocyte response to particulate biomaterials generated in vivo and in vitro. J Orthopaed Res 1995;13(5): 792-801.

77. Weihrauch D, Arras M, Zimmermann R, Schaper J. Importance of monocytes/macrophages and fibroblasts for healing of micronecroses in porcine myocardium. Molec Cell Biochem. 1995;147:13-19.

78. Concannon MJ, Barrett BB, Adelstein EH, Thorton WH, Puckett CL. The inhibition of fibroblast proliferation by a novel monokine: an in vitro and in vivo study. J Burn Care Rehabil 1993;14:141-147.

79. Dollery CM, Owen CA, Sukhova GK, Krettek A, Shapiro SD, Libby P. Neutrophil elastase in human atherosclerotic plaques: production by macrophages circulation 2003;107:2829-2836.

Chapter 2. Integrin-dependent monocyte interaction with ECM-derived peptide functionalized sIPN: Adhesion and Subsequent IL-1beta, MMP-2 and MMP-9 Protein and mRNA Regulation

2.1 Introduction

Migration and adhesion are the essential steps for macrophage function in the local site of inflammation. Integrins, a family of cell-surface receptors expressed in many cell types including monocytes/macrophages, fibroblasts and endothelial cells, can mediate cell adhesion and migration [1]. The integrins are dimeric proteins that contain an α and a β subunit. Currently seventeen α and eight β subunits have been identified, and these subunits can combine to make 23 different combinations of dimers [2, 3]. During the recruitment of monocytes into the site of inflammation, β1- and β3-containing integrins mediate monocyte adhesion and transmigration across the endothelium and binding to ECM proteins, such as fibronectin (FN) and collagen [4-6]. Peptide sequences from FN such as arginine-glycine-aspartic acid (RGD), proline-histidine-serine-arginine-aspragine (PHSRN) and leucine-aspartate-valine (LDV), are believed to be ligands for β1- and β3-containing integrins [5]. Integrins can also modulate a variety of gene and protein expression by affecting multiple signaling pathways [7, 8]. The RGD oligopeptide, located in the FN III-10 module, can be recognized by approximately half of all integrins [4]. PHSRN, a pentapeptide sequence in the FNIII-9 module is a synergy site that enhances the cell adhesive activity of RGD [9]. The α5β1 and the αvβ3 integrin receptors have been shown to mediate macrophage adhesion onto the biofunctional peptide sequence RGD that is ubiquitous in ECM proteins such as collagen, laminin and fibronectin [10-12]. Antibody inhibition and epitope

mapping studies for α5β1 integrin indicate that the binding site of the RGD sequence is on the β subunit while the binding site for the synergy sequence appears to be on the α subunit [13]. Though the RGD sequence proves important for macrophage adhesion and subsequent signaling, the orientation by which this peptide sequence is presented to the macrophages also impacts cell adhesion and function [14]. Moreover, FN-derived peptides on different surfaces, such as PEG-based networks or TCPS, have shown to affect selected intracellular signaling events in monocytes/macrophages, including protein tyrosine phosphorylation [15, 16].

Monocytes/macrophages exert important regulatory effects on immunoreaction, inflammation and wound healing. Macrophages not only remove debris by phagocytosis but can release a plethora of cytokines, growth factors, chemokines and enzymes, which can influence tissue healing. Interleukin-1beta (IL-1β) is a member of the IL-1 family which consists of two agonists, IL-1α and IL-1β, a specific receptor antagonist called IL-1Ra, and two different IL receptors. IL-1β is a major pleiotropic and pro-inflammatory cytokine which is mainly synthesized by activated monocytes/macrophages. IL-1β influences the host response in the presence of a foreign body, as well as cell proliferation, differentiation, apoptosis, inflammation and wound healing [17]. The activity of IL-1β is affected by IL-1Ra which competes with IL-1β for receptor binding but fails to activate cells [18,19]. The balance between IL-1β and IL-1Ra in local tissues influences the physiologic or pathophysiologic effects of IL-1β. An excess amount of IL-1β is related to the development of inflammatory and autoimmune diseases [22].

Macrophages not only direct the progression of inflammatory and immune response, and the healing of the host response system [21-23] but also play a critical role in ECM remodeling [24,25]. The ECM provides a microenvironment to mediate cell adhesion, proliferation and differentiation [26,27] and macrophages interact with the matrix mainly by integrin receptors.

Integrins also influence the expression of matrix metalloproteases (MMPs), a family of zinc and calcium dependent proteolytic enzymes that play a critical role in ECM proteolysis and turnover [28,29]. Human mononuclear phagocytes can directly modulate the ECM turnover by secreting MMPs and MMP inhibitors, tissue inhibitor matrix metalloproteases (TIMPs) [21,28]. ECM turnover by MMPs allows the removal of damaged tissue, vessel formation and cell migration, which are all critical processes in the normal progression of wound healing [30]. There have been studies on the relationship between the $\alpha 5\beta 1$, $\alpha v\beta 3$ integrin receptors and MMP-2/-9 [10,31-34]. MMP-2 and MMP-9 (or gelatinase A and gelatinase B, respectively) both degrade gelatin and basement membrane and *in vitro*, they have been shown to have similar substrate profiles [35]. However, most of the investigations have studied uveal melanoma, ovarian carcinoma, and glioma cells. Few studies to date have focused on MMP-2 and MMP-9 regulation in relation to integrin receptors using human monocytes/macrophages, especially those in the presence of gelatin-based biomaterials.

Monocytes directly influence physiological conditions such as tissue remodeling, inflammatory reactions, and wound healing and have been commonly observed at the biomaterial-tissue interface [36]. Thus, it is crucial to understand the intricate molecular mechanisms of macrophages, including the mechanism behind initial adhesion and the subsequent protein and gene regulation of cytokines such as MMPs. In this study, we investigated the hypothesis that $\beta 1$ and $\beta 3$ containing integrin receptors modulate monocyte adhesion onto surface-immobilized biofunctional peptides.

PEG is extensively employed in pharmaceutical and biomedical applications as PEG has low toxicity and good solubility in both aqueous and organic solvents [37-39]. Previously, we have synthesized sIPNs composed of PEG derivatives and chemically modified gelatin as drug

delivery and tissue engineering matrices [40-42]. The rationale of incorporating bioactive factors such as RGD to biomedical materials is widely adapted to facilitate cell-material interaction. However, these biofunctional molecules can also activate host inflammatory cells such as macrophages. We have reported that the adhesive activity of monocytes was promoted by gelatin-based sIPN immobilized with RGD [43]. In this study we extend our understanding of the mechanisms behind monocyte interaction with biomaterials containing FN-derived peptides and of the involvement of β1 or β3 containing integrins in the interaction. We hypothesized that the biomaterial substrate, the sequence of the FN-derived peptide and the β1 or β3 containing integrin receptors would modulate monocyte adhesion and the subsequent expression of IL-1β and MMP-2/-9 gene and protein. The elucidation of molecular mechanisms behind monocyte-biomaterial interaction will provide a basis for clinical applications of the novel multifunctional material. We also tested our hypothesis that the subsequent regulation of MMP-2 and MMP-9 protein and gene expression by monocytes would be upregulated in the presence of the gelatin and PEG based sIPN, and that β1 and β3 containing integrin receptors would be involved in modulating IL-1β and MMP-2/-9 protein and gene expression in the presence of sIPNs.

The hypothesis of investigating β1 and β3 containing integrin receptor-mediated adhesion and subsequent IL-1β and MMP-2/-9 protein and mRNA expression described above is outlined in Figure 2-1. Results from this study are analyzed to assess the interaction of ECM-derived peptide grafted sIPNs with integrins and the subsequent effects on cytokine release from monocytes.

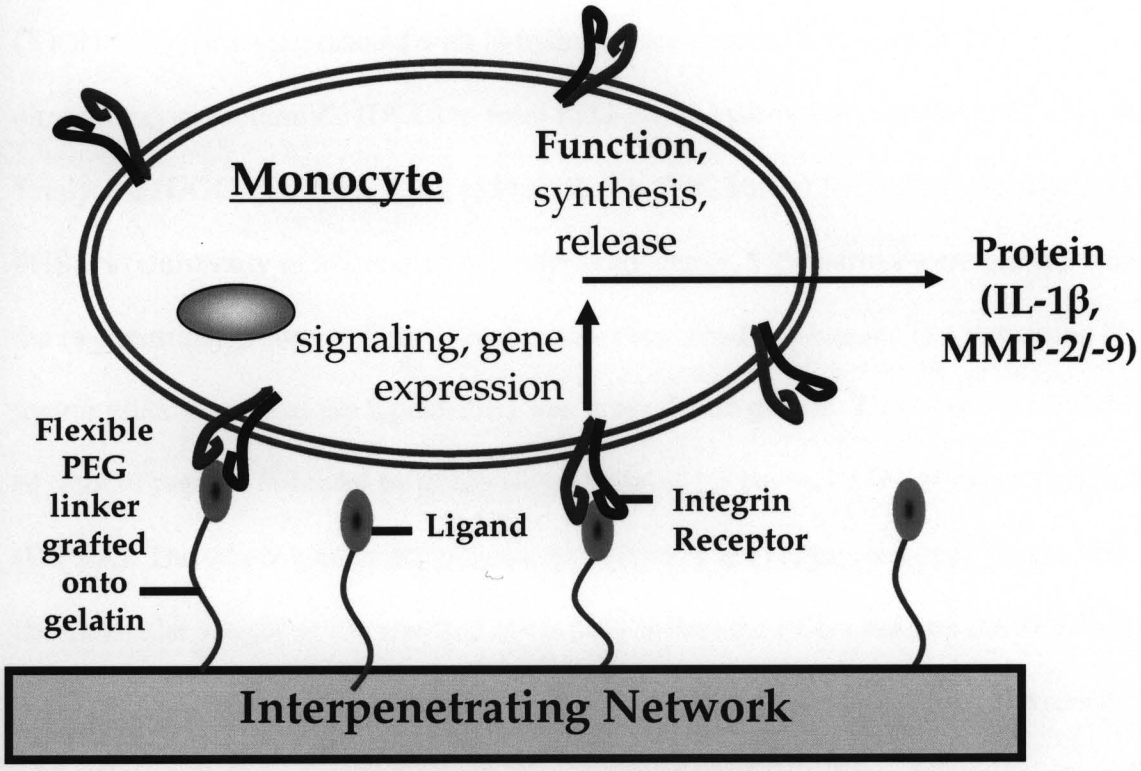

Figure 2-1. Integrin mediated adhesion and subsequent gene and protein expression.

2.2 Materials and Methods

2.2.1 Synthesis and characterization of gelatin-based sIPN grafted with PEGylated ECM-derived peptides

Synthesis and characterization of gelatin-based sIPN have been previously described [43]. The modification of PEG functional groups to conjugate ligand-PEG onto the gelatin backbone is outlined in Figure 2-2. Briefly, PEGylated ligand gelatin was synthesized by first converting the terminal alcohol groups of polyethylene glycol (2 kDa) alcohol to ethylacetate then to carboxylic acid. Bis-COOH-PEG was characterized using a reverse-phase column (Alltech, Inc., Nicholasville, KY) on an HPLC system (Gilson, Inc., Middleton, WI) coupled with a UV/Vis and an evaporative light scattering detectors. Both carboxylic acid groups of bis-

COOH-PEG were then reacted with N-hydroxysuccinimide (NSu) and N, N'-dicyclohexylcarbodimiide (DCC) to form PEG-bis-N-hydroxysuccinimide (PEG-bis-NSu). Triglycine (GGG) (Bachem, King of Prussia, PA, 99% purity) for control peptide, RGD or PHSRN (University of Wisconsin Biotechnology center, 98% purity) were grafted onto one of the two terminal groups to form N-hydroxysuccinimide-PEG-ligand. The remaining N-hydroxysuccinimide of the ligand-PEG was grafted onto gelatin. This was done by adding 1.5 eq. mol of peptide followed by dropwise addition of 1.5 eq. mol of N, N-diisopropyl ethylamine (DIPEA). The whole protein FN (Sigma-Aldrich) was not conjugated onto the bis-NSu -PEG as the molecular weight of FN was 225 times greater than the PEG used and the PEG molecules would be likely entrapped within the protein structures during conjugation. The remaining NSu of the ligand-PEG was grafted onto gelatin. This was carried out by adding one eq. mol of NSu-ligand-PEG to 1% gelatin in PBS and stirring at pH 8.0 for 1 h. A pressurized ultrafiltration system (Millipore, Bedford, MA) with a 30 kDa membrane filter under nitrogen at 60 psi was used to separate peptide-PEG grafted gelatin and to filter out residual unreacted side product. Methoxy-PEG modified gelatin was synthesized in a similar scheme, but monomethoxy PEG (mPEG) of 2 kDa was employed as the starting material rather than PEG diol 2 kDa without peptide conjugation. The degree of peptide-PEG grafted onto the lysyl residues of the gelatin backbone was analyzed via a well-established method based on trinitrobenzenesulfonic acid-based spectrophotometry [44]. The percent modification (n=3) for modified gelatin was 91-96% for MPEG-gelatin, 82-89% for GGG-PEG-gelatin, 65-78% for RGD-PEG-gelatin, and 72-92% for PHSRN-PEG-gelatin.

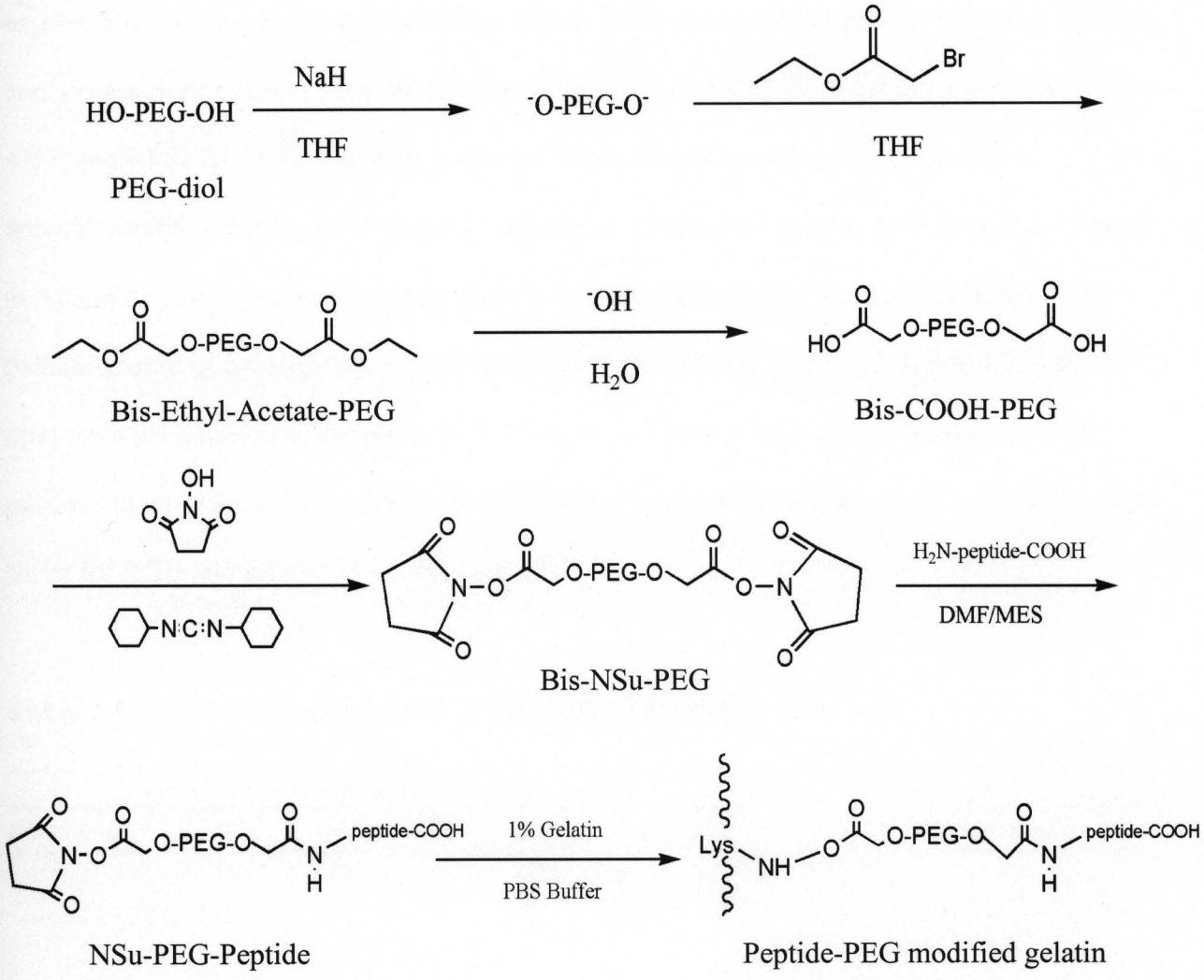

Figure 2-2. Schematic outline of peptide-PEG-modified gelatin synthesis.

Peptide-PEG-modified gelatin was also characterized with ^{1}H-NMR. All samples of modified gelatin contained PEG and gelatin, and thus all modified gelatin samples exhibited prominent PEG peaks approximately at 3.67 ppm. In addition, all ^{1}H-NMR spectra from modified gelatin samples displayed peaks from gelatin, which included a group of broad,

asymmetrical peaks spanning from 0.885 ppm to 4.803 ppm, a broad doublet peak at 7.250 ppm and a sharp peak at 8.411 ppm. In addition to those peaks, GGG-PEG-gelatin showed a triplet at 4.07 ppm while RGD-PEG-gelatin displayed an overlapped doublet of triplet peaks at approximately 1.36 ppm, a broad group of peaks at 1.40 ppm, a peak at 2.79 ppm, at 2.87 ppm, at 3.03 ppm, and two overlaid triplet peaks at approximately 3.38 ppm. For PHSRN-PEG-gelatin, groups of broad peaks were observed at approximately 1.6, 1.8, 1.9, 3.2, 4.3, 4.4, and 7.1 ppm from the addition to the gelatin and PEG peaks. These results were consistent to and outlined in more detail in our previous study [45]. Table 2-1 summarizes the ^{1}H-NMR chemical shifts for RGD and RGD-PEG grafted gelatin.

Table 2-1. ^{1}H-NMR chemical shifts for RGD and RGD-PEG grafted gelatin

Chemical Shifts of Designated Hydrogen (in Superscript)								
nCH$_2$	H$^{(1)}$	H$^{(2)}$	H$^{(3)}$	H$^{(4)}$	H$^{(5)}$	H$^{(6)}$	H$^{(7)}$	Chemical Group
–	4.02	1.96	1.73	2.96	3.71	4.1	3.25	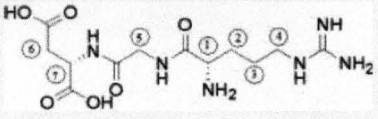
3.65[a]	3.35	1.4	1.36	2.87	3.03	3.38	2.79	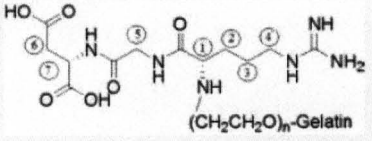

sIPNs were made by mixing the ligand-PEG-gelatin with polyethylene glycol diacrylate (PEGdA) (575 Da, Sigma, St. Louis, MO) with 2,2-dimethoxy-2-phenyl-acetophenone initiator (0.1 wt% of the initiator in the final mixture). sIPNs were made in 4:6 modified gelatin: PEGdA weight ratio, poured over Teflon® molds and crosslinked with UV light (maximal intensity at 365 nm, 21,700 μW/cm^2, UVP, model B 100AP) for 5 min. sIPNs were γ-irradiated (1 MRad) for sterility prior to cell culture. sIPNs were placed in 48-well TCPS (BD Falcon®) plates and

incubated with Roswell Park Memorial Institute 1640 (RPMI 1640) (Mediatech, Inc, Herndon, VA) medium at 37°C and 5% CO_2 for 24 h prior to monocyte seeding. To quantify the peptide surface density, the amount of RGD on the sIPN was measured by a modified protocol based on an indirect ELISA method described in more detail in Chapter 3, section 3.2.1 and 3.3.1 [46].

2.2.2 Preparation of glutaraldehyde fixed gelatin hydrogel and ligand adsorbed TCPS

To examine the effects of gelatin on monocyte adhesion and protein and mRNA expression, glutaraldehyde fixed gelatin was synthesized per established procedure [40]. Briefly, 10 wt % gelatin (type A: from porcine skin, 300 bloom, cell culture tested, Sigma-Aldrich) was dissolved in ddH_2O and heated to 70°C while stirring for 10 min, cooled overnight, cut into discs (0.7 mm dia x 0.8 mm thick) and fixed with 0.1% glutaraldehyde for 7 h. The discs were rinsed with sterile ddH_2O for 3 days under constant stirring to leach out all glutaraldehyde. The hydrogels were incubated with RPMI 1640 at 37°C and 5% CO_2 for 24 h prior to cell seeding.

To evaluate the effect of ligands presented via a flexible PEG linker, peptides were also adsorbed onto TCPS plates. FN or FN derived peptides, i.e., G_3, RGD or PHSRN, were adsorbed onto 48-well TCPS plates at a 1 μmole/ml concentration in PBS for 24 h then the wells were rinsed twice with PBS prior to seeding monocytes. For non-ligand treated TCPS surface, PBS without ligands were added 24 h prior to cell seeding.

2.2.3 Monocyte culture and adhesion assay

Human primary monocytes were isolated from citrated whole blood of healthy adult volunteer according to an established density gradient, nonadhesion method [47]. In culture

conditions, previous studies had confirmed that monocytes express both β1- and β3-containing integrins [50]. Freshly isolated cells were seeded onto each surface, i.e. TCPS and sIPN, at a concentration of 10^6 cells/ml in RPMI 1640 medium plus 10% autologous serum at 37°C and 5% CO_2. Isotype and endotoxin tested mouse anti-integrin β1 monoclonal antibody (JB1A) or anti-integrin β3 monoclonal antibody (B3A) (Chemicon International, Temecula, CA) was used for integrin blocking study. Integrin blocking was done by incubating freshly isolated monocytes at 37°C for 30min at a concentration of 50 μg/ml of antibody under gentle agitation (approx. 30 rpm on a battery-powered bidirectional rotator in a 37°C, 5% CO_2 incubator) [47]. With the same protocol, mouse monoclonal IgG1 (Chemicon International, Temecula, CA) was used to confirm the specificity of anti-integrin antibody. As the complete differentiation of cultured monocytes into macrophages occurs in approximately one week, the nomenclature "monocyte" is used throughout this study [49,50]. At 2, 24, 96 and 168 h, supernatants were collected for IL-1β protein assessment with commercial ELISA kit (Raybiotech, Inc., Norcross, GA). ELISA was carried out according to manufacturer's instruction. The sensitivity of the kit for IL-1β protein was 0.3 pg/ml. After the supernatants were collected at each time point, samples were washed twice with RPMI medium to remove nonadherent cells and cellular debris. The adherent monocytes were either continuously cultured with new RPMI plus 10% autologous serum or lysed with TRIzol® reagent (Invitrogen™, CA) for RNA isolation or imaged using a computer-assisted video analysis system (Metamorph v4.1) coupled to an inverted microscope (Nikon, Eclipse TE 300). The monocytes in sIPN samples were stained with Wright's stain before quantification of adherent cell density.

2.2.4 Monocyte mRNA analysis with RT-PCR

All reagents employed in RT-PCR assays were purchased from Bio-Rad, USA, unless indicated otherwise. Adherent cells were lysed with TRIzol® reagent (Invitrogen™, CA) for RT-PCR analysis. The DNA sequence database from NCBI (Bethesda, MD) was used to obtain oligonucleotide primers. Primer sets were designed using the Primers3 Output computer program (Whitehead Institute for Biomedical Research, Cambridge, MA, USA) which offers the possibility of selection based on G/C content, melting temperature and PCR product size. NCBI BLAST program was used to check the specificity of the primer sequences. Table 2-2 below outlines the primer sequences and the product size.

Table 2-2. Oligonucleotide primer sequences used for RT-PCR and expected PCR product sizes.

mRNA	Sense primer (5' → 3')	Antisense primer (5' → 3')	Product size (bp)
MMP-2	AGGATCATTGGCTACACACC	AGCTGTCATAGGATGTGCCC	535
MMP-9	CGCAGACATCGTCATCCAGT	GGATTGGCCTTGGAAGATGA	406
IL-1β	GAATCTCCGACCACCACTACA	CAACACGCAGGACAGGTACA	416
β-actin	AGGCATCCTCACCCTGAAGTA	AGCCTGGATAGCAACGTACA	229

A modification on the Chomczynski and Sacchi method [51] was carried out to isolate total RNA from adherent monocytes. The quality of the purified RNA was tested by 1.5% agarose gel/ethidium-bromide staining with a 260/280 nm absorbance ratio. For cDNA synthesis, RNAse-free DNAse (Sigma, MO) was used to treat the RNA before being reverse transcribed with Moloney Murine Leukemia Virus (M-MLV) reverse transcriptase (Invitrogen™, CA). Amplification of cDNA was done in a 25 µl PCR mixture containing 1x reaction buffer (Sigma, MO, USA), 0.24 µM of each primer, 0.2 mM of each dNTP, and 0.75 U RedTaq DNA

polymerase (Sigma, MO). The PCR was started at 94°C for 3 min, after which followed 35 cycles for IL-1β, MMP-2/-9 and β-actin. A denaturation step (at 94°C for 30 sec), an annealing step (at 62°C for IL-1β and 56°C for β-actin) and an extension step (at 72°C for 1 min), and a final elongation step (at 72°C for 7 min) took place at each cycle. The PCR reaction was performed in iCycler thermal cycler. 15 μl of the amplified products were electrophoresed on 1.5% agarose gel containing ethidium-bromide (0.5 μg/ml) and visualized under ultraviolet light. Contamination from genomic DNA was checked for with RT-PCR containing RNA but not M-MLV reverse transcriptase. The Scion imaging program (Frederick, Maryland, USA) was used to quantify the band density in the gels. PCR analysis was carried out for sIPN samples at 2, 24 and 96 h. At 168 h there were too few adherent monocytes left on the sIPN for isolating RNA. The level of IL-1β mRNA expression for each sample was normalized to β-actin.

PCR analysis was carried out for sIPN samples at 2, 24, and 96 h and the level of IL-1β, MMP-2/-9 mRNA expression for each sample was normalized to β-actin. mRNA levels in primary monocytes on different sIPNs were compared within each time point. Ligand identity and ligand mobility's role in intracellular events was of primary focus for this study and thus PCR analysis was not carried out on TCPS samples in which the effect of adsorbed proteins might be more pronounced. As the primary cell source was limited, RT-PCR analysis for sIPN samples without antibody pretreatment was carried out for one sIPN sample per ligand at all time points and thus was not subject to statistical analysis.

2.2.5 Statistical Analysis

Monocyte adhesion data (n=3) and ELISA data (n=3) were analyzed by two-way analysis of variance and Tukey post testing (SigmaStat v2.03, USA), $p < 0.05$ was considered

significantly different. RT-PCR data (n=2) from the individual sIPN at each time point were compared to the transcriptional level of IL-1β mRNA at 2 h. RT-PCR for the group without antibody pretreatment and the group with antibody pretreatment (n=1 and n=2 respectively) were not statistically tested due to low sample number and the antibody pretreated groups were expressed as mean ± standard error.

2.3 Results

2.3.1 Monocyte adhesion onto sIPN via β1 and β3 containing integrin receptors

Monocytes adherent density declined over time, characteristic of primary, nonproliferating cells. At 2 and 96 h, adherent monocyte density on RGD-adsorbed TCPS was significantly greater than adherent density of PBS or GGG treated TCPS samples. There was a decreasing trend in adherent cell density for all ligand-modified TCPS with culture time, especially from 2 to 24 h. Between 24 and 96 h this decrease was less significant and at 168 h, adherent monocyte density on all modified TCPS surfaces were detected at low levels compared to previous time points (Table 2-2). After either anti-integrin β1 or β3 antibody pretreatment there was a decrease in monocyte density on all ligand-treated TCPS compared to those monocytes without antibody pretreatment on TCPS modified with the corresponding ligand at all time points. Anti-integrin β3 antibody had a stronger inhibitory effect on monocyte adhesion than anti-integrin β1 antibody. After IgG1 antibody pretreatment, the cell density on all TCPS surfaces was comparable to that of that of monocytes without pretreatment on TCPS at 2 h. However, at 24 and 96 h a more dramatic decrease in cell adhesion of cells pretreated with IgG1

compared to those without antibody or IgG1 pretreatment was observed. At 168 h there were no adherent cells on TCPS among the IgG1 pretreated samples (Table 2-3).

Table 2-3. Adherent monocyte density (cell/mm^2) on TCPS treated with various ligands and on glutaraldehyde fixed gelatin at 2, 24, 96, and 168 h of culture.

	Culture Time:			
Surfaces/Ligand Treatment	**2 h**	**24 h**	**96 h**	**168 h**
No Antibody Pretreatment				
No Ligand Treatment	1536 ± 242	809 ± 85	562 ± 43	21 ± 10
GGG	2109 ± 624	860 ± 161	648 ± 63	90 ± 85
RGD	2627 ± 546†	929 ± 150	958 ± 95†	184 ± 98
PHSRN	2000 ± 782	1047 ± 261	721 ± 239	90 ± 90
FN	2352 ± 238	864 ± 106	728 ± 150	42 ± 26
Glutaraldehyde Fixed Gelatin Hydrogel	266 ± 153†	415 ± 215†	304 ± 14†	278 ± 73†
Anti-Integrin Beta1 Pretreated				
No Ligand Treatment	1380 ± 44§	137 ± 35*§	17 ± 3*	6 ± 2*
GGG	1489 ± 67§	283 ± 63*§	5 ± 3*	8 ± 0*
RGD	1491 ± 76*§	359 ± 39*§	10 ± 2*	8 ± 0*
PHSRN	1587 ± 113*	467 ± 112*§	10 ± 2*	7 ± 2*
FN	1244 ± 61*	346 ± 74*	8 ± 3*	7 ± 2*
Glutaraldehyde Fixed Gelatin Hydrogel	228 ± 101†	25 ± 18*	179 ± 32$^{\dagger *}$	92 ± 22$^{\dagger *}$
Anti-Integrin Beta3 Pretreated				
No Ligand Treatment	774 ± 184*	25 ± 22*	6 ± 2*	0 ± 0*
GGG	1007 ± 111*	155 ± 77*	15 ± 2*	4 ± 2*
RGD	1143 ± 83*	293 ± 43*	11 ± 0*	6 ± 3*
PHSRN	1203 ± 60*	393 ± 19*	19 ± 6*	4 ± 2*
FN	1235 ± 68*	341 ± 72*	22 ± 3*	6 ± 0*
Glutaraldehyde Fixed Gelatin Hydrogel	189 ± 166†	115 ± 72$^{\dagger *}$	122 ± 70$^{\dagger *}$	106 ± 52$^{\dagger *}$
Immunoglobulin G1 Pretreated				
No Ligand Treatment	2545 ± 289	285 ± 50^{i}	19 ± 5^{i}	0 ± 0^{i}
GGG	2178 ± 322	221 ± 99^{i}	15 ± 3^{i}	0 ± 0^{i}
RGD	2174 ± 337	127 ± 28^{i}	15 ± 3^{i}	0 ± 0^{i}
PHSRN	2112 ± 418	163 ± 73^{i}	13 ± 3^{i}	0 ± 0^{i}
FN	1940 ± 324	187 ± 62^{i}	15 ± 3^{i}	0 ± 0^{i}

all values expressed as mean ± s.e.m; n=3 ($p < 0.05$)

* significantly different from the corresponding TCPS surface without antibody or IgG1 treatment within time point

† significantly different from TCPS without ligand treatment

§ significantly different from β3 anti-integrin antibody treated monocytes within time point

^{i} significantly different from corresponding TCPS surface without antibody or IgG1 pretreatment within time point at $p<0.001$

* significantly different from corresponding glutaraldehyde fixed gelatin surface without antibody treatment (within time point)

To further probe the role of integrin β1 and β3 subunits in mediating monocyte adhesion onto the sIPN, we investigated the cell adhesive activity of monocytes pretreated with or without anti-integrin β1 or β3 antibody on sIPNs. Monocyte density on the sIPN was highly dependent on the presence of RGD. At 2 and 24 h, there were significantly higher monocyte cell densities on sIPN grafted with RGD than other sIPNs, especially compared to MPEG grafted sIPN, where cell density was the lowest among all sIPN samples. At 96 h monocyte cell densities on sIPN grafted with RGD was still significantly higher than sIPN grafted with MPEG or GGG but lower than sIPN grafted with PHSRN. At 168 h the adherent monocyte numbers on all sIPNs were comparable (Table 2-4). Compared to corresponding ligand-treated TCPS surfaces, the cell density on each sIPN was lower at all time points, with the exception of sIPN grafted with RGD at 24 h. Over the culture time a decrease in cell densities was observed at 96 h. Pretreatment of monocytes with either anti-integrin β1 or β3 antibody had a similar effect on monocyte adherent density in the presence of sIPNs. Pretreatment with antibody significantly decreased the monocyte adhesive activity on sIPN conjugated with RGD or PHSRN, but this decrease was not observed with sIPN grafted with MPEG. IgG1 pretreatment did not affect the monocyte density on RGD immobilized sIPN. Similar to monocytes without pretreatment of antibody, the samples in the presence of RGD had a greater cell density than other sIPNs at all time points (Table 2-4).

Table 2-4. Adherent monocyte density (cell/mm^2) on sIPN with various immobilized ligands at 2, 24, 96, and 168 h of culture.

	Culture Time:			
Surfaces/Immobilized Ligand	**2 h**	**24 h**	**96 h**	**168 h**
No Antibody Pretreatment				
Methoxy	39 ± 9	36 ± 10	83 ± 55	66 ± 5
GGG	340 ± 133	320 ± 106	114 ± 51	74 ± 40
RGD	1237 ± 470†	1398 ± 504†	147 ± 69†	125 ± 59
PHSRN	680 ± 287	643 ± 264	332 ± 309	69 ± 34
Anti-Integrin Beta1 Pretreated				
Methoxy	142 ± 59	65 ± 20	51 ± 26	7 ± 4*
GGG	187 ± 150	116 ± 41	54 ± 39	0 ± 0*
RGD	151 ± 39*	85 ± 12*	32 ± 12*	9 ± 4*
PHSRN	151 ± 44*	194 ± 88*	14 ± 3*	18 ± 8*
Anti-Integrin Beta3 Pretreated				
Methoxy	96 ± 56	77 ± 8	36 ± 22	6 ± 4*
GGG	177 ± 17	66 ± 44	28 ± 3	8 ± 0*
RGD	145 ± 75*	100 ± 47*	64 ± 17*	15 ± 6*
PHSRN	229 ± 163*	116 ± 13*	62 ± 4*	9 ± 3*
Immunoglobulin G1 Pretreated				
Methoxy	49 ± 10	84 ± 19	90 ± 11	30 ± 11
GGG	72 ± 7	178 ± 28	72 ± 17	51 ± 7
RGD	1086 ± 407†	622 ± 38†	484 ± 162†	59 ± 44
PHSRN	418 ± 87	183 ± 31	117 ± 8	24 ± 9

all values expressed as mean ± s.e.m.; n=3

† significantly different from methoxy-PEG grafted sIPN at $p<0.05$

* significantly different from corresponding sIPN surface without antibody or IgG1 pretreatment within time point at $p<0.05$

2.3.2 Monocyte IL-1β protein and mRNA expression on sIPN: the role of β1 and β3 containing integrins

There was a difference in IL-1β in secretion pattern between monocytes on ligand modified TCPS and on sIPN over time. IL-1β levels from modified TCPS samples were comparable to those of sIPN samples at 2 h, and concentrations decreased over time. IL-1β protein concentrations across different ligand treated TCPS surfaces were comparable at each time point (Table 2-5). After pretreatment with anti-integrin β1 or β3 antibody or IgG1, IL-1β levels were generally low compared to those without antibody pretreatment at 2 and 24 h. There was no detectable IL-1β protein at 168 h from the samples with antibody pretreatment. At 96 h, however, there were higher IL-1β levels from monocytes pretreated with anti-integrin β1 antibody in the presence of PHSRN and FN modified TCPS compared to other ligand treated TCPS surfaces. Increased IL-1β levels were also observed from samples pretreated with anti-integrin β3 antibody on GGG and RGD modified TCPS (Table 2-5).

Table 2-5. IL-1β protein levels in the supernatant of monocytes cultured in the presence of ligand pre-adsorbed TCPS.

Antibody Pretreatment	Surface Ligands	Culture Time (h)			
		2	24	96	168
None	PBS	35 ± 2 [0.15 ± 0.03]	39 ± 2 [0.21 ± 0.19]	22 ± 9 [0.27 ± 0.10]	13 ± 7 [4.76 ± 2.54]
	GGG	34 ± 4 [0.11 ± 0.02]	40 ± 14 [0.33 ± 0.16]	21 ± 5 [0.22 ± 0.06]	13 ± 8 [2.03 ± 2.24]
	RGD	40 ± 1 [0.10 ± 0.02]	36 ± 10 [0.26 ± 0.08]	27 ± 13 [0.19 ± 0.08]	13 ± 9 [0.57 ± 0.39]
	PHSRN	39 ± 0 [0.14 ± 0.05]	36 ± 4 [0.24 ± 0.08]	20 ± 6 [0.22 ± 0.15]	13 ± 9 [2.25 ± 2.81]
	FN	35 ± 2 [0.10 ± 0.01]	40 ± 19 [0.32 ± 0.17]	23 ± 11 [0.21 ± 0.07]	12 ± 7 [2.44 ± 2.02]
IgG1	PBS	21 ± 2 [0.06 ± 0.01]	22 ± 11 [0.56 ± 0.38]	ND	ND
	RGD	19 ± 4 [0.06 ± 0.02]	14 ± 5 [0.80 ± 0.46]	ND	ND
	FN	28 ± 2 [0.10 ± 0.04]	18 ± 2 [0.70 ± 0.29]	ND	ND
Anti-Integrin β1	PBS	17 ± 1 [0.08 ± 0.01]	15 ± 1 [0.76 ± 0.18]	ND	ND
	GGG	17 ± 0 [0.07 ± 0.01]	18 ± 1 [0.45 ± 0.12]	ND	ND
	RGD	18 ± 0 [0.10 ± 0.02]	21 ± 5 [0.08 ± 0.00]	28 ± 35 [17.62 ± 20.53]	ND
	PHSRN	22 ± 3 [0.09 ± 0.02]	20 ± 2 [0.29 ± 0.06]	101 ± 26 [72.97 ± 32.37]	ND
	FN	23 ± 2* [0.12 ± 0.02]	18 ± 3 [0.37 ± 0.11]	142 ± 32 [128.16 ± 73.04]	ND
Anti-Integrin β3	PBS	18 ± 4 [0.17 ± 0.08]	22 ± 6 [9.83 ± 7.58]	ND	ND
	GGG	21 ± 0 [0.14 ± 0.02]	21 ± 4 [1.26 ± 1.09]	44 ± 10 [19.80 ± 3.85]	ND
	RGD	17 ± 3 [0.10 ± 0.02]	19 ± 5 [0.45 ± 0.16]	58 ± 14 [35.09 ± 8.37]	ND
	PHSRN	24 ± 3 [0.13 ± 0.01]	25 ± 3 [0.43 ± 0.07]	ND	ND
	FN	21 ± 1 [0.11 ± 0.00]	24 ± 1 [0.48 ± 0.07]	ND	ND

IL-1β protein concentration (pg/ml) is shown as mean ± s.e.m, n=3. IL-1β protein amount per cell (fg/cell) normalized to supernatant volume is expressed as mean ± s.e.m, n=3, in brackets "[ ]". Data was analyzed by two-way ANOVA.

* Significantly different compared to the same pretreatment PBS control within respective time point ($p < 0.05$)

ND: not detectable (below 0.3 pg/ml)

At 2 h, IL-1β levels from monocytes without antibody pretreatment were lower than those from 24 and 96 h in the presence of sIPNs. IL-1β concentrations peaked at 24 h and decreased over time after 24 h. Individual ligands did not affect IL-1β protein expression as IL-1β levels from different sIPNs were comparable (Table 2-6). Pretreatment with anti-integrin β1 antibody strongly reduced IL-1β protein expression from monocytes on sIPNs at 24, 96 and 168 h compared to protein levels from sample without antibody pretreatment in the presence of sIPNs (within respective ligand and time point). This decreasing trend was more surface rather than ligand dependent as IL-1β levels from different sIPNs were still comparable at each time point. In other words, monocyte IL-1β expression was similar across those in the presence of TCPS and those in the presence of sIPNs, regardless of peptide adsorbed or ligand conjugated, respectively. IL-1β concentration also peaked at 24 h with anti-integrin β1 antibody pretreatment though the concentrations were significantly lower than those without antibody pretreatment (Table 2-6). Anti-integrin β3 antibody pretreatment more strongly inhibited IL-1β expression in monocytes in the presence of all sIPNs compared to anti-integrin β1 antibody pretreated samples. Pretreatment with IgG1 also inhibited IL-1β expression in monocyte on sIPNs. At 2 and 168 h the inhibition was almost complete for each sample on sIPN. However, at 24 and 96 h the suppressive effect of IgG1 was much less on IL-1β expression in monocytes on GGG and RGD grafted sIPNs (Table 2-6).

Table 2-6. IL-1β protein levels in the supernatant of monocytes cultured in the presence of sIPN with various covalently-immobilized ligands

Antibody Pretreatment	Surface Ligands	Culture Time (h)			
		2	24	96	168
None	MPEG	24 ± 1 [4.28 ± 0.88]	540 ± 197 [15.65 ± 0.88]	77 ± 18 [5.87 ± 2.76]	10 ± 2 [1.13 ± 0.11]
	GGG	60 ± 23 [1.37 ± 0.85]	816 ± 60 [17.96 ± 4.52]	67 ± 15 [3.36 ± 1.61]	12 ± 3 [1.38 ± 0.66]
	RGD	36 ± 20 [0.24 ± 0.22]	671 ± 147 [3.36 ± 0.73]	52 ± 6 [2.14 ± 0.17]	8 ± 3 [0.60 ± 0.31]
	PHSRN	40 ± 10 [0.42 ± 0.11]	475 ± 310 [3.53 ± 3.08]	76 ± 31 [1.26 ± 1.07]	14 ± 2 [1.40 ± 0.70]
IgG1	MPEG	ND	64 ± 79 [5.63 ± 7.08]	6 ± 5** [0.37 ± 0.42]	ND
	GGG	0.4 ± 0.2 [0.04 ± 0.03]	282 ± 162 [60.56 ± 75.62]	50 ± 32 [4.37 ± 2.50]	0.7 ± 0.2** [0.10 ± 0.04]
	RGD	ND	390 ± 27** [29.27 ± 10.83]	39 ± 12 [0.55 ± 0.05]	ND
	PHSRN	0.6 ± 0.4 [0.01 ± 0.01]	71 ± 8 [4.01 ± 0.17]	ND	ND
Anti-Integrin β1	MPEG	40 ± 20 [29.68 ± 18.99]	129 ± 108** [6.12 ± 5.84]	9 ± 2** [38.33 ± 19.41]	2 ± 1 [55.14 ± 38.61]
	GGG	21 ± 10 [60.62 ± 28.32]	133 ± 134** [7.29 ± 2.96]	1 ± 1** [478.12 ± 466.94]	1 ± 0 [57.14 ± 41.23]
	RGD	14 ± 3 [73.72 ± 29.23]	194 ± 97** [3.98 ± 3.20]	16 ± 7** [16.51 ± 9.91]	1 ± 0 [11.07 ± 7.89]
	PHSRN	48 ± 16 [21.34 ± 3.83]	197 ± 92** [6.91 ± 1.73]	12 ± 7** [11.07 ± 7.89]	1 ± 0 [109.92 ± 22.21]
Anti-Integrin β3	MPEG	6 ± 5 [0.56 ± 0.43]	8 ± 7**† [0.47 ± 0.60]	0 ± 0** [0.11 ± 0.12]	1 ± 0 [5.02 ± 6.46]
	GGG	4 ± 2 [0.16 ± 0.09]	9 ± 6**† [0.48 ± 0.59]	4 ± 3** [1.04 ± 0.89]	1 ± 2 [1.13 ± 1.40]
	RGD	6 ± 1 [0.32 ± 0.16]	28 ± 13**† [2.04 ± 1.13]	3 ± 2** [0.35 ± 0.24]	1 ± 1 [0.43 ± 0.34]
	PHSRN	8 ± 2 [0.37 ± 0.36]	15 ± 1**† [0.85 ± 0.10]	4 ± 2** [0.44 ± 0.34]	1 ± 1 [1.01 ± 1.17]

IL-1β protein concentration (pg/ml) is shown as mean ± s.e.m, n=3. IL-1β protein amount per cell (fg/cell) normalized to supernatant volume is expressed as mean ± s.e.m, n=3, in brackets "[ ]". Data was analyzed by two-way ANOVA.

**: Significantly different from corresponding sIPN surface without antibody treatment within respective time point: $p < 0.001$

†: Significantly different from β1 pretreated antibody groups from the corresponding surface and respective time point. $p < 0.05$

ND: not detectable (below 0.3 pg/ml)

As the effects of ligands were more pronounced with sIPN than TCPS samples, the transcriptional level of IL-1β in adherent monocytes on sIPN modified with various peptide ligands were characterized with RT-PCR. For monocytes without antibody pretreatment, the highest level of IL-1β mRNA was at 2 h and decreased through 24 h and 96h, and only a trace amount of IL-1β mRNA was detected at 96 h. There were no significant differences in mRNA expression across ligands within respective time points for samples without antibody pretreatment and thus not marked on Figure 2-3. Similar trends were observed for IgG1 pretreated samples (i.e., decrease over time in IL-1β mRNA after 2 h). However, IL-1β mRNA levels from MPEG grafted sIPN samples increased 4-fold at 24 h with IgG1 pretreatment (Figure 2-3A-D).

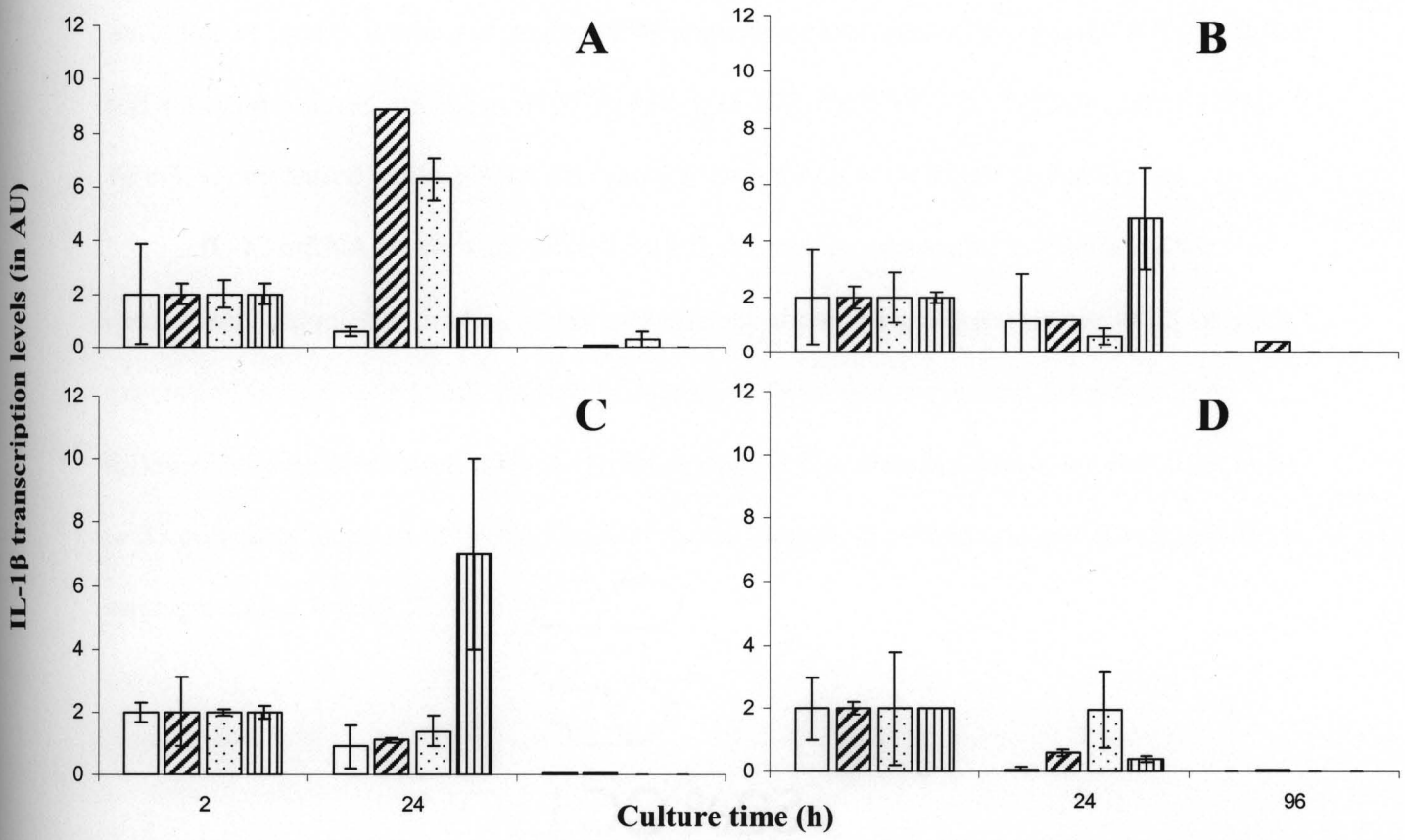

Figure 2-3. IL-1β mRNA expression of cells on MPEG (A), GGG (B), RGD (C) and PHSRN (D) modified sIPN without antibody pretreatment (open bars), with IgG1(hatched bars), or anti-integrin β1 antibody (dotted bars), or with anti-integrin β3 antibody pretreatment (striped bars) The expression levels of IL-1β mRNA were normalized to β-actin.

The effect of antibody pretreatment on IL-1β mRNA expression in adherent monocytes was different with the identity of the ligand grafted onto sIPNs. With anti-integrin β1 antibody pretreatment, IL-1β mRNA from MPEG grafted sIPN samples increased from 2 to 24 h. However, with GGG, RGD or PHSRN grafted sIPNs, there was a slight downregulation of IL-1β mRNA. Only a trace amount of IL-1β mRNA was detected by 96 h for all ligand-grafted sIPN

samples. Pretreatment with anti-integrin β3 antibody also led to different IL-1β mRNA levels according to ligand. All ligand-grafted sIPN samples yielded similar IL-1β mRNA levels at 2 h, and a trace amount of mRNA at 96 h. However, at 24 h, for MPEG or PHSRN-grafted sIPNs, IL-1β mRNA increased while mRNA decreased at 24 h for GGG or RGD-grafted sIPNs.

IL-1β mRNA levels were plotted with IL-1β protein expression in Figure 2-4 for comparison. Samples with no antibody pretreatment showed a gradual decrease in IL-1β mRNA expression from 2 to 96 h, but showed increased IL-1β protein expression from 2 to 24 h, followed by a decrease from 24 to 96 h. The change in IL-1β mRNA levels for anti-integrin β1 or β3 pretreated samples did not correlate with the changes in protein concentrations within the same group and ligand.

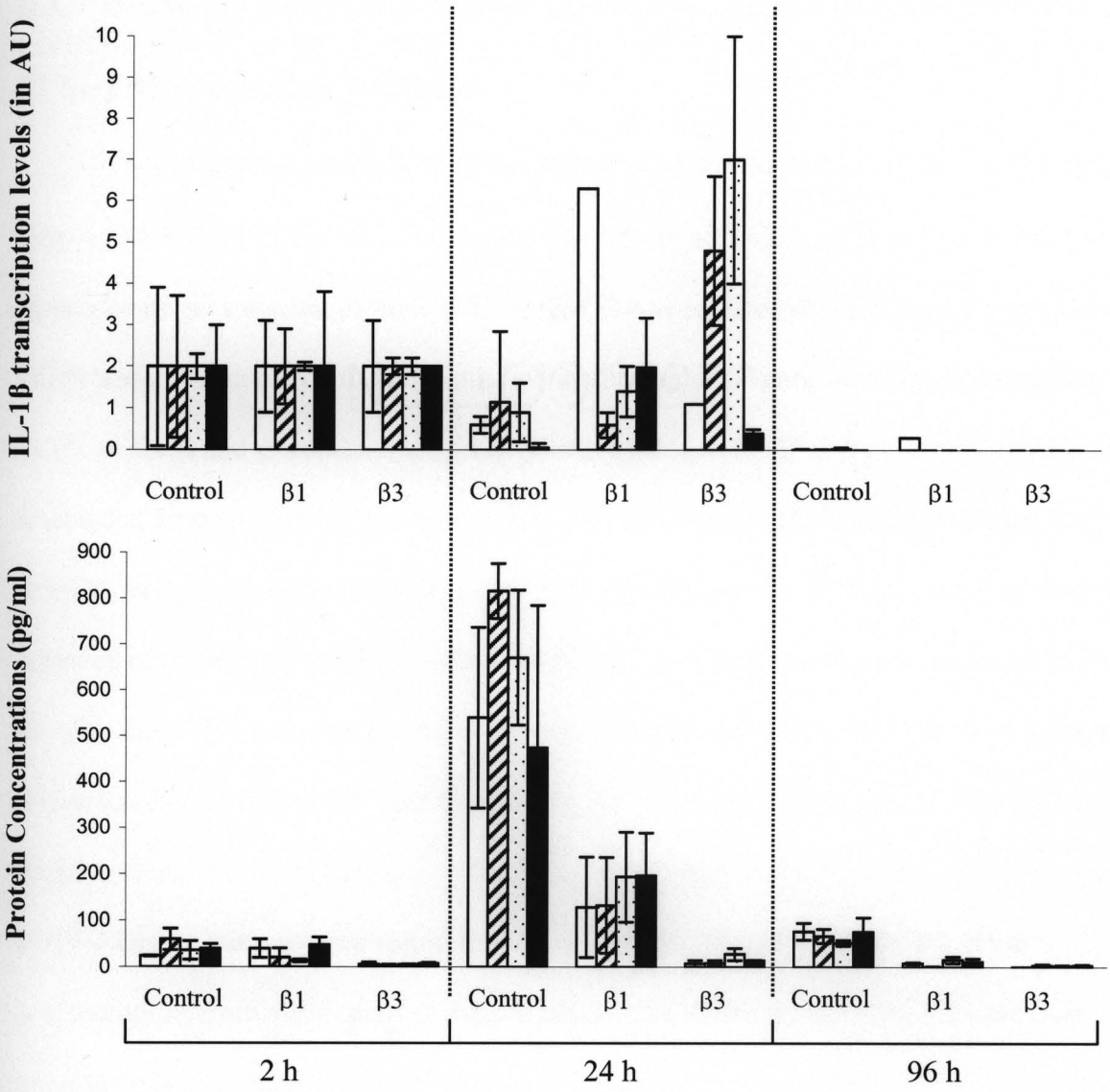

Figure 2-4. IL-1β mRNA and IL-1β protein expression in the presence of sIPNs (from samples with different antibody pretreatments) plotted over time for comparison. IL-1β mRNA expression of cells with anti-integrin β1 or β3 antibody pretreatment did not correlate with IL-1β protein levels. The expression levels of IL-1β mRNA were normalized to β-actin.

Open bars: MPEG modified sIPN; hatched bars: GGG modified sIPN; dotted bars: RGD modified sIPN; black bars: PHSRN modified sIPN.

2.3.3 Monocyte MMP-2/-9 protein and mRNA expression on sIPN: the role of β1 and β3 containing integrins

To characterize MMP-2/-9 protein secretion of monocytes, MMP-2/-9 concentrations were measured via ELISA at 2, 24, 96 and 168 h from all TCPS, sIPN and glutaraldehyde fixed gelatin hydrogel samples. From 2-168 h, MMP-2 was undetectable (below 140 pg/ml) from TCPS and glutaraldehyde fixed gelatin hydrogel samples (Figure 2-5A-D). In the presence of all TCPS surfaces and glutaraldehyde fixed gelatin hydrogel, MMP-9 protein concentration was detected at a range of 1406 to 1926 pg/ml at 2 h, but from 24-168 h, concentrations from TCPS samples were over the maximum detectable level (6000 pg/ml). MMP-2 concentrations in the presence of glutaraldehyde fixed gelatin hydrogel were more comparable to that of TCPS samples than sIPN samples. In various ligand-PEG grafted sIPN, high MMP-2 concentrations of approximately 11,000 pg/ml were detected at 2 h, which were decreased 10-fold by 24 h and concentrations did not significantly change by 96 h (Figure 2-5A,B,C). By 168 h, however, MMP-2 concentrations were approximately 200 pg/ml (Figure 2-5C and D). MMP-2 concentrations from sIPN samples did not statistically differ across ligands within each time point from 2-96 h. MMP-9 concentrations in the presence of all sIPN surfaces were over the detectable limit at all time points except at 24 h, where concentrations in the range of 1133 to 2387 pg/ml were measured. At 24 h, MMP-9 was measured with the lowest MMP-9 concentration for GGG-PEG grafted sIPN compared to all other ligand-PEG grafted sIPN.

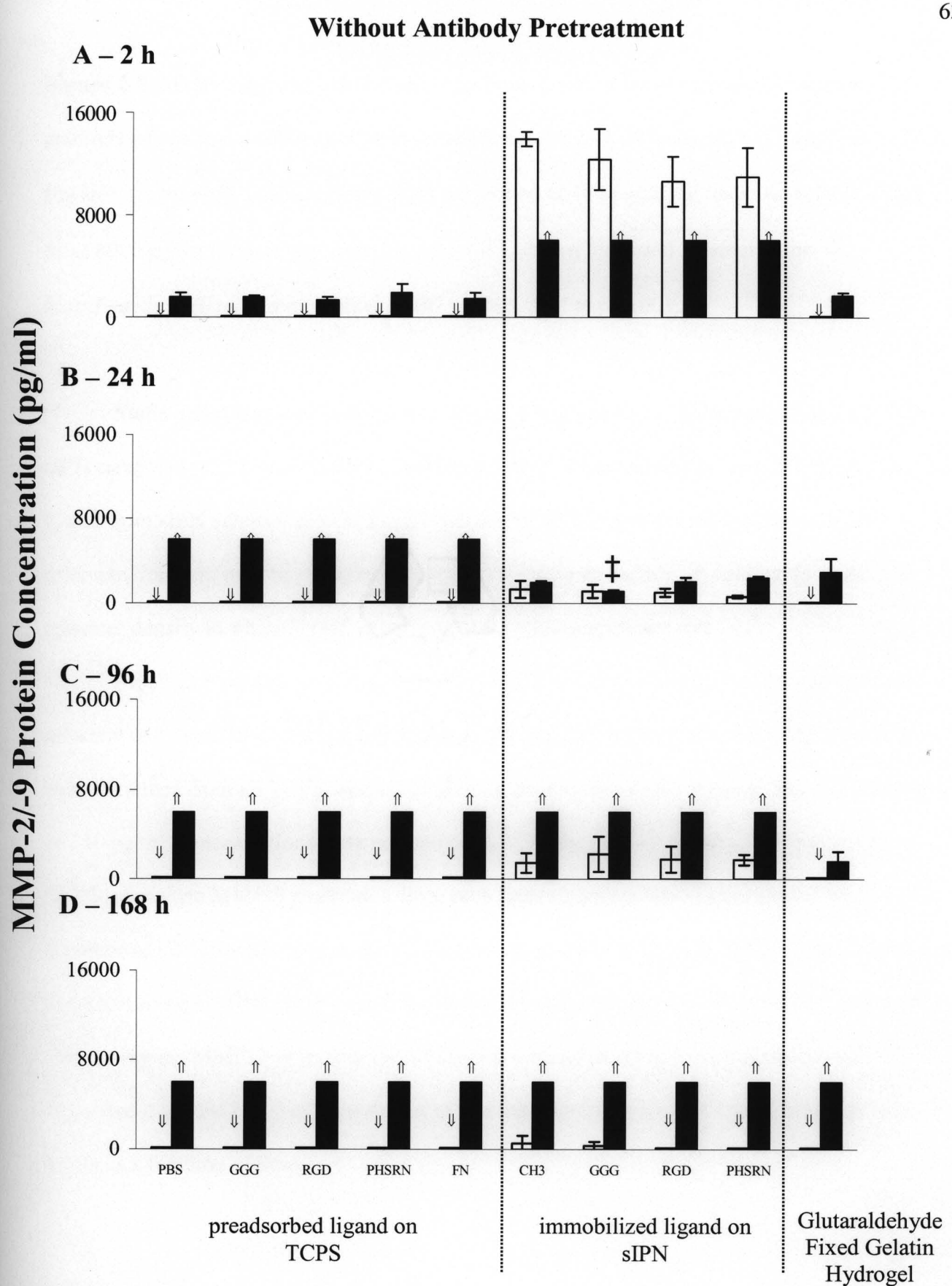
Without Antibody Pretreatment
A – 2 h
B – 24 h
C – 96 h
D – 168 h
16000
8000
0
MMP-2/-9 Protein Concentration (pg/ml)
PBS
GGG
RGD
PHSRN
FN
CH3
GGG
RGD
PHSRN
preadsorbed ligand on TCPS
immobilized ligand on sIPN
Glutaraldehyde Fixed Gelatin Hydrogel

Figure 2-5. MMP-2 (□) and MMP-9 (■) expression levels in human monocytes without antibody pretreatment adhered to various surfaces at 2 h (A), 24 h (B), 96 h (C) and 168 h (D) (mean + s.e.m, n=3). Undetectable values are plotted as 140 pg/ml for under detectable limit (⇓) or as 6000 pg/ml for over the detection limit (⇑), shown for visual representation. ╪ Significantly different from methoxy-PEG grafted sIPN at $p<0.001$.

Statistical analysis of MMP-2 protein concentrations from TCPS samples at 24 h, from sIPN samples at 2, 24, and 96 h, and analysis of MMP-9 concentrations from TCPS samples at 2 h, and from sIPN samples at 24 h, suggested that MMP-2/-9 protein concentration in the microenvironment may be influenced more by the substrate surface, in contrast to monocyte adherent density in which ligand identity played a more significant role.

MMP-2/-9 protein concentrations from TCPS and sIPN samples were normalized to adherent cell densities and presented in Tables 2-7 and 2-8, respectively. As MMP-2 protein concentrations from all TCPS samples at all time points were under the detectable concentration of 140 pg/ml, concentrations were not normalized to adherent cell density. In the presence of TCPS, monocyte MMP-9 production from each ligand samples was similar from 2-96 h. In the presence of sIPNs, monocytes in the presence of methoxy-, GGG-grafted sIPN samples appeared to secrete more MMP-2 protein per cell compared to other ligand-grafted sIPNs at 2 and 24 h. Correlating the MMP-2/-9 protein concentrations with normalized protein concentrations suggested that MMP-2/-9 concentrations within the microenvironment was regulated at specific levels as a function of time.

Table 2-7. MMP-2 and MMP-9 protein concentrations over time normalized to a per cell basis in the presence of TCPS.

	Culture Time (h):			
Surfaces/Ligand Treatment	**2**	**24**	**96**	**168**
MMP-2 Concentration (pg/ml)*	*	*	*	*
MMP-2 Concentration (pg/cell)*	*	*	*	*
MMP-9 Concentration (pg/ml)				
PBS	1571 ± 402	OD	OD	OD
GGG	1546 ± 141	OD	OD	OD
RGD	1406 ± 158	OD	OD	OD
PHSRN	1926 ± 681	OD	OD	OD
FN	1706 ± 476	OD	OD	OD
MMP-9/adherent cell (pg/cell)				
PBS	0.7 ± 0.1	>4.9	>7.1	>145
GGG	0.4 ± 0	>4.6	>6.2	>37
RGD	0.3 ± 0	>4.3	>4.2	>8.2
PHSRN	0.5 ± 0.2	>3.8	>5.5	>52
FN	0.3 ± 0.1	>2.2	>1.4	>11

*All samples from TCPS contained no detectable amount of MMP-2 and thus neither the concentration nor the concentration normalized to adherent cell density is displayed.

OD = over the detection limit of the ELISA kit, 6000 pg/ml. OD was treated as 6000 pg/ml when normalizing to adherent cell density and thus the concentrations for MMP-9/adherent cell (pg/cell) are expressed as >value).

Table 2-8. MMP-2 and MMP-9 protein concentrations over time normalized to a per cell basis in the presence of sIPNs.

	Culture Time (h):			
Surfaces/Ligand Treatment	**2**	**24**	**96**	**168**
MMP-2 Concentration (pg/ml)				
Methoxy	13905 ± 588	1328 ± 794	1441 ± 879	544 ± 700
GGG	12346 ± 2387	1153 ± 615	2244 ± 1589	342 ± 350
RGD	10625 ± 1938	1028 ± 396	1787 ± 1185	ND
PHSRN	11003 ± 2307	650 ± 129	1731 ± 472	ND
MMP-2/adherent cell (pg/cell)				
Methoxy	239 ± 10	25 ± 15	12 ± 7	6 ± 7
GGG	24 ± 5	2 ± 1	13 ± 9	3 ± 3
RGD	6 ± 1	0.5 ± 0.2	8 ± 5	<1
PHSRN	11 ± 2	0.7 ± 0.1	3 ± 1	<1
MMP-9 Concentration (pg/ml)				
Methoxy	OD	1935 ± 173	OD	OD
GGG	OD	1133 ± 119	OD	OD
RGD	OD	2023 ± 415	OD	OD
PHSRN	OD	2387 ± 149	OD	OD
MMP-9/adherent cell (pg/cell)				
Methoxy	>103	36 ± 3	>48	>61
GGG	>112	2 ± 0.2	>35	>54
RGD	>3	1 ± 0.2	>27	>48
PHSRN	>6	2 ± 0.1	>12	>59

ND = not detectable due to the sensitivity of the ELISA kit (below 140pg/ml). ND was treated as 140 pg/ml when normalizing to adherent and thus the concentrations for MMP-2/adherent cell (pg/cell) are expressed as <value).

OD = over the detection limit of the ELISA kit, 6000 pg/ml. OD was treated as 6000 pg/ml when normalizing to adherent cell density and thus the concentrations for MMP-9/adherent cell (pg/cell) are expressed as >value).

To explore the modulation of MMP-2/-9 protein expression by β1 containing integrin receptors, monocytes were treated with anti-integrin β1 antibody prior to seeding onto sIPN and TCPS surfaces and onto glutaraldehyde fixed gelatin hydrogel. MMP-2/-9 protein expressions in these samples were analyzed at each culture time point. As described above, MMP-2 protein levels in TCPS samples without antibody pretreatment were undetectable at all time points. In contrast, when monocytes were pretreated with anti-integrin β1 antibody and in the presence of TCPS, MMP-2 concentrations were measured at steady concentration in the range of 1488-4004 pg/ml from 2-96 h, but undetectable by 168 h (Figure 2-6A-D).

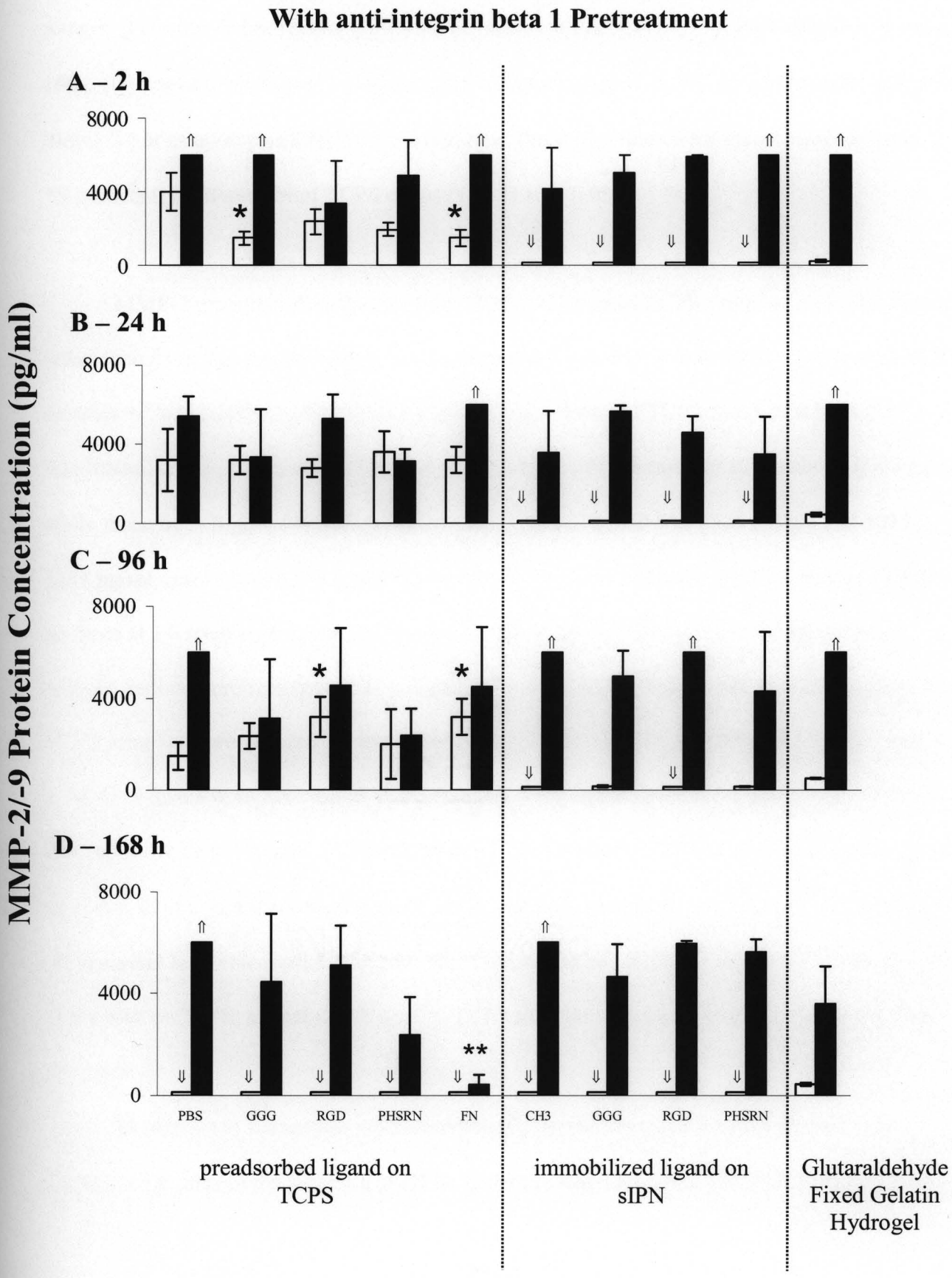
With anti-integrin beta 1 Pretreatment
A – 2 h
B – 24 h
C – 96 h
D – 168 h
MMP-2/-9 Protein Concentration (pg/ml)
8000
4000
0
PBS
GGG
RGD
PHSRN
FN
CH3
GGG
RGD
PHSRN
preadsorbed ligand on TCPS
immobilized ligand on sIPN
Glutaraldehyde Fixed Gelatin Hydrogel

Figure 2-6. MMP-2 (□) and MMP-9 (■) expression levels in human monocytes with anti-integrin β1 antibody pretreatment adhered to various surfaces at 2 h (A), 24 h (B), 96 h (C) and 168 h (D) (mean + s.e.m, n=3). Undetectable values are plotted as 140 pg/ml for under detectable limit (⇓) or as 6000 pg/ml for over the detection limit (⇑), shown for visual representation. *Significantly different from TCPS control (PBS) at $p<0.05$.

MMP-2 protein concentrations from GGG-, FN-treated TCPS samples were significantly lower than from non-ligand treated TCPS samples at 2 h. MMP-2 from RGD-, FN-treated TCPS samples were significantly higher than from non-ligand treated TCPS samples at 96 h. At 2 h, non-ligand, GGG-, FN- treated TCPS samples yielded MMP-9 concentrations above 6000 pg/ml while those from RGD-, PHSRN-treated samples yielded MMP-9 at 3896 ± 2404 and 4015 ± 1247 pg/ml, respectively. The MMP-9 concentrations from the RGD-, PHSRN-treated TCPS surfaces at 2 h were significantly higher than MMP-9 concentrations from TCPS samples without antibody pretreatment at 2 h (Figure 2-5A). From 24-168 h, MMP-9 concentrations from TCPS samples were generally detected between 2300 and 5100 pg/ml (Figure 2-5A-D). At 168 h, MMP-9 levels from FN-treated TCPS samples were significantly lower than concentrations from all other ligand-treated TCPS except non-ligand treated TCPS samples, which had over the detection limit concentrations and could not be statically compared. Anti-integrin β1 antibody pretreatment led to elevated MMP-2 protein expressions but generally decreased MMP-9 expression on TCPS surfaces compared to TCPS samples with no antibody pretreatment from 24-168 h.

In contrast to monocytes without antibody pretreatment, anti-integrin β1 antibody pretreated samples in the presence of sIPNs generally had no detectable MMP-2 (Figure 2-6A-

D). While MMP-9 levels from non-antibody pretreated monocytes on sIPN samples decreased from 2-24 h and increased from 24-96 h, MMP-9 levels from anti-integrin β1 antibody pretreated samples in the presence of sIPNs were generally detected at a constant level of approximately 4800 pg/ml from 2 through 168 h. Comparing samples within detectable MMP-9 concentrations, no statistical differences were observed across various ligand-grafted sIPNs at all time points. MMP-2 from glutaraldehyde fixed gelatin hydrogel samples were detected at a constant level of approximately 400 pg/ml from 2-168 h, while MMP-9 was over 6000 pg/ml from 2-96 h and 2654 ± 992 pg/ml at 168 h.

To examine the effect of β3 containing integrin receptors in modulating MMP-2/-9 expression, monocytes were pretreated with anti-integrin β3 antibody prior to being seeded on various surfaces. Anti-integrin β3 antibody pretreated monocytes on non-ligand and RGD-treated TCPS, MMP-2 concentrations were detected approximately at 1000 pg/ml from 2-96 h (Figure 2-7A-C). The MMP-2 expressions were similar to that of anti-integrin β1 antibody pretreated monocytes in the presence of TCPS. However, concentrations from anti-integrin β3 treated monocytes were approximately half the concentration from β1 antibody treated samples. At 96 h, significantly higher MMP-2 concentrations were detected from GGG-treated TCPS sample compared to no ligand-treated TCPS samples. MMP-2 concentrations from PHSRN-, FN-treated TCPS were similar in their two-fold increase in concentration from 2-24 h and three-fold decrease in concentration by 96 h (Figure 2-7A-C).

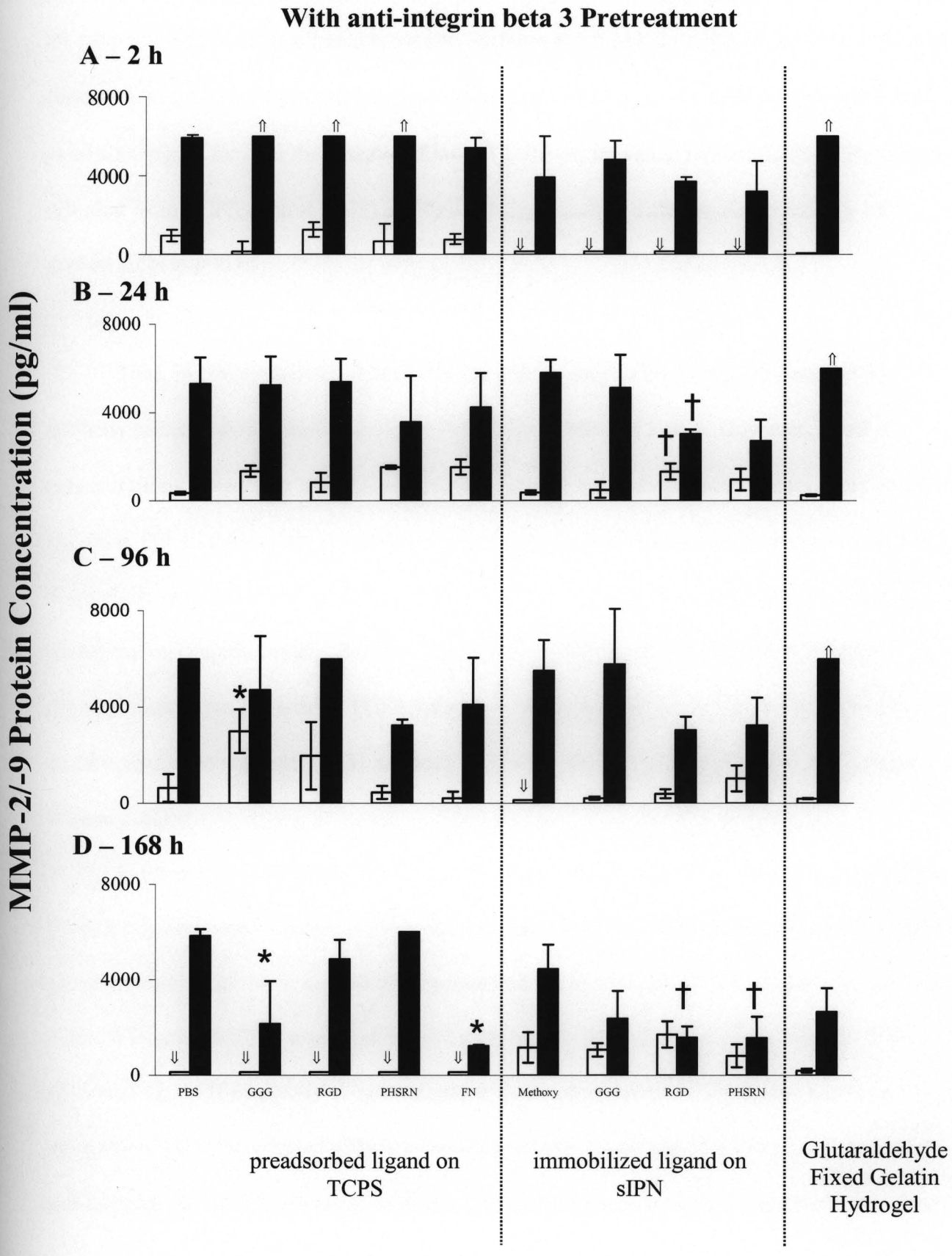
With anti-integrin beta 3 Pretreatment
A – 2 h
B – 24 h
C – 96 h
D – 168 h
MMP-2/-9 Protein Concentration (pg/ml)
8000
4000
0
PBS
GGG
RGD
PHSRN
FN
Methoxy
GGG
RGD
PHSRN
preadsorbed ligand on TCPS
immobilized ligand on sIPN
Glutaraldehyde Fixed Gelatin Hydrogel

Figure 2-7. MMP-2 (□) and MMP-9 (■) expression levels in human monocytes with anti-integrin β3 antibody pretreatment adhered to various surfaces at 2 h (A), 24 h (B), 96 h (C) and 168 h (D) (mean + s.e.m, n=3). Undetectable values are plotted as 140 pg/ml for under detectable limit (⇓) or as 6000 pg/ml for over the detection limit (⇑), shown for visual representation. *Significantly different from TCPS control (PBS) at $p<0.05$. † Significantly different from methoxy-PEG grafted sIPN at $p<0.05$.

Thus, in contrast to non-antibody pretreated monocytes on TCPS, anti-integrin β3 antibody pretreated monocytes expressed detectable MMP-2 at 2-96 h. However, MMP-2 concentrations were lower compared to anti-integrin β1 antibody pretreated monocytes on TCPS at 2-96 h. For all three antibody pretreatment conditions, MMP-2 could not be detected at 168 h. From either anti-integrin β1 or β3 treatments, MMP-9 from TCPS samples were detected at concentrations approximately 5000-6000 pg/ml or above from 2-96 h. At 168 h, MMP-9 concentrations from FN-treated TCPS samples were lower than the no ligand treated TCPS surface, similar to anti-integrin β1 antibody pretreated samples on FN-treated TCPS samples (Figure 2-6D).

In the presence of sIPNs, MMP-2 levels were not detected at 2 h, similar to anti-integrin β1 antibody pretreated samples in the presence of sIPNs at 2 h. From 24-168 h, however, MMP-2 concentrations similar to non-antibody pretreated monocytes on sIPNs were detected. At 24 h, RGD-PEG grafted sIPNs expressed significantly higher MMP-2 compared to methoxy-PEG grafted sIPN. At 168 h, MMP-2 concentrations were approximately 1000 pg/ml, significantly higher from all sIPN samples without antibody pretreatment or with anti-integrin β1 antibody pretreatment. MMP-9 levels were comparable to that from anti-integrin β1 antibody pretreated

samples on sIPNs from 2-96 h. At 168 h, MMP-9 concentrations were lower than that from anti-integrin β1 antibody pretreated samples on sIPNs, particularly from RGD-, PHSRN-PEG grafted sIPNs.

For cells pretreated with IgG1, MMP-2 protein levels in the presence of RGD-treated TCPS surfaces were not detectable from 2-24 h, but 2238 ± 1252 pg/ml at 96 h and in the presence of methoxy-, RGD-grafted sIPN samples, not detectable from 2-96 h. Glutaraldehyde fixed gelatin samples yielded non-detectable MMP-2 protein concentrations for IgG1 pretreated monocytes from 2-24 h, but at 96 h, 4599 ± 2491 pg/ml was measured. MMP-9 protein concentrations were over the detectable concentration of 6000 pg/ml for RGD-treated TCPS, methoxy-, RGD-grafted sIPN, and glutaraldehyde fixed gelatin hydrogel samples from 2-168 h.

In summary, from 2-96 h, anti-integrin β3 antibody pretreated monocytes expressed less MMP-2 compared to anti-integrin β1 antibody pretreated monocytes in the presence of TCPS. In the presence of sIPNs, however, anti-integrin β3 antibody pretreatment led to an increased MMP-2 expression at times 24-168 h compared to anti-integrin β1 antibody pretreated monocytes. In the presence of sIPNs anti-integrin β1 antibody pretreated monocytes expressed similar MMP-9 concentrations to that of anti-integrin β3 antibody pretreated cells from 2-96 h. However, at 168 h, β3 antibody pretreated monocytes expressed less MMP-9 than β1 antibody pretreated monocytes. Both antibody treatments elicited a significantly lower MMP-9 expression on FN-treated TCPS compared to the non-ligand treated TCPS surface at 168 h.

From glutaraldehyde fixed gelatin hydrogel samples, both MMP-2 and MMP-9 expression patterns from anti-integrin β1 antibody pretreated samples were similar to that of anti-integrin β1 antibody pretreated samples on glutaraldehyde fixed gelatin hydrogels (Figure 2-6A-D). To test the correlation between protein expression profiles and regulatory trends of those

proteins at the genetic level, mRNA levels in monocytes with or without antibody pretreatment conditions were characterized.

As the effects of ligands on cell adhesion and protein release were more pronounced with sIPN than TCPS samples and we focused on ligand identity and ligand mobility, transcript levels of MMP-2/-9 in adherent monocytes in the presence of various modified sIPNs were characterized with RT-PCR. MMP-2 mRNA analysis was carried for all sIPN samples under all antibody pretreatment conditions from 2-96 h. However, as no visible bands could be detected in any of the samples by the Scion imaging program, MMP-2 mRNA levels could not be measured and thus the data is not shown.

With methoxy-PEG grafted sIPN samples, there was an upregulation of MMP-9 mRNA over time for non-antibody pretreated and anti-integrin β1 antibody pretreated monocytes (Figure 2-8). When pretreated with anti-integrin β3 antibody, adherent monocytes on methoxy-PEG grafted sIPN showed similar MMP-9 mRNA as anti-integrin β1 antibody pretreated samples at 2 h, but mRNA was barely detectable from 24-96 h. Monocytes under all three pretreatment groups (i.e. no antibody, anti-integrin β1 or β3 antibody pretreated) from GGG-PEG grafted sIPN appeared to exhibit an upregulation of MMP-9 mRNA from 2-24 h (Figure 2-9). At 96 h, MMP-9 mRNA was downregulated for anti-integrin β1 pretreated monocytes by 7-fold. Anti-integrin β3 antibody pretreated monocytes' mRNA patterns deviated from the other pretreatment groups, similar to that of methoxy-PEG grafted sIPN samples, and upregulated MMP-9 mRNA by 3-fold. Adherent monocytes without antibody pretreatment from RGD-PEG grafted sIPN samples showed a consistent increase in MMP-9 mRNA expression from 2-96 h (Figure 2-10).

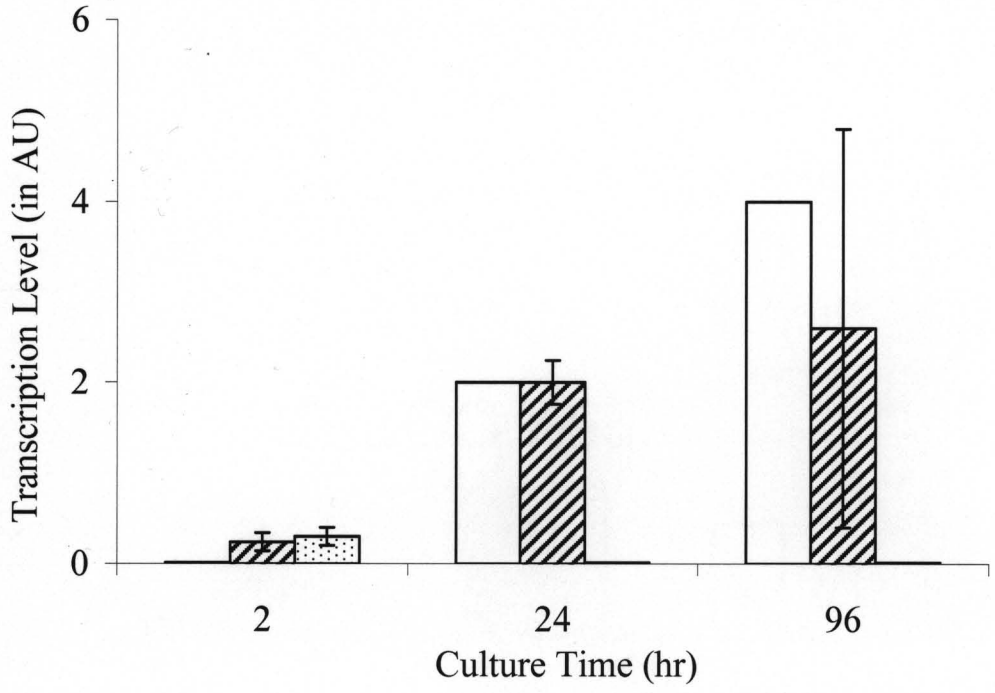

Figure 2-8. MMP-9 mRNA expression in adherent monocytes on methoxy-PEG grafted sIPN at 2, 24, and 96 h, with no Ab pretreatment (▭), with anti-integrin β1 Ab pretreatment (▨), or with anti-integrin β3 Ab pretreatment (▭). mRNA MMP-9 levels were normalized to β-actin (presented in mean ± s.e.m, n=2 except no antibody pretreatment, n=1).

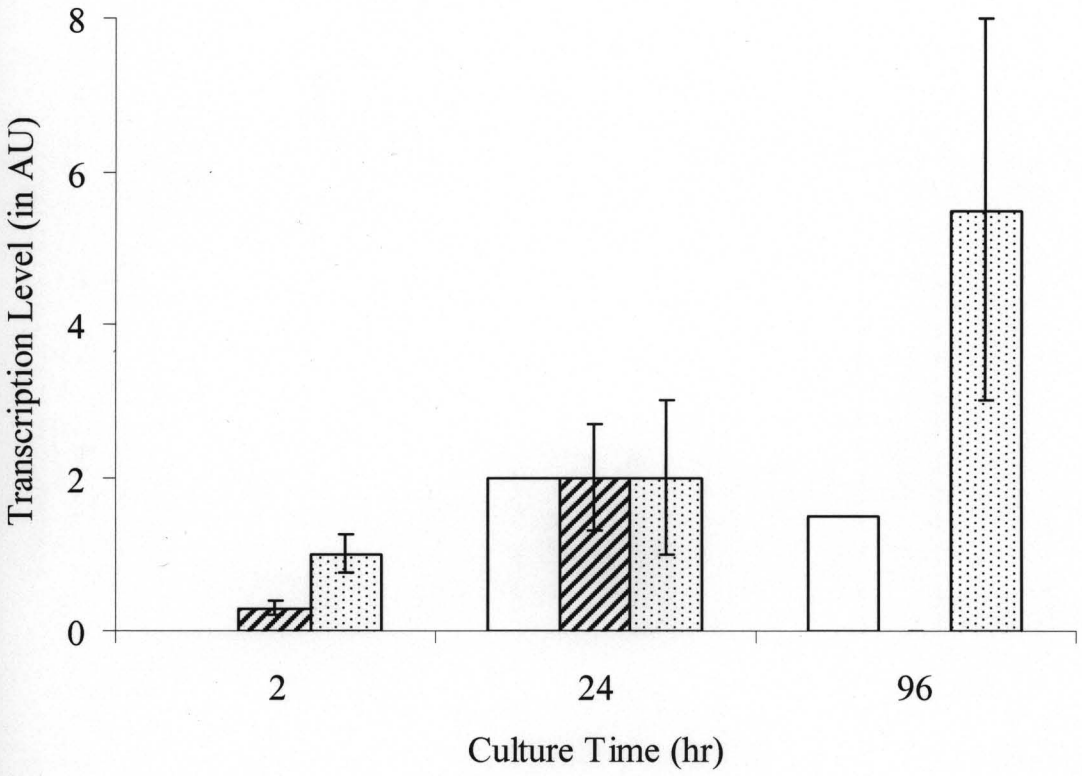

Figure 2-9. MMP-9 mRNA expression in adherent monocytes on GGG-PEG grafted sIPN at 2, 24, and 96 h, with no antibody pretreatment (▭), with anti-integrin β1 antibody pretreatment (▨), or with anti-integrin β3 antibody pretreatment (▭). mRNA MMP-9 levels were normalized to β-actin (presented in mean ± s.e.m, n=2 except no antibody pretreatment, n=1).

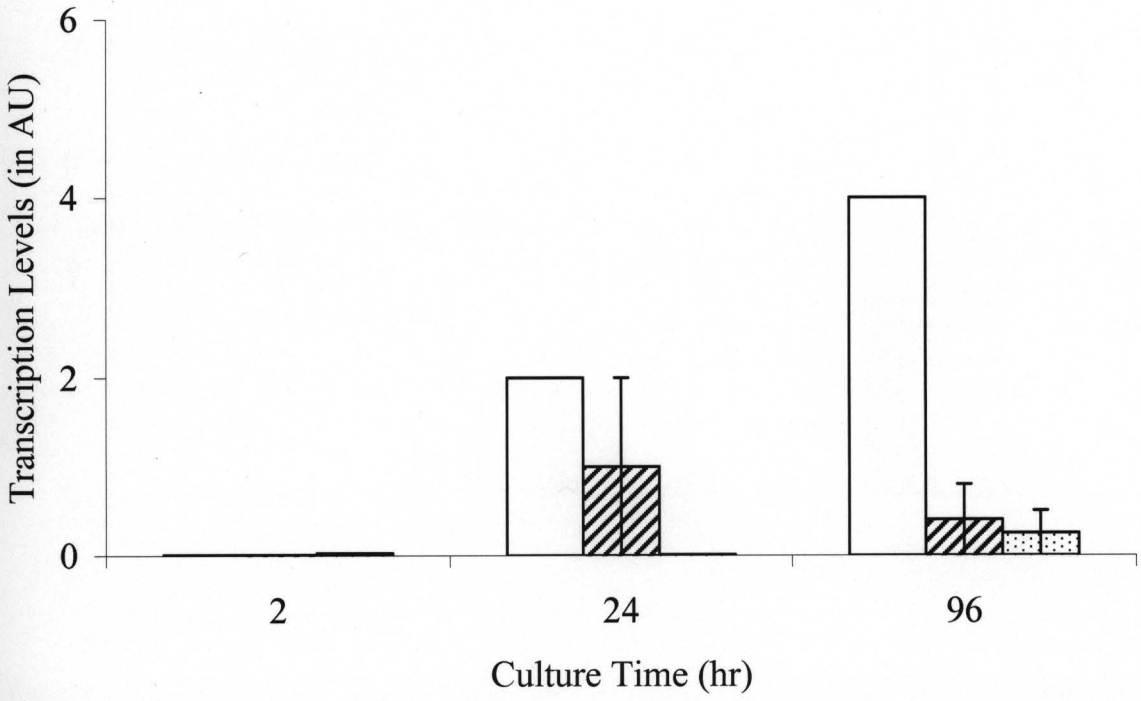

Figure 2-10. MMP-9 mRNA expression in adherent monocytes on RGD-PEG grafted sIPN at 2, 24, and 96 h, with no antibody pretreatment (▭), with anti-integrin β1 antibody pretreatment (▨), or with anti-integrin β3 antibody pretreatment (▭). mRNA MMP-9 levels were normalized to β-actin (presented in mean ± s.e.m, n=2 except no antibody pretreatment, n=1).

Samples from the anti-integrin β1 antibody pretreatment group also showed a 200-fold increase in mRNA expression from 2 to 24 h and did not significantly change in expression by 96 h. Unlike the anti-integrin β1 antibody pretreatment group, anti-integrin β3 antibody pretreated samples appeared to increase only at 96 h. In the presence of PHSRN-PEG grafted sIPN, adherent monocytes from all three antibody pretreatment conditions showed a general increase in MMP-9 mRNA over time (Figure 2-11).

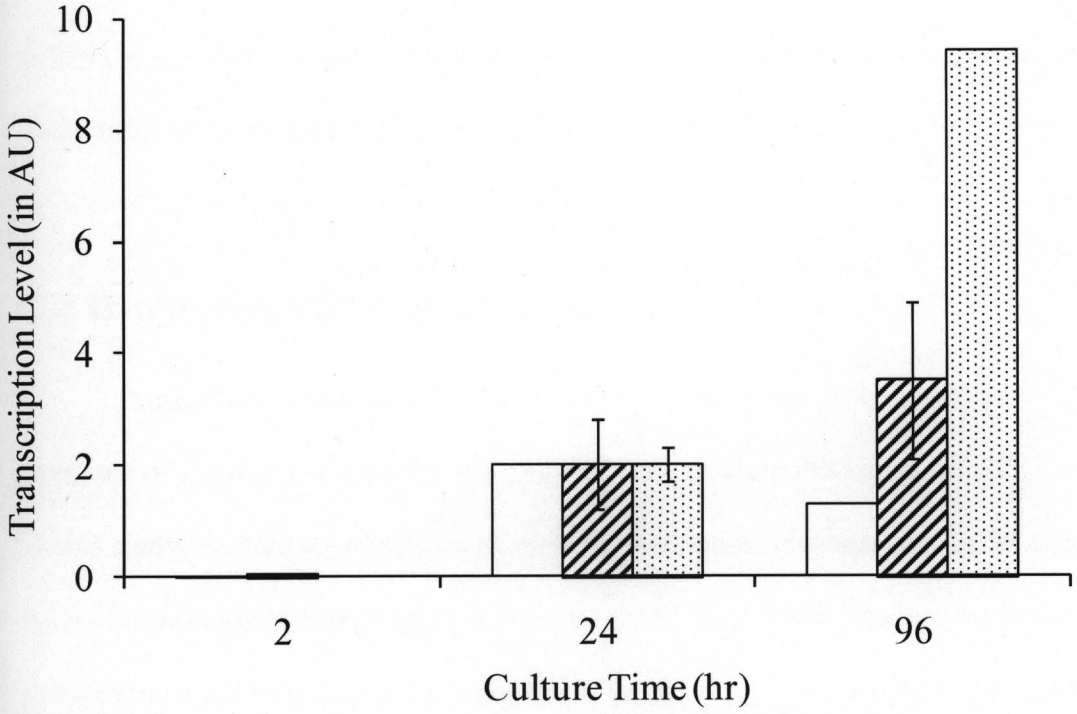

Figure 2-11. MMP-9 mRNA expression in adherent monocytes on PHSRN-PEG grafted sIPN at 2, 24, and 96 h, with no antibody pretreatment (▭), with anti-integrin β1 antibody pretreatment (▨), or with anti-integrin β3 antibody pretreatment (▭). mRNA MMP-9 levels were normalized to β-actin (presented in mean ± s.e.m, n=2 except no antibody pretreatment, n=1).

In summary, without antibody pretreatment, MMP-9 mRNA was generally upregulated with time and downregulated less than 1-fold at 96 h only for GGG-, PHSRN-PEG grafted sIPN samples. Ligand independent upregulation in MMP-9 mRNA at 24 and 96 h correlated with a significant increase in ligand independent protein concentrations measured at 96 and 168 h, respectively (Figure 2-5C). Anti-integrin β1 antibody pretreated cells upregulated MMP-9 mRNA over time, with the exception of RGD-grafted sIPN, where downregulation of mRNA was observed from 24-96 h. Anti-integrin β3 antibody pretreated monocytes in the presence of all sIPNs, except methoxy-grafted sIPN, increased MMP-9 mRNA production from 24-96 h.

However, with anti-integrin β1 or β3 pretreated groups, neither up or downregulatory patterns of mRNA from 2-96 h correlated with the protein expression patterns, which were relatively high and consistent from 2-96 h (Figures 2-6A-C and 2-7A-C).

2.4 Discussion and Conclusions

Integrin mediated monocyte adhesion and subsequent protein and gene expression in the presence of FN-derived peptides immobilized onto flexible PEG arms on sIPNs were examined in this study. As monocytes play a crucial role in immune response and ECM turnover, which are both critical in the normal progression of wound healing, understanding the intricate responses of monocytes at the biomaterial-tissue interface is essential. Here, we characterized monocyte adhesion and subsequent IL-1β and MMP-2/-9 protein and mRNA expression in the presence of gelatin-based sIPNs.

Though monocyte adhesion and subsequent protein release to peptide adsorbed materials are characterized in literature, not many reports on the monocyte behavior in response to peptide grafted hydrogel surfaces currently exist, though rapidly growing. There is much literature on the integrin-mediated interaction of cells with bioadhesive sequences presented onto a biomaterial [52]. In 1992, McNally and Anderson demonstrated the critical role of β1 and β2 integrins in mediating macrophage adhesion and foreign body giant cell formation onto a RGD adsorbed TCPS surface. This important work explored monocyte adhesion and fusion as controlled by RGD, and our work sheds light on human derived monocyte response to the RGD peptide as presented on a biomaterial scaffold designed to be in contact with the human dermis rather than adsorbed onto TCPS [12]. This work presents one of the first studies in which the molecular

mechanisms behind human blood derived monocyte response to peptides covalently grafted and presented by a linker is examined.

Higher adherent cell density on RGD modified TCPS and grafted sIPN indicates that RGD was an important factor in promoting monocyte adhesion on these surfaces. It is shown above that monocyte adhesion on FN-derived peptides immobilized on flexible PEG arms is mediated by β1 and β3 containing integrin receptors. Compared to corresponding peptide-treated TCPS surfaces, adherent monocyte densities on sIPNs were generally lower. PEG, one of the components of sIPN, may have contributed to the low cell density. This phenomenon suggests that the physicochemical characteristics of the substratum modulate monocyte adhesion. Monocyte adherent density was drastically higher for RGD-PEG grafted sIPN samples compared to sIPNs with other ligands grafted onto the flexible PEG arm (Tables 2-3 and 2-4). When monocytes were treated with anti-integrin β1 or β3 antibody, adherent cell density on RGD-, PHSRN-PEG grafted sIPNs was greatly reduced, demonstrating that both β1 and β3 containing integrins play a critical role in monocyte adhesion onto FN-derived peptides immobilized on flexible PEG arm. This is consistent with other findings where integrin-mediated cell adhesion was dependent on both ligand identity as well as ligand presentation [22,12,16].

Pretreatment with anti-integrin β1 or β3 antibody decreased monocyte cell densities on TCPS at 2 h. The data demonstrate that β1 or β3 containing integrins are involved in mediating monocyte adhesive activity on TCPS at earlier stages. After 2 h, adherent monocyte density on TCPS was decreased further by incubation with either of the anti-integrin β antibodies or IgG1, suggesting that non-specific IgG1 inhibits monocyte attachment on TCPS and this attachment may not be specifically mediated by β1- or β3-containing integrins. Monocyte adhesion on RGD immobilized sIPN is mediated by either β1- or β3-containing integrin as anti-integrin β1 or β3

antibody rather than IgG1 pretreatment affects the adherent monocyte densities. The binding of anti-integrin β1 or β3 antibody to β1 or β3 integrins, respectively, disrupts the receptors' dimerization, leading to a subsequent loss binding capability to the RGD grafted on the sIPN. Thus, on sIPNs, both the ligand identity and the substrate are involved in mediating monocyte adhesion. The integrin receptor can also bind other ligands besides the RGD motif, such as collagen and the C-terminal heparin-binding domain of FN [4,53]. Moreover, the activation of other adhesive molecules, such as β2 integrin, L-selectins ICAM, VCAM, also promotes cell adhesion with varying circumstances [54-56]. In this study the antibody incubation also inhibited monocyte adhesion on the surfaces that did not contain the RGD sequence suggesting that the pretreatment with antibody also affected monocyte binding onto other ligands.

IL-1β plays a critical role in the inflammatory process. It has been reported that in inflamed tissue the IL-1β was increased compared to the normal tissue and [57]. In this study, the decrease in IL-1β levels in each microenvironment in the presence of TCPS over time may have been partly due to the low adherent cell numbers. IL-1β expression in monocytes from all sIPN samples at 24 and 96 h increased, but this increase did not occur in monocytes with modified TCPS, suggesting that the substrate property is important in modifying cell behavior [58,59]. The increase in IL-1β protein at 24 h in sIPN samples unlike the decreasing IL-1β protein over time in the presence of TCPS suggests that the components in the sIPNs induce IL-1β in monocytes. It has been reported that the ligand-integrin binding can modulate the efficiency of intracellular signaling pathways, such as MAP kinase cascade, resulting in the change of gene and protein expressions [60,61]. Monocytic IL-1β protein expression in the presence of sIPNs did not correlate with adhesion cell density as the monocyte densities on each sIPNs were similar between 2 and 24 h while the IL-1β concentration at 24 h was significantly higher than at 2 h.

Moreover, cell density was dependent on the presence of the RGD sequence, but monocytes on RGD grafted sIPN did not express higher levels of IL-1β protein. The overall concentration of IL-1β protein microenvironment may play a significant role in monocytic IL-1β protein and mRNA expression. In a previous study, we described that in the presence of various ligand grafted sIPN, IL-1β concentration in inflammatory exudates of subcutaneous cage implantation decreased from day 4 to day 7 [62]. The concentration of IL-1β in this study had a similar trend in sIPN samples from 24 h.

After antibody pretreatment, lower IL-1β protein levels from monocytes on TCPS may have been partly the result of lower cell densities. At 96 h, however, there was an increase in IL-1β protein expression in some of peptide modified TCPS samples, indicating that the binding of anti-integrin β1 or β3 antibody increases IL-1β expression in monocytes from 24 to 96 h, depending on the ligand identity. After antibody pretreatment a ligand-independent decrease in IL-1β protein expression from sIPN samples at 24 h was observed compared to samples without antibody pretreatment within 24 h. This decrease in IL-1β concentration suggests that the blocking of integrin β1 or β3 subunit decreases the stimulating effect of integrin signaling pathways, which can induce cells to express IL-1β. These results imply that either β1 or β3 integrin are involved in modulating IL-1β expression in monocytes on sIPNs. The pretreatment with either of anti-integrin β1 or β3 antibody or IgG1 decreased IL-1β expression, but the increased IL-1β protein expression on sIPNs at 24 h was still maintained in the samples treated by anti-integrin β1 antibody or IgG1. These results show that β3 integrin involvement in IL-1β expression in monocytes plays a more significant role in the presence of sIPNs.

IL-1β mRNA expression in monocytes pretreated with antibody was influenced by the peptide identity. At 24 h the pretreatment with anti-integrin β1 or β3 antibody changed IL-1β

mRNA expression in monocytes on sIPNs. The change in IL-1β mRNA, however, did not accompany changes at the translation level, as low IL-1β protein levels for all sIPN samples at 96 h were observed. The results showed that the increase in IL-1β mRNA transcription was not necessarily followed by the translation of IL-1β protein. Our results suggest that anti-integrin antibody serves to regulate gene expression in the cell and the mRNA transcription in the presence of the peptide-modified sIPN substrate is regulated by the activation of unique signaling pathways modulated by peptide identity after integrin complexation with antibody [63].

As integrins may mediate monocyte attachment to ECM proteins and possibly the localization of MMPs [33], we also characterized monocyte MMP-2/-9 protein regulation in the presence ligand-PEG grafted sIPN. In contrast to monocyte adhesion, MMP-2/-9 protein and mRNA expression was influenced by surface rather than ligand identity. MMP-2 protein was not detected in the presence of TCPS or glutaraldehyde fixed gelatin hydrogels at any time. However, in the presence of sIPNs, an initially high concentration of MMP-2 followed by a gradual decrease in concentration over time was measured (Figure 2-5A-D). MMP-9 protein expression trends were similar to MMP-2 trends from 2-96 h in the presence of sIPNs. Both MMP-2 and MMP-9 levels were normalized to adherent cell density and presented in Tables 2-7 and 2-8 and MMP-9 protein amount per cell did not differ across various ligand treated TCPS surface at 2 h and possibly through 168 h. However, in the presence of methoxy-grafted sIPNs, the data suggests that monocytes produced MMP-2 protein and possibly MMP-9 protein in higher concentrations compared to GGG-, RGD-, or PHSRN-grafted sIPNs at 2 and 24 h. Comparing trends between not normalized MMP-2/-9 protein concentrations and normalized concentrations (to adherent cell densities) as a function of time suggested that MMP-2/-9 concentrations in the microenvironment was regulated in the presence of different substrates.

Representative MMP-2 and MMP-9 concentrations over time from sIPN groups without antibody treatment are shown in Figure 2-12 and the data also suggests that the gelatinases may be coordinated in their secretion into their microenvironment in the presence of sIPNs.

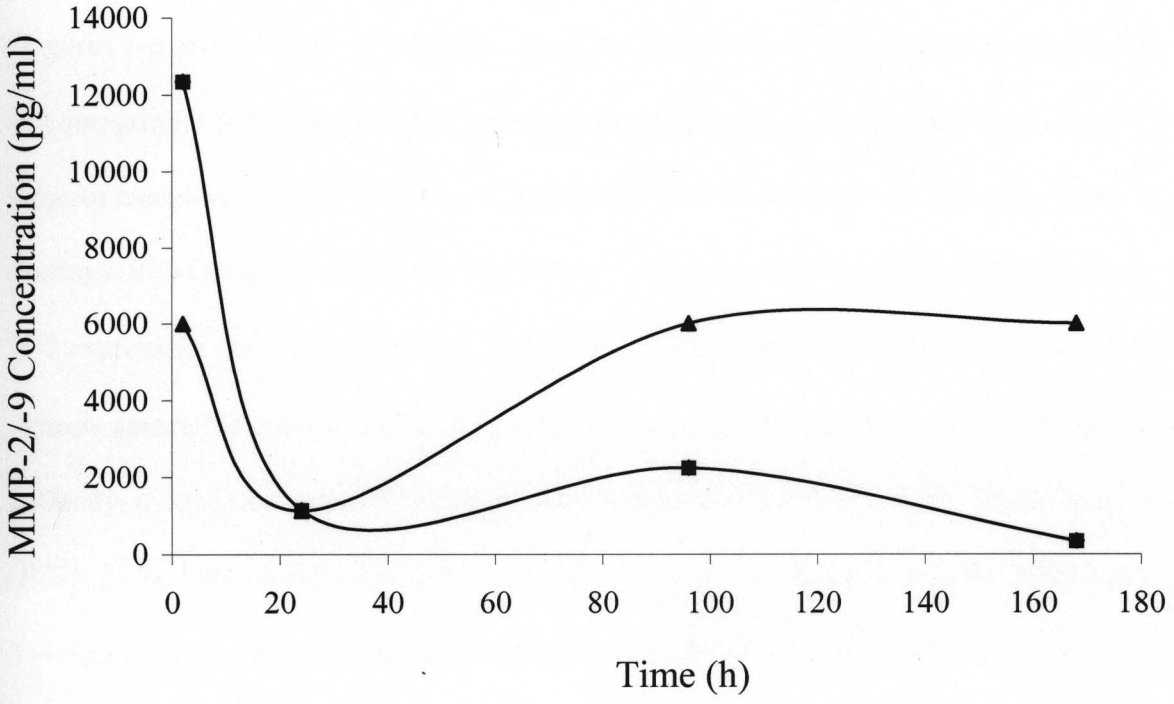

Figure 2-12. Overlay of MMP-2 (▲) and MMP-9 (■) profiles over time from monocytes without antibody treatment adhered to GGG-PEG grafted sIPN. Curves are representative of MMP-2/-9 expression patterns for sIPNs grafted with other ligands.

Collagen type IV has been reported to expose a cryptic site when degraded to gelatin and αVβ3 integrin receptors can bind to this site [31,64]. The gelatin backbone of the sIPNs may allow a clearer exposure of this site than the rigid gelatin strands fixed by glutaraldehyde in the gelatin hydrogels. Thus, not only is the presence of gelatin critical in inducing MMP-2 concentrations, but the physicochemical state of gelatin also plays an important role. Further

examination of the activity of MMP-2/-9 proteins and the amount of active MMP-2/-9 proteins present in the sIPN environment as a function of time may also allow investigation in design for actuated drug delivery incorporating MMP sensitive sequences into tissue engineering scaffolds.

In the presence of TCPS and glutaraldehyde fixed gelatin hydrogels, MMP-2 protein expression trends were similar between anti-integrin β1 and β3 antibody pretreated groups (Figures 2-6 and 2-7), but with MMP-2 protein concentrations being higher in the presence of anti-integrin β1 antibody pretreated monocytes. RGD-independent interactions between αVβ3 integrin receptors and MMP-2 as demonstrated by Silletti and others [31] could explain these findings. In the presence of sIPNs, protein expression was significantly different from the MMP-2/-9 expression in the presence of TCPS. Anti-integrin β1 antibody pretreated monocytes did not express detectable concentrations of MMP-2 protein, but when pretreated with anti-integrin β3 antibody, monocytes secreted increased concentrations of MMP-2 protein. Thus, in the presence sIPNs, β1 containing integrins may have played a more significant role in the induction of MMP-2 proteins, in contrast to the increased MMP-2 protein expression patterns with β3 containing integrins in the presence of TCPS. MMP-9 protein expression, however, was influenced more by β3 containing integrins, especially at 168 h, as RGD-, PHSRN-PEG grafted sIPN expression significantly lower MMP-9 protein compared to that from methoxy-PEG grafted sIPN samples (Figure 2-8).

With respect to gene regulation, as MMP-2 mRNA was not detectable at any time point, the MMP-2 protein may be synthesized and stored in granules [65] and released over time in the presence of sIPNs. Without antibody pretreatment, MMP-9 mRNA was generally upregulated over time in the presence of sIPNs. MMP-9 regulation may not be ligand specific as monocytes in the presence of methoxy-, RGD-PEG grafted sIPN both appeared to upregulate MMP-9

mRNA expression (Figure 2-8 and 2-10), but GGG-, PHSRN-PEG grafted sIPN may have slightly downregulated mRNA expression from 24-96 h (Figure 2-9 and 2-11). When pretreated with antibody, there was a lack of clear, consistent mRNA regulatory trends across ligands from 24-96 h, although there was an upregulation of MMP-9 mRNA from 2-24 h from either antibody pretreated groups. RT-PCR data, however, was not statistically analyzed due to sampling number.

By investigating the molecular mechanisms behind monocyte adhesion and subsequent protein and mRNA regulation of MMP-2 and MMP-9 in the presence of tissue engineering scaffolds, we can gain further insight not only into the intricate intracellular signaling processes and cell response to biomaterials, but we can also elucidate important details involved in wound healing including ECM remodeling, biomaterial degradation, and neovascularization.

Primary monocyte adhesion was modulated by both the substrate surface and the identity of the bioactive peptide. The expression of IL-1β protein in monocytes was affected predominately by the biomaterial substrate. Blocking the β1 or β3 subunit of the integrin receptor reduced both monocyte adhesive activity and IL-1β protein expression, particularly in the presence of RGD grafted sIPN. Ligand identity influenced the regulation of mRNA transcription in monocytes pretreated with anti-integrin β1 or β3 antibody. The results indicate that the substrate, bioactive peptide, and either β1 or β3 containing integrins mediate cell adhesion and IL-1β gene and protein expression in monocytes. Thus, we show in this work that both integrin subunit β1 and β3 are involved in mediating monocyte adhesion, IL-1β protein and mRNA expression in response to surfaces functionalized with fibronectin-derived peptides.

Monocyte adhesion is dependent on the identity of the bioactive peptide as well as the peptide's presentation on different substrates. RGD-PEG grafted sIPNs promoted monocyte

adhesion via β1 and β3 containing integrin receptors. MMP-2/-9 protein and mRNA expressions in the presence of sIPNs were not mediated by ligand identity, but by the presence of gelatin based sIPN. sIPNs initially induced MMP-2 and MMP-9 protein expression and modulated the expression over time. MMP-2 and MMP-9 were modulated in coordination at earlier stages of the experiment. Monocyte adhesion and subsequent MMP-2/-9 protein and mRNA expression in the presence of sIPNs provides an important insight into the matrix degrading activities. Though the exact mechanisms involving β1 or β3 containing integrins in modulating MMP-2/-9 protein and mRNA expression are to be further explored, elucidating these mechanisms will provide critical insight into the monocyte response to biomaterials.

Though monocyte adhesion and subsequent protein release to peptide adsorbed materials are characterized in literature, not many reports on the monocyte behavior in response to peptide grafted hydrogel surfaces currently exist, though rapidly growing. There is much literature on the integrin-mediated interaction of cells with bioadhesive sequences presented onto a biomaterial (Massia and Hubbell) In 1992, McNally and Anderson demonstrated the critical role of β1 and β2 integrins in mediating macrophage adhesion and foreign body giant cell formation onto a RGD adsorbed TCPS surface. This important work explored monocyte adhesion and fusion as controlled by RGD, and our work sheds light on human derived monocyte response to the RGD peptide as presented on a biomaterial scaffold designed to be in contact with the human dermis rather than adsorbed onto TCPS [12]. This work presents one of the first studies in which the molecular mechanisms behind human blood derived monocyte response to peptides covalently grafted and presented by a linker is examined.

2.5 References

1. Ruoslahti E. RGD and other recognition sequences for integrins. Annu Rev Cell Dev Biol 1996;12:697-715.
2. Miyamoto S, Katz BZ, Lafrenie RM and Yamada KM. Fibronectin and integrins in cell adhesion, signaling, and morphogenesis. Ann NY Acad Sci 1998;857:119-129.
3. Cox EA and Huttenlocher A. Regulation of integrin-mediated adhesion during cell migration. Microsc Res Tech. 1998;43:412-419.
4. Johansson S, Svineng G, Wennerberg K, A. Arumulik and L. Lohikangas. Fibronectin-integrin interactions. Frontier in Biosci 1997;2:d126-146.
5. Weerasinghe D, McHugh KP, Ross FP, Brown EJ and Gisler RH, Imhof BA. A role for the α vβ 3 integrin in the transmigration of monocytes. J Cell Biol 1998;42:595-607.
6. Imhof BA and Aurrand-Lions M. Adhesion mechanisms regulating the migration of monocytes. Nat Rev Immunol 2004;4:432-444.
7. Humphries MJ, Travis MA, Clark K and Mould AP. Mechanisms of integration of cells and extracellular matrices by integrins. Biochem Soc Trans 2004;32:822-825.
8. Ginsberg MH, Partridge A and Shattil SJ. Integrin regulation. Curr Opin Cell Biol 2005;17:509-516.
9. Aota S, Nomizu M and Yamada KM. The short amino acid sequence Pro-His-Ser-Arg-Asn in human fibronectin enhances cell-adhesive function. J Biol Chem 1994;269:24756-24761.
10. Chintala SK, Sawaya R, Gokaslan ZL, Rao JS. Modulation of matrix metalloprotease-2 and invasion in human glioma cells by α3β1 integrin. Cancer Letters 1996;103:201-208.
11. Liu Y, Kao WJ. Human macrophage adhesion on FN: the role of substratum and intracellular signaling kinases. Cell Signal 2002;14:145-152.
12. McNally AK, Anderson JM. β1 and β2 integrins mediate adhesion during macrophage fusion and multinucleated foreign body giant cell formation. Am J Path 2002;160:621-630.
13. Mould AP, Askari JA, Aota S, Yamada KM, Irie A, Takada Y, Mardon HJ and Humphries MJ. Defining the topology of integrin α5β1-fibronectin interactions using inhibitory anti-α5 and anti-β1 monoclonal antibodies. Evidence that the synergy sequence

of fibronectin is recognized by the amino-terminal repeats of the α5 subunit. J Biol Chem 1997;272:17283-17292.

14. Phillips JM, Kao WJ. Macrophage adhesion on gelatin-based interpenetrating networks grafted with PEGylated RGD. Tissue Eng 2005;11:964-973.

15. Kao WJ and Liu Y. Intracellular signaling involved in macrophage adhesion and FBGC formation as mediated by ligand-substrate interaction. J Biomed Mater Res 2002;62:478-487.

16. Chen X, Zuckerman ST and Kao WJ. Intracellular protein phosphorylation in adherent U937 monocytes mediated by various culture conditions and fibronectin-derived surface ligands. Biomaterials 2005;26:873.

17. Rosenwasser LJ. Biologic activities of IL-1 and its role in human disease. J Aller and Clinl Immunol 1998;102:344-350.

18. Arend WP. Interleukin-1 receptor antagonist. Adv Immunol 1993;54:167-227.

19. Arend WP, Malyak M, Guthridge CJ, Gabay C. Interleukin-1 receptor antagonist: role in biology. Annu Rev Immunol 1998;16:27-55.

20. Arend WP. The balance between IL-1 and IL-1Ra in disease. Cytokine & Growth Factor Reviews 2002;13:323-340.

21. Welgus HG, Campbell EJ, Cury JD, Eisen AZ, Senior RM, Wilhelm SM, Goldberg GI. Neutral metalloproteinases produced by human mononuclear phagocytes: enzyme profile, regulation, and expression during cellular development. J Clin Inv 1990;86:1496-502.

22. Kao WJ, Lee D, Schense JC, Hubbell JA. Fibronectin modulates macrophage adhesion and FBGC formation: the role of RGD, PHSRN, and PRRARV domains. J Biomed Mater Res 2000;55:79-88.

23. Kao WJ, Zhao QH, Hiltner A, Anderson JM. Theoretical analysis of in vivo macrophage adhesion and foreign body giant cell formation on poly-dimethylsiloxane, low density polyethylene, and polyetherurethanes. J Biomed Mat Res 1994;28:73-79.

24. Xie BL, Laouar A, Huberman E. Fibronectin-mediated cell adhesion is required for induction of 92-kDa type IV collagenase/gelatinase (MMP-9) gene expression during macrophage differentiation. The signaling role of protein kinase C-β. J Biol Chem 1998; 273: 11576-11582.

25. Maillard JL, Favreau C, Reboud-Ravaux M. Role of monocyte/macrophage derived matrix metalloproteinases (gelatinases) in prolonged skin inflammation. Clin Chim Acta 1995;233:61-74.

26. Yang Hu, Kao, WJ. Synthesis and characterization of nanoscale dendritic RGD clusters for potential applications in tissue engineering and drug delivery. Int J Nanomed 2007;2:89-99.

27. Lutolf MP, Hubbell JA. Synthetic biomaterials as instructive cellular microenvironments for morphogenesis in tissue engineering. Nat Biotechnol 2005;23:47-55.

28. Dabiri G, DiPersio CM. Matrix metalloproteinases (MMPs). In: Falabella AF; Kirsner RS, editors. Wound Healing. New York: Taylor and Francis, 2005:49-58.

29. Werb Z. ECM and cell surface proteolysis: regulating cellular ecology. Cell (Cambridge, Massachusetts) 1997;91:439-442.

30. Gillard J, Reed M, Buttle D, Cross S, Brown N. Matrix metalloproteinase activity and immunohistochemical profile of matrix metalloproteinase-2 and -9 and tissue inhibitor of metalloproteinase-1 during human dermal wound healing. Wound Repair Regen 2004; 12:295.

31. Silletti S, Kessler T, Goldberg J, Boger DL, Cheresh DA. Disruption of matrix metalloproteinase 2 binding to integrin αvβ3 by an organic molecule inhibits angiogenesis and tumor growth in vivo. Proc Natl Acad Sci USA 2001;98:119-124.

32. Leroy-Dudal J, Demeilliers C, Gallet O, Pauthe E, Dutoit S, Agniel R, Gauduchon P, Carreiras F. Transmigration of human ovarian adenocarcinoma cells through endothelial extracellular matrix involves αV integrins and the participation of MMP2. Int J Cancer 2005;114:531-543.

33. Elshaw SR, Sisley K, Cross N, Murray AK, MacNeil SM, Wagner M, Nichols CE, Rennie IG. A comparison of ocular melanocyte and uveal melanoma cell invasion and the implication of α1β1, α4β1 and α6β1 integrins. Br J Ophthamol 2001;85:732-8.

34. Zhang H, Li C, Baciu PC. Expression of integrins and MMPs during alkaline-burn-induced corneal angiogenesis. Invest Ophthalmol Vis Sci 2002;43:955-62.

35. Whatling C, McPheat W, and Hurt-Camejo E. Matrix management: assigning different roles for MMP-2 and MMP-9 in vascular remodeling. Arterioscler Thromb Vasc Biol 2004;24:10-11.

36. Laquerriere P, Grandjean-Laquerriere A, Addadi-Rebbah S, Jallot E, Laurent-Maquin D, Frayssinet P, Guenounou M. MMP-2, MMP-9 and their inhibitors TIMP-2 and TIMP-1 production by human monocytes in vitro in the presence of different forms of hydroxyapatite particles. Biomaterials 2004;25:2515-2524.

37. Nakayama Y, Matsuda T. Photocurable surgical tissue adhesive glues composed of photoreactive gelatin and poly(ethylene glycol) diacrylate. J Biomed Mater Res 1999;48:511-521.

38. Elisseeff J, McIntosh W, Anseth K, Riley S, Ragan P, Langer R. Photoencapsulation of chondrocytes in poly(ethylene oxide)-based semi-interpenetrating networks. J Biomed Mater Res 2000;51:164-171.

39. Okino H, Nakayama Y, Tanaka M, Matsuda T. In situ hydrogelation of photocurable gelatin and drug release. J Biomed Mater Res 2002;59:233-245.

40. Stevens KR, Einerson NJ, Burmania JA, Kao WJ. In vivo biocompatibility of gelatin-based hydrogels and interpenetrating networks. J Biomat Sci Polym Ed 2002;13:1353-1366.

41. Jing L, Kao WJ. Synthesis of Polyethylene Glycol (PEG) Derivatives and PEGylated-Peptide Biopolymer Conjugates. Biomacromolecules 2003;4:1055-1067.

42. Burmania JA, Martinez-Diaz GJ, Kao WJ. Synthesis and physicochemical analysis of interpenetrating networks containing modified gelatin and poly(ethylene glycol) diacrylate. J Biomed Mater Res 2003;67:224-234.

43. Phillips JM, Kao WJ. Macrophage adhesion on gelatin-based interpenetrating networks grafted with PEGylated RGD. Tissue Eng 2005;11:964-973.

44. Einerson NJ, Stevens KR, Kao WJ. Synthesis and physicochemical analysis of gelatin-based hydrogels for drug carrier matrices. Biomaterials 2002;24:509-523.

45. Waldeck HM, Chung AS, Kao WJ. Interpenetrating polymer networks containing gelatin modified with PEGylated RGD and soluble KGF: Synthesis, characterization, and application in in vivo critical dermal wound. J Biomed Mater Res 2007;82:861-871.

46. Benoit DSW, Anseth KS. The effect on osteoblast function of colocalized RGD and PHSRN epitopes on PEG surfaces. Biomaterials 2005;26:5209-5220.

47. McNally AK, Anderson JM. Complement C3 participation in monocyte adhesion to different surfaces. Proc Natl Acad Sci USA 1994;91:10119-10123.

48. Klingemann HG, Dedhar S. Distribution of integrins on human peripheral blood mononuclear cells.Blood 1989;74:1348-1354.

49. Cabrero A, Cubero M, Llaverias G, Alegret M, Sanchez R, Laguna JC, Vazquez-Carrera M. Leptin down-regulates peroxisome proliferator-activated receptor γ (PPAR γ) mRNA levels in primary human monocyte-derived macrophages. Mol Cell Biocehm 2005;275:173-179.

50. Ronni T, Matikainen S, Sareneva T, Melen K, Pirhonen J, Keskinen P, Julkunen I Regulation of IFN-alpha/beta, MxA, 2',5'-oligoadenylate synthetase, and HLA gene expression in influenza A-infected human lung epithelial cells. J Immunol 1997;158: 2363-2374.

51. Chomczynski P, Sacci N. Single-step method of RNA isolation by acid guanidinium thiocyanate-phenol-chrloroform extraction. Anal Biochem 1987;162:156-159.

52. Massia SP and Hubbell JA. An RGD spacing of 440 nm is sufficient for integrin alphaVbeta3 mediated fibroblast spreading and 140 nm for focal contact and stress fiber formation. J Cell Biol 1991;14:1089-1100.

53. Mohri H. Interaction of fibronectin with integrin receptors: evidence by use of synthetic peptides. Peptides 1997;18:899-907.

54. Mayadas TN, Cullere X. Neutrophil beta2 integrins: moderators of life or death decisions. Trends Immuno 2005;26:388-395.

55. McNally AK and Anderson JM. Beta1 and beta2 integrins mediate adhesion during macrophage fusion and multinucleated foreign body giant cell formation. Am J Path 2002;160:621-630.

56. Issekutz TB. In vivo blood monocyte migration to acute inflammatory reactions, IL-1 alpha, TNF-alpha, IFN-gamma, and C5a utilizes LFA-1, Mac-1, and VLA-4. The relative importance of each integrin. J Immunol 1995;154:6533-6540.

57. Honig J, Rordorf-Adam C, Siegmund C, Wiedemann W, Erard F. Increased interleukin-1 beta (IL-1 beta) concentration in gingival tissue from periodontitis patients. J Periodontal Res 1989;24:362.

58. Shen M, Horbett TA. The effects of surface chemistry and adsorbed proteins on monocyte/macrophage adhesion to chemically modified polystyrene surfaces. J Biomed Mater Res 2001;57:336-345.

59. Liu Y, Kao WJ. Human macrophage adhesion on FN: the role of substratum and intracellular signaling kinases. Cell Signal 2002;14:145-152.

60. Miyamoto S, Katz BZ, Lafrenie RM, Yamada KM. Fibronectin and integrins in cell adhesion, signaling, and morphogenesis. Ann NY Acad Sci 1998;857:119-129.

61. Calderwood DA. Integrin activation. J Cell Sci 2004;117:657-666.

62. Zilinski JL and Kao WJ.Tissue adhesiveness and host response of in situ photopolymerizable interpenetrating networks containing methylprednisolone acetate. J Biomed Mater Res 2004;68:392-400.

63. Lafrenie RM, Bernier SM, Yamada KM. Adhesion to fibronectin or collagen I gel induces rapid, extensive, biosynthetic alterations in epithelial cells. J Cell Phys 1998;175:163-173.

64. Seftor RE, Seftor EA, Gehlsen KR, Stetler-Stevenson WG, Brown PD, Ruoslahti E, Hendrix MJ. Role of the αvβ3 integrin in human melanoma cell invasion. Proc Natl Acad Sci USA 1992;89:1557-1561.

65. Kjeldsen L, Sengelov H, Lollike K, Nielsen MH, Borregaard N. Isolation and characterization of gelatinase granules from human neutrophils. Blood 1994;83:1640-1649.

Chapter 3. Monocyte Response to Varying Ligand Concentration on ECM-derived sIPN Substrate: Inflammatory and Matrix Remodeling Protein and mRNA Regulation

3.1 Introduction

Monocytes are one of the early cells to appear at the site of injury and actively respond to biomaterials including polymers, ceramics, and metals.[1-3] The highly complex monocytic response to biomaterials involves cellular attachment, recognition and secretion of a myriad of factors important in the wound healing process, such as matrix remodeling proteins and inflammatory cytokines. Monocytes communicate with the extracellular matrix (ECM) environment through various means, including through cell adhesion receptors called integrins. Integrin complexation with the ECM modulates cell adhesion, signaling, cytokine and gene expression and survival.[4] The cell adhesion motif found in many adhesive proteins, arginine-glycine-aspartic acid (RGD), has been utilized extensively to modify biomaterials to promote integrin-mediated cell attachment, focal adhesion contact formation, motility and protein expression.[5-10]

In Chapter 2, the role of integrin mediated monocyte adhesion on materials grafted with ECM-derived peptides and subsequent cell response was demonstrated.[2,11,12] It was shown that adherent monocyte density was increased by RGD tethered onto a flexible polyethylene glycol (PEG) linker on the gelatin based semi-interpenetrating network (sIPN), and that subsequent protein and genetic regulation was also influenced by sIPNs.[11,12] RGD-PEG grafted sIPNs also enhanced cellularity and

organized ECM reconstruction over time *in vivo* in dermal wound healing models.[13] These data are consistent with literature describing RGD influence on cell-biomaterial interactions.[14,15] Cell-substratum interactions, specifically the effects of peptide density on cell adhesion and migration, have been investigated using fibroblasts, osteoblasts, and neurite cells.[6],[15-18] However, the effects of peptide density on monocyte adhesion and subsequent behavior has received little attention. As we have previously characterized integrin-mediated monocyte interaction with ECM-derived peptide-PEG presented on the sIPN surface, in this study, monocyte response to varied ECM-derived peptide amount presented on the sIPN surface was investigated.[11,12] The amount of cell adhesion peptides on the sIPN surface was controlled by varying the wt% ratio of ECM derived peptide-PEG grafted gelatin to polyethylene glycol diacrylate (PEGdA) in the total network. We hypothesized that the increasing amount of bioactive peptides would modulate monocyte adhesion, cytokine expression and gene regulation. In addition to altering peptide amount, the wt% of ligand-PEG modified gelatin or of PEGdA in the sIPN also affects structural properties such as crosslinking density, elasticity, topography and other physical properties of the sIPN. This may potentially affect subsequent cell behavior.[19]

In this study we specifically examine monocyte release of matrix metalloproteases type 2 and 9 (MMP-2 and MMP-9), which are also known as gelatinase A and B respectively, in the gelatin based sIPN environment. In addition to matrix remodeling, MMPs are also involved in cell signaling via cytokine regulation.[20] The interactions between MMP-2/-9 and other cytokines, including a major inflammatory cytokine interleukin-1β (IL-1β), have been described in literature.[21,22] IL-1β release in

response to biomaterials has been a reliable marker of macrophage activation and allows prediction of potential *in vivo* immune reactions.[23] Inflammation is also influenced by the presence of MMPs during tissue remodeling and wound healing. In this study, monocyte expression of IL-1β and MMP-2/-9 and the relationship among these proteins in the context of ECM-derived peptide grafted sIPN were investigated.[24]

3.2 Methods and Materials

3.2.1 sIPNs with varied ligand concentration: formulation and characterization

Synthesis and characterization of ligand-PEG grafted gelatin is outlined in detail in Chapter 2, section 2.2.1. sIPN discs were made in three different formulations, based on the modified gelatin:PEGdA wt% ratio. 26:74, 35:65 and 41:59 wt% ratio sIPNs were made, noted as 3:7, 4:6, and 5:5 sIPN, respectively, in this paper. Between 3:7 and 4:6 sIPNs, there was a 9% increase in gelatin content from but between 4:6 and 5:5 sIPNs, there was a 6% increase in gelatin wt%. Beyond the 5:5 wt% ratio, increased gelatin content compromised the robustness of the sIPN to withstand handling. The schematics of the 3:7 and 5:5 sIPN are outlined in Figure 3-1. sIPNs were placed in 48-well tissue culture polystyrene (TCPS; BD Falcon) plates and incubated with RPMI 1640 at 37°C and 5% CO2 for 24 h prior to monocyte seeding.

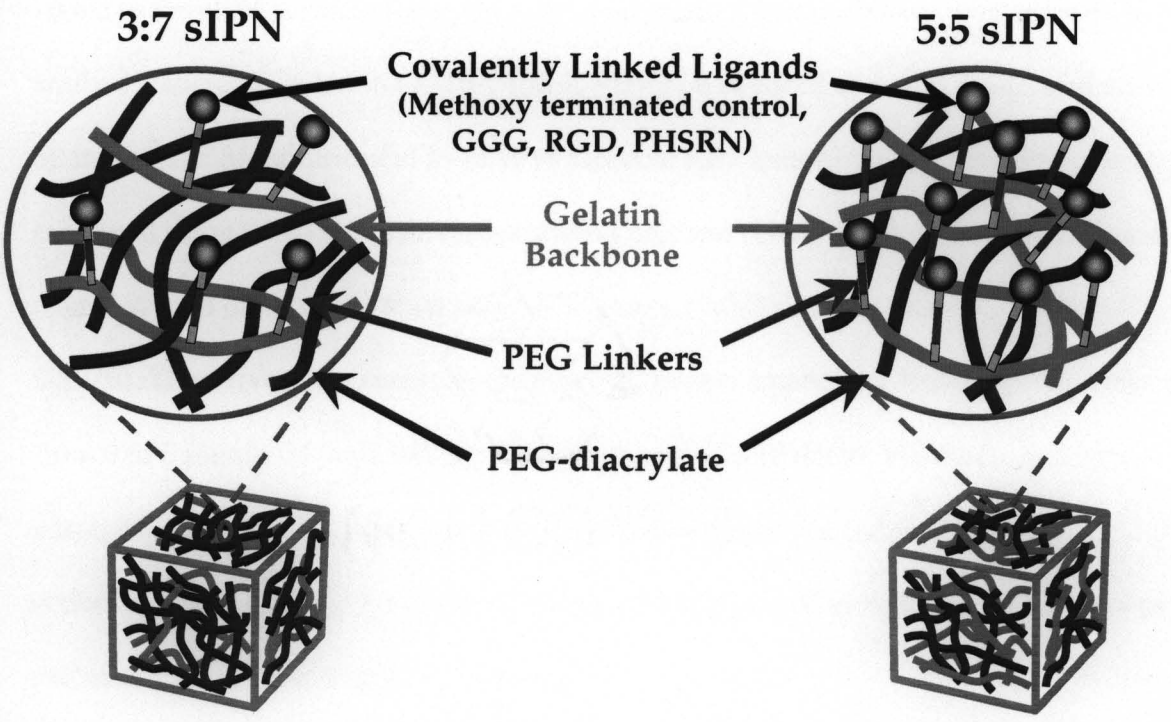

Figure 3-1. Schematic representation of the semi-interpenetrating network (sIPN) with varied ligand-PEG grafted gelatin:PEG wt%.

The RGD concentration on the surface of the sIPN discs was characterized via a previously reported indirect enzyme linked immunosorbent assay (ELISA).[28] sIPNs were equilibrated overnight in sterile PBS then incubated at room temperature for two hours in blocking solution containing 1% bovine serum albumin (BSA) in PBS. sIPNs were washed five times with wash buffer containing 1% Tween-20 in sterile PBS and incubated for 2 h at room temperature with RGD directed primary antibody (polyclonal rabbit anti-RGD domain antibody, EMD Biosciences), diluted 1:1000 in 1% BSA. Surfaces were then rinsed five times with wash buffer after incubation to remove non-adhered primary antibody. Secondary antibody (horseradish peroxidase-conjugated goat IgG fraction to rabbit whole IgG, MP Biomedicals) was diluted 1:20000 in 1% BSA then

added to the sIPN surfaces for a two hour incubation. After incubation with secondary antibody, substrate solution (TMB-ELISA, Pierce) was added and then inactivated after 30 min with 2 M sulfuric acid in order to measure HRP concentration. Absorbance was measured using a 450 nm plate reader (BIO-TEK) and converted to surface RGD density from a second order polynomial standard curve ($y = -0.0003x2 + 0.0068x + 0.0416$, $R^2 = 0.9926$). The curve was generated by adsorbing known amounts of RGD peptide, ranging from 0 to 5 μmole/ml, onto untreated polystyrene plates (Falcon). However, as 100% adsorption of the RGD peptide onto the polystyrene plates was assumed, the RGD concentrations on sIPNs presented in Figure 3-2 are expected to be lower than what was calculated using the standard curve above.

3.2.2 Monocyte adhesion and protein measurement assay

Human peripheral blood monocytes were isolated from citrated whole blood of a healthy adult volunteer using a density-gradient, non-adhesion method previously described in detail.[29] The same donor was used throughout the experiment for adhesion, cytokine and gene expression assays to minimize donor-centered variability. To verify that the cytokines observed after seeding were not a result of the isolation procedure, cell lysates collected by sonication (5 pulses) as well as the media containing the freshly isolated monocytes prior to sonication were immediately saved then analyzed for MMP-2 and MMP-9 using ELISA. The data from these samples are noted as "0 h" (i.e. immediately upon isolation and prior to seeding on surface). Freshly isolated monocytes were seeded onto various ligand-PEG grafted sIPN at a concentration of 106 cells/ml in RPMI 1640 culture medium and 10% autologous serum at 37°C and 5%

CO2.[2] At 2, 24, 96 and 168 h, supernatant was collected and analyzed with commercial ELISA kits (Raybiotech, Inc., Norcross, GA). Three 100 μl aliquots were obtained from each well in the experiment to test a variety of conditions, and these aliquots were used for the testing MMP-2/-9 and IL-1β concentrations with ELISA. The sensitivity of the kits ranged from 140-18,000 pg/ml for MMP-2, 8.2-6000 pg/ml for MMP-9 and 0.3-1000 pg/ml for IL-1β. ELISA was carried out according to manufacturer's instructions. After the supernatants were collected at 2, 24, 96 and 168 h, at each time point, all samples were washed twice with RPMI medium to remove nonadherent cells. Samples were resupplied with 10% autologous serum in RPMI and allowed to incubate further. At 2, 24, 96 and 168 h, sIPN samples were stained with Wright's stain. Adherent monocytes on all surfaces were imaged using a computer-assisted video analysis system (Metamorph v4.1) coupled to an inverted microscope (Nikon, Eclipse TE 300). The adherent cells were quantified and expressed as number of cells/mm2 surface area.

3.2.3 mRNA characterization with RT-PCR

All reagents employed in RT-PCR assays were purchased from Bio-Rad, USA, unless indicated otherwise. Adherent cells were lysed with TRIzol® reagent (InvitrogenTM, CA) for RT-PCR analysis. A modification of the Chomczynski and Sacchi method using TRIzol® reagent was carried out to isolate total RNA from adherent monocytes.[30] The quality of the purified RNA was tested by 1.5% agarose gel/ethidium-bromide staining with a 260/280 nm absorbance ratio. At the cDNA synthesis step, RNAse-free DNAse (Sigma, MO) was used to treat the RNA before being reverse transcribed with Moloney Murine Leukemia Virus (M-MLV) reverse

transcriptase (InvitrogenTM, CA). Oligonucleotide primers for MMP-2/-9, IL-1β and internal standards β-actin, and glyceraldehydes-3-phosphate-dehydrogenase (GAPDH) were obtained using the DNA sequence database from NCBI (Bethesda, MD). The primer sequences, of which the reproducibility has been previously demonstrated, are described in Table 2-1 in Chapter 2.[31,12] Primers3 Output computer program (Whitehead Institute for Biomedical Research, Cambridge, MA) which bases selection on G/C content, PCR product size, and melting temperature, was used to design primer sets. The specificity of the primer sequences was verified by the NCBI BLAST program. The primer sequences and product size are outlined in Chapter 2, Table 2-2. In addition, GAPDH was employed as a housekeeping gene due to the growing controversy over β-actin's reliability as a stable housekeeping agent. The GAPDH primer sequences were 5'- CATCATCCCTGCCTCTACTG-3' AND 3'- GGTGGTCCAGGGGTCTTACT-5' and the product size was 409.

cDNA was amplified in a 25 μl PCR mixture containing 1x reaction buffer (Sigma, MO, USA), 0.24 μM of each primer, 0.2 mM of dNTP (InvitrogenTM, CA), and 0.75 U RedTaq DNA polymerase (Sigma, MO). The PCR reaction was started at 94°C for 3 min, after which followed 35 cycles for MMP-2, MMP-9, IL-1β, β-actin, and GAPDH. A denaturation step (at 94°C for 30 sec), an annealing step (at 56°C for 45 sec) and an extension step (at 72°C for 1 min), and a final elongation step (at 72°C for 7 min) took place at each cycle. The reaction was performed with iCycler thermal cycler. 15 μl of the amplified products were run under electrophoresis through a 1.5% agarose gel containing ethidium-bromide (0.5 μg/ml) and visualized under ultraviolet light. Contamination from genomic DNA was checked for with RT-PCR containing RNA but

not M-MLV reverse transcriptase. The band densities in gels were quantified using the Scion imaging program (Frederick, MD). PCR analysis was carried out for sIPN samples at 2, 24, and 96 h for MMP-2/-9 and IL-1β. β-actin, a function of cell motility, and GAPDH, a function of cell metabolism, was observed for comparison as internal controls. Due to the unresolved issue over the consistency and the choice of housekeeping genes, MMP-2/-9, and IL-1β were normalized to β-actin as well as GAPDH.[32] mRNA levels in primary monocytes on different sIPNs were compared within each time point and within material formulation.

3.2.4 Statistical Analysis

All data, including surface RGD concentration, adherent cell density, cytokine concentration and transcriptional levels, were analyzed by two-way analysis of variance and Tukey post testing (SigmaStat, v2.03) and expressed as mean ± standard deviation (n=3). *p*-values of less than 0.001 were considered statistically significant for adherent cell density and protein concentrations and less than 0.05 for all other data. Transcriptional levels are expressed as arbitrary units (AU) as levels were normalized to either β-actin or GAPDH. Due to the semi-quantitative nature of RT-PCR, statistical comparisons were reserved within each RT-PCR runs, and thus were reserved within time points and within sIPN formulation groups.

3.3 Results

3.3.1 Accessible RGD concentration on sIPNs

Accessible RGD concentration (μmole/ml) on the sIPN surface is shown in Figure 3-2. Unmodified sIPNs showed significantly ($p<0.05$) less RGD concentration compared to RGD-PEG grafted sIPNs for 3:7 and 4:6 but not for 5:5 sIPN. Unmodified 3:7 sIPN also exhibited significantly ($p<0.05$) less RGD on the surface compared to unmodified 4:6 and 5:5 sIPNs. Comparing across RGD-PEG grafted sIPN, 3:7 sIPN showed significantly ($p<0.05$) less RGD on the surface compared to 4:6 sIPN. Significant differences were not observed between RGD-PEG grafted 4:6 and 5:5 sIPN and this may be due to the less incremental increase in RGD-PEG grafted gelatin content wt% from 4:6 to 5:5 sIPN compared to the gelatin content increase from 3:7 to 4:6 sIPN. The adherent concentration of RGD on unmodified sIPNs increases with increasing gelatin due to the endogenous RGD on the gelatin backbone.

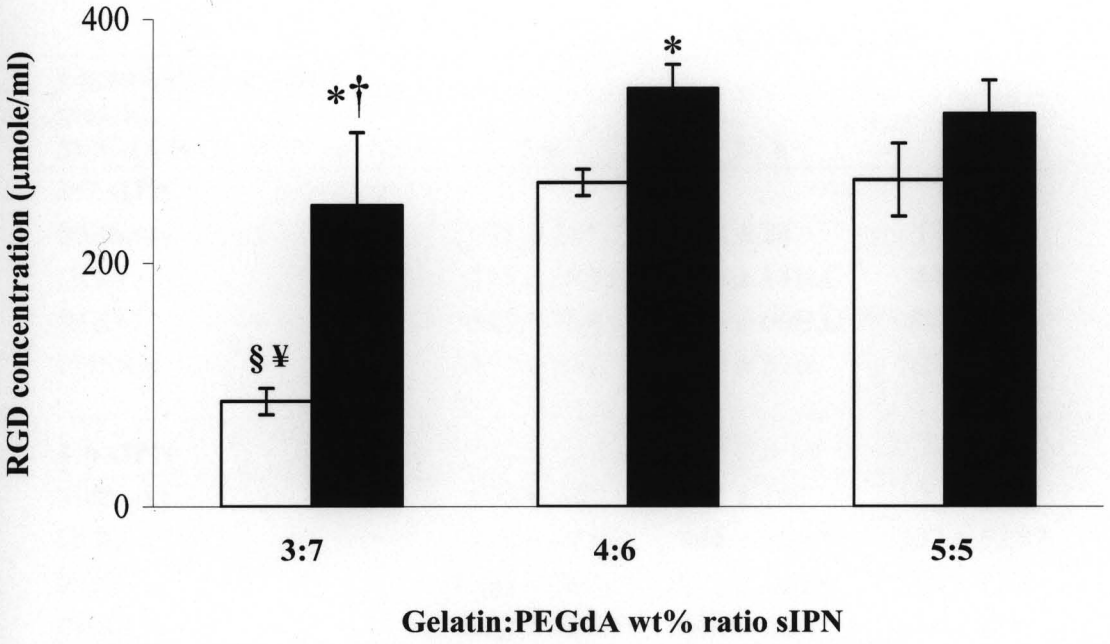

Figure 3-2. RGD concentration (µmole/ml) on unmodified (□) or RGD-PEG grafted gelatin (■) combined with varying wt % ratios of gelatin:PEGdA in the sIPN. Data expressed as mean ± s.d. *Significantly different (p<0.05) from respective unmodified sIPN. [§]Significantly different (p<0.05) from unmodified 4:6 sIPN. [¥]Significantly different (p<0.05) from unmodified 5:5 sIPN. [†]Significantly different (p<0.05) from RGD-PEG grafted 4:6 sIPN.

3.3.2 Adherent monocyte density on sIPN with varied ligand concentration

Adherent cell density was dependent on ligand identity and concentration. RGD-PEG grafted 4:6 and 5:5 sIPNs exhibited significantly (p<0.001) greater adherent cell density as compared to all other ligand-PEG grafted respective sIPNs from 2 to 96 h (Table 3-1).

Table 3-1. Adherent monocyte density (cell/mm2) on sIPNs with varying ligand-PEG grafted gelatin:PEGdA wt% ratio.

	Culture Time:			
Ligand-PEG grafted gelatin: PEGdA wt% sIPN surface	**2 h**	**24 h**	**96 h**	**168 h**
3:7 sIPN				
Methoxy	71 ± 14*	73 ± 24	57 ± 26	33 ± 6
GGG	155 ± 38B,C	108 ± 14B,C	46 ± 7B,C	32 ± 8C
RGD	327 ± 76B,C	166 ± 60B,C	88 ± 8B,C	66 ± 6B,C
PHSRN	172 ± 69B	180 ± 33B	105 ± 15	87 ± 9
4:6 sIPN				
Methoxy	145 ± 18*	233 ± 14*	106 ± 2*	95 ± 12
GGG	328 ± 69A*	444 ± 16A*	207 ± 52A*	74 ± 40
RGD	1321 ± 74A	1071 ± 190A	350 ± 42A	157 ± 8A
PHSRN	442 ± 26A*	399 ± 49A*	154 ± 41*	84 ± 14
5:5 sIPN				
Methoxy	113 ± 55*	102 ± 51*	67 ± 22*	87 ± 8
GGG	448 ± 189A*	407 ± 195A*	118 ± 14A*	135 ± 31A
RGD	1192 ± 384A	1133 ± 320A	434 ± 77A	173 ± 41A
PHSRN	314 ± 65*	381 ± 91*	169 ± 64*	101 ± 35

A Significantly different from 3:7 sIPN (within each ligand and within each time point) $p<0.001$

B Significantly different from 4:6 sIPN (within each ligand and within each time point) $p<0.001$

C Significantly different from 5:5 sIPN (within each ligand and within each time point) $p<0.001$

* Significantly different from RGD-PEG grafted sIPN (within ligand-grafted gelatin:PEGdA wt% ratio and within each time point) $p<0.001$

Adherent density of RGD-PEG grafted 3:7 sIPN was higher only compared to methoxy-PEG grafted sIPNs at 2 h. Comparing across RGD-PEG grafted sIPN formulations, significantly ($p<0.001$) lower adherent cell density was observed on 3:7 as compared to 4:6 and 5:5 sIPNs at all time points. Adherent cell density between RGD-PEG grafted 4:6 and 5:5 sIPN did not significantly differ over time and this may be contributed to the lack of significant differences in RGD concentration between these two

formulations. Methoxy-PEG grafted sIPN did not show significant differences in adherent cell density across all formulations and time points. Comparing across GGG-PEG grafted sIPNs, 3:7 sIPNs showed significantly ($p<0.001$) less adherent cell density compared to both 4:6 and 5:5 sIPNs from 2 to 96 h, but at 168 h, only 5:5 sIPN had a higher density than 3:7 sIPN. Adherent cell density on PHSRN-PEG grafted 3:7 sIPN was significantly ($p<0.001$) lower than PHSRN-PEG grafted 4:6 sIPNs at 2 and 24 h.

3.3.3 Monocyte MMP-2/-9 and IL-1β protein concentration

MMP-2 concentration over time was influenced by ligand identity as well as by concentration, though the impact of ligand concentration was greater at later time points (Fig. 3-3). Both the cell lysate and the media yielded non-detectable MMP-2 concentrations (0 ± 0 pg/ml) immediately after isolation. From 0 to 2 h, a dramatic increase in MMP-2 secretion was observed for 4:6 and 5:5 but not for 3:7 sIPN. All except methoxy-PEG grafted 4:6 sIPNs showed significantly ($p<0.001$) higher MMP-2 concentrations than 5:5 sIPN, and methoxy-PEG grafted 5:5 sIPNs showed significantly ($p<0.001$) higher concentrations than RGD-, and PHSRN-PEG grafted 5:5 sIPN. From 24 to 168 h, MMP-2 concentrations for 3:7 sIPN gradually increased, but did not exceed 2000 pg/ml. At 24 and 96 h, all 4:6 sIPNs had significantly ($p<0.001$) higher concentrations compared to respective 3:7 and 5:5 sIPNs except versus GGG-PEG grafted 5:5 sIPN at 96 h. At 168 h, all 3:7 sIPNs showed significantly ($p<0.001$) higher concentrations than respective 5:5 sIPNs but lower than respective 4:6 sIPNs.

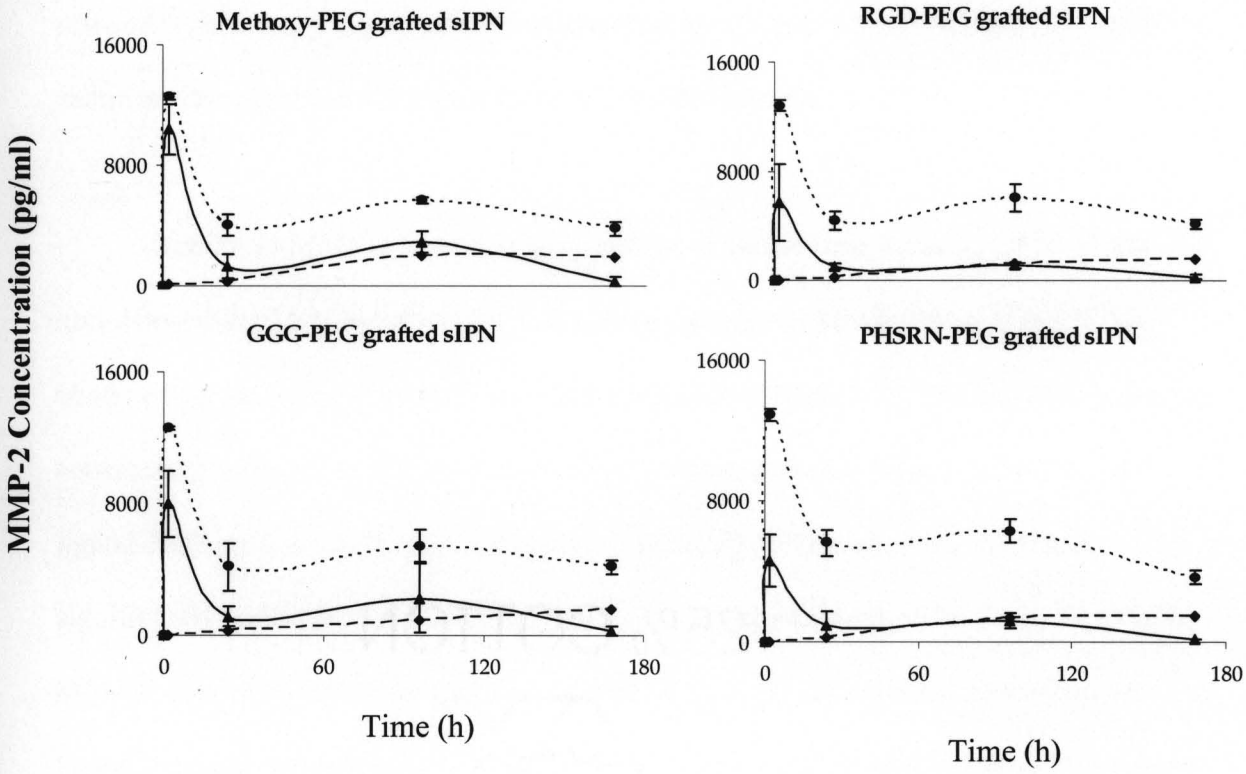

Figure 3-3. MMP-2 concentrations (pg/ml) over time from human monocytes in the presence of sIPNs with various wt% ratios of ligand-PEG grafted gelatin:PEGdA: 3:7 sIPN (−◆−), 4:6 sIPN (···●···), or 5:5 sIPN (—▲—). Data are shown per ligand group and are expressed as mean ± s.d. Comparing within each time point and each ligand identity at $p<0.001$: i.) at 2 h, all ligand-PEG grafted 3:7 sIPNs showed a significantly lower concentration compared to that of 4:6 and 5:5 sIPNs and all except methoxy-PEG grafted 4:6 sIPNs showed significantly higher concentrations compared to 5:5 sIPNs while within 5:5 sIPNs, RGD-, PHSRN-PEG grafted sIPNs were significantly lower than methoxy-PEG grafted sIPNs; ii.) from 24 to 96 h, concentrations from all ligand-PEG

grafted 4:6 sIPNs were significantly higher than all 3:7 sIPN and 5:5 sIPN samples except versus GGG-PEG grafted 5:5 sIPN at 96 h; iii.) at 168 h, all 4:6 sIPN samples showed significantly higher concentrations than all 3:7 and 5:5 sIPNs and all 3:7 sIPN samples were significantly higher than all 5:5 sIPN samples.

Similar to MMP-2 protein concentrations at earlier time periods, MMP-9 was non-detectable (0 ± 0 pg/ml) at 0 h, but a sharp increase in MMP-9 from 0 to 2 h was observed for all ligand type and material formulation (Figure 3-4). The increase in protein concentration from 0 to 2 h was followed by a drastic decrease from 2 to 24 h for all ligand-PEG grafted sIPN. At 2 h, methoxy- and RGD-PEG grafted 3:7 sIPN had significantly ($p<0.001$) higher concentrations than respective 4:6 sIPN. From 24 to 96 h, MMP-9 concentrations increased for all sIPNs, but to varying degrees depending on ligand type and concentration. For example, all methoxy-PEG grafted sIPN at 96 h were statistically similar while both GGG- and PHSRN-PEG grafted 4:6 sIPNs exhibited significantly ($p<0.001$) higher values compared to that of respective 3:7 and 5:5 sIPNs. RGD-PEG grafted 4:6 sIPN at 96 h had significantly ($p<0.001$) higher concentrations than that of 3:7 sIPN but significantly ($p<0.001$) lower than 5:5 sIPN. At 168 h, concentrations from methoxy-PEG grafted 4:6 sIPN were significantly higher than 3:7 but significantly lower than 5:5 sIPN. GGG-, PHSRN-PEG grafted 4:6 sIPN continued to show significantly ($p<0.001$) higher values than 3:7 and 5:5 sIPNs. RGD-PEG grafted 4:6 and 5:5 sIPNs displayed significantly ($p<0.001$) higher concentrations than 3:7 sIPN.

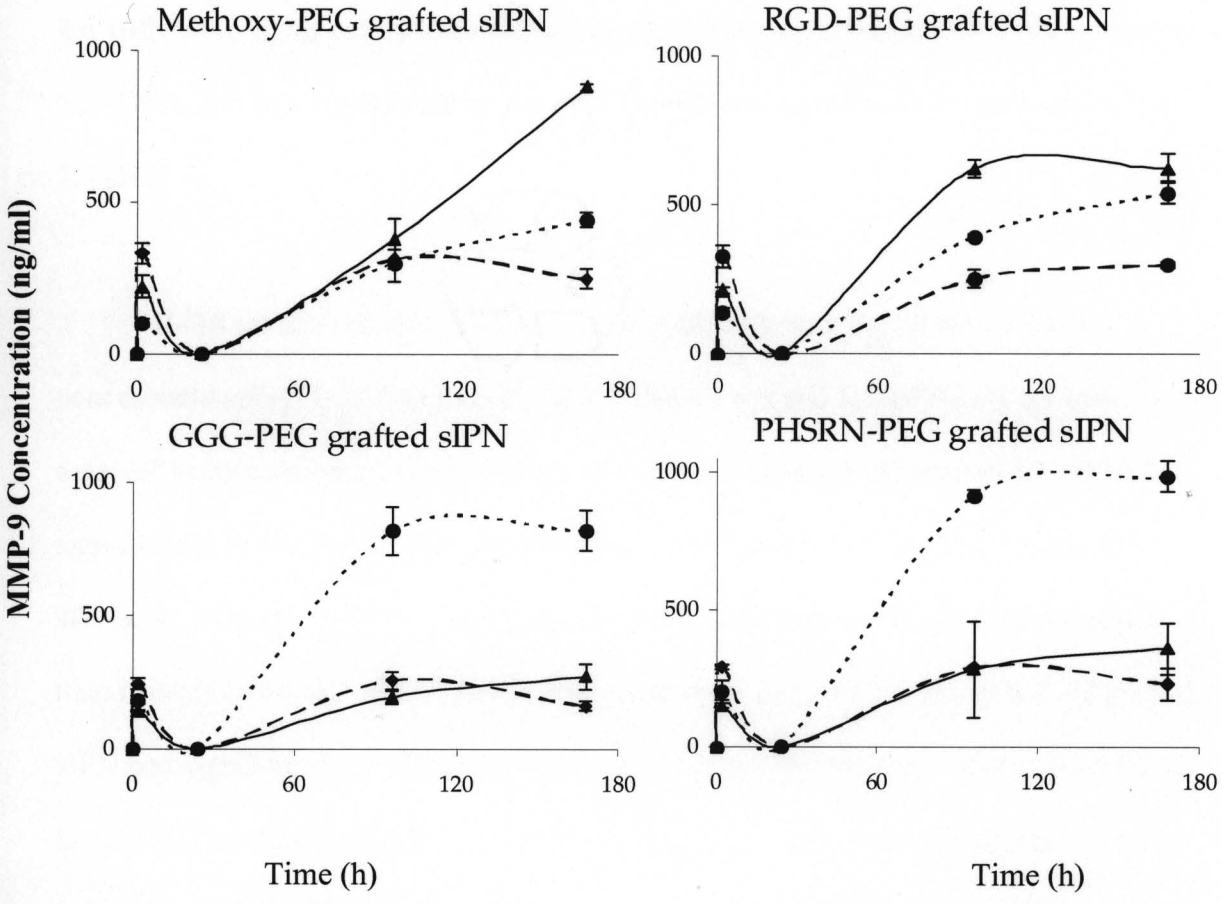

Figure 3-4. MMP-9 concentrations (ng/ml) over time from human monocytes in the presence of sIPNs with various wt% ratios of ligand-PEG grafted gelatin:PEGdA: 3:7 sIPN (−◆−), 4:6 sIPN (··●··), or 5:5 sIPN (—▲—). Data are shown per ligand group and are expressed as mean ± s.d. Comparing within each time point and each ligand identity at $p<0.001$: i.) at 2 h, methoxy-, RGD-PEG grafted 3:7 sIPNs had significantly higher values than 4:6 sIPNs; ii.) at 96 h, both GGG- and PHSRN-PEG grafted 4:6 sIPNs exhibited significantly higher values compared to that of 3:7 and 5:5 sIPNs while for RGD-PEG grafted sIPN, 4:6 sIPNs had significantly higher values than that of 3:7 but

lower than 5:5 sIPNs; iii.) at 168 h, GGG-, PHSRN-PEG grafted 4:6 sIPN had significantly higher values than 3:7 and 5:5 sIPNs while values for methoxy-PEG grafted 4:6 sIPN were significantly higher than those of 3:7 but significantly lower than those of 5:5 sIPNs, and RGD-PEG grafted 4:6 and 5:5 sIPN had significantly higher values than 3:7 sIPN.

IL-1β protein concentrations were modulated by both ligand identity and concentration (Fig. 3-5). For 3:7 sIPN at 2 h and for 4:6 and 5:5 sIPNs, IL-1β was detected at concentrations below 200 pg/ml. At 2 h, PHSRN-PEG grafted 5:5 sIPNs had significantly ($p<0.001$) higher concentrations than PHSRN-PEG grafted 3:7 and 4:6 sIPNs. At 24 h, all 3:7 sIPN showed significantly ($p<0.001$) less IL-1β concentrations than respective 4:6 and 5:5 sIPN. Within 4:6 sIPNs at 24 h, RGD-, PHSRN-PEG grafted sIPN had significantly ($p<0.001$) lower concentrations than methoxy- and GGG-PEG grafted sIPN. At 24 and 96 h, no significant differences were observed between 4:6 and 5:5 sIPN. All 3:7 sIPNs continued to show significantly ($p<0.001$) less IL-1β concentrations compared to 4:6 and 5:5 sIPNs at 96 h. RGD-PEG grafted 4:6 sIPN exhibited significantly ($p<0.001$) higher concentrations than all other ligand-PEG grafted 4:6 sIPN at 96 h.

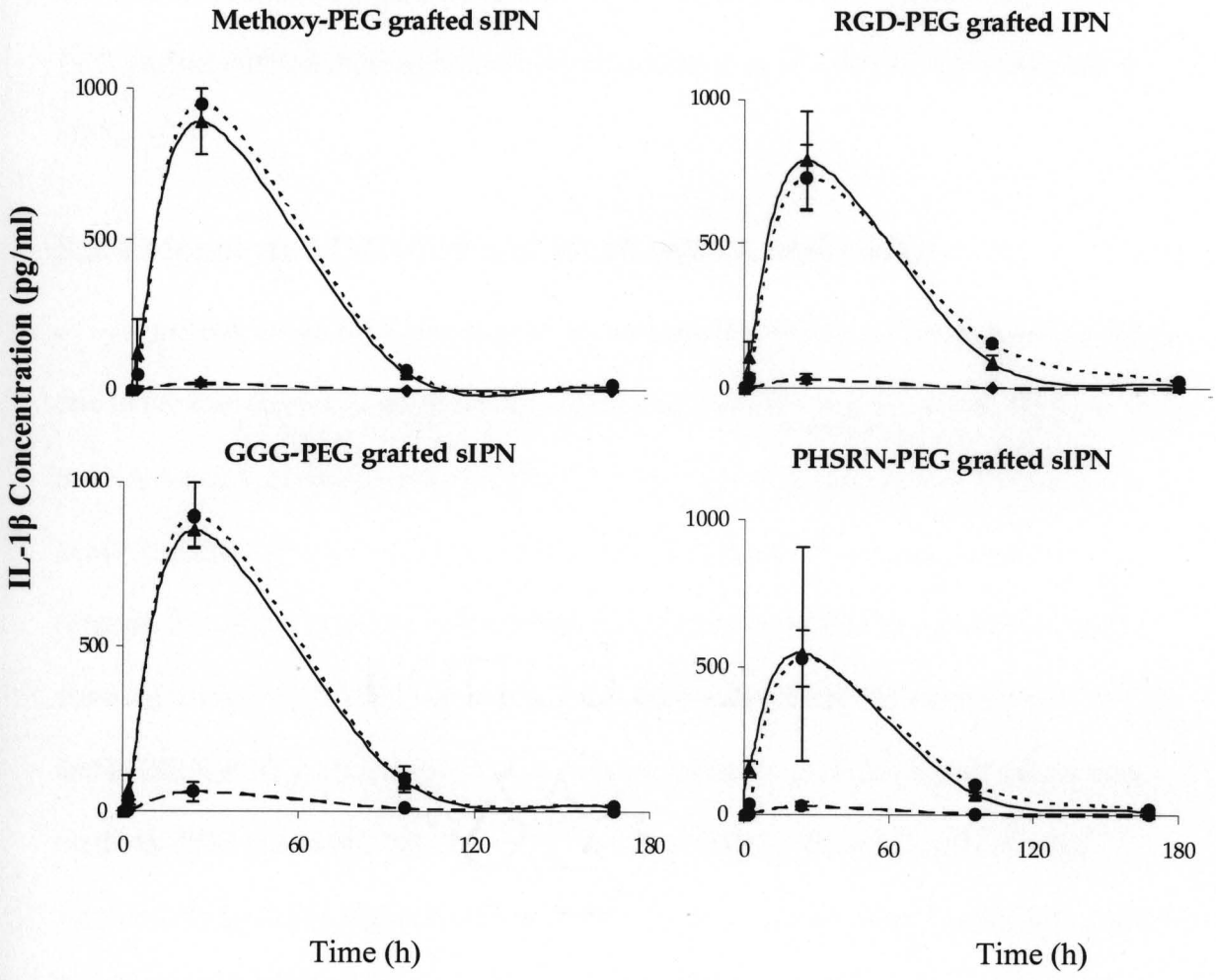

Figure 3-5. IL-1β concentrations (pg/ml) over time from human monocytes in the presence of sIPNs with various wt% ratios of ligand-PEG grafted gelatin:PEGdA: 3:7 sIPN (−◆−), 4:6 sIPN (··●··), or 5:5 sIPN (—▲—). Data are shown per ligand group and are expressed as mean ± s.d. Comparing within each time point and each ligand identity at $p<0.001$: i.) at 2 h, PHSRN-PEG grafted 5:5 sIPNs had significantly higher concentrations than 3:7 and 4:6 sIPNs; ii.) at 24 h, all 4:6 and 5:5 sIPNs showed higher values than 3:7 sIPN, and within 4:6 sIPNs, RGD-, PHSRN-PEG grafted sIPNs had

lower concentrations than methoxy- and GGG-PEG grafted sIPNs; iii.) at 96 h, all 4:6 and 5:5 sIPNs showed higher values than 3:7 sIPN, and within 4:6 sIPNs, only RGD-PEG grafted sIPNs exhibited higher concentrations than all other ligand-PEG grafted sIPN.

3.3.4 Monocyte MMP-2/-9 and IL-1β mRNA expression

mRNA levels were investigated for all samples from 2 to 96 h, but not for 168 h, due to the low density of adherent cells from which mRNA was extracted. MMP-2 mRNA was not detectable (i.e. 0 ± 0 AU) for all sIPN at all time points. For all sIPN, MMP-9 mRNA levels were undetectable at 2 h, but generally increased over time (Figures 3-6 and 3-7). At 24 h, MMP-9/β-actin levels for RGD-PEG grafted 3:7 sIPN were significantly ($p<0.05$) higher than methoxy- and PHSRN-PEG grafted sIPN. RGD- and PHSRN-PEG grafted 4:6 sIPNs showed significantly ($p<0.05$) higher values than methoxy-PEG grafted sIPN at 24 h. At 96 h, GGG-PEG grafted 3:7 sIPN showed significantly ($p<0.05$) higher levels of MMP-9/β-actin than all other ligand-PEG grafted 3:7 sIPN. RGD-PEG grafted samples within 4:6 sIPN showed significantly higher transcriptional levels than all other ligand-PEG grafted 4:6 sIPNs at 96 h. When normalized to GAPDH, MMP-9 mRNA levels from PHSRN-PEG grafted 4:6 sIPN samples were significantly ($p<0.05$) higher than all other ligand-PEG grafted 4:6 sIPNs at 24 h (Fig. 3-7). At 96 h, MMP-9/GAPDH levels for GGG-PEG grafted 3:7 and 5:5 sIPN were significantly ($p<0.05$) higher than methoxy-, and PHSRN-PEG grafted sIPNs. GGG-PEG grafted 4:6 sIPNs were also significantly higher than methoxy-, and RGD-PEG grafted 4:6 sIPN at 96 h.

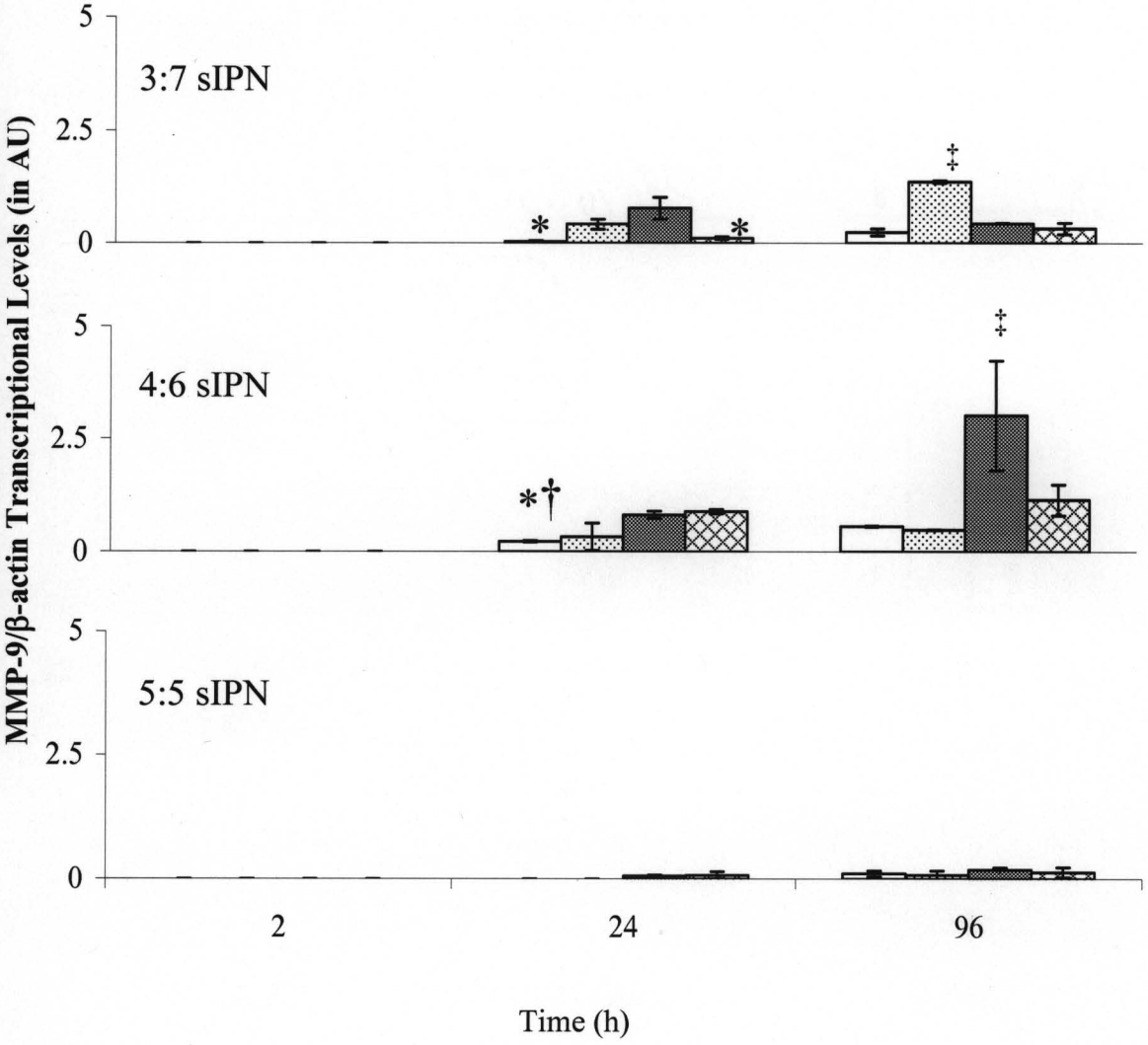

Figure 3-6. RT-PCR analysis for MMP-9/ β-actin mRNA levels from adherent monocytes in the presence of 3:7, 4:6 and 5:5 wt% ratio of ligand-grafted gelatin:PEGdA sIPNs: methoxy-(▭), GGG-(▭), RGD-(▭), and PHSRN-PEG grafted sIPN (▭). Data are expressed as mean ± s.d. * Significantly different (p<0.05) from RGD-PEG grafted sIPN (within sIPN group and time point). † Significantly different (p<0.05) from PHSRN-PEG grafted sIPN (within sIPN group and time point). ‡ Significantly different (p<0.05) from all other ligand-PEG grafted sIPN (within sIPN group and time point).

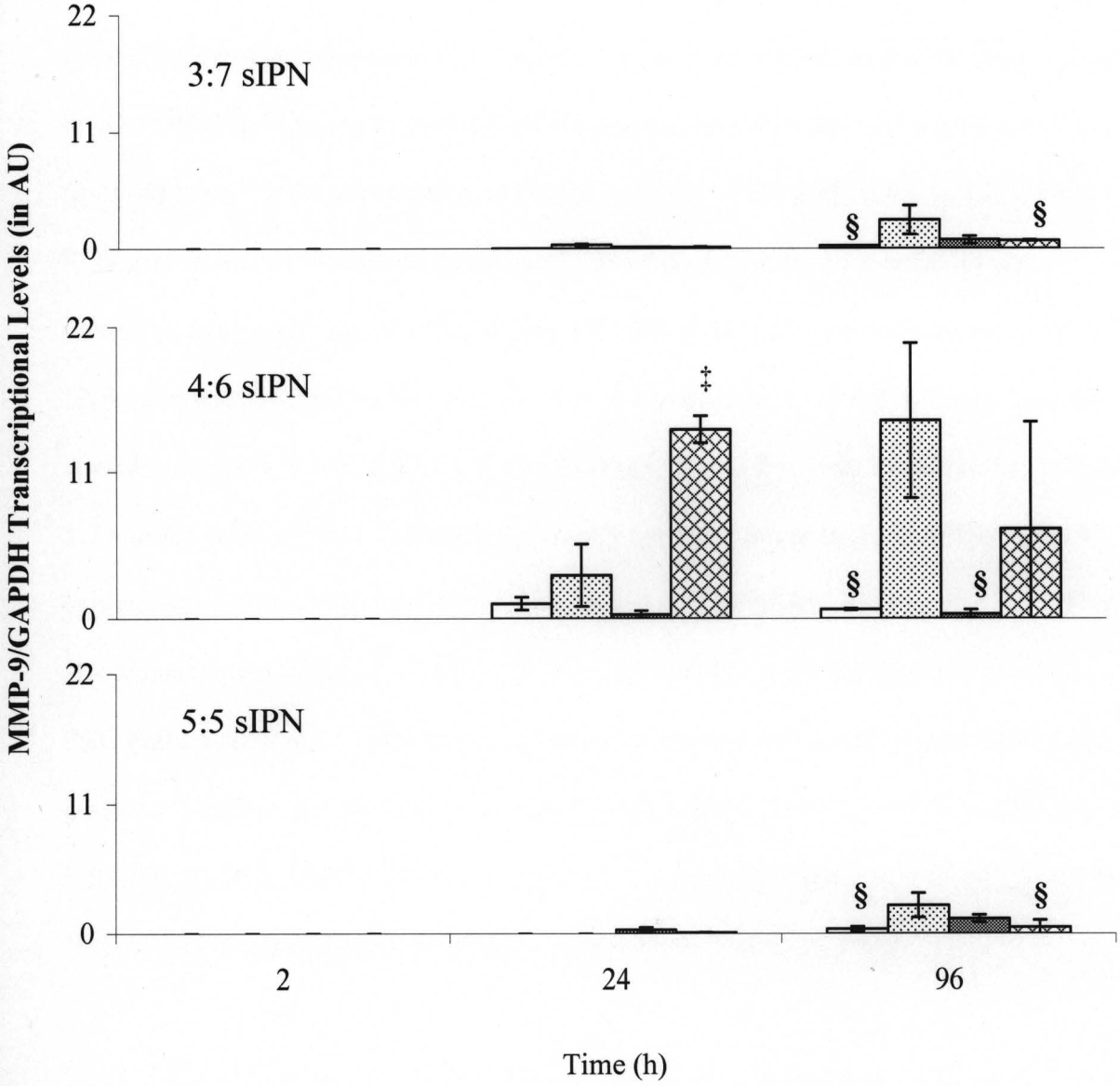

Figure 3-7. RT-PCR analysis for MMP-9/GAPDH mRNA levels from adherent monocytes in the presence of 3:7, 4:6 and 5:5 wt% ratio of ligand-PEG grafted gelatin:PEGdA sIPNs: methoxy-(▭), GGG-(▭), RGD-(▭), and PHSRN-PEG grafted sIPN (▭). Data are expressed as mean ± s.d. §Significantly different (p<0.05) from GGG-PEG grafted sIPN (within sIPN group and time point). ‡Significantly different (p<0.05) from all other ligand-PEG grafted sIPN (within sIPN group and time point).

While MMP-9 mRNA levels increased over time in general, IL-1β mRNA levels generally decreased over time. IL-1β levels were also normalized to β-actin (Fig. 3-8) or to GAPDH (Fig. 3-9). At 2 h, PHSRN-PEG grafted 4:6 sIPNs showed significantly ($p<0.05$) lower levels as compared to GGG-, and RGD-PEG grafted 4:6 sIPNs. RGD-PEG grafted 4:6 sIPN showed significantly ($p<0.05$) higher IL-1β/β-actin levels compared to all other ligand-PEG grafted 4:6 sIPN at 24 h. Only a trace amount or no IL-1β/β-actin was detected by 96 h for all sIPN. A decrease in IL-1β mRNA over time was also observed when normalized to GAPDH (Fig. 3-9). At 2 h, both PHSRN-PEG grafted 3:7 and 4:6 sIPN samples showed significantly ($p<0.05$) lower IL-1β/GAPDH mRNA expression than the respective RGD-PEG grafted sIPN. PHSRN-PEG grafted 5:5 sIPNs also showed significantly ($p<0.05$) lower IL-1β/GAPDH levels compared to methoxy-PEG grafted sIPN at 2 h. At 24 h, IL-1β/GAPDH levels from methoxy- and GGG-PEG grafted 5:5 sIPN were significantly ($p<0.05$) higher than RGD-, and PHSRN-PEG grafted 5:5 sIPN. At 96 h, GGG-PEG grafted 4:6 sIPNs showed significantly ($p<0.05$) higher IL-1β/GAPDH levels compared to all other ligand-PEG grafted 4:6 sIPNs.

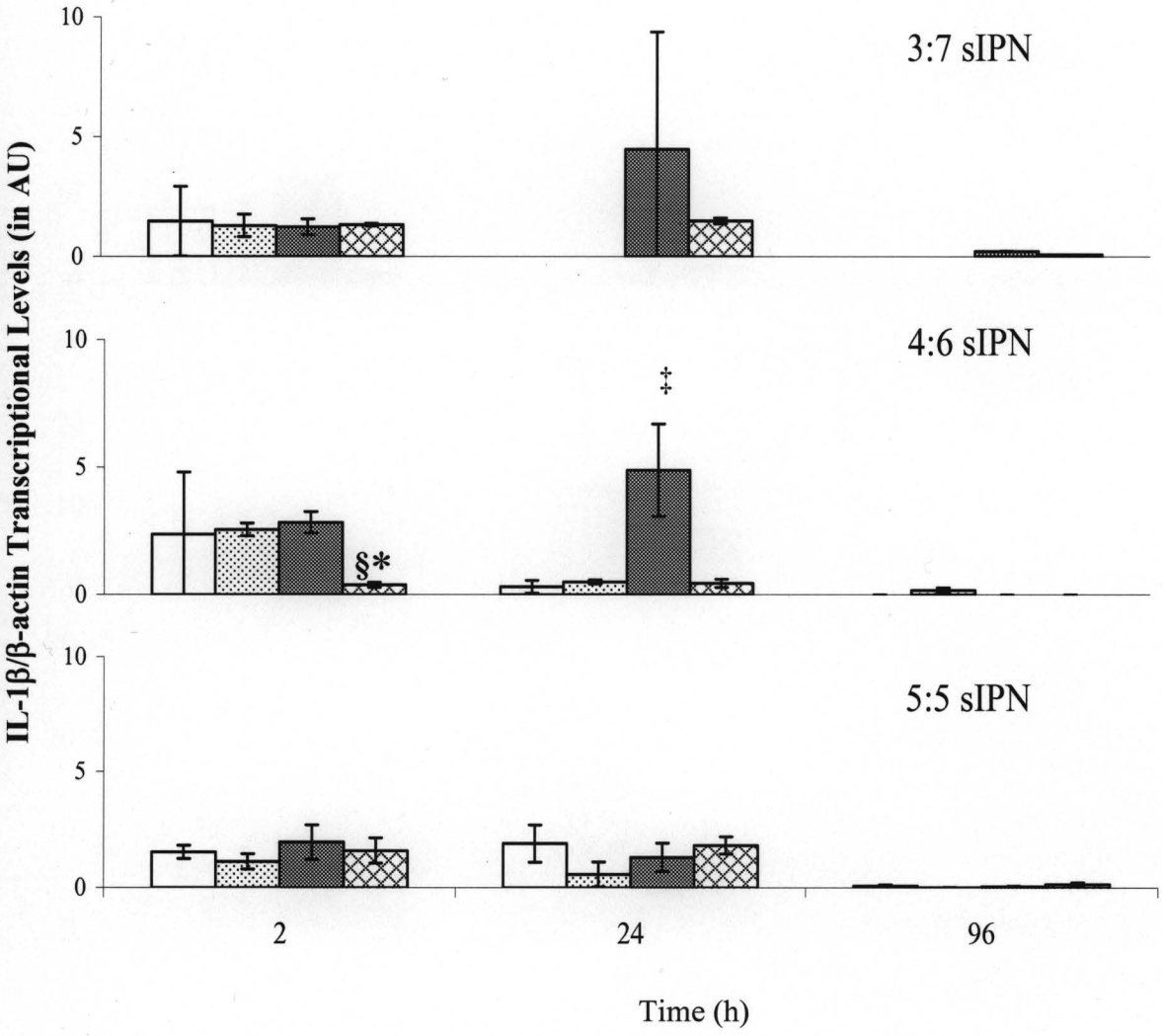

Figure 3-8. RT-PCR analysis for IL-1β/β-actin mRNA levels from adherent monocytes in the presence of 3:7, 4:6 and 5:5 wt% ratio of ligand-PEG grafted gelatin:PEGdA sIPNs: methoxy-(▭), GGG-(▭), RGD-(▭), and PHSRN-PEG grafted sIPN (▭). Data are expressed as mean ± s.d. §Significantly different (p<0.05) from GGG-PEG grafted sIPN (within sIPN group and time point). *Significantly different (p<0.05) from RGD-PEG grafted sIPN (within sIPN group and time point). ‡Significantly different (p<0.05) from all other ligand-PEG grafted sIPN (within sIPN group and time point).

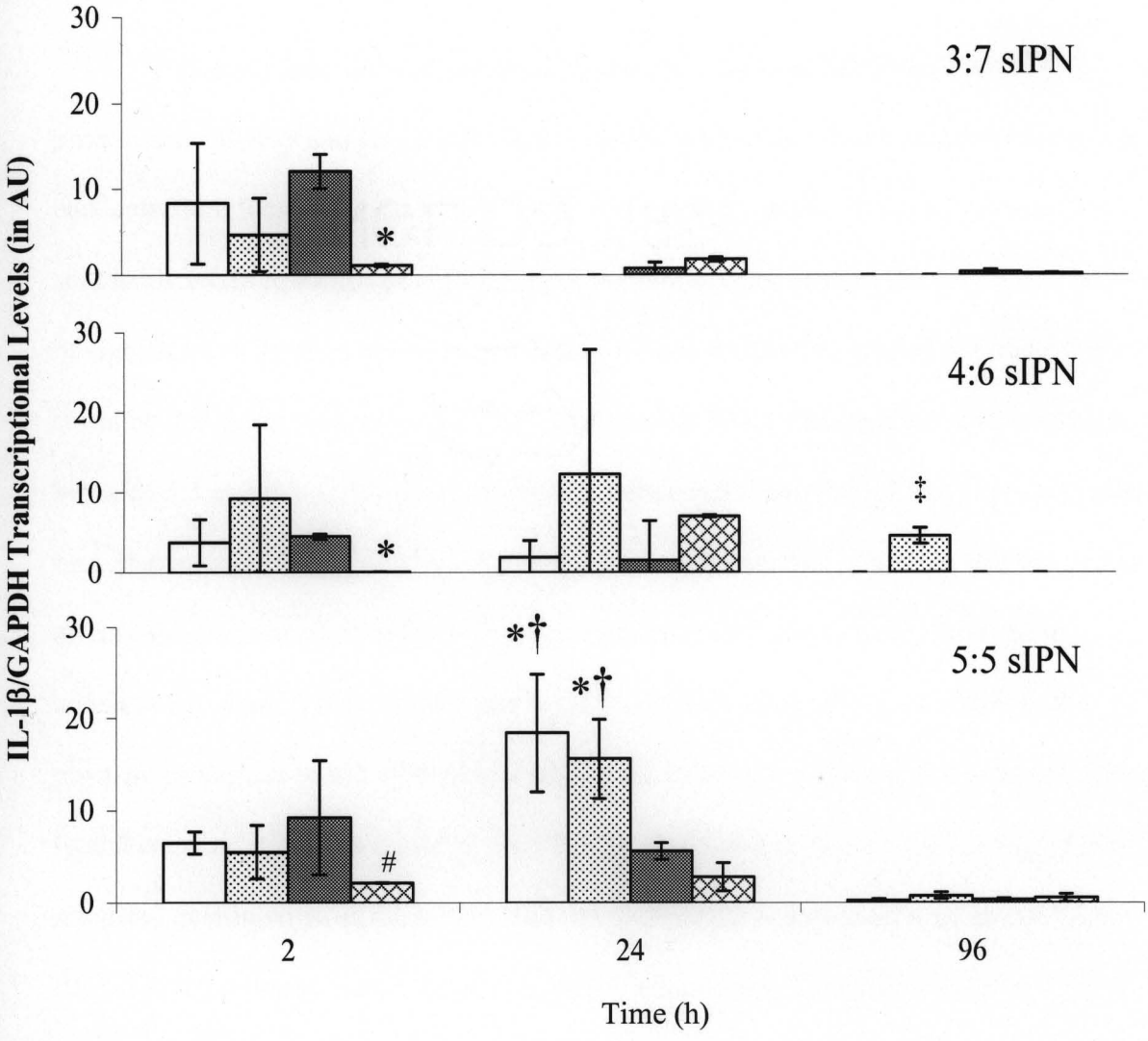

Figure 3-9. RT-PCR analysis for IL-1β/GAPDH mRNA levels from adherent monocytes in the presence of 3:7, 4:6 and 5:5 wt% ratios of ligand-PEG grafted gelatin:PEGdA sIPNs: methoxy-(▭), GGG-(▭), RGD-(▭), and PHSRN-PEG grafted sIPN (▭). Data are expressed as mean ± s.d. #Significantly different ($p<0.05$) from methoxy-PEG grafted sIPN (within sIPN group and time point). *Significantly different ($p<0.05$) from RGD-PEG grafted sIPN (within sIPN group and time point). †Significantly different ($p<0.05$) from PHSRN-PEG grafted sIPN (within sIPN group and time point). ‡Significantly different ($p<0.05$) from all other ligand-PEG grafted sIPN (within sIPN group and time point).

3.4 Discussion and Conclusion

This study has shown that human monocyte adhesion, MMP-2/-9 and IL-1β protein and MMP-9 and IL-1β mRNA expression were influenced by ligand identity and concentration. Increasing the wt% of RGD-PEG grafted gelatin in the sIPN increased accessible RGD concentration on the sIPN surface, but not beyond the 4:6 wt%. The lack of significant difference in accessible RGD between RGD-PEG grafted 4:6 and 5:5 sIPNs could be due to the less incremental wt% increase in RGD-PEG grafted gelatin content between 5:5 and 4:6 sIPNs compared to that between 3:7 and 4:6 sIPNs. There may also be a plateau after which RGD accessibility on the sIPN surface is limited and the ligand effects are diminished. Similar to this, no significant differences were observed in adherent cell density between 4:6 and 5:5 RGD-PEG grafted sIPNs. In addition, the physical properties of the sIPN play a role in the monocyte response. As the accessible ligand concentration was varied in the sIPN by increasing or decreasing the ligand-PEG modified gelatin wt % in the sIPN construct, the change in gelatin as well as the ligand-PEG that was conjugated on the gelatin backbone was also changed. Furthermore, the endogenous RGD in the gelatin backbone was also changed, and the Young's modulus and topography of the sIPN construct. Thus, conclusions on the monocyte adherent density as well as the IL-1β and MMP-2/-9 expression must be made with the accessible RGD concentration as examined by RGD targeted antibody (Figure 3-2) in mind. The effectiveness of the RGD concentration, in this case, then, should be taken in the context of the nature of the background substrate. The data may also suggest that the minimum concentration required for the effectiveness of the RGD peptide on monocyte adhesion and protein expression is also dependent on the nature of the background substrate.

As shown in our previous work, initial monocyte adhesion was regulated by β1 and β3 containing integrin complexation onto RGD presented on the sIPN surface. However, other cell-material interaction involving various gelatin domains in the sIPN is likely to influence cell adhesion and subsequent behavior. For example, cells can adhere to gelatin via αVβ3-RGD complexation as well as α5β1-fibronectin bridge.[33,34] The mannose receptor expressed on the macrophage surface also specifically binds to gelatin.[35] Further, monocyte interactions with the sIPN are not limited to gelatin but also involve interactions with PEG. In another study, human monocytes are shown to adhere comparable to TCPS and respond to PEG-only hydrogels.[36]

Clear differences in MMP-2 and IL-1β protein release profiles over time were observed at initial time points from 3:7 sIPN as compared to those from 4:6 and 5:5 sIPN. Although this could be a result of the more significant incremental increase in gelatin wt% from 3:7 to 4:6 sIPNs compared to that between 4:6 and 5:5 sIPNs, a "threshold effect" of gelatin or PEG content at which MMP-2 and IL-1β release is suppressed may also exist. Though the kinetic pattern of MMP-2 protein release over time between 4:6 and 5:5 sIPN was similar, MMP-2 concentrations were generally higher for 4:6 compared to that of 5:5 sIPN. Even with the initial burst of MMP-2 protein release at 2 h for 4:6 and 5:5 sIPNs, MMP-2 mRNA was not observed from any sample at any time point. However, the disconnect between MMP-2 protein and mRNA expression has been reported by others.[20,38] The MMP-2 gene, containing few conserved *cis*-elements in the promoter region, has been speculated to transcribe MMP-2 protein, then to store the protein in the matrix until activation.[39, 40]

MMP-9 protein release was modulated by ligand identity, material formulation and time. Increasing MMP-9 protein concentration was consistent with generally increasing MMP-9/ β-actin and MMP-9/GAPDH over time. Ligand specific expression of MMP-9 protein and MMP-9/GAPDH mRNA was observed. For example, GGG-, and PHSRN-PEG grafted 4:6 sIPN showed a drastic increase in MMP-9 protein concentration from 24 to 96 h. This correlates with higher MMP-9/GAPDH mRNA levels at 96 h for GGG-, and PHSRN-PEG grafted 4:6 sIPNs, though the MMP-9/GAPDH level for PHSRN-PEG grafted 4:6 sIPN was not statistically significant.

Decreasing IL-1β protein concentrations were paralleled by decreasing IL-1β mRNA levels over time. At 24 h, RGD-PEG grafted 4:6 sIPNs showed higher IL-1β/β-actin mRNA levels compared to all other ligand-PEG grafted 4:6 sIPN. This was partly a result of low β-actin levels, perhaps due to specific receptor-ligand interactions and/or perhaps to the lack of cytoskeletal rearrangement on the sIPN surface. Ligand specific expression of IL-1β protein and mRNA expression was also observed. For example, relatively low IL-1β mRNA levels were observed for PHSRN-PEG grafted 4:6 sIPNs at 2 h and this correlated with significantly lower IL-1β protein concentrations for PHSRN-PEG grafted 4:6 sIPN as compared to methoxy-, and GGG-PEG grafted 4:6 sIPNs at 24 h. Only a trace amount or no IL-1β/β-actin and IL-1β/GAPDH mRNA were detected by 96 h, consistent with the decrease in IL-1β protein concentration at 96 h and beyond. The decrease in IL-1β protein levels was observed with an increase in MMP-9. The increase in MMP-9 protein from 24 to 96 h following the increase in IL-1β from 2 to 24 h correlates well with previous findings on IL-1β induction of MMP-9.[22] MMP-9 has also been shown to degrade IL-1β, and the decrease in IL-1β protein from 24 to 96 h

could correspond with an increase in MMP-9 concentrations from 24 to 96 h.[21] Thus, in the context of sIPNs, monocyte expression of MMP-9 and IL-1β showed a potential autocrine regulation.

Thus, we have demonstrated that human monocyte adhesion, MMP-2/-9 and IL-1β protein and MMP-9 and IL-1β mRNA expression were influenced by ligand identity and concentration. These interrelationships are not always a positive correlation but a complex, time-dependent phenomenon.

3.5 References

1. Noda M, Wataha J, Lockwood P. Low-dose, long-term exposures of dental material components alter human monocyte metabolism. J Biomed Mater Res 2002;62(2):237-243.

2. Phillips JM, Kao WJ. Macrophage adhesion on gelatin-based interpenetrating networks grafted with PEGylated RGD. Tissue Engineering 2005;11(5/6):964-973.

3. Xia Z, Triffitt JT. A review on macrophage responses to biomaterials. Biomed Mater 2006;1(1):R1-R9.

4. Kao WJ, Lee D, Schense JC, Hubbell JA. Fibronectin modulates macrophage adhesion and FBGC formation: the role of RGD, PHSRN, and PRRARV domains. J Biomed Mater Res 2000;55(1):79-88.

5. Maheshwari G, Brown G, Lauffenburger DA, Wells A, Griffith LG. Cell adhesion and motility depend on nanoscale RGD clustering. J Cell Sci 2000;113(10):1677-1686.

6. Massia SP, Hubbell JA. An RGD spacing of 440 nm is sufficient for integrin αvβ3-mediated fibroblast spreading and 140 nm for focal contact and stress fiber formation. J Cell Bio 1991;114(5):1089-1100.

7. Mann BK, Tsai AT, Scott-Burden T, West JL. Modification of surfaces with cell adhesion peptides alters extracellular matrix deposition. Biomaterials 1999;20(23/24):2281-2286.

8. Mann BK, West JL. Cell adhesion peptides alter smooth muscle cell adhesion, proliferation, migration, and matrix protein synthesis on modified surfaces and in polymer scaffolds. J Biomed Mater Res 2002;60(1):86-93.

9. Cutler SM, Garcia AJ. Engineering cell adhesive surfaces that direct integrin α5β1 binding using a recombinant fragment of fibronectin. Biomaterials 2003;24(10):1759-1770.

10. Liu JC, Heilshorn SC, Tirrell DA. Comparative cell response to artificial extracellular matrix proteins containing the RGD and CS5 cell-binding domains. Biomacromolecules 2004;5(2):497-504.

11. Chung AS, Gao Q, Kao WJ. Macrophage matrix metalloproteinase-2/-9 gene and protein expression following adhesion to ECM-derived multifunctional matrices via integrin complexation. Biomaterials 2006;28(2):285-298.

12. Chung AS, Gao Q, Kao WJ. Either integrin subunit beta1 of beta3 is involved in mediating monocyte adhesion, IL-1beta protein and mRNA expression in response to surface functionalized with fibronectin-derived peptides. J Biomater Sci Polym Ed 2007;18(6):713-729.

13. Waldeck HM, Chung AS, Kao WJ. Interpenetrating networks containing gelatin modified with PEGylated RGD and soluble KGF: synthesis: characterization, application in *in vivo* critical dermal wound. J Biomed Mater Res 2007;82A(4):861-871.

14. Garcia AJ. Interfaces to control cell-biomaterial adhesive interactions. Adv Polym Sci 2006;203:171-190.

15. Neff JA, Tresco PA, Caldwell KD. Surface modification for controlled studies of cell-ligand interactions. Biomaterials 1999;20(23/24):2377-2393.

16. Shin H, Jo S, Mikos AG. Modulation of marrow stromal osteoblast adhesion on biomimetic oligo[poly(ethylene glycol) fumarate] hydrogels modified with Arg-Gly-Asp peptides and a poly(ethylene glycol) spacer. J Biomed Mater Res 2002;61(2):169-179.

17. Garcia AJ, Ducheyne P, Boettiger D. Cell adhesion strength increases linearly with adsorbed fibronectin surface density. Tissue Engineering 1997;3(2):197-206.

18. Schense JC, Hubbell JA. Three-dimensional migration of neurites is mediated by adhesion site density and affinity. J Biol Chem 2000;275(10):6813-6818.

19. Martinez-Diaz GJ, Nelson D, Crone WC, Kao WJ. Mechanical and chemical analysis of gelatin-based hydrogel degradation. Macromol Chem Phys 2003;204:1898-1908.

20. Parks WC. Matrix metalloproteinases in repair. Wound Repair Regen 1999;7(6):423-432.

21. Ito A, Mukaiyama A, Itoh Y, Nagase H, Thogersen IB, Enghild JJ, Sasaguri Y, Mori Y. Degradation of interleukin 1β by matrix metalloproteinases. J Biol Chem 1996;271(25):14657-14660.

22. Rao VH, Singh RK, Delimont DC, Schaefer GB, Bridge JA, Neff JR, Sanger WG, Sappenfield JW, Buehler BA, Finnell RH. Interleukin-1β upregulates MMP-9 expression in stromal cells of human giant cell tumor of bone. J Interf Cytok Res 1999;19(10):1207-1217.

23. Miller KM, Anderson JM. Human monocyte/macrophage activation and IL-1 generation by biomedical polymers. J Biomed Mater Res 1988;22:713-731.

24. McCawley LJ, Matrisian LM. Matrix metalloproteinases: They're not just for matrix anymore. Curr Opin Cell Biol 2001;13(5):531-540.

25. Einerson NJ, Stevens KR, Kao WJ. Synthesis and physicochemical analysis of gelatin-based hydrogels for drug carrier matrices. Biomaterials 2002;24:509-523.

26. Lin-Gibson S, Bencherif S, Cooper JA, Wetzel SJ, Antonucci JM, Vogel BM, Horkay F, Washburn NR. Synthesis and characterization of PEG dimethacrylates and their hydrogels. Biomacromolecules 2004;5(4):1280-1287.

27. Gattas-Asfura KM, Weisman E, Andreopoulos FM, Micic M, Muller B, Sirpal S, Pham SM, Leblanc RM. Nitrocinnamate-functionalized gelatin: synthesis and "smart" hydrogel formation via photo-cross-linking. Biomacromolecules 2005;6(3):1503-1509.

28. Benoit DS, Anseth KS. The effect on osteoblast function of colocalized RGD and PHSRN epitopes on PEG surfaces. Biomaterials 2005;26(25):5209-5220.

29. McNally AK, Anderson JM. Complement C3 participation in monocyte adhesion to different surfaces. P Natl Acad Sci USA 1994;91(21):10119-10123.

30. Chomczynski P, Sacchi N. Single-step method of RNA isolation by acid guanidinium thiocyanate-phenol-chloroform extraction. Anal Biochem 1987;162(1):156-159.

31. Gao Q, Meijer MJW, Kubben FJGM, Sier CFM, Kruidenier L, van Duijn W, van den Berg M, van Hogezand RA, Lamers CBHW, Verspaget HW. Expression of

matrix metalloproteinases-2 and -9 in intestinal tissue of patients with inflammatory bowel diseases. Digest Liver Dis 2005;37(8):584-592.

32. Bas A, Forsberg G, Hammarstroem S, Hammarstroem ML. Utility of the housekeeping genes 18S rRNA, β-actin and glyceraldehyde-3-phosphate-dehydrogenase for normalization in real-time quantitative reverse transcriptase-polymerase chain reaction analysis of gene expression in human T lymphocytes. Scand J Immunol 2004;59(6):566-573.

33. Davis GE. Affinity of integrins for damaged extracellular matrix: αvβ3 binds to denatured collagen type I through RGD sites. Biochem Bioph Res Co 1992;182(3):1025-1031.

34. Tuckwell DS, Ayad S, Grant ME, Takigawa M, Humphries MJ. Conformation dependence of integrin-type II collagen binding. Inability of collagen peptides to support α2β1 binding, and mediation of adhesion to denatured collagen by a novel α5β1-fibronectin bridge. J Cell Sci 1994;107(4):993-1005.

35. Martinez-Pomares L, Wienke D, Stillion R, McKenzie EJ, Arnold JN, Harris J, McGreal E, Sim RB, Isacke CM, Gordon S. Carbohydrate-independent recognition of collagens by the macrophage mannose receptor. Eur J Immunol 2006;36(5):1074-1082.

36. Schmidt DR, Kao WJ. Monocyte activation in response to PEG hydrogels grafted with RGD and PHSRN separated by interpositional spacers of various lengths. J Biomed Mater Res e-published May 2007.

37. Agren MS. Gelatinase activity during wound healing. Brit J Dermatol 1994;131(5):634-640.

38. Van den Steen PE, Dubois B, Nelissen I, Rudd PM, Dwek RA, Opdenakker G. Biochemistry and molecular biology of gelatinase B or matrix metalloproteinase-9 (MMP-9). Crit Rev Biochem Mol 2002;37(6):375-536.

39. Werb Z. ECM and cell surface proteolysis: regulating cellular ecology. Cell 1997;91(4):439-442.

40. Murphy G, Gavrilovic J. Proteolysis and cell migration: creating a path? Curr Opin Cell Biol 1999;11(5):614-621.

Chapter 4. Fibroblasts Regulate Monocyte Response to ECM-derived Matrix: The Effects on Monocyte Adhesion and the Production of Inflammatory, Matrix Remodeling and Growth Factor Proteins

4.1 Introduction

As displayed in Figures 1-1 and 1-2 in Chapter 1, fibroblasts and collagen have been found in close proximity to inflammatory cells such as monocytes at the wound bed during repair, we examined monocyte adhesion and subsequent protein expression on the ECM-derived sIPN in the presence of fibroblasts. RGD has been utilized extensively to modify biomaterials to promote integrin-mediated cell attachment and we have previously demonstrated that RGD grafted onto an ECM-based sIPN enhances cell adhesion and modulates signaling, and cytokine and gene expression [1-4]. We demonstrated in Chapter 2 that adherent monocyte density was increased by RGD tethered onto a PEG linker on the gelatin based sIPN, and that subsequent protein and genetic regulation of IL-1β and MMP-2/-9 was increased in response to sIPNs. RGD-PEG grafted sIPNs also enhanced cellularity and organized ECM reconstruction over time *in vivo* in dermal wound healing models [5].

As inflammation and matrix remodeling are complex interweaving event with monocytes/macrophages and fibroblasts playing key roles in the progression of wound healing, we hypothesized that monocytes and fibroblasts in the context of the ECM analog sIPN would provide a more accurate analysis of the temporal wound healing proteins compared to monoculture investigations. Thus, a monocyte-fibroblast co-culture system in the presence of the sIPN was constructed as shown in Figure 4-1.

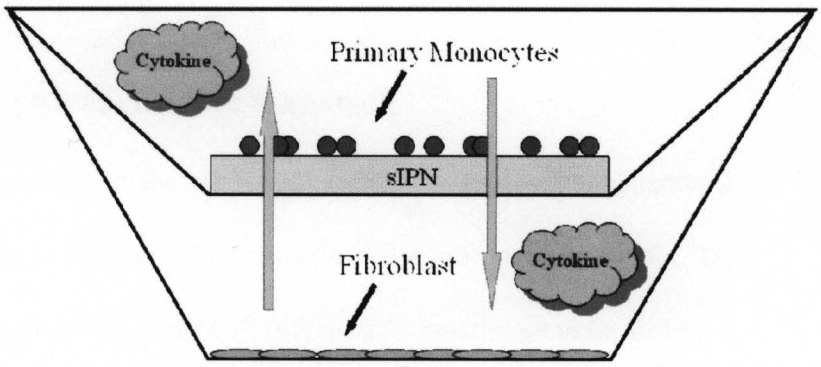

Figure 4-1 Monocyte/fibroblast co-culture set up

In this study, we sought to investigate the influence of fibroblasts on monocyte response to this ECM mimic. Both fibroblasts and monocytes are present during the granulation stage of wound healing and they coordinate a highly controlled set of inflammatory, ECM production and breakdown events during wound healing [6,7]. An understanding of the endothelial cell/blood/biomaterial interactions is central to advancing the field of bioengineering and drug delivery. As a highly controlled set of inflammatory, ECM production and breakdown events exists in wound healing, examining the monocyte-fibroblast protein-mediated communication in the context of the ECM-mimic sIPN will provide crucial insight into the sIPN's role in wound healing facilitation. However there are few studies investigating the role of fibroblasts in directly regulating human monocyte response to ECM components [8-10]. As current reports of a monocyte-fibroblast co-culture system in an ECM-derived scaffold setting nearly absent, this work sheds critical insight into the intermolecular paracrine communication between monocytes and fibroblasts as well as into the sIPN's role in wound healing facilitation. Key wound healing factors in inflammation, matrix remodeling and regeneration were analyzed to gain insight into the interrelated role of regulation in fibroblast-monocyte interaction.

4.2 Methods and Materials

4.2.1 Preparation of sIPN cast polycarbonate transwell

Ligand-modified gelatin preparation for the sIPN is described extensively in Chapter 2, section 2.2.1. sIPNs were cast and polymerized directly onto the polycarbonate transwells. The mPEG-gelatin, GGG-PEG-gelatin, RGD-PEG-gelatin, PHSRN-PEG-gelatin, or unmodified gelatin was dissolved in ddH_2O (10% w/v) by heating at 60°C. The gelatin solution was added to PEG diacrylate (PEGdA, $M_n \approx 575$ Da) to form a 4:6 gelatin:PEGdA weight ratio. 20 μl of 2,2-dimethoxy-2-phenyl-acetophenone (DMPA) initiator solution (0.02 g DMPA in 0.5g PEGdA) was added to the gelatin/PEGdA mixture, vortexed, and 175 μl was transferred to the polycarbonate transwell insert (3.0 μm pore size, d = 12 mm, Corning Inc., Corning, NY) and polymerized directly in the insert via exposure to light emitting diode (λ_{max} = 365 nm at 10 cm) for 5 min. The resultant sIPNs were dipped into a 70% ethanol solution for 30 min for sterilization, rinsed three times with 1 x PBS and transferred to 12 well plates to equilibrate for 3 days in 1 x PBS all under 4°C. Density of peptide-PEG-sIPN was previously analyzed on RGD-PEG grafted sIPNs via ELISA using RGD directed antibody [11]. We found that accessible RGD concentration (μmole/ml) on the unmodified sIPN surface was significantly ($p<0.05$) lower compared to that of RGD-PEG grafted sIPN [12]. sIPN containing transwells and polycarbonate transwells were equilibrated in RPMI 1640 at 37°C and 5% CO_2 for 2 h prior to monocyte seeding.

4.2.2 Protein diffusion through the sIPN

The diffusion of three proteins of varying molecular weights through the sIPN from one chamber to another were examined: rhGM-CSF (ProSpec-Tany TechnoGene Ltd., Rehovot, Israel), BSA-FITC (Sigma, St. Louis, MO) and MMP-2 (EMD Chemicals, Inc., San Diego, CA), of 14.5 kDa, 65 kDa, and 72 kDa, repectively. As the highest concentration from the in vitro assays were observed approximately at 20 ng/ml, that concentration of each protein was added to either chamber A or B and the diffusion into the other chamber was observed over 2, 24, and 96 h. rhGM-CSF or rhMMP-2 was added to either chamber A or B and the diffusion into the other chamber was measured via ELISA (R&D Systems, Minneapolis, MN and EMD Chemicals, Inc., San Diego, CA, respectively). Quantification of BSA-FITC was carried out with a spectrofluorometer (Thermo-Spectronic AB/2 luminescence spectrometer) with excitation and emission wavelength of 495 and 520 nm, respectively.

In separate experiments, small molecule diffusion across the sIPN was also examined with fluorescein (332.31 g/mol, Sigma, St. Louis, MO) at 67 μg/ml in PBS where 0.5 ml of this solution was place in chamber A and 1.5 ml of PBS without the dye molecule was placed in chamber B and absorbance was measured at 469 nm at 5, 30, 60 and 120 min, all under ambient temperature. Diffusion across chambers was observed as early as 5 min, and by 120 min both chambers had equilibrated with 16.4 μg/ml in chamber A and 13.4 μg/ml in chamber B. A portion of the fluorescein was entrapped within the sIPN thus absorbance readings in both chambers did not reflect the total concentration throughout 120 min. We also observed previously that time to maximum percent released of basic fibroblast growth factor out of the sIPN was 2 h [15].

4.2.3 Monocyte/fibroblast monoculture and co-culture

Neonatal human dermal fibroblasts (NHDF) (Lonza Group Ltd, Switzerland) between passages 4 through 7 were seeded in a 12-well TCPS plate (Corning Inc., Corning, CA) and cultured to a monolayer confluency (approx > 90%) in fibroblast growth media (FGM) plus 5% FBS as previously described [13]. Once fibroblasts reached confluency, the media was removed and replaced with RPMI 1640 (GIBCO, Carlsbad, CA) containing 10% human serum for 3 days prior to the experiment. Effects of the media transition were optimized prior to the experiment and fibroblast confluency/cell density, morphology and viability on TCPS were monitored at 48 and 168 h. Confluency was unaffected by RPMI with 10% human serum through 168 h and LIVE/DEAD assay (Invitrogen, Carlsbad, CA) confirmed > 95% fibroblast viability was also maintained by this media, as observed with FGM supplemented with 5% FBS (n = 3). Morphological observations also revealed that the characteristic spindle shape (shown in Appendix, Figure i) was unaltered by RPMI supplemented with 10% human serum. This indicates that the culture medium employed in the co-culture sets in the current study did not adversely affect the behavior of fibroblasts.

Human peripheral blood monocytes were isolated from citrated whole blood of a healthy, medication-refrained adult volunteer using a density-gradient, non-adhesion method previously described in detail [14]. Briefly, citrated blood (100~150 ml) was diluted 1:2 with PBS/5mM EDTA (PBSE), layered onto Ficoll-Paque (GE Healthcare, Uppsala, Sweden), and centrifuged at 400 × g for 30 min (no brake). The resultant mononuclear cells were serially washed three times with 50 volumes of PBSE by centrifugation at 350, 200 and 150 × g for 10 min each. Cells were resuspended in 2~3 ml of PBSE, layered onto two 10-ml columns of FBS, and centrifuged at 120 × g for 10 min. The same procedure was repeated, after which cells were resuspended in 3.5 ml

of PBSE, added to 6.7 ml of Percoll (Sigma, St. Louis, MO), mixed and centrifuged at 2000 × g for 25 min (no brake). The resultant topmost cell layer (1 ml) was washed twice with 50 volumes of cold RPMI 1640 medium resuspended in cold RPMI 1640, and seeded immediately.

Co-culture set up: Freshly isolated cells were seeded onto each surface on the transwell insert (i.e. polycarbonate transwell or ligand-PEG grafted sIPN surface) at a concentration of 10^6 cells/ml in RPMI 1640 culture medium and 10% autologous serum at 37°C and 5% CO_2 and cultured up to 96 h. Once the monocytes were seeded onto the transwell insert with or without sIPN, it was immediately but gently placed into the well with a confluent layer of fibroblasts. Figure 4-2 outlines the monocyte and fibroblast co-culture schematic in the presence of the sIPN. Chamber A refers to the upper chamber where monocytes were seeded and chamber B refers to the bottom chamber where a confluent layer of fibroblasts were cultured. Monocultures were constructed in the same set up as co-cultures, but with only monocytes in chamber A for monocyte monocultures and only fibroblasts in chamber B for fibroblast monocultures. While monocytes in monocultures were in direct contact with sIPNs or polycarbonate transwell, a confluent layer of fibroblasts on TCPS in chamber B in fibroblast monocultures were in the presence of, but were not in direct contact with the various surfaces. Supernatants were collected from both chamber A and B at all time points and all monocultures and co-cultures.

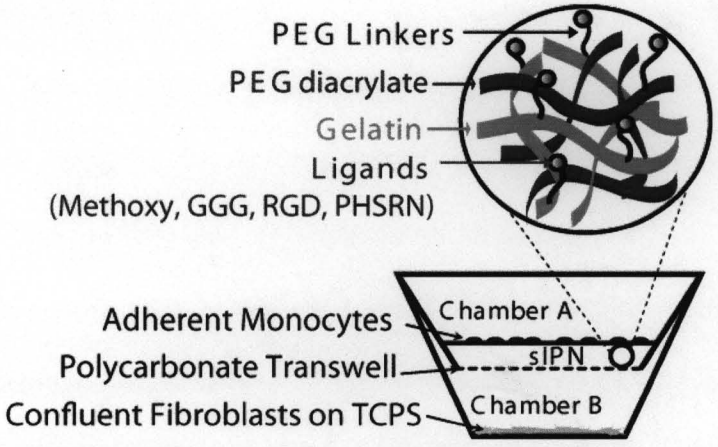

Figure 4-2. Monocyte/fibroblast co-culture setup with the sIPN.

4.2.4 Cell based assays: LIVE/DEAD, ELISA, microsphere-based multiplex protein assay and immunoblotting

At 2, 24, and 96 h, all surfaces were rinsed with D-PBS and stained with LIVE/DEAD (Invitrogen, Carlsbad, CA). Working dilutions of calcein-AM (2 μM) and ethidium homodimer-1 (4 μM) were made in D-PBS immediately before use. For each sample well in chamber A, a minimum of two different areas at 0.55 mm^2 each were imaged using an inverted microscope. Confluent fibroblasts in chamber B were not quantified but LIVE/DEAD assay was still carried out for verification of fibroblast viability. Supernatants were collected from both chamber A and B at 2, 24, and 96 h. With the supernatant collected at 2, 24 and 96 h, all proteins were analyzed with the microsphere-based multiplex protein assay (Linco Research, St. Charles, MO), except MMP-2 and MMP-9, where the ELISA (Raybiotech Inc., Norcross, GA) method was used. The ELISA and the microsphere-based multiplex protein assays were carried out according to manufacturers' instructions. The protein concentrations reported contain the concentrations in addition to the protein concentrations from the 10% autologous serum in the media.

Immunoblotting procedures were carried out by collecting the adhered cells with trypsin and lysing the cells in mammalian protein extraction reagent (Thermo Scientific, Rockford, IL). Cell lysate was incubated with a 10% protease inhibitor cocktail in M-PER at 4°C for 15 min then briefly sonicated. The cell lysate solution was centrifuged to rid of cell debris and the solution was analyzed for total protein concentration with the bicinchoninic acid (BCA) protein assay then 0.142 μg of protein was resolved by 12% SDS-PAGE. Resolved proteins were transferred to a nitrocellulose blotting membrane and incubated overnight in blocking solution, 5% milk in phosphate buffer saline tween-20 (PBST), at 4°C. Samples were incubated with anti-human vinculin monoclonal antibody (hVIN-1) (Sigma, St. Louis, MO) overnight, then washed

with washing buffer (1%PBST) then incubated with horse radish peroxidase (HRP) conjugated an anti-mouse polyclonal antibody (Cell Signaling Technology, Inc., Danvers, MA) for 1 h. The resulting samples were washed twice with PBST, rinsed with PBS and developed via chemiluminescence. Tubulin protein expression was used as a positive control for all immunoblots.

4.2.5 Statistical analysis

Cell adhesion and ELISA data were expressed as the mean of triplicate wells ± standard deviation (n = 3). Adherent live cell density data and protein concentrations were analyzed by unpaired Student *t*-test where $p < 0.05$ was considered statistically significant.

4.3 Results

4.3.1 Protein diffusion through the co-culture system

The diffusion of three proteins of varying molecular weights rhGM-CSF (14.5 kDa), BSA-FITC (66 kDa) and rhMMP-2 (72 kDa) through the sIPN from one chamber to another were examined. Protein was added to either chamber A or B and the diffusion into the other chamber through the sIPN was observed over 2, 24, and 96 h.

Diffusion of GM-CSF from chamber A to B through the polycarbonate transwell insert without sIPN was observed as early as 2 h (Figure 4-3) and for all surfaces, the total concentration of both chambers does not yield the original concentration of 20 ng/ml at any time point.

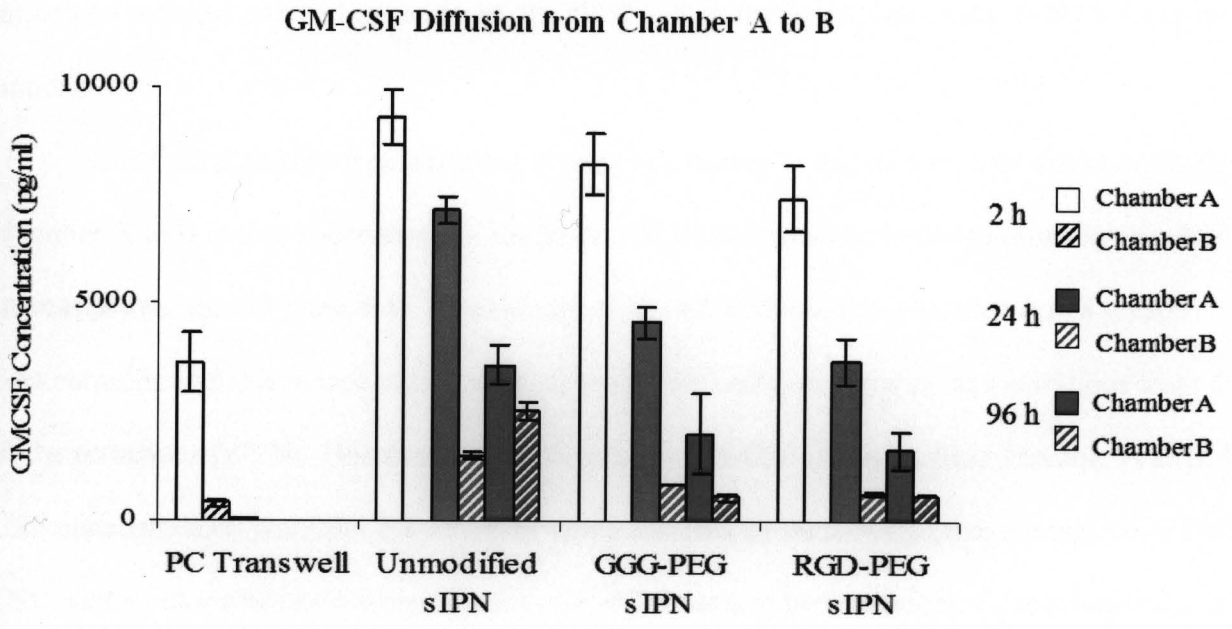

Figure 4-3. GM-CSF concentrations over time in chamber A and B in the presence of various surfaces. GM-CSF diffusion was from chamber A to chamber B.

However, concentrations decreased to nondetectable levels by 96 h, possibly due to adsorption of proteins onto the transwell insert and/or the TCPS surface in chamber B. With sIPNs cast transwell inserts, diffused GM-CSF concentrations in chamber B were not detected until 24 h, due to the protein interaction with the sIPN. By 96 h, GM-CSF levels were comparable in unmodified sIPN samples, but concentrations in chamber B in the presence of GGG and RGD-PEG grafted sIPNs were not as high as that from unmodified sIPN samples. This phenomenon is likely due to the ligand-PEG grafting onto the gelatin backbone theoretically decreasing the sIPN's pore size and making the diffusive path more tortuous for the proteins compared to the unmodified sIPN. The highest concentration at 2 h was 9300 pg/ml in the presence of unmodified sIPN, and by 96 h, the GM-CSF concentration from chamber A and B together is 6096 pg/ml. GM-CSF could be

adsorbing onto the polycarbonate insert, the sIPN cast on the insert, and/or the TCPS surface on the bottom.

GM-CSF diffusion from chamber B to A was similar to that of GM-CSF diffusion from chamber A to B in that concentrations in chamber B decreased while concentrations in chamber A increased over time (Figure 4-4). As expected, GM-CSF diffused into chamber A at a greater concentration in the presence of the polycarbonate transwell compared to concentrations from those in the presence of sIPNs. However, as observed with GM-CSF diffusion from chamber A to B, GM-CSF concentrations were not detectable in either chamber by 96 h, suggesting adsorption of GM-CSF on the polycarbonate transwell and/or the TCPS surface in chamber B. Concentrations at 2 h in the presence of polycarbonate transwell also suggests GM-CSF adsorption onto the insert and/or TCPS.

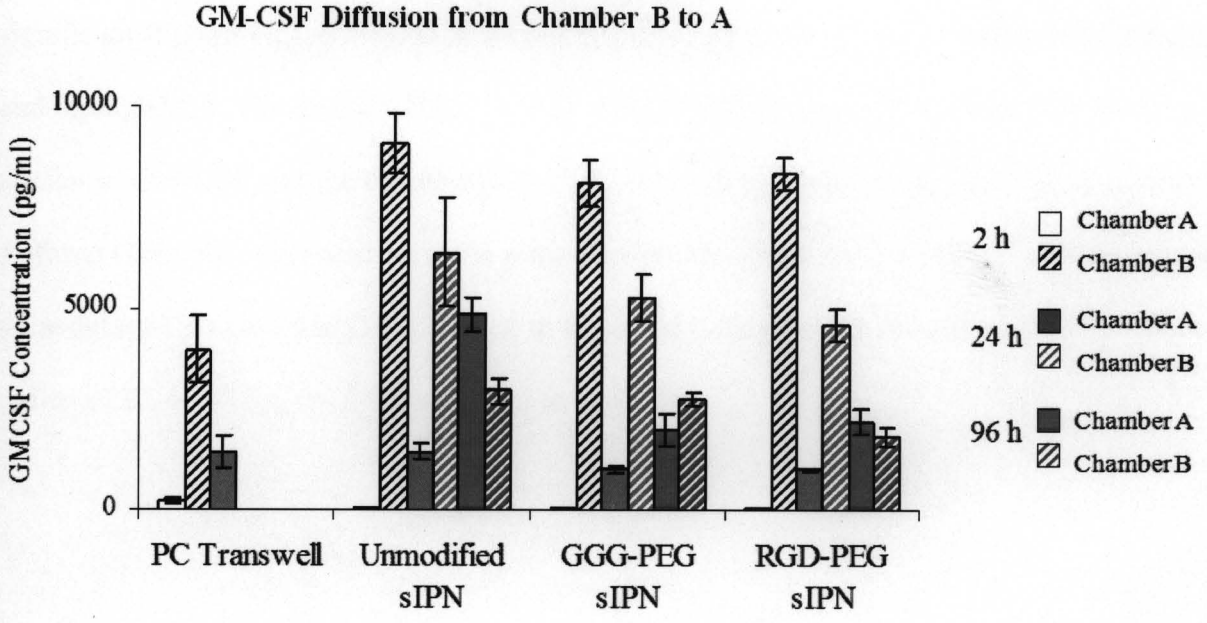

Figure 4-4. GM-CSF concentrations over time in chamber A and B in the presence of various surfaces. GM-CSF diffusion was from chamber B to chamber A.

For example, total GM-CSF concentration at 2 h in the presence of the polycarbonate transwell was 4195 pg/ml while those in the presence of sIPN cast transwell yielded an average GM-CSF concentration of 8537 pg/ml. GM-CSF adsorption onto the polycarbonate transwell is likely the dominant factor in the undetectable levels of GM-CSF by 96 h, observed in either direction (i.e. from chamber A to B, from chamber B to A) of GM-CSF diffusion. Concentrations in the presence of sIPNs were similar over time and while GM-CSF diffusion from chamber A to B was not observed until 24 h, GM-CSF had diffused to chamber A from B by 2 h in the presence of all sIPNs. By 96 h, concentrations in both chambers in the presence of sIPNs were comparable, except for that from unmodified sIPN, where concentrations from chamber A were higher than that from chamber B.

BSA-FITC diffusion was similar to GM-CSF diffusion through the sIPN over time, but adsorption of the protein on to the polycarbonate transwell and/or the TCPS surface was also significant (Figure 4-5). Diffusion of BSA-FITC through the sIPN, was observed beginning at 24 h and through 96 h. The diffused BSA-FITC molecule through the sIPN was observed starting at 24 h, similar to GM-CSF, but the diffused BSA-FITC concentrations were less than that compared to the diffused GM-CSF concentration at the same time points. The diffusion of BSA-FITC was predicted to be delayed compared to GM-CSF due to the larger molecular weight and larger hydrodynamic radius of BSA-FITC (~36.5 Å) compared to GM-CSF.

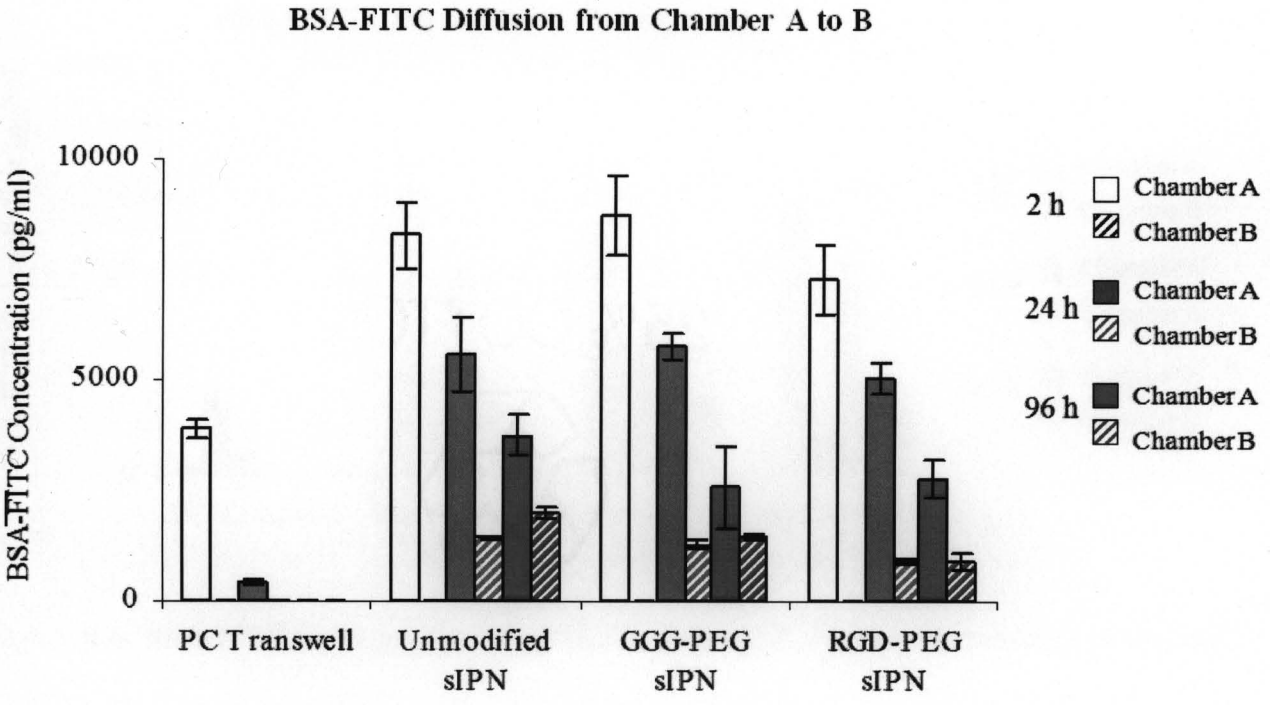

Figure 4-5. BSA-FITC concentrations over time in chamber A and B in the presence of various surfaces. BSA-FITC diffusion was from chamber A to chamber B.

BSA-FITC diffusion from chamber B to A was similar to that of BSA-FITC diffusion from chamber A to B in that diffusion through the sIPN into the other chamber was observed beginning at 24 h and through 96 h (Figure 4-6). Similar to the diffusion from chamber A to B, BSA-FITC concentrations were undetectable by 24 h in chamber B, likely due to the adsorption of the protein onto the polycarbonate transwell and/or the TCPS surface. The BSA-FITC concentration of 20 ng/ml was not detected at any time point, due to the protein's interaction with the polycarbonate transwell, the sIPN, and/or the TCPS surface.

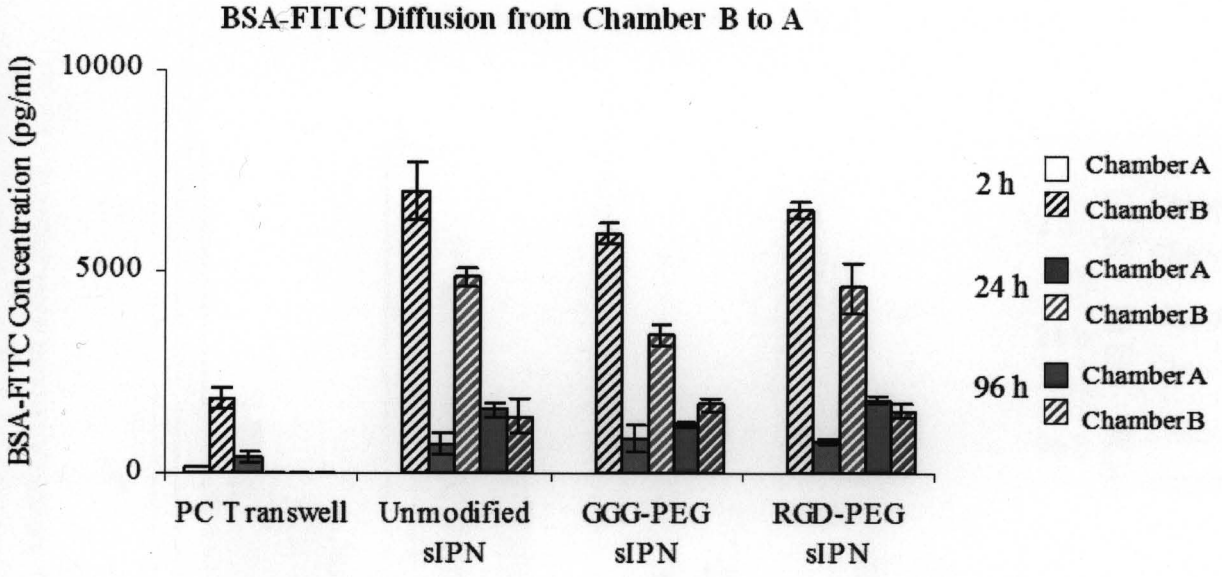

Figure 4-6. BSA-FITC concentrations over time in chamber A and B in the presence of various surfaces. BSA-FITC diffusion was from chamber B to chamber A.

MMP-2 diffusion from chamber A to B was observed starting from 2 h in the presence of polycarbonate transwell without sIPN and by 96 h, concentrations between chamber A and chamber B were comparable (Figure 4-7). MMP-2 also adsorbed to the transwell insert and/or the TCPS surface in chamber B as the starting MMP-2 concentration of 20 ng/ml was decreased to approximately 7 ng/ml by 96 h. In the presence of sIPNs, MMP-2 diffusion was not observed from 2 through 96 h, likely due to the large molecular weight of the enzyme. However, MMP-2 concentrations in chamber A decreased over time, suggesting that the MMP-2 is interacting with the gelatin of the sIPN. Ionic interactions and the activity of the MMP-2 gelatinase may play an important role in this phenomenon. If the MMP-2 enzymes are bound to the gelatin substrate in the sIPN diffusional effects would be masked.

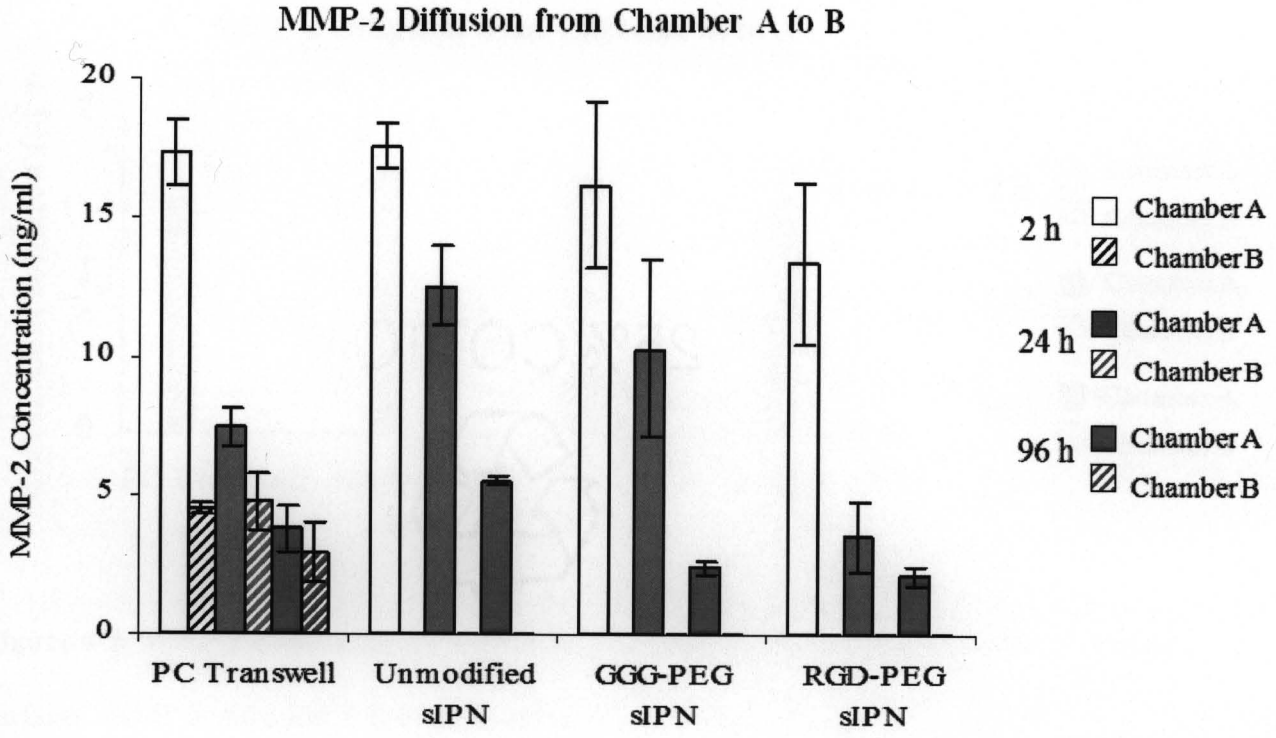

Figure 4-7. MMP-2 concentrations over time in chamber A and B in the presence of various surfaces. MMP-2 diffusion was from chamber A to chamber B.

MMP-2 diffusion from chamber A to B was observed only at 2 h in chamber B for all surfaces and not observed at any other time point in the presence of all surfaces. (Figure 4-8). MMP-2 is either too large to diffuse through and remaining in chamber B then adsorbing onto the TCPS surface or MMP-2 is diffusing through but remains bound to the gelatin substrate present in the sIPN. MMP-2 may have a much higher affinity toward the TCPS surface compared to GM-CSF.

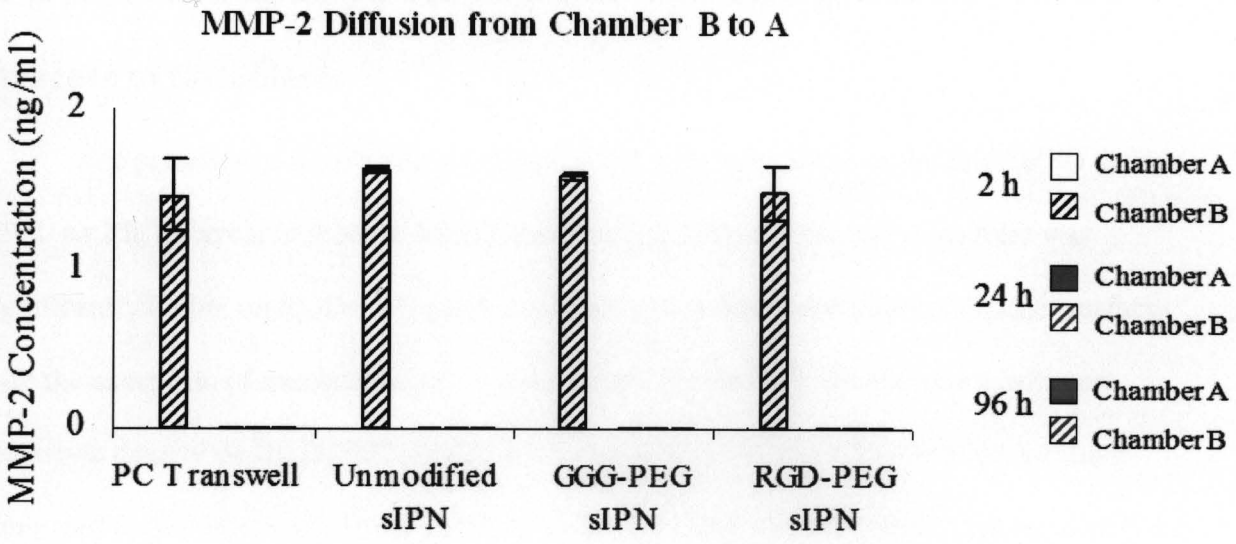

Figure 4-8. MMP-2 concentrations over time in chamber A and B in the presence of various surfaces. MMP-2 diffusion was from chamber B to chamber A.

For MMP-2 diffusion from chamber B to A, diffusion through the sIPN and PC transwell was not observed as MMP-2 concentrations were observed only at 2 h at ~1.5 ng/ml in chamber B and not detectable beyond 2 h for all surfaces. Both the polycarbonate transwell and the TCPS surface are hydrophobic and given the plasma treatment of both surfaces, there are likely strong adsorptive interactions, particularly with MMP-2, that are driving the adhesion of proteins onto the surfaces and leading to nondetectable protein levels. With proteins observed in the co-culture system, a confluent layer of fibroblasts covers the TCPS surface and thus will reduce adsorption. However, the protease and fibroblast processing of the proteins will add more dynamic components to the detection of proteins.

4.3.2 Decreased monocyte adhesion onto RGD-PEG grafted sIPN in the presence of fibroblasts

The presence of fibroblasts decreased initial monocyte adhesion on RGD-PEG grafted sIPN. At 2 h, adherent monocyte density in monocyte monoculture and co-culture was significantly higher on RGD-PEG grafted sIPNs when compared to that on all other surfaces with the exception of unmodified sIPN in co-culture (Table 4-1). Furthermore, adherent monocyte density on RGD-PEG grafted sIPN was approximately 2 fold less in co-culture compared to that in monocyte monoculture at 2 h. On other surfaces, there were no significant differences in adherent monocyte density when comparing between monocyte monoculture and co-culture at 2 and 24 h. Our previous studies had shown that monocytes adhered at significantly low levels on methoxy-/GGG-PEG grafted sIPN when compared to tissue culture polystyrene (TCPS) and PEG-only hydrogels [16]. RGD-PEG grafted sIPN mediated enhanced monocyte adhesion in a ligand-integrin dependent fashion and that subunit β1- and β3-containing integrins were critical in mediating this observation. Although enhanced monocyte adhesion on RGD grafted surfaces is consistent with others' findings, fibroblasts inhibiting this enhanced monocyte adhesion is unexpected.

Table 4-1. Adherent live monocyte density (cell/mm^2) on various surfaces at 2, 24, and 96 h under monocyte monoculture or monocyte/fibroblast co-culture conditions.

		Culture Time (h):		
	Surface/Ligand-PEG grafted sIPN	**2**	**24**	**96**
Monocyte Monoculture	Polycarbonate Transwell	62 ± 25	27 ± 7*	18 ± 5*
	Unmodified Gelatin	138 ± 15^{t}	72 ± 20^{g,p}	85 ± 31^{m,p}
	Methoxy-PEG	156 ± 74	125 ± 47	30 ± 5
	GGG-PEG	158 ± 38^{t}	142 ± 18	53 ± 21
	RGD-PEG	609 ± 90^{t§†}	296 ± 43†	174 ± 27§†
	PHSRN-PEG	121 ± 35	126 ± 12	76 ± 22§
Monocyte/ Fibroblast Co-Culture	Polycarbonate Transwell	39 ± 7*	48 ± 20*	27 ± 4
	Unmodified Gelatin	225 ± 58$^{\#}$	111 ± 31	73 ± 7^{t}
	Methoxy-PEG	92 ± 2	126 ± 14	54 ± 20
	GGG-PEG	95 ± 23	114 ± 11	30 ± 13^{u}
	RGD-PEG	273 ± 24‡	340 ± 48†	99 ± 18^{t,m,g}
	PHSRN-PEG	116 ± 23	141 ± 35	24 ± 9

All values expressed as the mean of triplicate wells ± standard deviation (n=3). Significantly different within time point and surface ($p < 0.05$): §Higher than those under co-culture conditions. Significantly different within time point and culture condition ($p < 0.05$): *Lower than all surfaces, †higher than all surfaces, $^{\#}$higher than all surfaces except RGD-PEG grafted sIPN, ‡higher than all surfaces except unmodified gelatin sIPN, ^{t}higher than polycarbonate transwell surface, ^{m}lower than methoxy-PEG grafted sIPN, ^{g}lower than GGG-PEG grafted sIPN, ^{p}lower than PHSRN-PEG grafted sIPN.

Another data set on monocyte adhesion on sIPNs with or without fibroblasts is shown in Table 4-2 to display the decreased monocyte adhesion onto RGD-PEG grafted sIPN in the presence of fibroblasts. The adhered but dead monocyte density on the polycarbonate transwell surface is also shown. From the low dead adhered monocyte number on the polycarbonate transwell surface in both monocyte monoculture and monocyte fibroblast co-culture, dead monocytes do not appear to remain adhered on the surface but detach.

Table 4-2. Adherent live monocyte density (cell/mm^2) on various surfaces at 2, 4, and 24 h under monocyte monoculture or monocyte/fibroblast co-culture conditions, with dead adherent monocyte density on polycarbonate transwell inserts.

		Culture Time (h):		
	Surface/Ligand-PEG grafted sIPN	**2**	**4**	**24**
Monocyte Monoculture	Polycarbonate Transwell (Live)	140 ± 19*	146 ± 6	122 ± 8
	Polycarbonate Transwell (Dead)	22 ± 5	16 ± 3	12 ± 8
	Unmodified Gelatin	263 ± 20	167 ± 14	148 ± 22
	GGG-PEG	297 ± 42	163 ± 22	73 ± 14*
	RGD-PEG	560 ± 59$^{\#\S}$	329 ± 14$^{\#\S}$	119 ± 6
Monocyte/ Fibroblast Co-Culture	Polycarbonate Transwell (Live)	111 ± 3*	139 ± 19	103 ± 7
	Polycarbonate Transwell (Dead)	29 ± 7	14 ± 6	15 ± 3
	Unmodified Gelatin	206 ± 31	279 ± 37	139 ± 19
	GGG-PEG	283 ± 76	231 ± 14	83 ± 22
	RGD-PEG	280 ± 46	194 ± 10	135 ± 13

All values expressed as the mean of triplicate wells ± standard deviation (n=3). Significantly different within time point and surface ($p < 0.05$): §Higher than those under co-culture conditions. Significantly different within time point and culture condition ($p < 0.05$): *Lower than all surfaces, †higher than all surfaces, $^{\#}$higher than all surfaces except RGD-PEG grafted sIPN

4.3.3 Nonadherent monocyte analysis: viability and vinculin regulation in the presence of fibroblasts in co-culture

There was an unexpected nonspecific interaction between the sIPN and the ethidium homodimer-1 that stains for damaged DNA of dead cells. Thus, the nonadhered cells were analyzed via the LIVE/DEAD assay to examine how much of the nonadhered monocytes were dead. Nonadhered monocyte analysis was carried out at 2, 4, and 24 h. Table 4-3 below shows the ratio of live to dead nonadhered monocytes with or without the presence of fibroblasts.

Table 4-3. Ratio of nonadherent live to nonadherent dead monocytes from various surfaces at 2, 4, and 24 h under monocyte monoculture or monocyte/fibroblast co-culture conditions.

		Culture Time (h):		
	Surface/Ligand-PEG grafted sIPN	**2**	**4**	**24**
Monocyte Monoculture	Polycarbonate Transwell	20 ± 8	46 ± 14	9 ± 7
	Unmodified Gelatin	12 ± 4	5 ± 2	11 ± 5
	GGG-PEG	19 ± 7	4 ± 1	46 ± 13
	RGD-PEG	7 ± 4	2 ± 1	33 ± 3
Monocyte/Fibroblast Co-Culture	Polycarbonate Transwell	30 ± 9	20 ± 10	47 ± 15*
	Unmodified Gelatin	26 ± 13	10 ± 2	23 ± 8
	GGG-PEG	8 ± 1	6 ± 2	48 ± 11
	RGD-PEG	8 ± 4	6 ± 0*	50 ± 29

All values expressed as the mean of triplicate wells ± standard deviation (n=3). Significantly different within time point and surface ($p < 0.05$): *Compared to that under monoculture conditions.

Thus, from table 4-3, the ratio of live to dead nonadhered monocytes do not appear to significantly differ between those under monoculture and those under co-culture conditions within surface, especially at the initial 2 h. At 4 h, the ratio of live to dead monocytes detached from RGD-PEG grafted sIPN appear to be significantly higher under co-culture conditions, and from the raw detached monocyte count (shown in Appendix, Table i), there are more detached live monocytes in co-culture versus detached live monocyte count in monoculture. In other words, the significantly higher ratio observed at 4 h is a result of higher live detached monocytes in co-culture. Thus, at 4 h, the increased detachment of monocytes from RGD-PEG grafted sIPN could be due to an effect related to adhesive molecular mechanisms rather than to viability. In other words, rather than monocytes detaching because their viability is decreased by fibroblasts, monocytes are detaching likely due to an effect related to an adhesive molecular mechanism such as the downregulation of focal adhesion proteins.

Thus, the regulation of the monocyte focal adhesion protein vinculin was analyzed over time to gain insight on the molecular mechanism related decreased monocyte adhesion onto RGD-PEG grafted sIPN. Monocytes on the polycarbonate transwell or RGD-PEG grafted sIPN was investigated. The limiting factor for monocyte vinculin regulation over time was the limited protein amount. Though faint bands at ~72 kDa could be observed as a possible fragment of the vinculin protein [38], the expected band at 116 kDa was not observed from the monocyte lysates (Appendix, Figure ii). The expected 116 kDa bands were faintly visible from the fibroblast lysates. Due to limited protein source from the primary monocyte, definitive conclusions on monocyte vinculin regulation on RGD-PEG grafted sIPNs as modulated by fibroblasts cannot be made. Immunoblot analysis of several focal adhesion proteins (i.e. not just limited to vincuin) and at more time points at the initial stages of co-culture will yield definitive conclusions. For example, vincluin binds to talin that binds to tensin and α-actinin. Fak also binds to paxillin which binds to vinculin. Thus, observing the expression and regulation of these proteins over time on RGD-PEG grafted sIPNs in the presence of fibroblasts should provide a more comprehensive and detailed insight into the modulation of focal adhesion proteins on the ECM-derived scaffold by fibroblasts.

4.3.4 Monocyte-fibroblast protein regulation: attenuated inflammatory and upregulated growth and matrix remodeling factors

To gain insight into monocyte-fibroblast regulated proteins in the presence of the ECM-derived matrix as a communication conduit, we quantified several growth factors and inflammatory and remodeling proteins. We found that monocytes and fibroblasts in co-culture

resulted in increased GM-CSF concentrations in chambers A and B at 24 and 96 h, except with RGD- and PHSRN-PEG grafted sIPN at 96 h (Figure 4-9).

Under monoculture conditions, GM-CSF was expressed by both monocytes and fibroblasts; however only low levels were expressed in our fibroblast monocultures. Under monocyte monocultures in the presence of the RGD- and PHSRN-grafted sIPN, a significant increase in GM-CSF concentration was observed from 2 to 24 h as observed with other surfaces, but by 96 h, levels were significantly decreased. It has been reported that the integrin β5 subunit mRNA is downregulated by GM-CSF in a dose dependent manner [17]. In this study, we observed drastically increased GM-CSF levels from 2 to 24 h along with decreased monocyte adhesion on RGD-PEG grafted sIPN at 2 and 96 h in co-culture compared to monoculture. Hence, our results suggest that the decreased monocyte adhesion on RGD-PEG grafted sIPN in the presence of fibroblasts may be a result of a monocyte-fibroblast regulation that has been indicated in wound healing and likely the downregulation of monocyte integrin by the increased GM-CSF levels up until 24 h.

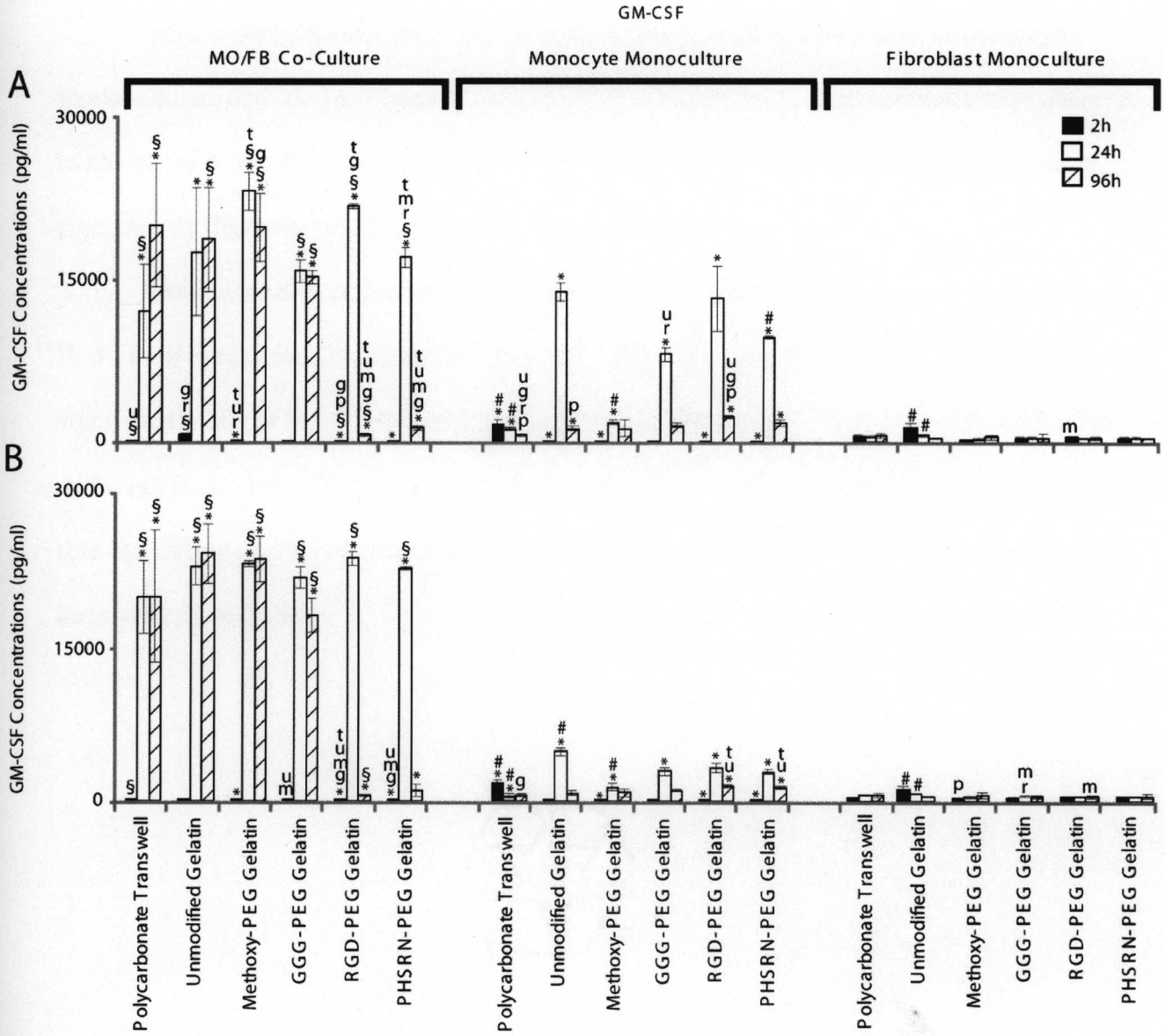

Figure 4-9. GM-CSF concentrations (pg/ml) over time from the upper chamber (A) and the bottom chamber (B) under various culture conditions and substrates. All values expressed the mean of triplicate wells ± standard deviation (n = 3). Significantly different ($p < 0.05$) within time, surface, and chamber: [§]from monocyte monoculture, [*]from fibroblast monoculture, [#]from all other surfaces, [t]from polycarbonate transwell surface, [u]different from unmodified sIPN, [m]from methoxy-PEG grafted sIPN, [g]from GGG-PEG grafted sIPN, [r]from RGD-PEG grafted sIPN, [p]from PHSRN-PEG grafted sIPN.

Inflammatory factors were also directed by the present of fibroblasts. In monocyte monocultures, high IL-1α (Figure 4-10) and TGF-α (Figure 4-11) concentrations were observed in chambers A and B at 2 h in the presence of polycarbonate, but the presence of fibroblasts significantly decreased those concentrations in co-culture.

Monocytes also attenuated initial fibroblast IL-1α and TGF-α expression. For example, IL-1α concentrations in chambers A and B from fibroblast monoculture were generally significantly higher at 2 h compared to that from co-culture at 2 h, in the presence of all surfaces. Although IL-1α and TGF-α were expressed more in monocytes/macrophages, our results indicate that significant expression was also observed in our fibroblast monocultures that was initially decreased in co-cultures.

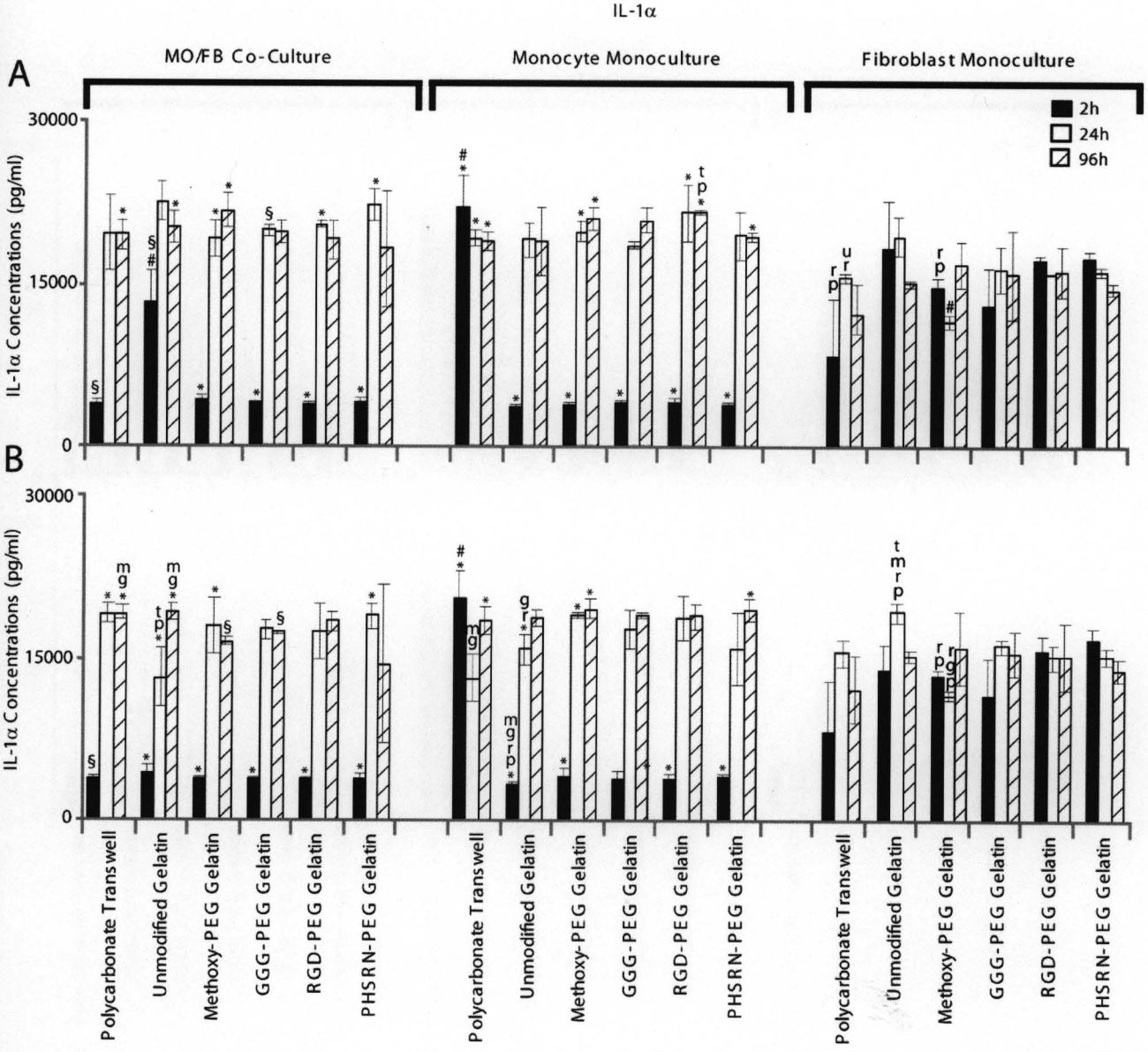

Figure 4-10. IL-1α concentrations (pg/ml) over time from the upper chamber (A) and the bottom chamber (B) under various culture conditions and substrates. All values expressed as the mean of triplicate wells ± standard deviation (n = 3). Significantly different ($p < 0.05$) within time, surface, and chamber: §from monocyte monoculture, *from fibroblast monoculture, $^{\#}$from all other surfaces, ^{t}from polycarbonate transwell surface, ^{m}from methoxy-PEG grafted sIPN, ^{g}from GGG-PEG grafted sIPN, ^{r}from RGD-PEG grafted sIPN, ^{p}from PHSRN-PEG grafted sIPN.

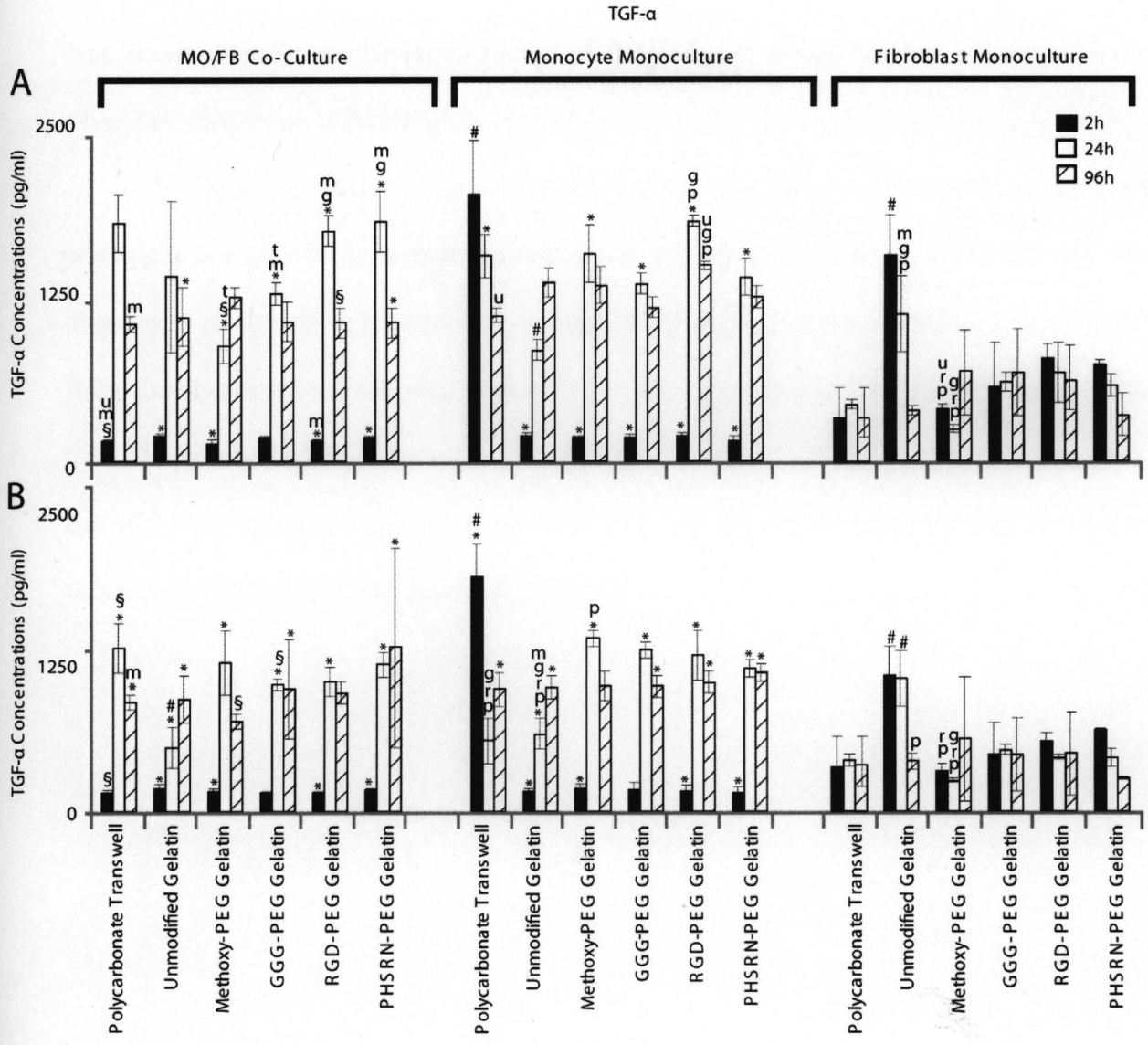

Figure 4-11. TGF-α concentrations (pg/ml) over time from the upper chamber (A) and the bottom chamber (B) under various culture conditions and substrates. All values expressed as the mean of triplicate wells ± standard deviation (n = 3). Significantly different ($p < 0.05$) within time, surface, and chamber: [§]from monocyte monoculture, [*]from fibroblast monoculture, [#]from all other surfaces, [t]from polycarbonate transwell surface, [u]different from unmodified sIPN, [m]from methoxy-PEG grafted sIPN, [g]from GGG-PEG grafted sIPN, [r]from RGD-PEG grafted sIPN, [p]from PHSRN-PEG grafted sIPN.

In addition to inflammatory and growth factors, we characterized matrix remodeling factors critical in the proliferation and remodeling phase of wound healing. Monocytes induced fibroblast expression of MMP-2 (Figure 4-12).

For example, MMP-2 levels from chamber B in fibroblast monocultures were generally consistent from 2 to 96 h. In monocyte monocultures, subtle increases in MMP-2 levels were observed from 2 to 96 h. However, in co-cultures versus monocultures, MMP-2 concentrations from chamber B were drastically increased at 96 h to concentrations beyond the detection limit (>18000 pg/ml). This high concentration was also observed in chamber A only on polycarbonate and sIPN containing unmodified gelatin at 96 h, indicating different protein transport properties between the unmodified and ligand grafted sIPNs.

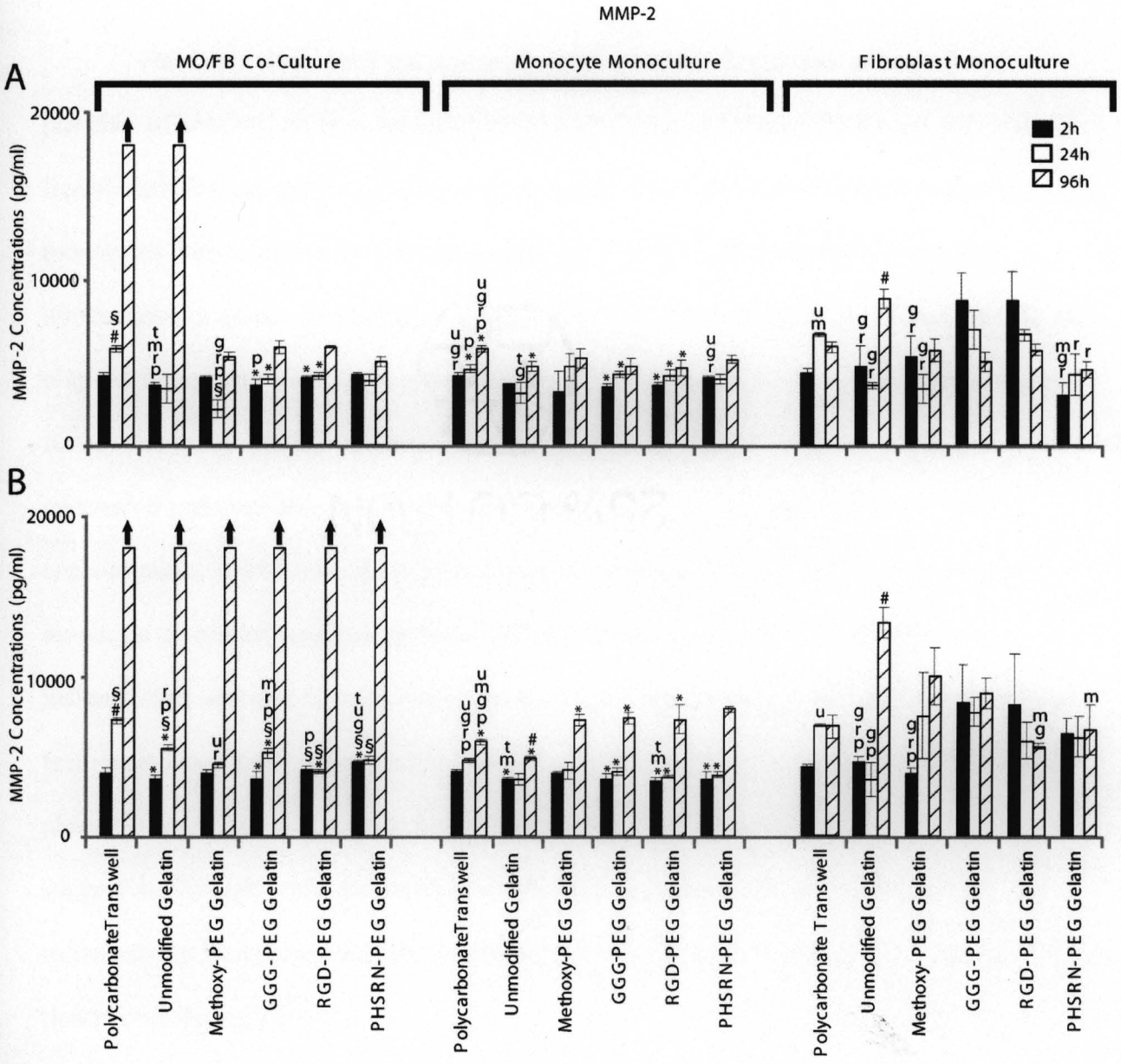

Figure 4-12. MMP-2 concentrations (pg/ml) over time from the upper chamber (A) and the bottom chamber (B) under various culture conditions and substrates. All values expressed as the mean of triplicate wells ± standard deviation (n = 3). Significantly different ($p < 0.05$) within time, surface, and chamber: [§]from monocyte monoculture, [*]from fibroblast monoculture, [#]from all other surfaces, [t]from polycarbonate transwell surface, [u]different from unmodified sIPN, [m]from methoxy-PEG grafted sIPN, [g]from GGG-PEG grafted sIPN, [r]from RGD-PEG grafted sIPN, [p]from PHSRN-PEG grafted sIPN. ⬆Over the detection limit of 18000 pg/ml.

While both fibroblasts and monocytes express MMP-2, our data indicate that the presence of both cell types enhanced fibroblast MMP-2 expression at 96 h especially with ligand-immobilized sIPN suggesting the synergistic interaction between fibroblasts and monocytes during the matrix remodeling process. While MMP-2 possesses important implications in tissue remodeling, angiogenesis and foreign body giant reaction, GM-CSF also plays an important role in these processes and a closely regulated relationship between growth factors and matrix metalloproteases exists [18,19]. GM-CSF has been reported to induce MMP-2 expression and our data shows drastically increased GM-CSF levels at 24 h and MMP-2 concentrations at 96 h only in co-cultures and not in monocultures [20]. This suggests a monocyte-fibroblast paracrine mediated MMP-2 induction by GM-CSF in co-culture. Inflammatory proteins can also induce growth factors and matrix remodeling agents as these factors are also closely intertwined players in activation and regulation of the inflammatory phase that eventually progress through the proliferative and remodeling stage [21]. Our data suggest that though initial fibroblast inflammatory factors could be attenuated, these inflammatory factors increased in concentration with time and they could upregulate growth and matrix remodeling factors.

4.3.5 ECM-derived matrix mediated monocyte-fibroblast protein regulation: expression and transport are dependent on sIPN and ligand immobilization of the sIPN

Though culture condition (i.e. co-culture versus monoculture) mediated IL-1α, TGF-α, GM-CSF and MMP-2 expression, the ECM-based sIPN predominantly mediated the expression of other monocyte inflammatory and remodeling proteins such as IL-1β, TNF-α, MIP-1β and

MMP-9. In both monocyte monoculture and co-culture, the presence of sIPNs significantly elevated IL-1β (Figure 4-13), TNF-α (Figure 4-14), and MIP-1β (Figure 4-15) concentrations from 2 to 24 h in chamber A when compared with the polycarbonate controls.

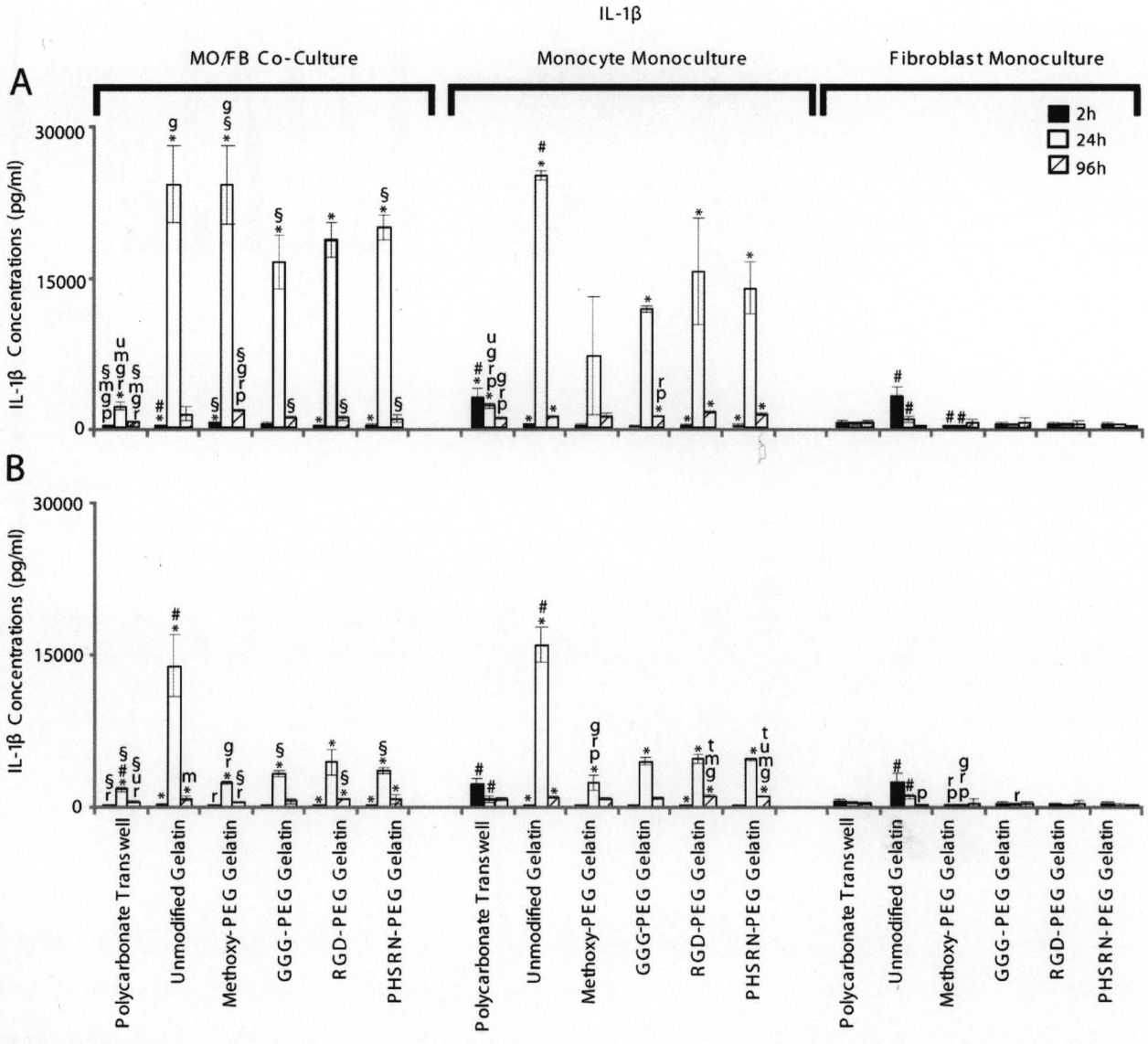

Figure 4-13. IL-1β concentrations (pg/ml) over time from the upper chamber (A) and the bottom chamber (B) under various culture conditions and substrates.. All values expressed as the mean of triplicate wells ± standard deviation (n = 3). Significantly different ($p < 0.05$) within time, surface, and chamber: [§]from monocyte monoculture, [*]from fibroblast monoculture, [#]from all other surfaces, [t]from polycarbonate transwell surface, [u]different from unmodified sIPN, [m]from methoxy-PEG grafted sIPN, [g]from GGG-PEG grafted sIPN, [r]from RGD-PEG grafted sIPN, [p]from PHSRN-PEG grafted sIPN.

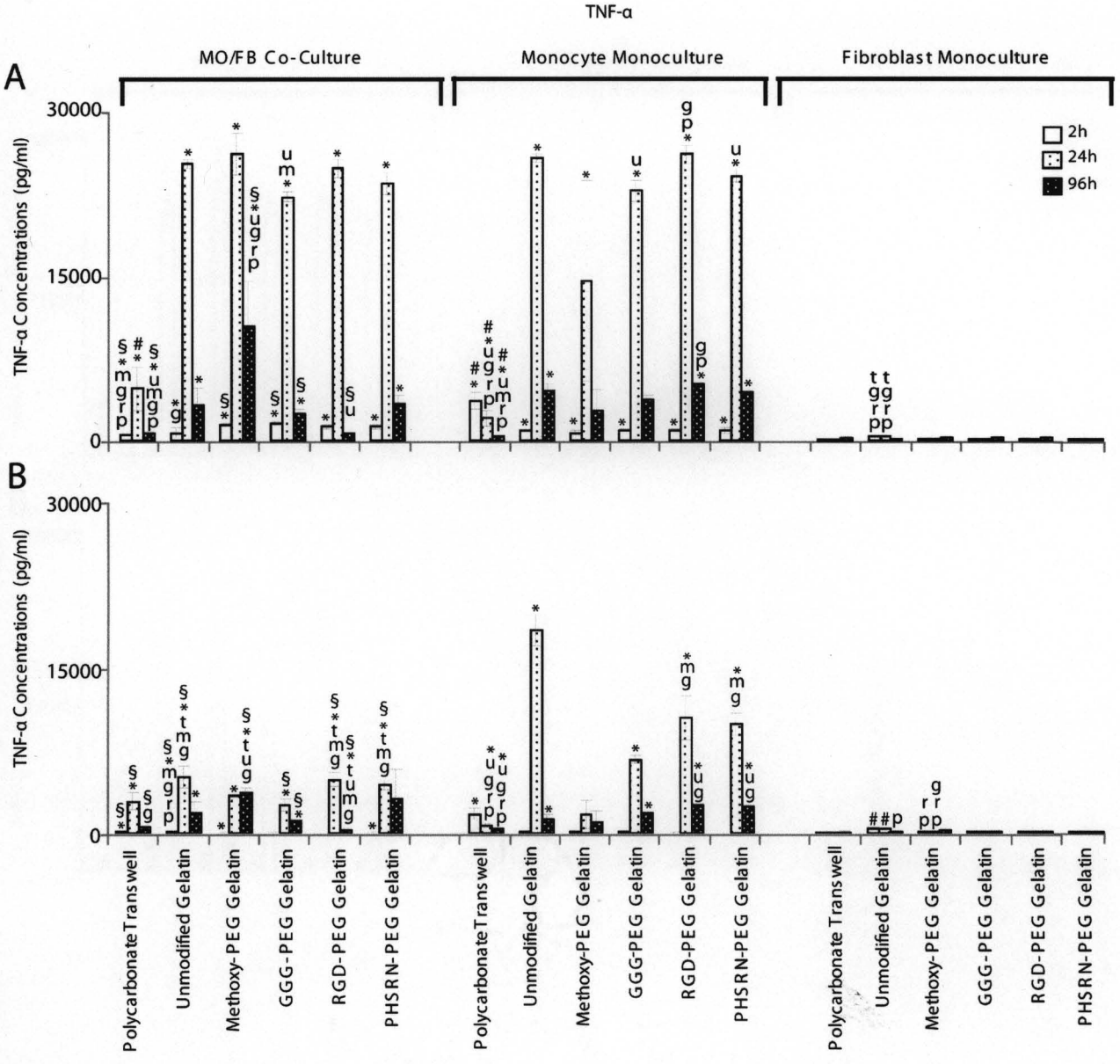

Figure 4-14. TNF-α concentrations (pg/ml) over time from the upper chamber (A) and the bottom chamber (B) under various culture conditions and substrates. All values expressed as the mean of triplicate wells ± standard deviation (n = 3). Significantly different ($p < 0.05$) within time, surface, and chamber: [§]from monocyte monoculture, [*]from fibroblast monoculture, [#]from all other surfaces, [t]from polycarbonate transwell surface, [u]different from unmodified sIPN, [m]from methoxy-PEG grafted sIPN, [g]from GGG-PEG grafted sIPN, [r]from RGD-PEG grafted sIPN, [p]from PHSRN-PEG grafted sIPN.

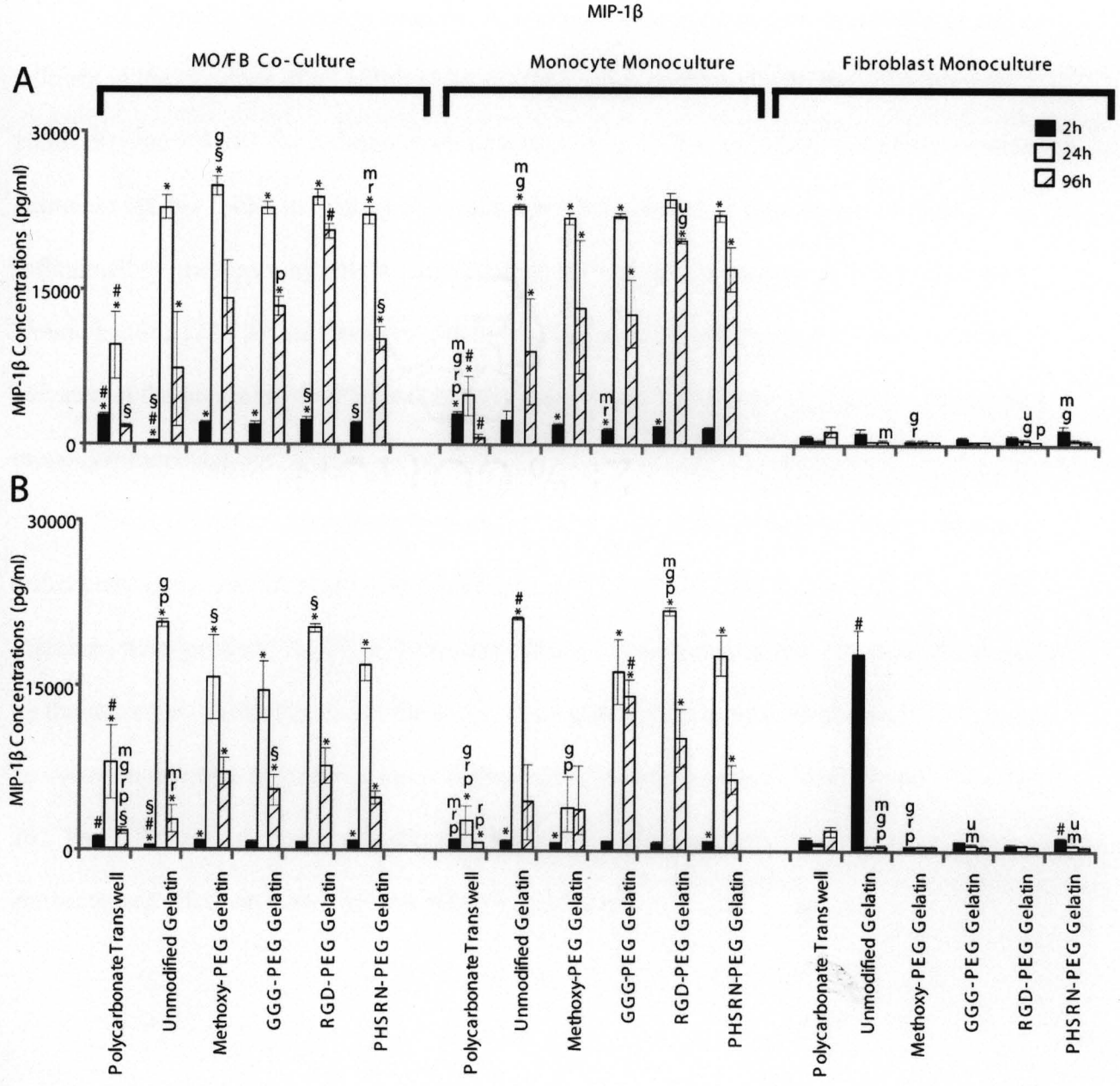

Figure 4-15. MIP-1β concentrations (pg/ml) over time from the upper chamber (A) and the bottom chamber (B) under various culture conditions and substrates. All values expressed as the mean of triplicate wells ± standard deviation (n = 3). Significantly different ($p < 0.05$) within time, surface, and chamber: §from monocyte monoculture, *from fibroblast monoculture, $^{\#}$from all other surfaces, ^{t}from polycarbonate transwell surface, ^{u}different from unmodified sIPN, ^{m}from methoxy-PEG grafted sIPN, ^{g}from GGG-PEG grafted sIPN, ^{r}from RGD-PEG grafted sIPN, ^{p}from PHSRN-PEG grafted sIPN.

MCP-1 concentrations in chamber A also increased in monocyte monocultures and co-cultures in the presence of all sIPNs at 24 and 96 h when compared with the polycarbonate controls (Figure 4-16). As inflammatory factors such as TNF-α and IL-1β have been reported to stimulate MCP-1 levels in various cell types, the sIPN substrata's modulation of these inflammatory proteins may hold a critical role in activation of a cascade of events crucial to wound healing [22,23]. Furthermore, MMP-9 levels at 96 h in chamber A were significantly elevated in the presence of sIPNs and not the polycarbonate controls in both co-cultures and monocyte monocultures (Figure 4-17).

These results are consistent with others' findings that the ECM substratum can play a critical role in increasing MMP-9 levels over time [24,25]. GM-CSF levels at 24 h were also increased in response to the ECM-derived matrix, but in co-cultures, this increase was amplified by the presence of fibroblasts. Additionally, TNF-α and IL-1β have been shown in literature to be common inducers of matrix remodeling and growth factors such as MMP-9 and GM-CSF [26-28]. The inflammatory proteins and the ECM-derived sIPN are likely to have a cooperative enhancement effect on GM-CSF and MMP-9 expression.

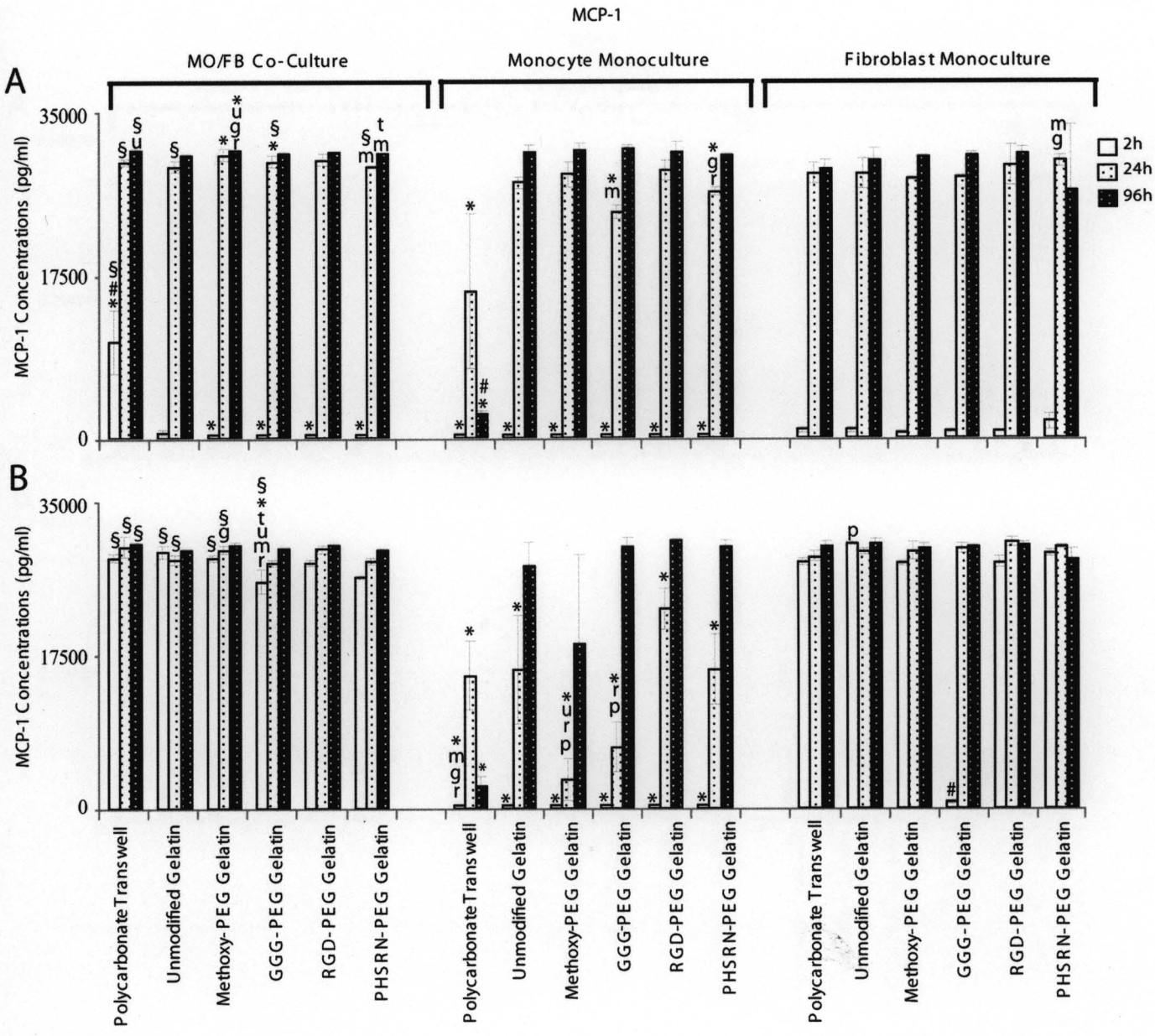

Figure 4-16. MCP-1 concentrations (pg/ml) over time from the upper chamber (A) and the bottom chamber (B) under various culture conditions and substrates. All values expressed as the mean of triplicate wells ± standard deviation (n = 3). Significantly different ($p < 0.05$) within time, surface, and chamber: [§]from monocyte monoculture, [*]from fibroblast monoculture, [#]from all other surfaces, [t]from polycarbonate transwell surface, [u]different from unmodified sIPN, [m]from methoxy-PEG grafted sIPN, [g]from GGG-PEG grafted sIPN, [r]from RGD-PEG grafted sIPN, [p]from PHSRN-PEG grafted sIPN.

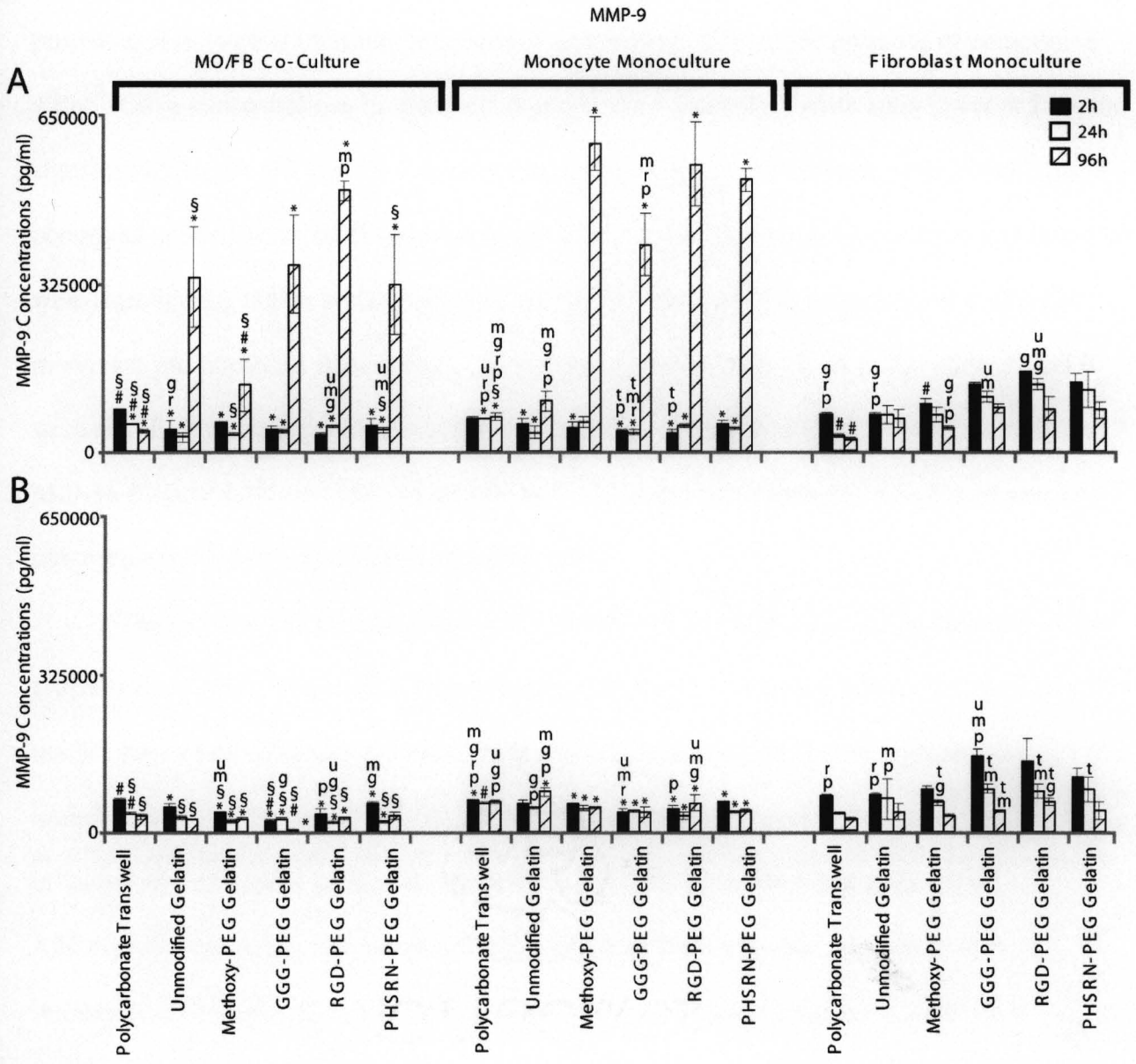

Figure 4-17. MMP-9 concentrations (pg/ml) over time from the upper chamber (A) and the bottom chamber (B) under various culture conditions and substrates. All values expressed as the mean of triplicate wells ± standard deviation (n = 3). Significantly different ($p < 0.05$) within time, surface, and chamber: §from monocyte monoculture, *from fibroblast monoculture, $^{\#}$from all other surfaces, ^{t}from polycarbonate transwell surface, ^{u}different from unmodified sIPN, ^{m}from methoxy-PEG grafted sIPN, ^{g}from GGG-PEG grafted sIPN, ^{r}from RGD-PEG grafted sIPN, ^{p}from PHSRN-PEG grafted sIPN.

In addition to sIPN mediated effects, ligand immobilization on the sIPNs led to varied protein expression and transport compared to unmodified sIPN. In the presence of unmodified sIPN, TGF-α concentrations in chambers A and B were generally significantly lower at 24 h and significantly higher at 2 and 24 h in monocyte and fibroblast monocultures, respectively, when compared with sIPN immobilized with ligand. IL-1β concentrations in chambers A and B at 24 h were significantly higher with unmodified sIPN when compared with ligand-grafted sIPN in monocyte and fibroblast monocultures. In fibroblast monoculture, IL-1β in chambers A and B were significantly higher with unmodified sIPNs versus ligand-grafted sIPN at 2 h as well, and MIP-1α (Figure 4-18) and MIP-1β also showed higher concentrations at 2 h in the presence of unmodified sIPN compared to ligand-grafted sIPN.

The increase inflammatory agents IL-1β, MIP-1α and MIP-1β could be the result of the greater rate of gelatin dissolution from the unmodified sIPN versus the ligand-PEG grafted sIPN that we have observed previously and in separate experiments [29]. Taken together, the immobilization of the ligand-PEG on the sIPN appears to downregulate certain key pro-inflammatory mediators such as IL-1β, MIP-1α and MIP-1β in fibroblast monocultures. Additionally, the matrix also regulated the transport of these proteins, depending on ligand immobilization on the sIPN. For TNF-α (Figure 4-15), we observed concentrations at 24 h in chamber B that were significantly higher in the presence of unmodified gelatin compared to all other ligand immobilized sIPN in monocyte monocultures, though concentrations in chamber A at 24 h did not differ in the presence of unmodified sIPN compared to other ligand immobilized sIPN.

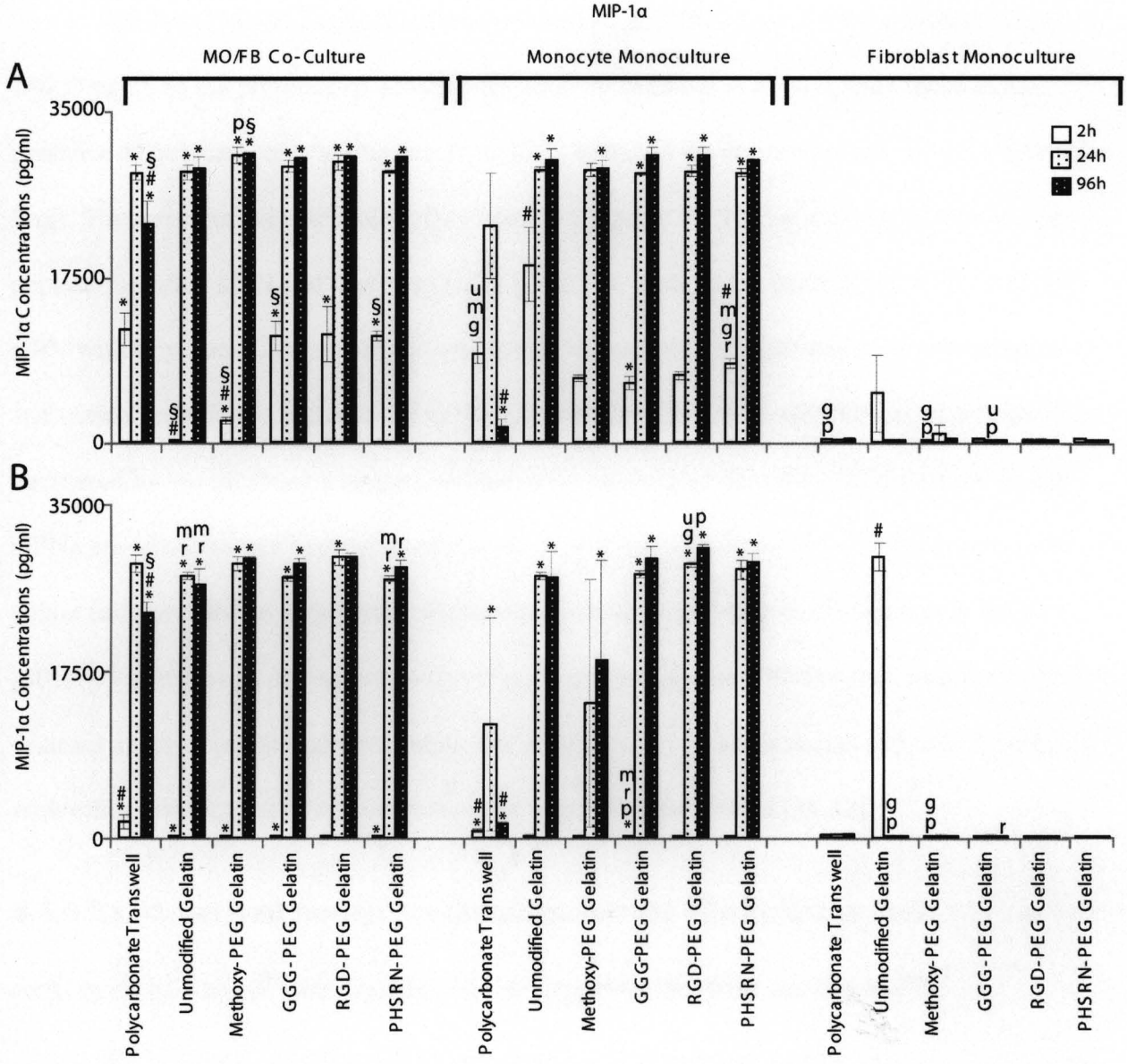

Figure 4-18. MIP-1α concentrations (pg/ml) over time from the upper chamber (A) and the bottom chamber (B) under various culture conditions and substrates. All values expressed as the mean of triplicate wells ± standard deviation (n = 3). Significantly different ($p < 0.05$) within time, surface, and chamber: [§]from monocyte monoculture, [*]from fibroblast monoculture, [#]from all other surfaces, [t]from polycarbonate transwell surface, [u]different from unmodified sIPN, [m]from methoxy-PEG grafted sIPN, [g]from GGG-PEG grafted sIPN, [r]from RGD-PEG grafted sIPN, [p]from PHSRN-PEG grafted sIPN.

Similarly, MMP-2 concentrations in chamber B at 96 h were over the detection limit of 18000 pg/ml in the presence of all surfaces while, in chamber A at 96 h, only those in the presence of polycarbonate and unmodified sIPN reflected the concentrations over the detection limit. These results indicate a selective transport property for TNF-α and MMP-2 across the peptide-modified sIPN and that this selectivity is less observed in unmodified sIPN. Although sIPN with or without grafted peptides enhanced the expression of monocyte pro-inflammatory and matrix remodeling regulator, the effect of these proteins on an effector cell would be decreased by the inhibited transport of these proteins through the sIPN ECM mimics. These sIPNs are rather porous hydrogels and the mesh structure would restrict diffusive movement of a solute and the addition of polymer chains would cause an increase in diffusion path length [30,31]. Furthermore, diffusive passage of proteins through the sIPNs as well as other hydrogel systems depends on the protein's molecular weight, hydrodynamic radius and ionic interactions with other solutes, properties that remain incompletely understood [31,32].

4.3.6 ECM-derived matrix mediated monocyte-fibroblast protein regulation: expression is mediated by identity of peptide grafted on the sIPN

We have observed that ligand immobilized sIPN induced varied protein expression and transport from unmodified sIPN. In addition to these findings, we observed that the identity of grafted peptides also induced peptide specific protein expression. We identified decreased GM-CSF levels in the presence of RGD and PHSRN grafted sIPN as described above. We also measured elevated TGF-α concentrations at 24 h in co-cultures in the presence of RGD and PHSRN grafted sIPN compared with other ligand grafted sIPN. Also in co-cultures, we observed increased concentrations of MIP-1β at 96 h and VEGF (Figure 4-19) at 24 h and in the presence

of grafted RGD but not PHSRN and RGD and PHSRN, respectively, when compared with other sIPN.

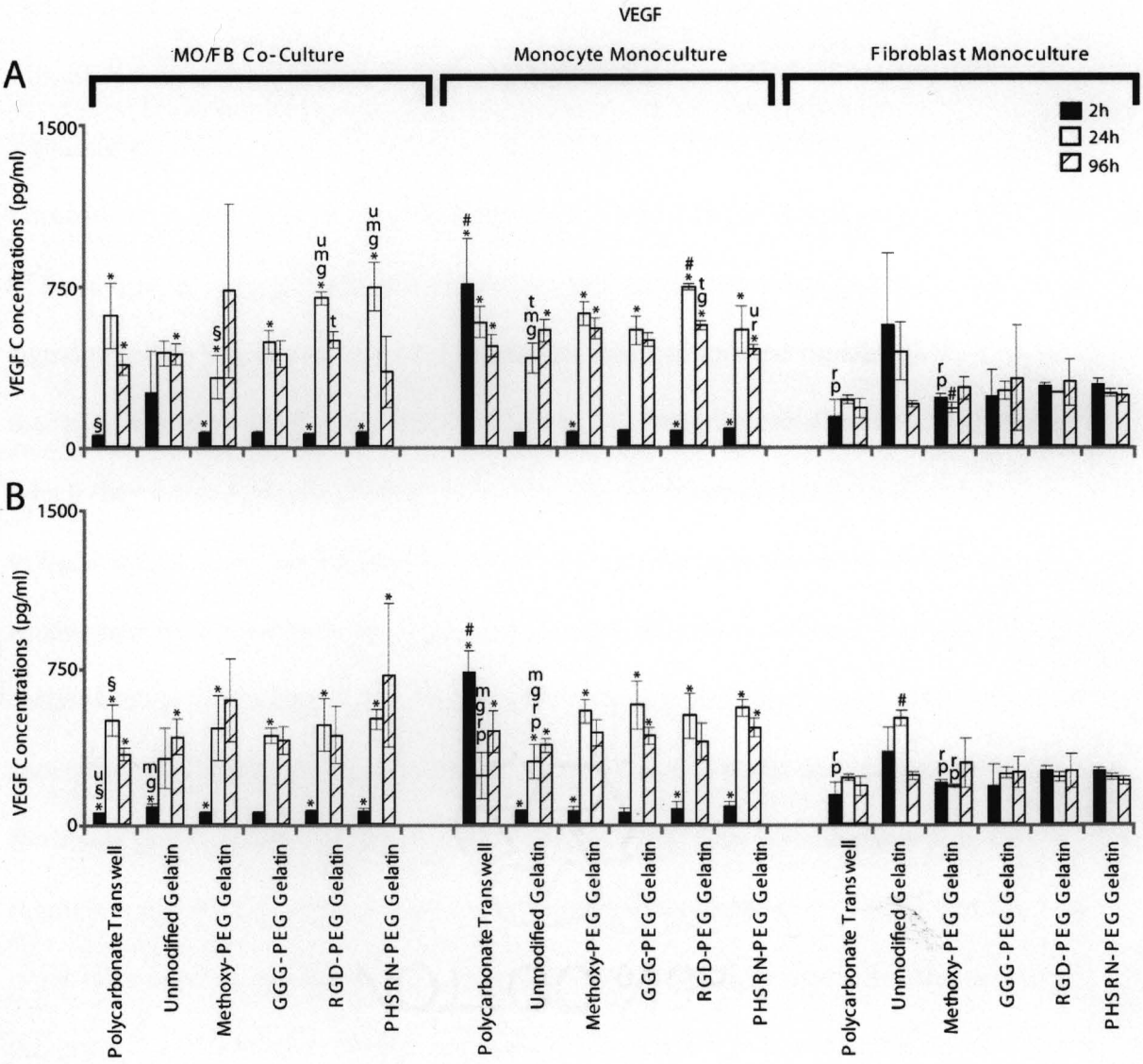

Figure 4-19. VEGF concentrations (pg/ml) over from the upper chamber (A) and the bottom chamber (B) under various culture conditions and substrates. All values expressed as the mean of triplicate wells ± standard deviation (n = 3). Significantly different ($p < 0.05$) within time, surface, and chamber: [§]from monocyte monoculture, [*]from fibroblast monoculture, [#]from all other surfaces, [t]from polycarbonate transwell surface, [u]different from unmodified sIPN, [m]from methoxy-PEG grafted sIPN, [g]from GGG-PEG grafted sIPN, [r]from RGD-PEG grafted sIPN, [p]from PHSRN-PEG grafted sIPN.

It has been reported that integrin αvβ3 mediates and activates various intracellular signaling pathways involved in proliferation and differentiation secondary to multiple growth factor receptors such as VEGF [33]. Furthermore, the presence of monocytes and sIPN enhanced fibroblast matrix remodeling expression in terms of elevated GM-CSF and MMP-2. Post-ligation signaling and phenotypic expression modulated by RGD and PHSRN in monocyte and fibroblasts are unclear at the moment. However, these data indicate divergent downstream effects of these ligands in monocytes and fibroblasts, perhaps in response to other stimuli as a part of signal proofreading and cooperative regulation. Recognition and signaling activities can be mediated solely by integrins (private functions), but integrins can also have public activities in which they interact physically with other plasma membrane receptors to elicit cellular responses to ligands that do not bind directly to integrins. In monocytes, this relationship has been established for several systems: (i) monocyte α4β1 integrin is activated through the G protein-coupled receptor binding of MCP-1 and MIP-1 chemokines; (ii) integrin (αvβ3, α5β1, αvβ5, β1 superfamily) crosstalk with growth factor receptors (i.e., platelet derived growth factor, basic fibroblast growth factor, epithelial growth factor, VEGF) has been implicated in the cooperative regulation of 100-120 monocyte genes when adhered to fibronectin [34-37]. For the latter, these cross-talks occur in several fashions including shared signaling molecules and co-clustering of receptors in the formation of focal adhesion. Thus fibroblasts in co-culture with monocytes can mediate physical and intermolecular monocyte interactions with the sIPN.

4.4 Discussion and conclusions

This monocyte-fibroblast co-culture investigation has shown that fibroblasts decrease monocyte adhesion onto RGD-PEG grafted sIPN. However, when the viability of the detached monocytes was examined, the live to dead nonadhered monocyte ratio was not significantly different between monoculture and co-culture conditions initially, but more live monocytes detached at 4 h, indicating detachment through an active molecular mechanism rather than a passive detachment through cell death. Observing the expression and regulation of several focal adhesion proteins over time on RGD-PEG grafted sIPNs in the presence of fibroblasts should provide a more comprehensive and detailed insight into the modulation of focal adhesion proteins on the ECM-derived scaffold by fibroblasts.

From the diffusion of proteins without the presence of cells or serum, it was observed that proteins up to approximately 65 kDa in molecular weight (~ 36.5 Å hydrodynamic radius) can diffuse through the sIPN cast polycarbonate transwell barrier within 24 h. Thus, proteins under 65 kDa are likely to diffuse through and serve to mediate the communication between monocytes and fibroblasts approximately at 24 h and through 96 h. Thus, the drastic increases in GM-CSF and MMP-2 at 96 h observed in co-culture (Figures 4-9 and 4-12, respectively) can thus be attributed to monocyte-fibroblast protein mediated communication at a time before 96 h. It is difficult to speculate whether proteins approximately 72 kDa are able to diffuse through, as the MMP-2 interacted heavily with the sIPN, the transwell, and/or the TCPS surface. Larger proteins such as MMP-9, a 92 kDa protein may not be diffusing through the sIPN within 96 h, as observed in Figure 4-11, and coupled with the MMP-2 diffusion data (Figures 4-7 and 4-8), MMP-9 from chamber A observed at 96 h may be interacting with the sIPN and not diffusing through.

With cells and serum in the actually experimental environment, the sIPN's degradation rate is likely increased, perhaps allowing for increased diffusive pathways for proteins. There are various factors in the dynamic co-culture system influencing protein diffusion through chambers: i.) the presence of serum that contain proteases and degradative agents that can process other proteins and degrade the sIPN scaffold, ii.) enzymes and degradative agents that the cells express and secrete into the environment, iii.) monocytes' direct contact with the sIPN that influence sIPN degradation, and iv.) the cells' own ECM deposition on the sIPN. Hence, the diffusion data (Figures 4-3 through 4-8) yield insight into the correlation between molecular weight and hydrodynamic radius as it relates to diffusion rate, but in the co-culture system with cells and serum, dynamic factors will influence the diffusion of the protein through chambers. The presence of fibroblasts increased monocyte GM-CSF except on RGD and PHSRN grafted sIPNs at 96 h. The presence of monocytes decreased initial fibroblast IL-1α, TGF-α and VEGF, but increased MMP-2 and GM-CSF at later time points. Furthermore, the ECM-derived sIPNs led to increased monocyte IL-1β, TNF-α, MIP-1β, MCP-1, MMP-9 and GM-CSF expression. Ligand immobilization of the sIPNs led to a downregulation of fibroblast IL-1β, MIP-1α, MIP-1β compared to unmodified sIPN. When the ligand immobilized on the sIPN was RGD, increased TGF-α, MIP-1β and VEGF but decreased GM-CSF expression at selected time points was observed. Figure 4-20 summarizes the effects of a secondary cell type and of the sIPN substrata on monocyte and fibroblast protein expression.

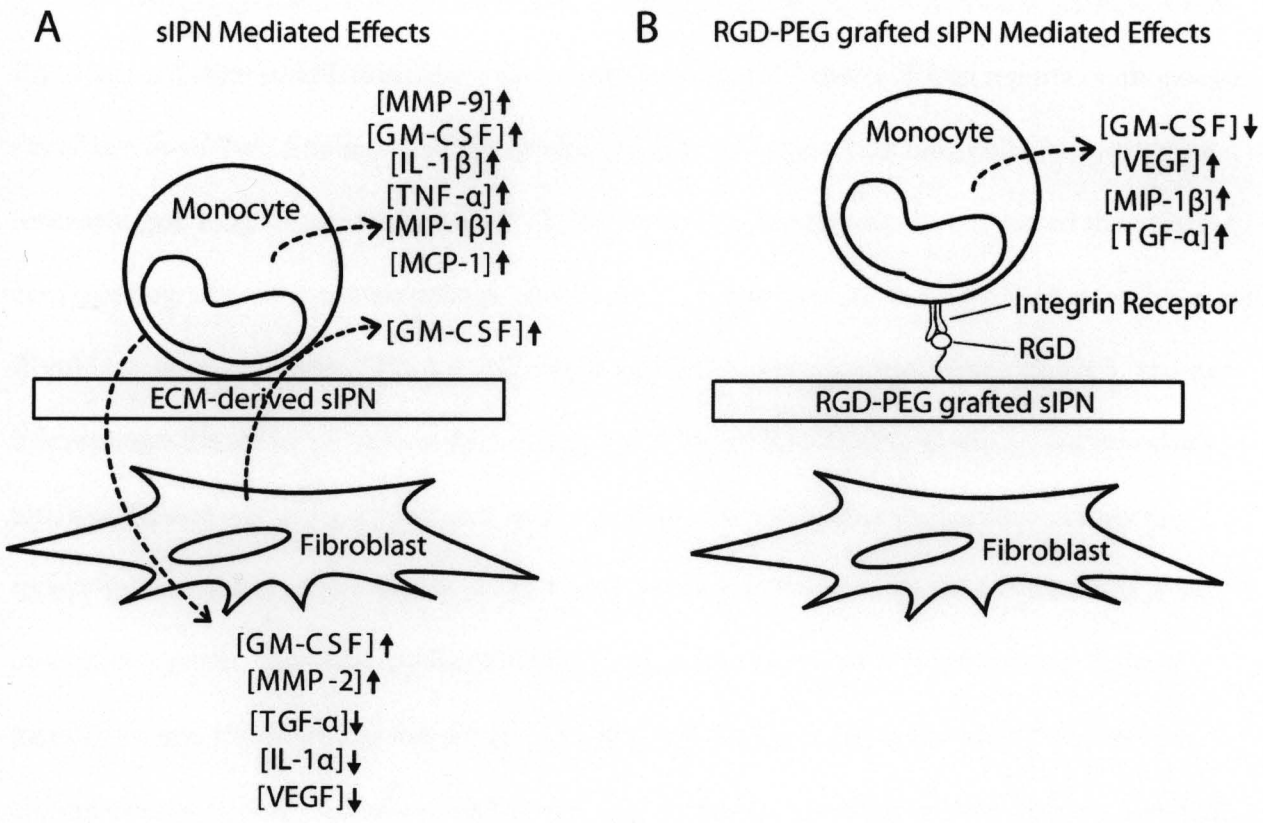

Figure 4-20. Monocyte response to the ECM-derived sIPNs (A) and monocyte response to RGD-PEG grafted sIPN (B). Monocyte interaction with sIPN led to increased IL-1β, TNF-α, MIP-1β, MCP-1, MMP-9 and GM-CSF concentrations over time. Elevated levels of monocyte GM-CSF as a result of interaction with the sIPN were amplified by the presence of fibroblasts. Monocytes attenuated fibroblast TGF-α, IL-1α and VEGF at selected time points but drastically increased fibroblast GM-CSF and MMP-2 release. On RGD-PEG grafted sIPN at selected time points, monocyte TGF-α, MIP-1β and VEGF were increased, but GM-CSF was decreased.

The first co-culture study dates back to 1983, highlighting human monocyte regulation fibroblast collagen production. Since then, there has been less than a dozen reports on monocyte-fibroblast co-culture findings, and the existing literature is mainly on lung cells (e.g., alveolar macrophages, lung fibroblasts) [8-10,22,39-43]. In 1993, Janusz and Hare reported the effects of cartilage degradation in a macrophage-fibroblast co-culture system, but both the macrophage and fibroblasts were cell lines, J774A.1 and 10ME HD A.DR.1, respectively [41]. In 2005, another macrophage-fibroblast co-culture system was reported by Kashchak and others, but this study too, was carried out using murine cell lines, J774A.1 and L929 fibroblasts [40]. Neither the report by Janusz and others nor the work by Kashchak and others involved biomaterials in the co-culture system. The work by Bonfield and others reported in 1991 human blood derived monocytes and fibroblasts in the context of a polydimethylsiloxane is the most "similar" co-culture system thusfar, because of the use of primary monocytes derived from human blood [8]. However, rather than a "true" co-culture system with both cell types present in the same microenvironment, the effects of monocyte enriched media on fibroblasts was examined. Thus, this work presents a novel and important work in which monocyte interaction with the sIPN scaffold is examined in the presence of fibroblasts. The results described in this chapter shed light into the dynamic monocyte adhesion, and inflammatory, matrix remodeling and growth factor response to the ECM mimic in the presence of fibroblasts in wound healing.

4.5 References

1. Shin HS, Jo SB, Mikos AG. Modulation of marrow stromal osteoblast adhesion on biomimetic oligo[poly(ethylene glycol) fumarate] hydrogels modified with Arg-Gly-Asp peptides and a poly(ethylene glycol) spacer. J Biomed Mater Res 2002;61:169-179.
2. Kantlehner M, Schaffner P, Finsinger D, Meyer J, Jonczyk A, Diefenbach B, Nies B, Holzemann G, Goodman SL, Kessler H. Surface coating with cyclic RGD peptides stimulates osteoblast adhesion and proliferation as well as bone formation. Chembiochem 2000;1:107-114.
3. Rezania A and Healy KE. Integrin subunits responsible for adhesion of human osteoblast-like cells to biomimetic peptide surfaces. J Orthop Res 1999;17:615-623.
4. Massia SP and Stark J. Immobilized RGD peptides on surface-grafted dextran promote biospecific cell attachment. J Biomed Mater Res 2001;56:390-399.
5. Waldeck HM, Chung AS, Kao WJ. Interpenetrating polymer networks containing gelatin modified with PEGylated RGD and soluble KGF: Synthesis, characterization, and application in in vivo critical dermal wound. J Biomed Mater Res 2007;82:861-871.
6. Weihrauch D, Arras M, Zimmermann R, Schaper J. Importance of monocytes/macrophages and fibroblasts for healing of micronecroses in porcine myocardium. Mol Cell Biochem 1995;147(1/2):13–19.
7. Concannon MJ, Barrett BB, Adelstein EH, Thorton WH, Puckett CL. The inhibition of fibroblast proliferation by a novel monokine: An in vitro and in vivo study. J Burn Care Rehabil 1993;14(Part 1):141–147.

8. Bonfield TL, Colton E, Anderson JM. Fibroblast stimulation by monocytes cultured on protein adsorbed biomedical polymers.I. Biomer and polydimethylsiloxane. J Biomed Mater Res 1991;25:165–175.

9. Skold CM, Liu XD, Umino T, Zhu YK, Ertl RF, Romberger DJ, Rennard SI. Blood monocytes attenuate lung fibroblast contraction of three-dimensional collagen gels in coculture. Am J Physiol Lung Cell Mol Physiol 2000;279:L667–L674.

10. Zhu Y, Liu XD, Skold CM, Wang H, Kohyama T, Wen FQ, Ertl RF, Rennard SI. Collaborative interactions between neutrophil elastase and metalloproteinases in extracellular matrix degradation in three-dimensional collagen gels. Respir Res 2001;2:300–305.

11. Benoit DS, Anseth KS. The effect on osteoblast function of colocalized RGD and PHSRN epitopes on PEG surfaces. Biomaterials 2005;26(25):5209-5220.

12. Chung AS, Waldeck HM, Schmidt DR, Kao WJ. Monocyte inflammatory and matrix remodeling response modulated by grafted ECM-derived ligand identity and concentration. J Biomed Mater Res Published online Dec 2, 2008.

13. Witte RP, Kao WJ. Keratinocyte-fibroblast paracrine interaction: the effects of substrate and culture condition. Biomaterials 2005;26(17):3673-3682.

14. McNally AK, Anderson JM. Complement C3 participation in monocyte adhesion to different surfaces. Proc Natl Acad Sci USA 1994;91(21):10119.

15. Burmania JA, Martinez-Diaz GJ, Kao WJ. Synthesis and physicochemical analysis of interpenetrating networks containing modified gelatin and poly(ethylene glycol) diacrylate. J Biomed Mater Res 2003;67A(1):224–34.

16. Schmidt DR, Kao WJ. Monocyte activation in response to polyethylene glycol hydrogels grafted with RGD and PHSRN separated by interpositional spacers of various lengths. J Biomed Mater Res 2007;83A(3):617-625.

17. Feng X, Teitelbaum SL, Quiroz ME, Towler DA, Ross FP. Cloning of the murine beta5 integrin subunit promoter: identification of a novel sequence mediating granulocyte-macrophage colony stimulating factor-dependent repression of beta5 integrin gene transcription. J Biol Chem 1999;274(3):1366-1374.

18. Jansen PL, Kever M, Rosch R, Krott E, Jansen M, Alfonso-Jaume A, Dooley S, Klinge U, Lovett DH, Mertens, PR. Polymeric meshes induce zonal regulation of matrix metalloproteinase-2 gene expression by macrophages and fibroblasts. FASEB J 2007;21(4):1047-1057.

19. Kuzuya M, Iguichi A. Role of matrix metalloproteinases in vascular remodeling. J Atheroscler Thromb 2003;10(5):275-282.

20. Tomita T, Fujii M, Tokumaru Y, Kanke M, Yamashita T, Ishiguro R, Kanzaki J, Kameyama K, Otani Y. Granulocyte macrophage colony-stimulating factor upregulates matrix metalloproteinase-2 (MMP-2) and membrane type-1 MMP (MT1-MMP) in human head and neck cancer cells. Cancer Lett 2000;156(1):83–91.

21. Boughton II G, Janis JE, Attinger CE. The basic science of wound healing. Plast. Reconst Surg 2006;117(7S):12S-34S.

22. Zickus C, Kunkel SL, Simpson K, Evanoff H, Glass M, Strieter RM, Lukacs NW. Differential regulation of C-C chemokines during fibroblasts-monocyte interactions: adhesion vs. inflammatory cytokine pathways. Med Inflamm 1998;7(4):269-274.

23. Ozaki K, Hanazawa S, Takeshita A, Chen Y, Watanabe A, Nishida K, Miyatay Y, Kitano S. Interleukin-1 and tumor necrosis factor-alpha stimulate synergistically the expression of monocyte chemoattractant protein-1 in fibroblastic cells derived from human periodontal ligament. Oral Microbiol Immuno 1996;11(2):109-114.

24. Jacob SS, Sudhakaran PR. Molecular mechanism involved in matrix dependent upregulation of matrix metalloproteinases in monocyte/macrophage. J Biochem Mol Biol Biophys 2002; 6(5):335-340.

25. Sudhakaran PR, Radhika A, Jacob SS. Monocyte macrophage differentiation in vitro: fibronectin-dependent upregulation of certain macrophage-specific activities. Glycoconjugate J 2007;24(1):49-55.

26. Marom B, Rahat MA, Lahat N, Weiss-Cerem L, Kinarty A, Bitterman H. Native and fragment fibronectin oppositely modulate monocyte secretion of MMP-9. J Leukocyte Biol 2007;81(6):1466-1476.

27. Wilson SE Lloyd SA. Epidermal growth factor and its receptor, basic Fibroblast growth factor, transforming growth factor beta-1, and interleukin-1 alpha messenger RNA production in human corneal endothelial cells. Invest Ophthalmol Vis Sci 1991;32(10):2747-2756.

28. Yokoo T, Kitamura M. Dual regulation of IL-1 beta-mediated matrix metalloproteinase-9 expression in mesangial cells by NF-kappa B and AP-1. Am J Physiol 1996;270 (1 Pt 2):F123-F130.

29. Martinez-Diaz GJ, Nelson D, Crone WC, Kao WJ. Mechanical and chemical analysis of gelatin-based hydrogel degradation. Macromol Chem Physic 2003;2041(15):898-1908.

30. Burmania JA, Stevens KR, Kao WJ. Cell interaction with protein-loaded interpenetrating networks containing modified gelatin and poly(ethylene glycol) diacrylate. Biomaterials 2003;24(22):3921-3930.

31. Amsden B. Solute diffusion within hydrogels: mechanisms and models. Macromolecules. 1998;31(23):8382-8395.

32. Erikson A, Andersen, HN, Naess SN, Sikorski P, Davies CL. Physical and chemical modifications of collagen gels: impact on diffusion. Biopolymers 2007;89(2):135-143.

33. Soldi R, Mitola S, Strasly M, Defilippi P, Tarone G, Bussolino F. Role of αvβ3 integrin in the activation of vascular endothelial growth factor receptor-2. EMBO J. 1999;18(4):882-892.

34. Petty HR, Worth RG, Todd III, R.F. Interactions of integrins with their partner proteins in leukocyte membranes. Immunol Res 2002;25(1):75-95.

35. Chan JR, Hyduk SJ, Cybulsky MI. Chemoattractants induce a rapid and transient upregulation of monocyte a4 integrin affinity for vascular cell adhesion molecule 1 which mediates arrest: An early step in the process of emigration. J Exp Med 2001;193(10):1149-1158.

36. da Costa Martins PA, van Gils JM, Mol A, Hordijk PL, Zwaginga JJ. Platelet binding to monocytes increases adhesive properties of monocytes by up-regulating the expression and functionality of b1 and b2 integrins. J Leuk Bio 2006;79(3):499-507.

37. Newton RA, Thiel M, Hogg N. Signaling mechanisms and the activation of leukocyte integrins. J Leukoc Biol 1997;61(4):422-426.

38. Kilic F, Ball EH. Partial cleavage mapping of the cytoskeletal protein vinculin. J Biol Chem 1990;266:8734-8740.

39. deLustro F, Mackel AM, deLustro B, LeRoy EC. Human monocyte regulation of connective tissue growth. Amer Zool 1983;23:213-220.

40. Kashchak N, Tsaryk R, Stoika R. Bystander effect of normal fibroblasts for macrophages co-cultured with susceptible transformed target cells. Cell Biol Int 2005;29:41-50.

41. Janusz MJ, Hare M. Cartilage degradation by cocultures of transformed macrophage and fibroblast cell lines. J Immunol 1993;150:1922-1931.

42. Fitzgerald SM, Chi DS, Hall K, Reynolds SA, Aramide O, Lee SA, Krishnaswamy G. GM-CSF induction in human lung fibroblasts by IL-1beta, TNF-alpha, and macrophage contact. J Interf Cytok Res 2003;23:57-65.

43. Tipton DA, Pabst MJ, Dabbous MK. Interleukin-1beta and tumor necrosis factor-alpha-independent monocyte stimulation of fibroblast collagenases activity. J Cell Biochem 1990;44:253-264.

Chapter 5. Concluding Remarks and Suggested Future Studies

This work has outlined several critical and novel findings in monocyte response to the gelatin and PEG based sIPN: i.) beta 1 and 3 containing integrins modulate monocyte adhesion and subsequent protein release onto the sIPN, ii.) ligand density of the sIPN modulates monocyte adhesion and subsequent protein release and iii.) monocyte-fibroblast co-culture system with the sIPN reveals dynamic monocyte response to selected ECM components in the presence of fibroblasts.

Of particular importance is the monocyte-fibroblast co-culture study that highlights monocyte interactions with the sIPN as perturbed by fibroblasts as a closer mimic of the physiological environment. As described in Section 4.4 in the discussion section, since the first report of a monocyte-fibroblast co-culture study in 1983, there have only been less than a dozen monocyte-fibroblast co-culture studies, and the majority of them focus on alveolar macrophages and lung fibroblasts and employ cell lines with inherent deviations. In addition, the majority of the studies do not include a biomaterial in the co-culture system. Thus, this work presents a novel and important findings in which monocyte interaction with the sIPN scaffold as modulated by the presence of the fibroblasts is examined.

Co-culture analysis of cell-material interaction in the context of a biomaterial over time can be carried out but controls must be carefully and thoroughly prepared in order to maintain the ability to isolate the source of an effect or phenomenon. The core principles of the dynamic co-culture technique include the following parameters:

1.) Media optimization

For example, media used in the ultimate design of the co-culture system was optimized prior to the experiments, as described in Section 4.2.3. The effects of media transition on

fibroblast confluency/cell density, morphology and viability were all monitored so that the phenomenon observed in the co-culture study was not an artifact of the media conditions.

2.) **Monoculture conditions as controls**

In the monocyte adhesion data shown in Table 4-1 and the protein expression data, particularly in 4-9 (GM-CSF) and 4-12 (MMP-2), the effects of a co-culture condition where the two cells are in communication can be unsubtly observed. By having monocyte monoculture and fibroblast monoculture conditions in the design of the study, the effects of the co-culture versus monoculture conditions can clearly be distinguished. In addition, as both chambers were analyzed for protein concentration, even in monoculture conditions, insight into the diffusion of the proteins over time in this dynamic system could also be acquired.

3.) **Verification of communication between the cell types through the biomaterial.**

Section 4.3.1 describes the diffusion of proteins of varying molecular weight through the polycarbonate transwell network with or without the sIPN cast on the membrane. Three proteins of varying molecular weight were tested to verify the communication of cells in the co-culture system, and solute transport through the chambers should be verified in future works as well.

These guiding principles in the co-culture study design allow more control for a clearer analysis of data, but additional studies can also be carried out to parse out the precise details of the molecular mechanisms by studying cell-cell contact or cell response in "enriched media." The co-culture study outlined in this thesis describes a system in which the two cell types are not

in contact but are communicating via molecules diffusing through the matrix barrier. Monocyte-fibroblast cell contact may lead to altered response and as a result cell contact may lead to a decreased or increased expression of cytokines, growth factors or enzymes. However, with cell contact, it becomes difficult to isolate the origin of an effect. In other words, if there is an upregulation of a protein observed, it will be difficult to ascertain from which cell type this upregulated expression is being observed. With thorough controls, perhaps through single cell assays, it may provide powerful information. Alternatively, monocyte or fibroblast enriched media can be tested on fibroblasts or monocytes, respectively. While cell contact assays will describe two cell types that communicate directly to and with each other, the work described in this thesis describes two cells communicating through molecules in solution. Enriched media assays can provide information on the paracrine mechanisms between the two cell types, even in the absence of the one cell type.

The project that has been outlined in this thesis, particularly Chapter 2, has probed the molecular mechanisms behind the cell-material interaction. However, the mechanisms behind the decreased monocyte adherent density on RGD-PEG grafted sIPN in the presence of fibroblasts described in Chapter 4 needs to be further investigated. Though fibroblasts did not decrease monocyte adherence onto RGD-PEG grafted sIPN by affecting their viability, this is not a direct confirmation of monocyte function, and though they may be viable, their adherent function may not be preserved. Plating the nonadhered monocytes onto other adhesive substrates such as collagen or fibronectin coated TCPS surfaces can provide information about their functionality as perturbed by fibroblasts. If the adhesive functionality but not the viability of the monocytes are affected by fibroblasts, that can provide a broader picture into the adherent mechanism, and immunoblotting for specific focal adhesion proteins can identify the key molecular players

behind this phenomenon. Immunoblotting should be targeted toward several focal adhesion proteins (i.e. not just limited to vinculin). For example, vinclulin binds to talin that binds to tensin and α-actinin. Fak also binds to paxillin which binds to vinculin. Thus, observing the expression and regulation of these proteins over time on RGD-PEG grafted sIPNs in the presence of fibroblasts should provide a more comprehensive and detailed insight into the modulation of focal adhesion proteins on the ECM-derived scaffold by firboblasts. In addition, the investigation should include more time points at the initial stages of co-culture. The western blot analysis of vinculin and other proteins, coupled with RT-PCR, can also provide a much more comprehensive analysis of monocyte focal adhesion on the RGD-PEG grafted sIPN as modulated by fibroblasts.

With regard to monocyte protein response to the sIPNs, as MMPs in the wound and the ECM-derived matrix scaffold have demonstrated a dynamic interaction, and taking advantage of these complex interactions and guiding the degradation of the wound healing scaffold through cells will be a possible route of therapy. Chemically introducing MMP cleavable sequences in the PEG tether that presents the ligands on the scaffold will be able to control not only the release of the ligands but also the subsequent infiltration of the surround cells into the matrix scaffold and lead to the degradation of the material. Not only is the evaluation of the MMPs imperative for the design of this degradation directed material, but the analysis of the matrix metalloproteinase inhibitors, tissue inhibitor matrix metalloproteinase, will also provide a critical insight into the wound environment as degradative environment to which the material is introduced. Once the inhibitors and activators of MMPs are evaluated in the wound site in which the sIPN will be placed, the host site may provide an environment where different PEG tether lengths can be used in the sIPN. In other words, one drug or agent of interest can be conjugated

onto a longer PEG tether with the cleavable sequence and can "mask" the shorter chain lengths with another drug entity conjugated onto the tether, outlined in Figure 5-1. With this design, actuated drug delivery through the sIPN matrix may be achieved taking advantage of the host environment.

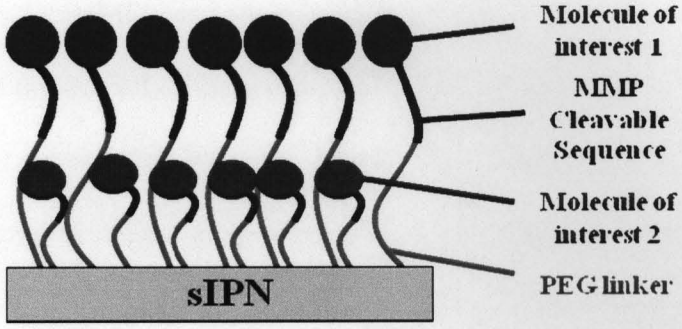

Figure 5-1. Schematic of a sIPN scaffold with two different molecules conjugated to PEG tethers of varying chain lengths.

Dovetailing the control over mechanical properties and the biofunctional characteristics of the sIPN material (i.e. RGD presentation, concentration, spacing) along with a thorough investigation of the wound healing environment to which the sIPN scaffold will be placed will prove crucial in the successful integration and in the assistance of the wound healing progression by the sIPN in the host tissue.

In addition, analysis of the infiltration of the surrounding wound healing cells into the sIPN as well as ECM deposition onto the material will also provide insight into short term inflammatory response and long term biocompatibility. Thus, comprehensive yet detailed cell-material interaction investigations will ultimately play critical roles in the successful integration of this biodegradative and compatible wound healing scaffold in the wound site.

Peptide conjugated polymer systems are a newly emerging class of biomaterials that can combine select advantages from biological and synthetic components to create a uniquely functionalized material. Advances in peptide conjugated materials have been exponential and a wealth of knowledge has been gained about the effect of peptide conjugated materials on the host response. Peptides offer stability and specific induction of cell events, but there remains much to be understood about the impact of these peptides' selectivity and presentation on the biomaterial surface and how that impacts cell behavior. For example, while some report the importance of αvβ3 integrin-mediated fibroblast focal adhesion and stress fiber formation in fibroblasts to a RGD presenting surface, others have demonstrated the key role of β2 containing integrins on monocyte adhesion onto a RGD presenting surface [1-3]. It is also becoming clearer that the density of peptides on the material plays a critical role in host response. For example, while Massia and Hubbell reported that a RGD density of 1 fmol/cm^2 grafted on a glass surface induced maximal fibroblast adhesion and spreading while Rowley and Mooney showed a 30 fmol/cm^2 RGD density on an alginate surface induced maximum myoblast adhesion and proliferation [1,4]. In addition, Sawyer and others have demonstrated a threshold for RGD density's impact on mesenchymal stem cells (MSC), where a high RGD concentration coated on the hydroxyapatite surface actually deterred MSC binding and spreading [5]. However, these studies report *in vitro* findings and the impact of the complex and dynamic interaction between blood proteins and a variety of host cells on the RGD presenting surface is even less understood. Even in *in vitro* systems the cause and effect based mechanisms behind cell-material interaction (i.e. enhance adhesion, proliferation and ECM production, etc.) are yet to be clearly deciphered and remain critical to the ultimate goal of directed host response.

And though peptides are more stable than the whole protein, they are not exempt from thermal instability and hydrolysis and are thus subject to short shelf lives. Peptides can also be costly to synthesize and may be impractical for large scale treatments, but with rapid developments in recombinant DNA technologies that allows the synthesis of these sequences, the overcoming the hurdle of high scale up cost is becoming more plausible. The biggest challenge will still be controlling the dynamic and spatial arrangement of multiple signals and ultimately translating this to a controlled surface into directed host response.

With current developments in our increasingly sophisticated understanding of protein structure-function through technologies such as crystallography, the trend in peptide conjugated systems is shifting toward peptide conjugated natural polymers. Natural biopolymers such as chitosan, collagen and hyaluronic acid have gained much interest, and the literature on peptide conjugated natural polymers is growing at a faster rate than peptide conjugated synthetic polymer systems. However, synthetic polymers are more robust than natural polymers and continue to be a more prevalent application in the clinical setting, and thus the endeavor to impart biological activity onto polymer surfaces to create uniquely advantageous biomaterials will continue.

References

1. Massia SP and Hubbell JA. An RGD spacing of 440 nm is sufficient for integrin alphaVbeta3 mediated fibroblast spreading and 140 nm for focal contact and stress fiber formation. J Cell Biol 1991;14:1089-1100.
2. Yahalom D, Wittelsberger A, Mierke DF, Rosenblatt M, Alexander JM, Chorey M. Identification of the principal binding site for RGD-containing ligand in the alphaVbeta3 integrin: a photoaffinity cross-linking study. Biochem 2002;41:8321-8331.
3. McNally AK and Anderson JM. Beta1 and beta2 integrins mediate adhesion during macrophage fusion and multinucleated foreign body giant cell formation. Am J Path 2002;160:621-630.
4. Rowley JA and Mooney DJ. Alginate type and RGD density control myoblast phenotype. J Biomed Mater Res 2001;60:217-223.
5. Sawyer AA, Hennessy KM, Bellis SL. The effect of adsorbed serum proteins, RGD and proteoglycan-binding peptides on the adhesion of mesenchymal stem cells to hydroxyapatite. Biomaterials 2007;28:383-392.

Appendix

Figure i. Confluent fibroblast morphology and viability incubated in FGM or RPMI with human serum for 3 days after reaching confluency (100x).

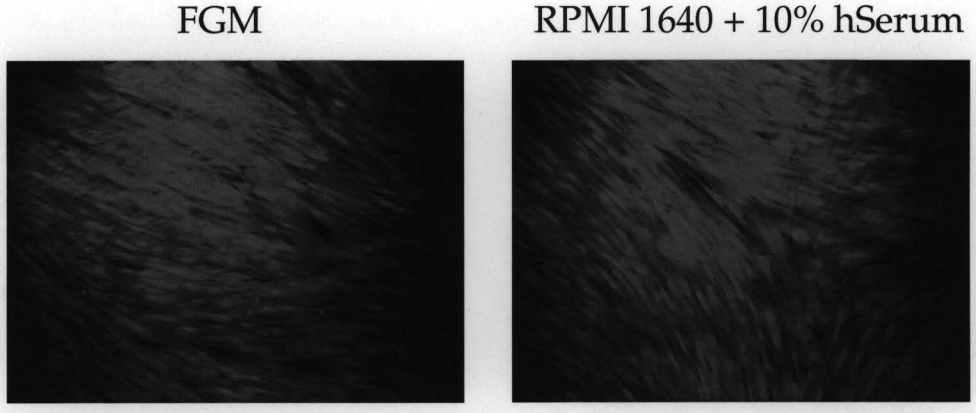

Figure ii. Immunoblot of monocyte and fibroblast vinculin on the polycarbonate transwell or RGD-PEG grafted sIPN at 2 h. *Fibroblasts are adhered on the TCPS surface and in the presence of the polycarbonate transwell or RGD-PEG grafted sIPN.

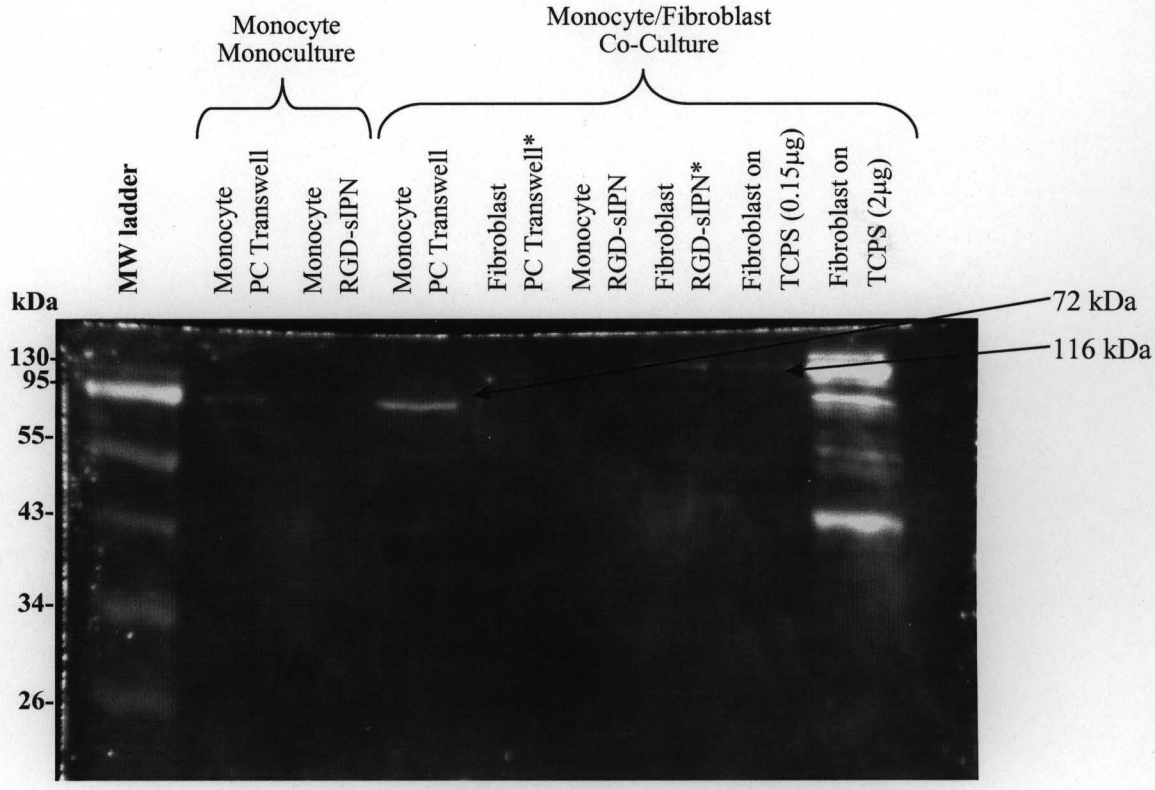

Table i. Nonadherent live and dead monocyte number from various surfaces at 2, 4, and 24 h under monocyte monoculture or monocyte/fibroblast co-culture conditions.

			Culture Time (h):								
	Surface/Ligand-PEG grafted sIPN		2			4			24		
Monocyte Monoculture	Live	Polycarbonate Transwell	67917	±	4161	33854	±	12756	22188	±	14221
		Unmodified Gelatin	26146	±	4126	14063	±	2049	21458	±	3341
		GGG-PEG	36771	±	8067	10938	±	313	34479	±	4701
		RGD-PEG	11979	±	2658	9792	±	2387	128125	±	28566
	Dead	Polycarbonate Transwell	3854	±	1477	833	±	477	2708	±	651
		Unmodified Gelatin	2188	±	541	2188	±	1740	2292	±	1301
		GGG-PEG	1458	±	786	2813	±	488	781	±	156
		RGD-PEG	1980	±	786	5208	±	1443	3958	±	1263
Monocyte/Fibroblast Co-Culture	Live	Polycarbonate Transwell	77188	±	12204	29583	±	15437	40833	±	6062
		Unmodified Gelatin	25938	±	3172	18958	±	7244	35104	±	10506
		GGG-PEG	21771	±	5316	21875	±	5303	52917	±	6920
		RGD-PEG	31250	±	2480	25000	±	2210	162292	±	6913
	Dead	Polycarbonate Transwell	2708	±	477	1458	±	180	938	±	313
		Unmodified Gelatin	1164	±	449	2188	±	1250	1875	±	1362
		GGG-PEG	2563	±	410	3721	±	239	1146	±	361
		RGD-PEG	4792	±	2009	3792	±	697	4063	±	2188